Cranfield University

Craig Lawson

Capacitance Tip Timing Techniques in Gas Turbines

2003

School of Engineering

Ph.D. Thesis

Cranfield University

School of Engineering

Ph.D. Thesis

1999 - 2003

Craig Lawson

Capacitance Tip Timing Techniques in Gas Turbines

Supervisor: Professor P. C. Ivey

November 2003

This thesis is submitted in fulfilment of the requirements for the Doctor of Philosophy.

Abstract

The vibration of turbomachinery blades is an important phenomenon to understand, observe and predict and is the reason for developing a tip timing measurement system. Vibration leads to High Cycle Fatigue (HCF), which limits blade durability and life. HCF can result in blade failure, having expensive consequences for the engine involved. The traditional method for monitoring blade vibration under test conditions is to use blade mounted strain gauges. However, strain gauges are costly and time consuming to install. They have a limited operating life as they are subjected to the harsh on-engine conditions. Only a limited number of blades can be monitored with strain gauges as the number that can be used is limited by the number of channels in the slip ring or telemetry. They can also interfere with the assembly aerodynamics. Consequently non-intrusive alternative techniques such as tip timing are sought.

Capacitance probe based clearance measurement systems see widespread use in turbomachinery applications to establish rotor blade tip clearance. This thesis reports investigations into an alternative and additional use in aero-engine rotor blade tip timing measurement for these commercially available systems. Tip clearance is of great importance in the gas turbine industry; this is clear from the fact that gas turbine efficiency has an inverse relationship with tip clearance. Large tip clearance leads to large leakage flows, hence low efficiency, thus the common use of the capacitance probe clearance measurement technique in monitoring turbomachinery.

Optical systems have been successfully used to measure rotor blade tip timing on test rigs with several optical probes mounted equally spaced around the turbomachine casing. However, there are practical problems associated with mounting such monitoring systems on in-service jet engines. Optical probes require high maintenance to keep the lenses clean, probably incorporating a purge air system to keep the lenses from fouling. Such impracticalities and added weight make it unlikely that an optical probe based tip timing system will be fitted on an in-service engine in the foreseeable future.

In this thesis the scope for a dual use sensor to measure both turbomachinery tip clearance and tip timing is investigated. Since it is impractical to measure blade tip clearance with an optical probe, then the obvious choice for such a sensor is a capacitance probe. Therefore, a commercially available FM capacitance probe based blade tip clearance measurement system is used in a series of tip timing practical investigations. The equipment and instrumentation designed, assembled and produced to facilitate this investigation is documented. These include the development of an optical once per revolution sensor and the design of an independent vibration measurement system based on blade mounted strain gauges.

Through an extensive body of experimental work the practicalities in this alternate use of the tip clearance measurement equipment have been assessed. System responses pertaining to tip timing measurement have been investigated, characterised and quantified. The accuracy by which tip timing can be measured using the system has been reported through the findings of an experimental programme carried out on a full-sized, low-speed compressor.

Specifically, dual capacitance probe tip timing derived vibration amplitudes have been compared to those derived from blade mounted strain gauge signals. Sources of error have been identified and quantified. Amplitudes were found to agree within the calculated error bands. Instantaneous resonant blade vibrations measured through single capacitance probe tip timing have been correlated with strain gauge derived vibration levels. This has also been done as the rotor traverses blade resonant speed. In this case the vibration phase change across resonance expected from theory was successfully detected through tip timing. Also, the accuracy by which blade time of arrival can be determined by using capacitance probe tip timing has been assessed using a precision OPR sensor and a non-vibrating compressor rotor blade. The characteristics of a DC capacitance probe based clearance measurement system's response to movement in 3D space in proximity to a blade tip have been mapped. Detection of small vibrations have also been investigated in a series of static impulse tests.

Acknowledgements

Thanks go to Professor Paul Ivey for initiating this project and for the continual advice, support and encouragement provided throughout the course of this research.

The author would like to acknowledge the United Kingdom Engineering and Physical Sciences Research Council for financially supporting this project. Rotadata Ltd., Derby, UK are also acknowledged for financial support and for providing hardware and technical advice.

The extensive experimental programme would not have been possible without the first-hand support and assistance from the team at the Cranfield University Low Speed Compressor Laboratory, Test House 3. Therefore, the author extends thanks to Bernard Charnley, Brian Stapleton and Pat Sweeney. The author also wishes to acknowledge Mark Erlund for willingly providing valuable instrumentation advice.

Thanks also to colleagues and friends for advice and assistance. Particular thanks to Martin Bayliss for lending his Fortran skills to the post processing automation task. Special thanks to Kelly Grant for continual and valuable input on the theoretical and practical aspects of this project, but most of all, thanks for making it fun to come to work every day.

Finally, the author wishes to gratefully acknowledge the continued support and encouragement throughout his period in full-time education of his parents, Jean and Ronald Lawson.

Table of Contents

List of Figures

List of Tables

Nomenclature

A	Electrode area
A/D	Analogue to Digital
A_{5mm}	Area of Light Spot 5 mm from Emitter Fibre
AC	Alternating Current
A_{inlet}	Compressor Inlet Area
$A_{receiver}$	Area of Receiver Fibre End
A_{seg}	Area of Segment
A_{vib}	Amplitude of Blade Tip Vibration
C	Capacitance
cal	Strain to Tip Deflection Calibration (m/Pa)
CBA	Cost Benefit Analysis
C_D	Discharge Coefficient
CDT	Capacitance Displacement Transducer
C_p	Specific Heat at Constant Pressure
CTF	Compressor Test Facility
C_v	Specific Heat at Constant Volume
CW	Coefficient of Work
d	Blade Tip Deflection
D_1	Blade Tip Deflection at Capacitance Probe 1
D_2	Blade Tip Deflection at Capacitance Probe 2
DC	Direct Current
DCF	Discounted Cash Flow
D_m	Dimensionless Mass Flow Rate
d_u	Mid Blade Radius
E	Modulus of Elasticity
Eo	Permittivity of free space
E_r	Relative permittivity of the dielectric between the electrodes
ESPI	Electronic Speckle Pattern Interferometry
f	Frequency of Blade Vibration
FEA	Finite Element Analysis
FFT	Fast Fourier Transform
FM	Frequency Modulated
G	Amplifier Gain
GF	Strain Gauge Factor

h	Distance from the probe centre to the blade edge
HCF	High Cycle Fatigue
Hz	Hertz
IC	Integrated Circuit
IGV	Inlet Guide Vane
IRR	Internal Rate of Return
LAN	Local Area Network
LED	Light Emitting Diode
m.	Mass Flow Rate
N	Newton
NGT	Normal Group Technique
NPV	Net Present Value
OPR	Once Per Revolution
P_0	Static Pressure at Compressor Intake
P_1	Static Pressure Upstream of IGVs
P_2	Static Pressure Upstream of Rotor
P_3	Static Pressure Downstream of Rotor
P_4	Static Pressure Downstream of Stator
Pa	Pascal
PC	Personal Computer
PCB	Printed Circuit Board
PSD	Power Spectral Density
PSU	Power Supply Unit
P_T	Total Pressure at Compressor Intake
PVI	Present Value Index
R	Resistance
R&D	Research and Development
R-C	Resistor-Capacitor
r_p	Radius of the probe head
RPM	Revolutions Per Minuite
SMA	Screw-Type Optical Fibre Connector
SME	Small to Medium Sized Enterprise
T_0	Compressor Inlet Temperature
t_1	Time of Arrival at Capacitance Probe 1
t_2	Time of Arrival at Capacitance Probe 2
U	Blade Tip Velocity
Va	Mass Flow Rate / A_{inlet}

δ	Electrode separation
Δt	Time of Blade Arrival Between Two Probes
ε	Strain
γ	C_p / C_v
τ	Torque
ω	Angular Velocity

1. Introduction

1.1 General Introduction

Capacitance probe based clearance measurement systems see widespread use in turbomachinery applications to establish rotor blade tip clearance. This thesis reports investigations into an alternative and additional use in aero-engine rotor blade tip timing measurement for these commercially available systems. Tip clearance is of great importance in the gas turbine industry; this is clear from the fact that gas turbine efficiency has an inverse relationship with tip clearance [1]. Large tip clearance leads to large leakage flows, hence low efficiency, thus the common use of the capacitance probe clearance measurement technique in monitoring turbomachinery.

The most suitable method of capacitance probe for turbomachine tip clearance measurement is the frequency modulated (FM) capacitance probe. This method was first developed by Chivers (1989) [2]. The paper suggests that it is superior to a DC system for on-engine applications as FM capacitance probes are uneffected by gas ionisation effects that are present in gas turbines.

The capacitance tip clearance system measures the capacitance between the probe and the blade tip. This is then related to tip clearance using a pre-determined calibration factor in conjunction with the fundamental relationship for capacitance.

The vibration of turbomachinery blades is an important event to understand, observe and predict and is the reason for developing a tip timing measurement system. Vibration leads to High Cycle Fatigue (HCF), which limits blade durability and life. HCF can result in blade failure, having expensive consequences for the engine involved. The traditional method for monitoring blade vibration under test conditions is to use blade mounted strain gauges. However, strain gauges are costly and time consuming to install. They have a limited operating life as they are subjected to the harsh on-engine conditions. Only a limited number of blades can be monitored with strain gauges as the number that can be used is limited by the number of channels in the slip ring or telemetry. They can also interfere with the assembly aerodynamics. Consequently non-intrusive alternative techniques such as tip timing are sought.

A survey of the open literature pertaining to blade tip timing shows that non-intrusive measurement systems are dominated by optical techniques. The laser Doppler method for tip timing measurement was first proposed in the 1970s [3]. The optical technique is appealing as it meets the high bandwidth requirements of tip timing measurements.

Optical systems have been successfully used on test rigs with several optical probes mounted equally spaced around the turbomachine casing. These systems can be used to obtain vibration amplitude through curve fitting and vibration frequencies by using Fourier analysis. Alternatively, outputs from algorithms applied to the signals from a number of probes over a

number of rotor revolutions may be used to determine vibration amplitude and frequency [4]. However, there are practical problems associated with mounting such monitoring systems on in-service jet engines. Optical probes require high maintenance to keep the lenses clean, probably incorporating a purge air system to keep the lenses from fouling. Such impracticalities and added weight make it unlikely that an optical probe based tip timing system will be fitted on an in-service engine in the foreseeable future.

As an alternative to optical probe tip timing, this programme of research set out to investigate the practicalities of developing a dual use capacitance probe based sensor that is capable of measuring both turbomachinery blade tip clearance and tip timing. The capacitance probe has greater potential than the optical probe as a dual use sensor as it is impractical to measure tip clearance on a turbomachine using an optical probe. This has been achieved by taking an existing commercially available FM capacitance probe based turbomachinery blade tip clearance measurement system and using it to measure blade tip timing. Thus, this programme of research involved an extensive body of practical experimental work in order to gain an understanding of the capacitance probe's application as a tip timing measurement device. This work culminates in blade tip vibration measurement through capacitance probe tip timing.

To date, there has been one published example where the performance of capacitance probes was compared to an optical system's performance in tip timing measurement [5]. That report found that the optical system showed superior amplitude resolution to the capacitance probe system. This suggests that optical tip timing systems can detect blade vibration amplitudes more accurately than the capacitance based system. Work has also been reported on specially designed capacitance probe head geometry, with the aim of improving the capacitance tip timing measurement [6]. This design is based on a multi-element probe head to improve spatial resolution. A lack of comparative measurement performance data prevents any meaningful conclusions from being drawn thus far from this work.

Since the capacitance probe system is already established as the on-rig tip clearance measurement system, if it can be shown (or developed) to have a dual use in also adequately measuring tip timing, then the need to also engine-mount an optical probe based system would be negated.

1.2 Management of the Project

This research project involved many distinct tasks, from computer simulations to laboratory experiments and Research and Development (R&D) management studies. Several tasks had to be performed in parallel as well as some following sequentially. Therefore, careful management of the project was required.

Work schedules were produced and continually reviewed and updated as events occurred throughout the project. Tasks were time-shifted in reaction to circumstances such as delays in obtaining experimental equipment. Consequently, despite setbacks the project was still able to be completed within the desired time-frame.

Quarterly meetings were held with the project's industrial sponsors. This allowed input and feedback from the industrial backers, ensuring that the project goals and outcomes were satisfactory to the sponsors. It also allowed the project to benefit from expertise and equipment from the gas turbine instrumentation industry.

The project was also managed through the university's annual review process. This involved assessing work completed at the time and scrutinising planned future work. Risks in future aims were identified and mitigating actions formulated.

1.3 Project Objectives

This programme of research set out to investigate turbomachinery blade tip timing using a commercially available FM capacitance probe tip clearance measurement system. An investigation into the practicalities of using such a system to make tip timing measurements is planned. The accuracy by which such measurements can be made is set out to be assessed. This broad objective is met by the successful accomplishment of several distinct smaller aims. These aims are summarised in the following list:

1. To satisfy the requirements of this Total Technology Ph.D. programme a review of R&D project selection models is an aim. This is followed by the application of such a model in a UK engineering SME.

2. To carry out a review of the literature pertinent to the broad objective. Thus, the areas of turbomachinery blade vibration in general, blade tip timing in particular and tip clearance measurement are studied.

3. To produce a solid model of the compressor blades to be used in the experimental investigations. Thus, facilitating through FEA blade natural frequency calculations, strain simulations and tip deflection simulations.

4. To commission a new compressor test facility to act as a vehicle with which to perform tip timing on.

5. To design and produce the instrumentation required to perform tip timing using the existing FM capacitance probe based tip clearance system; namely a precision OPR sensor.

6. To design and produce an instrumentation system to provide independent blade vibration measurements to assist in assessing the performance of the capacitance probe based tip timing blade vibration measurement.

7. To map the response characteristic of a DC capacitance probe clearance measurement system to movement in 3D space whilst in close proximity to a compressor rotor blade tip.

8. To Investigate a DC capacitance probe clearance measurement system's ability to measure small blade tip deflections by performing impulse response tests on a statically mounted blade.

9. To investigate the FM capacitance probe based turbomachinery tip clearance measurement system's ability to measure tip timing of a non-vibrating blade on the full-sized, low-speed compressor test facility.

10. To perform tip timing on a vibrating strain gauge instrumented blade using a single tip clearance FM capacitance probe to measure instantaneous blade tip deflections and to compare these tip deflections values with the values derived from the independent blade mounted strain gauge system.

11. To perform tip timing on a vibrating strain gauge instrumented blade using a single tip clearance FM capacitance probe to measure blade vibrations across resonance condition.

12. To perform dual capacitance probe tip timing on the vibrating blade to establish blade vibration amplitudes, and to compare these values with the amplitudes measured by the independent blade mounted strain gauge measurement system.

13. To assess the uncertainty associated with the tip timing and consequent blade vibration measurements performed through capacitance probe tip timing.

1.4 Thesis Structure

The main areas of work carried out during this project are each documented in a separate chapter in this thesis. With the exception of a few key diagrams contained in the chapters, the figures are presented in the appendices at the end of this thesis.

As a Total Technology Ph.D. project, this thesis contains a management aspect in the body of research reported. Six months were spent researching the application of an R&D project selection model within engineering SMEs. The work carried out to achieve this, and consequent findings are documented in Chapter 2.

In order to understand the state of the art, a review of the open literature was undertaken. The main areas of interest pertaining to the experimental investigations carried out were considered. The areas researched were turbomachinery blade vibration, turbomachinery blade tip timing and turbomachinery blade tip clearance measurement. Each of these three areas are reviewed in separate sections in Chapter 3.

Chapter 4 details blade simulation work carried out prior to the experimental testing programme. The production of a compressor rotor blade solid model is first described. This was followed by FEA of an FE mesh created from the solid model of the blade. This analysis begins by obtaining the blade's natural frequencies of vibration. Chapter 4 goes on to report on tests performed to validate the blade model. Subsequently, the model was used in a strain analysis to choose locations for surface mounted strain gauges. Next, blade tip deflection simulations are reported. This leads to the production of a model of a less stiff blade. Meshing, natural frequency, strain and tip deflection simulation results are also reported for this blade.

A large body of work was completed to assemble, design and manufacture the experimental equipment and instrumentation necessary to meet the experimental aims of this research project. This work is reported in Chapter 5. The assembly of a full-sized, low-speed compressor test facility is described in detail. The build schedule and budget for the compressor are documented. Some particular work carried out to enable instrument position control is outlined. Finally, the testing completed to commission the facility by mapping the compressor's characteristic is reported. The FM capacitance probe based turbomachinery blade tip clearance measurement system used for tip timing measurement, and the probe mounting arrangements designed are detailed.

Chapter 5 goes on to document the design and production of the instumentation systems used in the experimental testing programme. The process of developing an independent blade vibration monitoring system with which to test the capacitance probe tip timing techniques against is described. This system uses blade mounted strain gauges to derive tip deflections. The blade mounted strain gauges are described. This is followed by details of the electronics designed and produced to energise the strain gauges and amplify the resulting signals. The methods by which these electronics are physically and electrically integrated into the compressor are then described. The calibration carried out with the instrumented blades to relate strain to tip deflection is then covered. The development of a second instrumentation system required to carry out the tip timing tests is described. An optical OPR sensor was developed and

the laser, receiver and digitiser circuit designs are detailed. Finally, the performance of the OPR sensor is assessed. Chapter 5 ends by describing the data acquisition solutions used in this project. The capturing of the strain gauge signals is described. This is followed by the solution adopted for the acquisition of the capacitance probe signals. Finally, the hardware used and software developed to time the OPR sensor's digital output signal is detailed.

The experimental work carried out and the consequent findings are reported in Chapter 6. Initial off-rotor tests are performed with a DC capacitance probe clearance measurement system. The first section in Chapter 6 describes probe response characteristic mapping tests. The findings resulting from moving a capacitance probe in 3D space whilst in close proximity to a blade tip are reported. Next, further off-rotor testing is documented. This involved impulse tests performed with a strain gauge instrumented compressor rotor blade. Vibration levels and frequency were derived from the strain gauge signals. Simultaneously, vibrations are measured by a capacitance probe positioned in close proximity to the blade tip.

Chapter 6 goes on to report on the on-rotor testing programme. This starts by describing tests conducted with the FM capacitance probe based tip clearance measurement system. Tip timing is performed in the absence of blade vibration. Subsequently, a vibrating blade is used and tip timing is performed to measure blade vibration levels. These vibrations are compared to those derived from the blade mounted strain gauges. This is done in three ways. Firstly, single probe tip timing is reported where instantaneous blade tip deflections are measured. Secondly, blade vibration across resonance is investigated. Finally, dual capacitance probe tip timing experiments conducted to measure blade tip vibration amplitudes are reported. In each case, the results are analysed and the uncertainty is evaluated.

Conclusions from this programme of research are reported in Chapter 8. Conclusions are drawn from the findings resulting from the experimental work. This is followed by the original contributions resulting from this research. A list of publications generated from the work reported in this thesis is included in Chapter 8. The thesis ends by making recommendations for future work, based on findings obtained from this programme of research.

2. Management Aspects

2.1 Management Research Topic Justification

The development of novel and high-tech products is an effective way to give a company the edge over its competitors. Having a product of technical superiority in the market place can be a significant advantage. Hence the high importance of good research and development to firms involved in technological products.

Research and Development (R&D) is an ongoing process for forward thinking technology-based companies. Development of existing products is advisable to keep ahead of advances competitors may be making. Further, when a potential customer approaches a firm outlining its requirements for a product, R&D may be required to fulfil the request. Some more speculative, 'blue sky' research is also an option for firms. Speculative R&D is a valuable avenue to open new market opportunities. This type of research may lead to totally new products being developed and new markets being entered, thus strengthening the company's position through diversification.

A firm may seek to strike a balance between R&D in well-known areas to the company and more speculative R&D. The situation is analogous to a fleet of fishing trawlers. While most of the fleet will trawl waters known to be frequented by fish, a few boats may speculate by exploring uncharted waters. This can lead to new opportunities being discovered and thus reducing the fleet's dependence on its familiar areas for catches. Similarly, a technology-based company may guard against being damaged by downturns in its established sectors by seeking new sectors to move into through speculative 'blue sky' R&D.

The large numbers of potential R&D projects to pursue is clear when considering this R&D philosophy. The ability to consistently select the best projects to fund is therefore vitally important to firms. A great deal of academic research has been conducted over the past thirty-five years or so to produce methods to improve R&D project selection processes. Many project selection models have been developed over the years taking into account projects' financial aspects, risk considerations, or ranking projects by using scoring models. Research has shown that the most successful approach is to select projects by considering financial aspects, risk and project ranking, using a so-called hybrid selection model [7].

Relatively little research has been done to investigate the use of project selection processes within companies, particularly in small firms. This research therefore goes on to look at applying a hybrid R&D project selection model within a small engineering company. Such a field test provides rare and valuable insight into the practicalities of applying an academic model in industry. Insight is also gained into the R&D selection process currently used within a small UK based engineering firm. The factors that determine whether or not such a project selection model is likely to be adopted within a particular company are analysed, based on the field test results and the literature surveyed.

2.2 Research Project Selection Model

2.2.1 Introduction

When an organisation is tasked with deciding which research projects to proceed with, and which projects to reject, the selection process is often inconsistent. This research programme was designed to test the provision of a more formal, consistent and logical management tool to assist in project selection. This work builds on the findings of previous research students at Cranfield University. The test focuses specifically on the requirements of R&D managers in Small and Medium-sized Enterprises (SMEs).

A research project selection model has been developed at Cranfield University [8][9]. In this research programme, work has been done to enable the application of the model in a real company. The results are reported of a field test at a small engineering company in the aerospace instrument and telecommunications sectors. Conclusions are drawn on the applicability of such selection models within small companies.

2.2.2 Use of Project Selection Models in Industry

Despite the fact that many models for R&D project selection have been developed by academics, very few seem to have been tested in companies. Similarly, relatively little research has been published on the project selection techniques that are actually used in companies. There are a limited number of surveys that have been published into methods being employed in large firms [10][11][12][13][14][15][16][17][18]. There is no such information widely available on techniques being used in SMEs. In the absence of statistics on the application of project selection models in small firms, attention is turned to surveys of methods used in large companies to gain insight.

Large firms in the USA that are proven successes in R&D activities have previously been surveyed to establish the management practices they use [15]. Financial methods of project selection have been found to be the most widely used amongst large firms. However, companies that employ formalised project selection techniques that incorporate risk analysis and a scoring model as well as financial analysis generally outperform companies that rely solely on considering the financial aspects of projects [7].

Ongoing research at McMaster University, Canada, has surveyed over three hundred large companies throughout the world on their R&D projects portfolio management methods. From this, businesses have been sorted into four clusters based on the quality of their portfolio management technique and whether or not management is satisfied with the current method used. These clusters are illustrated below in the Table 2.1.

	Cluster			
Classification Criteria	Benchmark	Crossroads	Duds	Cowboys
Good portfolio management technique?	Yes	Yes	No	No
Technique fits management style?	Yes	No	No	Yes

Table 2.1 - Company Portfolio Management Technique Classification

As expected 'Benchmark' companies were found to perform best in terms of R&D project success, with 'Crossroads' second best. An interesting finding is that 'Duds' outperform 'Cowboys' [13]. This suggests that if a company has no good quality, structured portfolio management technique, it is at least better if management are dissatisfied with that state of affairs.

Application of structured and formal portfolio management has been found to have several benefits. The number and balance of projects is better, as is the number of projects in a firm's portfolio. Also, more projects are completed on time and R&D spending better reflects company strategy when good quality portfolio management techniques are used [12].

Surveys have shown that companies that employ formal project selection methods have better project launch success than those companies with no formal project selection technique. Sales and profit objectives have also been found to be significantly better where structured selection techniques are used [14].

Reports on in-house R&D management techniques used within the companies SEI of Japan and ABB show that formal documented portfolio management techniques are utilised successfully in these large firms [18][19].

2.2.3 Project Selection Model Study

The research project selection model being studied here was proposed at Cranfield University [9]. It is intended to be used as a tool to assist the engineer or manager to select the best project or projects from those put forward for consideration. The model does not set out to establish the best portfolio mix of research projects. It is designed to assess projects on their own merits, and to compare projects of similar types with each other.

The model is a hybrid, composed of three distinct and established project selection techniques. A scoring model is incorporated into the model, as is risk analysis and assessment. Financial considerations are also included in the form of Cost Benefit Analysis (CBA) or Discounted Cash Flow (DCF).

The selection tool is designed to be applicable to all types of research projects, but cannot be used to compare projects of different types. Three project type definitions are used, namely; Basic Research, Applied Research and Experimental Development.

The model uses an initial evaluation stage to quickly establish if a project shows potential and therefore merits a more detailed examination. This evaluation is qualitative and is in essence a scoring model. Quantitative and qualitative project criteria are set out. Scores are weighted and summed to give a single figure result. By weighting, the significance of each criteria and category are taken into account. The process by which the scores and weights are arrived at is vitally important in applying the model successfully. This process is discussed in detail in Section 2.2.4.

The project selection stages provide a more rigorous examination by conducting risk assessment and analysis on those projects that give promising results in the initial evaluation stage. Cost Benefit Analysis or Discounted Cash Flow is also applied to analyse the financial aspects of proposed projects. CBA and DCF are described in Appendix A.4.

A study of previous work shows that the model is yet to be tested at first hand. A rigorous set of field tests within companies of various sizes is essential to assess the applicability of the model. It is therefore necessary to conduct further work to allow the model to be applied in real companies.

2.2.4 Application of the Project Selection Model

In the previous section a need to validate the model in real firms was identified. In Section 2.2.2 a distinct lack of documented evidence testing model usage in SMEs was highlighted. This research programme therefore goes on to field test the model within a small engineering company in the telecommunications and aerospace sectors. A study of the project selection model allowed documents to be produced that enabled the model to be applied at the company. A step-by-step guide to model application has been developed and is shown in Appendix A.1. The process is represented diagrammatically in Figure A.1.1. Instructions and guidelines illustrating how to carry out each step have also been produced. These are shown in Appendix A.

Since the project selection model is applicable to all types of research project, but cannot compare projects of different types, the first step in using the model is to categorise the project either Basic Research or Applied Research and Experimental Development. Information on how to categorise a project is shown in Appendix A.1. However, the nature of the field test company's business means that they do not undertake Basic Research projects.

Once a project has been classified, a simple evaluation is carried out. This 'Filter' stage determines if the project can quickly be rejected as obviously being unpromising. The model suggests using six industry wide categories, consisting of company standard criteria. An example of such a Filter stage suitable for use within the company can be seen in Appendix A.2.

Scores assigned in the Filter stage should be established by standard group decision-making techniques. This could be by Normal Group Technique (NGT), where an anonymous ballot is followed by a discussion of the scores. A second ballot is then averaged to establish the final score. Alternatively, Delphi technique can be used; this is a remote survey with no group interaction. The score assignment guidelines are shown in Appendix A.2.

Further consideration of the application of the model assumes that the proposed project is not of classification Basic Research. As previously mentioned, the company being used in the field test does not undertake projects of that type.

Applied Research or Experimental Development projects that score sufficiently well in the Filter stage are next put forward for more detailed consideration. Further project classification is required as New Product projects (generally Applied Research) cannot be compared with Existing Product projects (generally Experimental Development). Once classified, projects can be ranked by their scores from the Filter stage.

For both types of project (New Product and Existing Product) the next stage is to conduct a Risk Assessment. This assessment establishes the appropriate level of risk analysis with which to scrutinise the proposed research project. This is done by finding a value 'x'. x is determined by considering available resources, budget and Benefit Cost Ratio. The equation for determining x can be seen in Appendix A.3.

Assigning values to the variables in the x equation should follow a consistent method. A single table should be constructed to assess the budget and manpower resources required for the range of projects being considered for approval. An example of assessing budget and manpower resources for risk assessment purposes is shown in Table A.3 in Appendix A.3.

Once values are assigned to the variables the value of x can be calculated, consequently the level of risk assessment corresponding to the calculated value of x can be read from Table A.2 in Appendix A.3.

Risk analysis level varies from no further assessment if values of $x \leq 2$ (low risk) are obtained, to detailed simulation modelling if $x > 4$ is derived. Appendix A.3 describes what is involved in each of the risk analysis levels.

After the suggested level of risk analysis is carried out mitigating action is taken in an attempt to reduce the chance of the project failing to meet expectations. The process then repeats from the risk assessment stage until either the risk is sufficiently low to approve the project, or it is the case that all mitigating action has been taken and the project is still deemed to risky to approve.

For projects that pass the risk analysis stage the next stage in the selection process depends upon the project's classification. A Cost Benefit Analysis should be conducted next for projects classified as New Product, while a Discounted Cash Flow study is the next stage for Existing Product projects. For an existing product cash flow information can be judged, hence the more informative DCF analysis is chosen over CBA. For a new product, cash flow information is

unlikely to be able to be predicted with any degree of confidence, hence CBA techniques are used for financial analysis. Applications of CBA and DCF are demonstrated in Appendix A.4.

The final stage in all cases is a Comparison Spreadsheet to allow selection between projects of the same type to be made. This brings together for review the scoring model scores, risk analysis results and financial assessment findings for a final comparison of the projects being considered for approval.

2.2.5 Project Selection Model Field Test

The project selection model field test sets out to gain insight into the model's potential for application within small engineering companies. A small UK-based engineering company operating in the telecommunications and instrumentation sectors was chosen for the field test. Work reported previously in this chapter has readied the project selection model for application at the company. This has been achieved by producing documents that were used by management at the company being considered in the field test. These documents have been developed following the framework for a project selection model set out in previous research work at Cranfield University [9].

The field test was facilitated by a meeting with a member of the company's senior management. This individual is in the position of making project selection decisions. The meeting allowed the project selection method identified and developed in this research programme to be applied to a project previously undertaken by the company. Throughout the process of applying the project selection model feedback was gathered on all aspects of the model. Comparisons were drawn with the method used when the company originally considered the project for selection.

Investigations into the project selection process at the company revealed that many of their normal considerations are reflected by those in the selection model. However, at the company the process is a mental one, done by an individual, and as such no data is on record.

Management at the company argued that the quality of decision making within the company is maintained without the use of a project selection model. Good decision making employees continue to consistently make good decisions, while bad decision makers are dismissed from the company.

Therefore, the field test found that the model would not be used for decision making within the company. Indeed it has been suggested before that management are unlikely to actually use formal models such as this for decision making [20]. In fact this has been found to be the case at the company being considered here.

The possibility exists to instead utilise the model as an information tool. In this case application of the model aids communication of decision making information down from senior management to project leaders. Management at the company considers that the value gained by using the model for this reason is outweighed by the cost of its implementation. This cost was

estimated to be fifteen thousand pounds per annum, as an additional staff member would be needed to administer the decision making records.

One aspect of the project selection model was considered by the company to be potentially worthwhile to formalise and document. The financial analysis section of the model allows documented Discounted Cash Flow to be linked to technical and financial project targets. The next section will therefore look at developing a project finances tracking framework that meets the company's requirements of being quick and easy to apply.

2.3 Multiple Project Cash Flow Tracking

The research project selection model field test has shown that such a formalised and documented management tool is unlikely to be implemented within the small engineering company tested. A need has been identified to enable management to closely track the cash flows within the company's portfolio of projects.

While the financial department will have a good understanding of company finances from the accounting processes, engineering management at the company currently lack this insight. What would be beneficial is a method which will allow management to conveniently track individual project, as well as the overall cash flow associated with the company's entire portfolio of projects. The tracking method should also allow management to easily predict the cash flow consequences of a project running over the initially estimated time schedule and budget. This should then be mapped to the portfolio cash flow to see the overall impact on finances.

To fulfil this need a simple extension to establish Discounted Cash Flow analysis techniques is proposed. By presenting DCF analysis information in a particular way, project costs over time can be efficiently tracked by management. By individually tabulating DCF information for each project in the company's portfolio in a spreadsheet, the overall portfolio cash flow can be calculated and displayed both numerically and graphically. Changes can easily be made to individual investment figures and time scales. The impact for the project finances in the future, as well as the impact on the portfolio cash flow is then automatically calculated, with results displayed numerically and graphically. Appendix A.5 shows spreadsheets containing DCF for sample projects and the resulting calculated overall portfolio cash flow and associated graphical representations.

2.4 Conclusions

The potential benefits of consistent and structured R&D project selection have long been recognised in both academia and industry. For about the last thirty-five years countless models have been developed to provide logic and structure to R&D project and portfolio management. Early development centred on scoring and financial models. Risk assessment is also a established technique used in project evaluation. Much of the more recent work has produced hybrid selection tools, where the three aforementioned techniques, scoring, financial and risk assessment are used to provide a more balanced project assessment tool.

While documentation of project selection model development in academia and industry are widespread, reports of model evaluation and usage within industry are relatively scarce. While some studies have been conducted on model usage in large companies, applications within SMEs remains largely undocumented. This research has produced valuable insight by testing a recently developed hybrid project selection model in a UK-based engineering SME.

The field test conducted in this research at a typical small engineering firm points to a general conclusion that small companies are unlikely to adopt structured hybrid project selection models such as the model considered here. However, the results are limited by the fact that this is only one example. Field tests at several more small companies are desirable to gain a better understanding of the applicability of the project selection model within small firms. Different companies and different styles of management may produce different field test results. For instance, the importance placed on recording the decision-making process by particular senior managers will have a significant effect on the likelihood of decision support systems being implemented within a firm.

The field test has shown that cost is a barrier to small firms implementing formal project selection techniques. Perceived benefits of such a decision support system are judged to be outweighed by the cost of using a model. Many larger companies already utilise structured project selection decision processes and could therefore adopt the particular model being considered here much more easily than a small firm with more limited financial resources.

One of the advantages of implementing the project selection model is that it allows a record of learning within the company to be kept. Such records are likely to be more valuable in large companies than in small firms. In large companies the scope to share decision-making knowledge is greater than in small firms where the number of decision-makers is less. Indeed in the test case here the number of decision makers is one and thus the value of keeping decision making records to share knowledge is very low. This offers an explanation as to why small firms in general and the company participating in this field test in particular are unwilling to invest the time and money to allow the implementation of a hybrid project selection model.

The field test identified a need for engineering management to track R&D project and portfolio finances more closely. Prompted by the willingness of management to formalise analysis and record keeping of financial aspects of R&D projects, a simple spreadsheet based tracking method has been developed. The method meets the requirements expressed by engineering management of being quick and easy to use. It clearly displays individual project and overall

portfolio finances over time. The method makes it straightforward for management to quickly establish the effect of changes to projects' budgets and time scales to the overall portfolio cash flow.

The company's interest in only formalising financial project aspects is not altogether surprising. Financial models have the most widespread use in large firms. This combined with the reduced value identified of sharing knowledge in small firms compared with large firms explains the greater reluctance of small companies to adopt a hybrid project selection model.

3. Literature Review

3.1 Turbomachinery Blade Vibration

3.1.1 Introduction

Turbomachinery blades will inevitably experience vibration throughout their working lives. Although blades are designed to avoid resonant excitation at engine harmonic frequencies, it is not possible to design a blade such that no significant vibration will be experienced. This vibration results in blade High Cycle Fatigue (HCF). HCF can result in sudden blade failure, which is likely to cause very expensive damage to the turbomachine. The higher the vibration amplitude that the blades are subjected to, the fewer cycles they will be able to complete before failure occurs due to HCF. Therefore, it is important to monitor blade vibrations.

One solution to blade vibration is to use shrouded rotors. This increases stiffness, reducing the vibrations that will be experienced. However, these cannot be used at high temperature, for example the first turbine stage after the combustion chamber. Shrouded rotors also have the draw back of not being able to operate at such high rotational speeds as non-shrouded rotors [21].

Unsteady flow in turbomachinery generated from, for example previous stage wakes may cause blade vibration at natural frequencies. Fan blades in particular can suffer from flutter, which is the undesirable blade vibration phenomenon driven by these unsteady flows that can cause self-excited blade oscillations [22]. Over recent years theory and experimental work have led to the hypothesis that flutter may be caused by acoustic properties of turbomachinery intakes [23] [24] [25].

3.1.2 Turbomachinery Blade Vibration Measurement

Traditionally, time consuming and expensive off-rig durability tests are carried out on turbomachinery blades. These tests are used to determine blade fatigue and the maximum vibration levels that a blade can withstand before failure occurs. These tests must be designed to account for the high temperature and centrifugal loading that blades are subject to on-rig. Fatigue strength is determined by destructive testing.

Predictions of blade life or durability can then be obtained by comparing the fatigue strength findings from the off-rig trials with the highest vibration level detected in the engine under consideration.

Vibration levels are normally measured by mounting strain gauges on the blades and performing an on-engine test. Strain gauges are positioned on the blade to gain an adequate

response in all modes of vibration. Modes of vibration can be predicted from finite element analysis. The blade tip vibration amplitude is determined from the strain gauge results. Calibration allows a strain-to-blade tip amplitude relationships to be established. Since calibration is performed cold, the on-engine measurements must be corrected to account for the heightened temperature.

As many gauges are blade mounted as possible, as a high percentage are expected to fail due to the high temperatures involved. The instrumentation capacity is usually the factor limiting the number of strain gauges that are blade mounted. That is to say, the number of gauges that can be used is limited by the number of telemetry or slip ring channels available to route the signals from the rotor to the ground station.

Engine tests are carried out by accelerating and decelerating the engine over it's operating range. The strain gauge results are in the form of multiple signals of varying frequencies and amplitudes. Fourier analysis must be performed on the data to get strain measurements in individual excitation modes.

The time consuming and expensive nature of this vibration measurement method makes the development of new techniques desirable. This has lead to the development of non-intrusive blade vibration monitoring methods such as blade tip timing. Tip timing is considered in detail in Section 3.2.

3.1.3 Conclusions

Blade vibration is a significant phenomenon in the case of turbomachinery rotors. Through complex unsteady flow, undesirable self-excited flutter can result. This leads to HCF, which in turn can result in catastrophic blade failure. Consequently serious and expensive damage can be done to turbomachinery.

To mitigate blade vibration, shrouded rotors are sometimes used. However, this type of turbomachinery stage is not suitable in all applications. As a result, blade life studies through vibration measurement are desirable.

Traditionally expensive, time consuming destructive testing is performed on test rigs to obtain blade life data. These tests typically use blade mounted strain gauges to measure vibration. Additional on-engine vibration data is also required to accurately establish blade life expectancy. Again, blade mounted strain gauges can be used to measure this vibration. This is expensive and impractical. Consequently, non-intrusive techniques of measuring blade vibration in place on in-service engines are sought. The leading technique is blade tip timing measurement, and this is considered in detail in Section 3.2.

3.2 Tip Timing Techniques

3.2.1 Introduction

The significance of blade vibrations in turbomachinery is discussed in Section 3.1. This leads to the desire to measure or monitor blade vibration levels on engines. Traditional intrusive methods for measuring blade vibrations are discussed in Section 3.1.2. These methods involve blade mounted strain gauges, and the disadvantages inherent in this for on-engine applications have been outlined. These disadvantages include the time and cost involved, the fact that only a limited number of blades can be monitored and the low life expectancy of the gauges. In addition, blade mounted strain gauges interfere slightly with turbomachinery aerodynamics.

These factors combine to make on-engine blade vibration measurement impractical using traditional methods. This has lead to the development of the non-intrusive blade vibration measurement method known as tip timing. In using this method the time of arrival of blades at fixed probes mounted on engine casings is used to monitor blade vibration. Vibration levels are deduced from the difference in this time of arrival from that expected from the rotor's speed.

3.2.2 Review of Current Work

A survey of the open literature in turbomachinery blade tip timing shows that non-intrusive measurement systems are dominated by optical techniques. The laser Doppler method for tip timing measurement was originally demonstrated by Kulczhk and Davis (1973). Later, optical systems were developed using lasers and blade mounted mirrors to also establish mode shapes from the laser beam deflections [26]. The optical technique is appealing as it meets the high bandwidth requirements of tip timing measurements. Modern systems typically have bandwidth capability of at least 100 MHz [27]. A typical optical tip timing measurement system is shown in Figure B.3.1.

Work has been reported involving experimental blade vibration measurements using case mounted optical probes. A shaft mounted OPR sensor was also used and tip timing vibration measurements were compared with frequency of vibration data obtained from Fourier analysis of blade mounted strain gauge signals [28]. This work continued with optical tip timing being performed on a compressor stage with vibration controlled blades. The vibration control was achieved by mounting piezoelectric crystal exciters on all 38 fan blades in the stage used for the testing programme [29].

A more complex system using optical probes to measure both blade tip timing and blade tip clearance was later proposed. Bench testing was reported that used triangulation with optical probes to measure blade tip position in both the clearance and timing directions [30]. Such a system requires numerous probes and as such appears impractical for use on an in-service engine.

Robinson *et al.* (1991) performed optical tip timing tests to measure blade tip vibration amplitudes. In these tests, tip timing blade vibration measurements are compared to blade

mounted strain gauge results of vibration amplitude. The strain to tip deflection conversion used is taken from look-up tables. It is suggested that such tables be generated from either blade FEA or from tests performed off-rig on a vibration table. It is unclear which method was used for the experiments presented, and comparisons between tip timing and strain gauge measurements are vague and inconclusive [31].

It has been shown that bending vibration can be measured using a single optical probe. By positioning the probe over the centre of the blade chord detection of torsional bending is minimised. By using more than one sensor, torsional deformations can be detected.

Optical tip timing measurement systems have been used to detect synchronous and asynchronous vibrations [27]. This can be achieved by using four probes mounted on the turbomachine's casing [32]. Systems have also been devised with two probes used at a known spacing around the turbomachine case. This type of system can detect asynchronous vibration, and synchronous vibration by speed traversing the engine resonance frequencies.

It is common to correlate optical tip timing measurements with the results from blade mounted strain gauges. This is because tip timing measurement has a limited results capability, especially when a small number of probes are used. Therefore, recent work in optical tip timing measurement has focused on data analysis, with the aim of raising the capability so that it can replace the need for blade mounted strain gauges.

The theory for an improved analysis technique for tip timing data was proposed by Heath and Imregun (1996). A multi-degree of freedom simulation was used to show the improvements of this technique over those previously proposed [33]. This work continues with an assessment of the state of the art in tip timing data analysis techniques. The pros and cons of various techniques are assessed [34].

A data processing technique to measure synchronous blade vibrations from a minimum of two engine case mounted optical probes is proposed by Heath (2000). The method is known as 'two parameter plot' and is investigated through bench testing. It's ability to measure resonant vibration amplitudes is evaluated [35].

Tip timing data analysis techniques are investigated numerically through simulations by Carrington *et al.* (2001). Three techniques including an new autoregressive method are reported and evaluated [36].

Systems have been successfully used with several optical probes mounted equally spaced around the turbomachine casing. These systems can be used to obtain vibration amplitude and frequency by using Fourier analysis on the signals from a number of rotor revolutions [4]. To date, there has been one published example where the performance of capacitance probes was compared to an optical system's performance in tip timing measurement [5]. That report found that the optical system showed superior amplitude resolution to the capacitance probe system. This suggests that optical tip timing systems can detect blade vibration amplitudes more accurately than the capacitance based system.

The importance of turbomachinery blade vibration measurement to the United States of America's military is clear from the work reported by Jones (1996). Optical probes are used to measure blade vibration amplitudes and frequencies through tip timing [37]. Efforts driven by the United States of America's military are also outlined by Strange (2000). This study compares current non-intrusive blade vibration instrumentation technology against the requirements set out by the 'HCF Programme' and 'National Turbine Engine Durability Initiative'. It is concluded that future and further R&D is required to meet the on-engine monitoring requirements [38].

The development and use of a capacitance probe based system to measure both blade tip clearance and blade time of arrival is reported by Drumm and Hasse (2000). The system includes a specially designed multi-element capacitance probe head used with the aim of improving spacial resolution over the traditional single element capacitance probe. A lack of published data regarding this system as a tip clearance and tip timing measurement device prevents any meaningful conclusions from being drawn on its performance capabilities [6] [39] [40].

3.2.3 Conclusions

The impracticalities in using traditional intrusive methods to measure turbomachinery blade vibrations on engines has lead to the development of the non-intrusive blade vibration measurement technique known as tip timing.

Tip timing measures blade vibration by determining blade tip times of arrival at fixed points on the turbomachinery casing where probes are mounted. Vibration levels are established from the differences in these arrival times and the arrival times expected from the independently measured rotor speed.

Tip timing measurements are dominated by the use of optical probes. There is some evidence of capacitance probes being used in tip timing applications.

Optical probe based tip timing systems have been successfully developed for test-rig use. Such systems are capable of determining blade vibration frequencies and amplitudes, given a sufficiently high number of case mounted probes. There are impracticalities associated with using optical probes for tip timing on in-service engines. These include the need to keep the probes' lenses clean. Thus adding to the weight penalty involved in mounting such a system on an aero-engine.

Data processing of tip timing results is an active field of R&D. Studies have looked into maximising the information extracted from a minimal number of case mounted probes.

3.3 Capacitance Tip Clearance Measurement

3.3.1 Introduction

Tip clearance is of great importance in the gas turbine industry. This is clear from the fact that gas turbine efficiency has an inverse relationship with tip clearance. Large tip clearance leads to large leakage flow and hence low efficiency.

As engine pressure rise per stage, aerodynamic loading and rotor speed have all increased over the years, it has become ever more important to consider and monitor losses such as the leakage flow due to tip clearances [41].

The capacitance tip clearance system measures the capacitance between the probe and the blade tip. This is then related to tip clearance using a pre-determined calibration factor in conjunction with the fundamental relationship for capacitance:

$$C = \frac{E_r E_o A}{\delta} \qquad 3.1$$

In the case of turbomachinery blade tip clearance measurement, one electrode is the blade tip and the other is a probe mounted on the engine casing.

3.3.2 Review of Current Work

The most suitable method of capacitance probe for turbomachinery tip clearance measurement is the FM based system. This method was first developed in 1989 and is preferred to a DC system as FM capacitance probe based systems are uneffected by gas ionisation effects that will be present in gas turbines [2].

When using a capacitance tip clearance probe to measure turbomachinery blade tip clearance, the blade tip presents a very small area end-on (in the region of 5 mm^2) to the probes. The distance between the electrodes is relatively large (in the region of 1 mm). These two facts mean that the capacitance detected will be very small, in the region of 0.04 pF. With such small signals involved, it is essential to isolate the sensing element from its surroundings in order to prevent unacceptably low signal to noise ratios occurring. This has been achieved by using a co-axial arrangement, with plastic acting as the insulator [42].

Further advances in capacitance probe technology have lead to much higher operating temperatures becoming possible. This is achieved by adopting a tri-axial arrangement for the probe and cable. In this way the need to use plastic to insulate is overcome. The use of plastics limits the operating temperature range of the probes to around 200 degrees Celsius. However, a plastic-free probe may be used in the hostile environs of a high-speed turbomachine at over 1000 degrees Celsius.

Two such tri-axial capacitance probes are illustrated in Figure B.1.1. Traditional tri-axial probes comprise a metallic and ceramic construction. However, an improved arrangement is also shown in Figure B.1.1, with an all-metallic construction [43]. This design includes a guard ring extending fully to the sensor tip. This results in minimised stray capacitance between the sensing electrode and the outer screen. Therefore, this design is the most suitable for turbomachinery tip clearance measurement systems.

With a tri-axial arrangement, the capacitance between the blade tip and the probe is still small, and consequently the stray capacitance between the probe tip and the cable guard could be around 1000 times the blade to probe capacitance. This would induce an unacceptably high error into the system. A tri-axial arrangement with inner and outer screens is a successful solution to eliminate stray capacitance. This works by grounding the outer screen while driving the inner screen to the same voltage as the conductor. Therefore, there will be no voltage difference between the shield and the sensing electrode and thus no stray capacitance.

Capacitance tip clearance measurement systems have been developed utilising such tri-axial probes that are fairly simple to operate and self-calibrating, meeting the requirements of the gas turbine industry. One such system includes an electrode and a FM capacitance probe recessed 0.1 mm further than the electrode. The stepper motor driven probe uses the electrode for a spark/ discharge technique to measure the distance of the longest blade to the casing. Each discharge leads to a 0.1 mm retraction of the probe assembly, hence eliminating the chance of the probe being damaged by coming into contact with a blade [44].

This system minimises the range required of the capacitance probe. Since the spark/discharge electrode is used to establish the distance to the longest blade, the capacitance probe is only required to measure the difference in length between the longest and shortest blades.

The capacitance probes' signals are typically fed to an engine mounted Capacitive Displacement Transducer (CDT) amplifier. The CDT amplifier includes an oscillator, amplifier and filter. The oscillator reacts to changes in capacitance caused by the blade passing the sensor by changing its signal's frequency. The amplifier ensures that the instantaneous voltage between the guard and the sensing electrode is zero, thus ensuring no stray capacitance.

A ground station is used to log and process the signals from the probes. A demodulator is used to convert the CDT amplifier's oscillator signal into a voltage pulse train. A blade analyser unit converts the analogue peak of each blade passing into a digital number.

The blade analyser units are linked to a signal processor unit. This unit will contain firmware to calibrate the probe on-line, and to calculate the tip clearance over each blade. The signal processor outputs are tip clearance against blade number. These data are passed to a PC running data acquisition software for data logging and analysis [45].

3.3.3 Conclusions

Turbomachinery blade tip clearance is a factor desirable to minimise in order to maximise engine efficiency. The most suitable technology to measure turbomachinery tip clearance utilises capacitance probes. The capacitance signals involved in such measurements are small. and as a result signal isolation is vital to prevent unacceptably high levels of noise corrupting the signals.

Current sensor technology employs tri-axial probes and cables, that through plastic-free construction allows high temperature operation. The most suitable systems are FM based, where electronics comprise a CDT amplifier and receiver arrangement. The CDT amplifier incorporates an oscillator, high gain differential amplifier and a filter. Such systems are commercially available to measure turbomachinery tip clearance.

4. Compressor Blade Solid Modelling and Vibration Simulation

4.1 Introduction

In this chapter the vibration of rotor blades on the one-and-a-half stage low speed compressor test facility is investigated through FEA. It is desirable to predict the blades' natural frequencies of vibration, strain profiles and tip deflections.

The natural frequencies of blade vibration are calculated by using FEA of a finite element mesh created from a solid model of the compressor blade. The reasons for doing this are two-fold. Blade vibration will be monitored using blade mounted strain gauges. Therefore, firstly it is essential to know the frequencies of blade vibration in order to successfully design the electronics used to energise the strain gauges and amplify the resulting signals. To achieve a thorough assessment of the capacitance probe system's tip timing measurement ability, it is necessary to excite sufficiently high levels of tip deflection. Secondly, a knowledge of the blade's natural frequencies is therefore essential when considering excitation schemes.

To successfully install the strain gauge based blade vibration monitoring system, it was necessary to carefully select the locations and orientations of the gauges that were mounted on the blade's surface. To enable this selection, FEA strain results were used to provide important blade surface strain profiles, on a mode-by-mode basis.

It is desirable to predict the levels of blade tip deflection that will be present during compressor operation. As previously noted, sufficiently high amplitudes of blade tip deflection are sought. To this end, forced response FEA simulations were performed based on the forcing functions expected to be present during compressor operation.

The blade in question was a three-times oversized, LM24 cast aluminium alloy rotor blade designed specifically to produce flow characteristics on the low-speed facility akin to those on high-speed turbomachinery [46]. It was first necessary to produce a solid model of the blade used in these investigations before the desired simulation results were obtained. The solid model was built using I-DEAS Masterseries software. This solution was chosen as it allows simulations to be performed within this software package.

This chapter goes on to report the production of blade solid models using I-DEAS. Also outlined are methods used to obtain frequency, strain and deflection calculation results, and these results are reported.

4.2 Solid Model Production

A solid model of one of the test compressor's rotor blades was produced. This allowed FEA of the blades to be performed. This analysis had two main aims. Firstly, allowing the appropriate locations for blade mounted vibration monitoring strain gauges to be chosen through modal analysis of blade surface strain. Secondly, performing vibration simulations allowed the levels of blade tip deflections expected when running the compressor to be predicted. The nature of the forcing functions required to excite the blades to levels of tip deflections that might reasonably be detected using tip timing measurements was also be investigated through FEA.

CFD grids of the rotor flow passage were obtained from the blade designers at the National Technical University of Athens. These grids contain blade surface geometry data at either side of the flow passage. This is illustrated in Figure C.1.1.

The CFD grids include the flow calculation nodes as well as the blade surface geometry. Therefore, the surface points were extracted from the grid. The surface points were then manipulated into a form compatible with importing the blade geometry into I-DEAS. The extraction and manipulation was then achieved by writing programs in FORTRAN.

4.2.1 Wire Frame Surface Creation

Since the CFD grid data files cannot simply be read by I-DEAS, the data is instead input by running programs in I-DEAS. The blade geometry data must be written to files in a format that will be able to be run as programs in I-DEAS. This is achieved by surrounding the blade geometry co-ordinates with commands conforming to the instructions understood by I-DEAS when a user manually keys in data points. The co-ordinates themselves must be written as x, y and z components separated by commas.

Programs were written in FORTRAN 77 to read in the CFD grid file and output files with only the data points on the blade suction and pressure surfaces. The CFD grid is structured, with the suction and pressure surfaces of the blade lying on the first and last plane of 'k' in the calculation domain respectively. The positions of the leading and trailing edges of the blade are known in the 'i' calculation plane. It is thus possible to use a simple algorithm to extract the blade surface points from the CFD calculation grid. The program code used to achieve this is shown in Appendix C.2. The programs read in a TURBO 3D CFD calculation grid file and output files with points on the blade suction and pressure surfaces in a form that can be run in I-DEAS as a program.

Surfaces can be created in I-DEAS from sets of splines. Therefore, splines were created from the surface data points. Due to the large number of surface data points involved (2295 on both surfaces) it was not feasible to do this by hand. More FORTRAN programs were produced to generate span-wise and stream-wise spline generation programs to be run in I-DEAS. One such program used to generate the span-wise splines on the blade's suction surface is shown in Appendix C.2.

4.2.2 Solid Blade Creation

The pressure and suction continuous surfaces of the blade were created by hand in I-DEAS from the wire frames by using 'Mesh of Curves' technique.

The pressure and suction surfaces of the blade had to be moved into suitable position relative to each other (see Figure C.1.1) and then joined together. There are 79 blades in the rotor, thus the pitch is 4.557 degrees. The pressure surface was therefore rotated by 4.557 degrees in the *z*-plane about the origin. This resulted in the edges of the pressure and suction blade surfaces being co-incident. The surfaces were then joined together using I-DEAS surface stitching techniques.

At this stage the model is an open shell consisting of the joined pressure and suction surfaces. Finally, the solid model can be created by forming the flat blade tip and root surfaces. This is done by using the I-DEAS lofting command. These surfaces were stitched to the suction and pressure surfaces. Thus an enclosed set of four joined surfaces is achieved, resulting in the blade solid model. The solid model of the compressor's rotor blade is illustrated in Figure C.1.2.

4.3 Natural Frequencies Simulation

The natural frequencies of vibration of the compressor rotor blades were obtained through FEA. This information was vital to the successful design of the electronic circuits associated with the strain gauge energising and signal amplification. This data is also important when considering steps that were required to excite sufficiently high levels of blade tip vibration to provide a meaningful test of the tip timing measurement system under investigation.

The compressor blade root was bolted firmly into the rotor disc, thus for simulation purposes the blade was assumed to be a cantilever fixed at the root. With this boundary condition in place the natural frequencies of blade vibration were calculated using I-DEAS, given the material properties of LM24 Aluminium of which the blade is made (see Table C.1).

The blade solid model was partitioned using I-DEAS into sub-volumes, these being the blade and the root. The root, where it was anticipated that deflections and stresses would be negligible, due to the displacement constraints here, was free meshed. In I-DEAS free meshes are generated using first or second order tetrahedral solid elements. For this modelling task first order tetrahedral elements were used as second order elements would not significantly improve the accuracy of the results.

For the blade itself, mapped meshing was used. This was for two reasons. Firstly, due to the blade suction and pressure surfaces being created from many data points, it was found that the dynamic memory constraints of the computer system prevented the I-DEAS automatic free meshing algorithm from working. Secondly, since the blade is where the significant stresses and displacements will occur, the use of a mapped (manually created, structured) mesh was made, in order to maximise accuracy [47]. To achieve continuity with the root's free mesh, the mapped mesh used brick elements also of first order. Additional volume partitioning of the blade part of the model was required to enable changes in the mapped mesh density over the volume, and to avoid creating elements with poor aspect ratios.

Lanczos solver method was employed for this normal mode dynamics solution as it is processor-efficient and is user-friendly to set up for solution [48]. The FEA mesh of the compressor rotor blade is illustrated in Figure C.1.3. The results of the FEA natural frequency calculations are shown below in Table 4.1. The blade's vibration modes are illustrated visually in Appendix C.3.

Mode	Deformation	Frequency
1	Bending	725 Hz
2	Torsional	2061 Hz
3	Bending	3478 Hz
4	Bending & Torsional	3950 Hz

Table 4.1 - FEA Compressor Blade Natural Frequency Calculations

4.4 Model Verification

It is desirable to verify the accuracy of the solid model FEA results. The natural frequency of vibration of the blade obtained through FEA was used in the design of the electronics employed to both energise the strain gauges and to amplify the resulting signals. Simulation results, obtained from finite element stress analysis were used to select the positioning of these surface mounted strain gauges. Therefore, a simple frequency of vibration test was carried out in the laboratory, in order to assess the accuracy of the FEA results.

The blade vibration natural frequencies predicted by simulation in I-DEAS were compared here with those measured in the laboratory. A rotor blade was mounted as for normal operation on the rotor disc for the test. Natural frequencies were measured using a blade mounted, small shear wave accelerometer. Sharp hammer taps were used to excite the blade. The accelerometer signal was passed to a charge amplifier, which was in turn fed to a second amplifier. The blade's resonance frequencies were obtained from the signal by using a spectrum analyser. The analyser employed the Hanning window method FFT to reduce leakage effects [49]. The experimental set-up is shown in Figure C.4.1.

The values of frequency obtained in the laboratory will have a small error associated with the effective mass addition to the blade of the accelerometer. The FEA results, by virtue of being obtained from an approximate numerical method, will also contain some inaccuracies. Sources of error include discretisation errors and the use of first order elements. However, the frequencies measured were in reasonable agreement with frequencies predicted by simulation in I-DEAS. This is illustrated below in Table 4.2.

Mode	Measured Frequency	Simulation Frequency	Discrepancy
1	690 Hz	725 Hz	5%
2	2050 Hz	2061 Hz	1%
3	3550 Hz	3478 Hz	2%
4	4500 Hz	3950 Hz	14%

Table 4.2 - Accelerometer Test Measured and Simulated Rotor Blade Natural Frequencies

4.5 Strain Gauge Locations

In order to assess the tip timing measurement performance of the capacitance probe tip clearance system, blade vibration was monitored using blade mounted strain gauges. An important initial step in achieving this is to carefully select the locations and orientations of the principal axis of each strain gauge. These locations and orientations must be selected to ensure a discernible voltage signal is produced from the strain gauge energising and signal amplification circuits in all modes of vibration under consideration. Therefore, gauges must be placed in locations and at orientations that experience sufficiently high strain during each of the first four modes of vibration. It is inconceivable that modes higher than mode four can be excited to significantly high levels of vibration.

To this end, simulations were performed in I-DEAS on a mode-by-mode basis to consider blade surface strain. By plotting the strain in various directions for the first four modes of vibration it was concluded that a gauge near the root, at the centre chord-wise, orientated radially could successfully detect vibration modes one, three and four. A second gauge oriented at 45° to this, and positioned near the leading edge would be best to detect vibration mode two, which is a torsional mode. Strain gauge locations are illustrated in Figure C.5.1. Strain plots generated from simulations can be seen in Appendix C.6.

4.6 Blade Tip Deflection Simulations

It was essential that the rotor blades vibrate at sufficiently high amplitudes when the compressor is operating. This will ensure a meaningful evaluation of the tip timing ability of the capacitance probe tip clearance measurement system. This vibration is investigated here through FEA.

The blade excitation forcing function magnitude can be estimated from the pressure change across the stage in conjunction with the surface area of the blade presented to the direction of the air flow. At compressor operating speeds of 800 RPM to 1200 RPM the pressure rise across the stage is approximately 800 Pa. The surface area of the blade presented to the flow is approximately 5×10^{-3} m^2. The magnitude of the forcing function is therefore approximately 4 Newtons for simulation purposes.

To find the frequencies of vibration that will be experienced by the blades when the compressor is in operation, the engine order frequencies must be considered. Since there are 72 IGVs and stators, engine order frequencies will be present at 72 times the frequency of the rotor's rotational frequency. Also, 16 times the rotational frequency will constitute engine order frequencies. This is due to the 16 struts at the compressor's intake. This is illustrated in Figure D.1.4.

The relevant rotational frequency range is therefore, 13 Hz to 20 Hz, since the operating speed range producing reasonably large air flow rates is 800 RPM to 1200 RPM. This gives forcing functions in two bands of approximately 210 Hz to 320 Hz from the 16 engine order, and 960 Hz to 1440 Hz from the 72 engine order.

Given the nature of the predicted forcing functions, the forced responses were calculated using FEA in I-DEAS for a variety of cases. Simulations showed that maximum tip deflections of the order of 10 microns were predicted under normal operating conditions.

A simulation was performed with the compressor operating at 800 RPM with a forcing function of therefore 930 Hz from the 72 engine order. Such a forcing function of magnitude 4 N was applied at mid chord, two-thirds of the way from root to tip. This results in a maximum tip deflection of 10 microns, as shown in Figure C.7.1. A second simulation shows that if it were possible to resonate the first vibration mode, a tip displacement amplitude of almost half of a millimetre could be attained. This is illustrated in Figure C.7.2. However, at 725 Hz the first mode of vibration is outside the forcing function ranges described earlier in this section.

4.7 Low Stiffness Quasi Blades

The magnitudes of blade tip deflections predicted from the FEA simulations in Section 4.6 were not expected to be large enough to provide a meaningful tip timing test to the capacitance probe tip clearance measurement system. Therefore, two blades of lower stiffness than the original blades were mounted on the rotor, in place of two of the existing blades. This ensures blade tip deflections of sufficient amplitudes to detect with the capacitance probes.

Flat, quasi blade geometry was chosen to achieve this, where the width and height remain the same as the original blades. FEA was performed on several such flat 'blades' of various thicknesses. Stresses and tip deflections were again obtained in response to the expected forcing functions, as described in Section 4.5 and Section 4.6.

As a result, two blades of thicknesses 2 mm and 3 mm were chosen. These were predicted, through simulations, to be flexible enough to provide sufficiently large tip deflections to detect with the capacitance probe system, while still being stiff enough not to bend or fracture when the compressor was in operation. The geometry is illustrated in Figure C.8.1.

The natural frequencies of vibration of these two quasi blades were obtained through FEA by using the method described for the original blades in Section 4.3. The results are shown below in Table 4.3. The mode shapes are presented graphically in Appendix C.9.

Mode	Deformation	2 mm Blade Frequency	3 mm Blade Frequency
1	Bending	243 Hz	353 Hz
2	Torsional	740 Hz	1075 Hz
3	Bending	1486 Hz	2146 Hz
4	Bending & Torsional	2540 Hz	3673 Hz

Table 4.3 - FEA Quasi Blades Natural Frequency Calculations

As with the original compressor blade, FEA strain results were obtained for the flat 'blade' to ensure suitable positioning of surface mounted strain gauges. With the criteria for location set out in Section 4.5, the strain gauge locations shown in Figure C.5.1 were also found to be suitable for the quasi blade. Strain plots generated from mode-by-mode simulations of the quasi blade can be seen in Appendix C.10.

The nature of the tip deflections that the two quasi blades experience during compressor operation was predicted. Given the forcing function criteria set out in Section 4.6, simulations were performed to establish the maximum blade tip deflection cases. The forced response was calculated to the aforementioned forcing function, which was applied at the node on the blade mid chord which is two-thirds of the way from root to tip. The Results are shown graphically in

Appendix C.11. Figure C.11.1 shows the case of the compressor operating at 938 RPM, where the dominant forcing function from the 16 engine order is close to the 2 mm quasi blade's first natural frequency of vibration. In this case tip deflections of up to 1.8 mm were predicted. Figure C.11.2 shows the forced response of the 3mm quasi blade resonating at it's first natural frequency. Here the tip deflection amplitude was predicted to be 0.9 mm.

5. Experimental Equipment and Instrumentation

5.1 Introduction

This chapter describes the design, development, production and assembly of the key experimental equipment and instrumentation used to carry out the investigation into the capacitance probe system's tip timing characteristics.

A major initial undertaking in terms of experimental equipment assembly was the commissioning of a new low-speed, full-sized one-and-a-half stage compressor test facility (CTF). This facility was commissioned to provide a vehicle to perform the tip timing tests for this research project. The facility subsequently provides Cranfield University with a test rig dedicated to instrumentation, on which many other investigations will be undertaken. The facility is described in Section 5.2.1.

The scheduling and budgeting of the CTF was managed during the first eighteen months of this research project. Work, purchasing and scheduling tasks that were undertaken are outlined in Section 5.2.2. Although most aspects of the CTF were designed prior to this research project commencing, one design task that was outstanding was pressure instrument position control. This is described in detail in Section 5.2.3.

Once the CTF build was complete and general instumentation was installed, the compressor's characteristic was plotted. The tests conducted and measurements made to achieve this are described in Section 5.2.4.

The particular capacitance probe based turbomachinery tip timing measurement system used in this project to measure tip timing is described in Section 5.3. This system, sold for tip clearance measurement is used in its original configuration in this project.

An independent blade vibration measurement system was developed, based on an existing technique, in order to provide a comparison to the capacitance probe tip timing measurements. A system to precisely measure rotor RPM speed was also developed to enable vibration levels to be determined from tip timing. Thus, two major pieces of instrumentation were designed and produced to achieve this research project; namely a strain gauge based blade vibration monitoring system and an optical once per revolution sensor.

The design and production of a strain gauge energising and signal amplification circuit is described. The layout design of these circuits on PCB, in a one PCB per strain channel arrangement is also described. Specifically, Section 5.4.2.1 covers the design of a constant current source based circuit to energise the strain gauges. The strain signal amplification problem is detailed in Section 5.4.2.2. Here, the cascade instrumentation amplifier solution developed is covered.

Each of the aforementioned strain gauge energising and signal amplification PCBs must be powered, and output signals must be routed through a slip ring. This is achieved using another board mounted circuit, which is described in Section 5.4.2.3. The design of a mechanical assembly to mount the electronics on the rotor is detailed in Section 5.4.2.4.

The final stage of the development of the strain gauge based blade vibration monitoring system was to establish the relationship between changes in strain and blade tip deflection. This work was carried out by Rolls-Royce plc using ESPI and is reported in Section 5.4.3.

As well as the capacitance probe tip clearance measurement system, the second instrumentation system involved in the tip timing method is the optical once per revolution sensor described in Section 5.5. An overall system description is given, including details of how it is mechanically incorporated into the compressor. Off-the-shelf laser and receivers were specified and used, details of these are given in Section 5.5.1 and Section 5.5.2 respectively. A custom designed digitiser circuit was developed and produced to digitise the receiver output signal. This Schmitt Trigger based circuit design is described in Section 5.5.3.

The performance of the optical OPR sensor is reported in Section 5.5.4. Tests carried out to assess its consistency are described and results are presented.

5.2 Compressor Test Facility

As part of this Ph.D. project a new compressor test facility was commissioned at Cranfield University's Gas Turbine Engineering Laboratories. Not only does this provide Cranfield with a unique instrument dedicated test facility, but also enabled the blade tip timing measurement technique to be investigated on a real turbomachine rotor. The test rig will also be utilised in the research of tip timing data interpretation routines, as well as airflow field characteristics observed when instruments are introduced into the flow downstream of the rotor [50].

5.2.1 Compressor Test Facility Description

The facility is a one and a half stage compressor comprising Inlet Guide Vane (IGV), rotor and stator stages. A 60 kW electric motor drives the compressor. The facility is classified as 'low speed' as its 850 RPM designed operating speed and 1200 RPM maximum speed are approximately 10% of the speed of a typical modern industrial turbomachine. The compressor test facility is illustrated in Figure D.1.3.

The diameter of the machine's hub at the rotor is approximately one meter. The diameter of the flow passage is 1.2 meters. The machine is approximately five meters long from inlet to exhaust exit. The exhaust outlet area is controlled by a back pressure valve, which is operated using a small electric motor. The back pressure valve is shown in Figure D.1.5.

The compressor's rotor is fitted with three times oversized blades. This results in an operating airflow more representative of the airflows found in high-speed engines [51]. The blades were designed with future machine airflow research in mind, rather than the blade tip timing measurement system researched in this project. The rotor is comprised of 79 blades, each measuring 90 mm in the radial direction and a 59 mm chord from leading edge to trailing edge. They were cast in LM24 aluminium alloy, and are illustrated in Figure D.1.6. The stator and IGV stages each contain 72 blades.

Pressures are measured at five stages in the compressor's airflow; namely at the inlet, upstream of the IGV, upstream of the rotor, downstream of the rotor and downstream of the stator. This is illustrated diagramatically in Figure D.3.1. Five pressure probes are positioned around the circumference of the flow passage at each of the five stages. Each of the twenty-five pressures are tapped to a bank of twenty-five manometers.

The inlet temperature of the compressor is measured using four PT100 platinum resistance probes positioned around the circumference of the inlet. These four signals are fed to a four-channel PT100 signal converter that is in turn fed to the rig's PC. The PC runs data acquisition software to store and display the temperatures over time. The system has an accuracy of 0.001 Kelvin.

The temperature of the shaft bearings is monitored as a safety precaution. This is done using thermocouples fed to a digital temperature meter.

The machine's rotational speed is measured using a fin mounted on the rotor in conjunction with a stationary laser and receiver arrangement. The laser beam is cut by the fin each rotor revolution. The receiver's signal is fed to a digitiser circuit, which is in turn fed to a rate meter with an LED display so that the RPM of the compressor can be read. This is a custom designed optical once per revolution sensor and electronics which are also used in the tip timing experiments to precisely establish the compressor's rotational speed. The sensor and electronics design and performance are described in detail in Section 5.5.

The torque on the machine's shaft is measured using a strain gauge based torque meter. The torque meter was calibrated during test facility commissioning. The strain signals are interpreted and displayed by a digital panel meter programmed with the calibration factor so that torque can be read directly from the meter's LED display.

The test facility is fitted with three dual-axis instrument actuators. These enable positional control of any probes being mounted on the compressor for particular tests. Control of the actuators is handled by a custom written programme running under Windows on the rig's PC.

The compressor includes a twenty-four channel slip ring. This allows rotor blade mounted instruments to be utilised.

A schematic diagram of the compressor test facility can be seen in Figure D.1.1.

5.2.2 Compressor Test Facility Build and Budget

During the first eighteen months of this Ph.D. project the building and commissioning of the one-and-a-half stage compressor test facility was managed. While the design of the facility was in its final stages when this project started, the engineering drawing production, manufacturing and purchasing still had to be managed. The build inventory was first split into three parts, namely; mechanical components, electrical components and instrumentation.

The mechanical parts of the compressor test facility were subdivided into three categories, namely; those that could be taken from stock, those that were in stock but required modification and finally, those that had to be manufactured. For the parts to be manufactured and modified, engineering drawings had to be produced and quotes for machining were obtained. Engineering drawings were scheduled to be produced by Cranfield University, School of Engineering Drawing Office. Quotes for machining were then subsequently gathered from outside machining companies, since the capability to machine such large parts does not exist within the university.

The test facility's major electrical component is the motor used to drive the compressor. This had to be specified in terms of RPM capability, power rating and physical size. The RPM and power ratings were specified at the compressor design stage as 1200 RPM and 60 kW respectively and were reported in Section 5.2.1. where the compressor test facility was described. The physical size of the electric motor is constrained by the space length-wise available behind the compressor stage and the diameter of the cavity space within the flow

passage, where the motor must be mounted. Figure D.1.2 illustrates the electric motor mounted behind the compressor stage.

Various general control and instrumentation components had to be installed on the compressor test facility, as described in Section 5.2.1. Particularly involving was the solution to the instrument position control problem. The work carried out to achieve this is described in detail in Section 5.2.3. Instrumentation particular to the tip timing experiments also had to be developed and installed and integrated into the compressor test facility. The details of this work is covered later in this chapter in Section 5.3, Section 5.4 and Section 5.5.

A component inventory, schedule and costing with details of the compressor test facility build can be seen in Table D.1. A Gantt chart showing the time frames associated with the building of the facility is shown in Figure D.2.1.

5.2.3 Instrument Position Control

Probes used in experiments with the compressor have the option to be position controlled using three dual-axis actuators. Each axis has a stepper motor which is powered by a stepper motor drive card. The actuators each have a traverse axis and a yaw axis. The traverse axes have encoders providing feedback, while the yaw axes feedback is an analogue resolver signal. Each axis also has forward and reverse limit switches.

Control of the six axes is achieved using two four-axis motion controller cards installed in the rig's PC. Connections to the controller cards are made via a universal motion controller interface wiring box.

The feedback signals from the actuators are not directly compatible with the motion controller cards. Therefore, additional circuits were designed and built to enable compatibility.

The controller card can be configured to accept active high or active low limit switch signals. The actuators limit switches provide an active low signal at DC level. However the signal carries an AC component and thus looks permanently active to the controller. To overcome this, a simple R-C low pass filter circuit is used to pass the DC component of the signal to the controller, while filtering off the AC component.

The controller card requires a digital feedback signal from each axis if closed loop control is to be achieved. The yaw axes provide analogue feedback signals from their resolvers. These signals are therefore incompatible with the controller hardware. In order to achieve closed loop control of the yaw axes, additional circuitry is required to convert the resolver signals to digital form, akin to that of an encoder. A circuit was designed and built by the author to accomplish this using a resolver-to-digital converter IC (integrated circuit) and an oscillator IC. A diagram of the circuit can be seen in Figure D.5.1. This circuit was then replicated for each resolver signal.

Although the traverse axes encoders provide digital feedback signals, they too are not fully compatible with the controller hardware. The controller hardware can operate a closed loop control system given either of the two standard encoder signal sets, namely; Index, Phase A and Phase B or these three signals and their inverses.

The actuators' encoders generate only the two phase signals. Therefore, rather than operating the hardware in closed loop mode, open loop mode is used while the custom software displays the encoder counts. The software also coverts these counts into the displacement moved and compares this to the requested distance that was required to be moved. This effectively provides closed loop control of the traverse axes through the software.

5.2.4 Compressor Test Facility Commissioning

Once the compressor test facility build was complete the rig was commissioned. Following some trial compressor runs at ever increasing speeds, the compressor characteristic was mapped at the designed operating speed of 850 RPM. This was achieved by holding the rotational speed constant at 850 RPM and noting the inlet temperature, shaft torque and pressures at strategically chosen points in the flow path. These readings were taken with the back pressure valve set at various positions from fully open through to the position just before the compressor stalled. The positions of the pressures measured are illustrated in Figure D.3.1, where a schematic of the compressor's flow passage is shown. Each pressure at the five points along the flow passage is in fact an average of five pressure tappings positioned around the circumference of the machine.

From these input data the compressor's mass flow rate, dimensionless mass flow, isentropic efficiency, work coefficient, Va/U and static pressure rise were all calculated using the equations shown in Appendix D.3. This then allows the compressor characteristic to be plotted in terms of pressure ratio against both dimensionless mass flow and Va/U. These plots are shown in Figure D.3.2 and Figure D.3.3 respectively.

5.3 Capacitance Probe Tip Clearance Measurement System

The capacitance probe based system being used in this investigation to measure tip timing is commercially available as a turbomachinery tip clearance measurement system.

The RotaCap system supplied by Rotadata Ltd., Derby, UK is an FM capacitance probe based tip clearance measurement system such as that described in Section 3.3. The system includes a mineral insulated capacitance probe (see Improved Arrangement in Figure B.1.1) connected to an oscillator module by a semi-rigid stainless-steel sheathed tri-axial cable which is filled with powdered mineral insulation. The oscillator module provides a 10 MHz frequency throughout the probe assembly. This connects via an interconnecting cable to a demodulator unit. The demodulator optimum operating bandwidth is 100 Hz to 70 kHz. The system electronics are calibrated by tuning the Phase Locked Loop (PLL) to the same frequency as the oscillator. This is achieved by turning a screw on the demodulator unit. The oscillator module, capacitance probe, semi-rigid cable and demodulator interconnector are illustrated in Figure B.2.1. A system schematic is shown in Figure B.2.2.

5.3.1 Capacitance Probe Mounting

The compressor test facility's rotor ring has four circumferential positions at which probes may be inserted into the flow over the rotor blades. These consist of two types of opening. There is one cassette window spanning the width of the rotor ring, of circumferential length approximately 100 mm. There are also three 19 mm diameter holes in the rotor ring at three different circumferential positions, all centred over the blades tips' path.

Two mounting sockets were designed and produced so that the capacitance probes could be mounted at the aforementioned two types of rotor ring window. A single probe may be mounted through each of the 19 mm diameter holes. Up to six probes may be mounted in the cassette.

In both cases the probe head was fixed in place by a custom hollow bolt screwing down onto the top of the probe head's flange. The bottom of the flange rested against the inside lip of the socket. The probe head itself protruded through the socket into the flow passage. The distance that the probe head protruded into the flow passage (and therefore, the probe's clearance from the blade tips) was set by placing a shim of the required thickness between the socket lip and the bottom of the probe head's flange. The securing arrangement is illustrated in Figure D.6.1. Engineering drawings of the socket and bolt are shown in Figure D.6.2 and Figure D.6.3 respectively.

The custom cassette design incorporates six capacitance probe sockets positioned over two adjacent rotor blades. Each row of sockets consists of three sockets, one over blade tip mid chord, one over blade tip leading edge and one over blade tip trailing edge. The sockets over the leading and the trailing edges provide the option of detecting torsional blade vibration. The cassette arrangement can be seen in Figure D.6.4.

5.4 Strain Gauge Based Blade Vibration Measurement System

5.4.1 Blade Mounted Strain Gauges

To provide an independent blade vibration measurement for comparison with the proposed vibration measurement through capacitance probe tip timing, blade mounted strain gauges were used to derive blade tip deflections. These instrumented blades, when calibrated provided a separate system to compare the capacitance probe tip timing against.

In Section 4.5 it was identified that two strain gauges per blade should be mounted to allow detection of the first four modes of the blade's vibration. The locations and orientations of the two gauges on the blade's surface were also determined in Section 4.5 through finite element stress analysis. Robust, high performance strain gauges were chosen for the task. The gauges were encapsulated in glass-fibre reinforced epoxy-phenolic resin to protect them. The foil is 1.57 mm^2, made from Nickel-Chromium Alloy and of electrical resistance 350 Ohms. The gauges used were manufactured by Measurements Group and were model WK-13-062AP-350.

Wires must of course be routed from the blade mounted strain gauges to the energising and amplification circuits. These electronics were mounted on the machine's axis to minimise the inertial forces that the components are subjected to. Thus, the wires were routed through the rotor hub via custom channels cut in the root of the instrumented blades.

5.4.2 Strain Gauge Energising and Signal Amplification Circuits

An electronic circuit was developed from first principles by the author to energise the blade mounted strain gauges and amplify the resulting signal. The circuit was designed with on-rotor operation in mind although it was initially used in static off-rotor tests.

On-rotor operation of the blade mounted strain gauges necessitates that the strain gauges' signals be passed through a slip ring to route the signals to the data acquisition PC. The slip ring introduces significant noise to the strain gauge signals. In order to greatly increase the strain gauge signal to system noise ratio, pre-slip ring (on-rotor) amplification of the strain signals was used. Figure D.5.2 shows a block diagram of the circuit concept.

This configuration necessitates a robust circuit solution. The circuits were mounted centred on the compressor's shaft, inside the stub shaft. To facilitate this mounting, the circuits are realised using PCBs. A modular one PCB per strain gauge configuration is preferred to enhance robustness and ease maintenance. Circuit design and PCB layout was achieved with the aid of IVEX schematic and PBC layout and mask creation software. A full circuit schematic diagram is shown in Figure D.5.3.

5.4.2.1 Current Source

The strain gauges are energised using constant current sources. This method was chosen over the traditional Wheatstone bridge arrangement as it provides greater accuracy, flexibility and reliability, and also does not require the bridge's tricky balancing requirements.

The current source circuit consists of a voltage reference and precision operational amplifier. The system provides a constant current of up to 10 mA, set by a single resistor. The constant current was chosen to be 8.5 mA. As high a constant current as possible is desired to maximise the change in voltage observed from changes in resistance of the gauges as they elongate and contract during blade vibration. The maximum current is limited to 10 mA by the power that can be dissipated by the strain gauges used. Therefore, an energising constant current of 8.5 mA was used to incorporate a margin of safety.

The current source has a linear operating bandwidth of 8 kHz. Above this frequency the current is no longer constant with small changes in resistance, this is due to the response characteristic of the operational amplifier used. The current source's performance was measured empirically by switching the load resistance at frequencies up to 10 kHz. The resistance was switched between 350 Ohms and 350.5 Ohms to simulate the strain gauge under blade vibration conditions. This was achieved by connecting one leg of a 350 Ohms resistor to the output of the current source, while the other leg was switched from being directly connected to ground and connected to ground through a 0.5 Ohms resistor. The switching was realised by driving a transistor into and out of saturation with a signal generator at frequencies up to 10 kHz. The current source circuit's performance characteristic is shown in Figure D.7.1. This linear operating bandwidth is clearly sufficiently high given that the frequencies of the modes of vibration of interest are all under 5 KHz, as reported in Chapter 4 and in Section 5.4.3.1.

5.4.2.2 Strain Signal Amplification

The strain gauge signal amplification is achieved using instrument amplifiers. These devices consist of three operational amplifiers on a single IC. A single resistor is used to set the gain of each instrument amplifier. Additional power rail de-coupling capacitors are also used. The required gain from each strain signal is achieved by using two instrument amplifiers in cascade.

Pre-amplification filtering is implemented before each amplification stage using high-pass R-C filters. Filtering is used to reduce the noise level introduced to the strain signal. The main source of noise is at the mains electricity frequency of 50 Hz. Therefore, the values of R and C in the filters were chosen to attenuate frequencies of this order. Also considered when choosing the cut-off frequency of the filter were the frequencies of vibration of the instrumented blades. The filters were also designed to pass these frequencies of interest. These frequencies were calculated in Section 4.3 and Section 4.7 and were verified through measurements in Section 4.4 and Section 5.4.3.1. Values of R and C of one thousand Ohms and one microfarad were chosen, giving a cut-off frequency of 160 Hz.

An important parameter to consider is the gain of the circuit. A signal of as large an amplitude as possible is desired to pass through the slip ring to the data acquisition hardware. The upper

limit that the magnitude of the signal could be is set by the $\pm 10V$ limit that can be used as an input to the data acquisition hardware that is available. When the circuit was developed during off-rotor testing (see Section 6.3) the maximum conceivable strain signal was found to be approximately $\pm 4mV$ for large tip deflections. A gain of approximately 2000 was therefore chosen to give maximum voltage magnitudes of 8V. This is realised by two amplification stages in cascade (series) of gains of 50 per stage. The amplification circuit's performance characteristics are shown in Figure D.7.2 and Figure D.7.3. This shows a fairly constant gain of just over 2000 for the frequencies of interest; namely those above 250 Hz and below 5 kHz.

5.4.2.3 Multi-Channel Strain Signal Connectivity

Two instrumented blades were mounted on the compressor's rotor for testing purposes. Therefore, four strain gauge energising and signal amplification channels were required. Each strain gauge energising and signal amplification circuit must be powered, and the output signals must be passed to the data acquisition hardware.

As shown in Figure D.5.3 two +15V power rails, two -15V power rails, two ground lines and two signal channels are required per strain gauge energising and signal amplification PCB. A junction and power circuit was thus designed, this is also to be mounted on the rotor on a single circuit board. This circuit involves four power rails being derived using two +15V and two -15V voltage regulator ICs, which are themselves powered by a $\pm 17V$ mains PSU. Also included are four eight-way connectors, one for each strain gauge energising and signal amplification PCB.

Wires connecting each strain gauge to the electronics module are shielded to prevent noise contaminating the signals. Guarding against noise influencing the signals is crucial at this point in the circuit since the signals are subsequently amplified 2000 times. Thus, it is critical to minimise the level that is introduced to the signals in these wires. The compressor's drive motor is a large source of noise due to the very high currents induced when the machine is accelerating. To ensure minimising of noise influencing the signals the sheilding is driven at zero Volts. This is achieved by electrically connecting the shielding to the junction and power board. The shield is thus driven at ground potential using an operational amplifier mounted on the board and configured in voltage follower mode (see Figure D.5.4, component LF356N).

Finally, an additional eight-way connector is included to accommodate the four strain signals being passed to the slip ring. The junction and power board circuit is shown in schematic form in Figure D.5.4.

5.4.2.4 Mechanical Assembly

Provision was made to mount four strain gauge energising and signal amplification PCBs and one junction and power circuit board within the rotor's stub shaft. A circular PCB shape is the logical choice for mounting purposes inside the compressor's cylindrical stub shaft. A circular layout for a single strain channel was achieved using a 60 mm diameter PCB. A four bar cage arrangement was designed to mount these boards in the stub shaft. The outside (front) end plate of the cage bolts onto the front of the stub shaft. This plate houses a bayonet connector to connect the slip ring to the junction board. The inside (back) end of the cage also houses a

bayonet connector to connect the four strain gauges to the four strain gauge energising PCBs. The PCB is illustrated in Figure D.6.5, while the cage assembly is shown in Figure D.6.6 and Figure D.6.7, with the complete assembly illustrated in Figure D.6.8.

5.4.3 Strain Gauge Signal to Tip Deflection Calibration

In order to relate the changes in resistance of the blade mounted strain gauges to blade tip deflections, calibration tests were carried out at Rolls-Royce plc. During these tests the first four modes of vibration of the compressor rotor blades and quasi blades were investigated by measuring the natural frequencies of vibration and capturing the mode shapes.

5.4.3.1 Blade Vibration Mode Shapes Using ESPI

The Electronic Speckle Pattern Interferometry (ESPI) tests were carried out by Rolls-Royce plc at their Derby facility. The blades and quasi blades were mounted on a V-block and excited on a crystal exciter vibration table. The natural frequencies were measured using ESPI and the results are shown in Table 5.1 and Table 5.2 for the compressor rotor blades and quasi blades respectively. Here the results are also compared to the frequencies obtained through the vibration acclerometer tests described in Section 4.4 and the FEA results reported in Section 4.3 and Section 4.7.

Mode	ESPI Measured Frequency	Accelerometer Measured Frequency	Simulation Frequency	ESPI / Simulation Discrepancy
1	687 Hz	690 Hz	725 Hz	5.5%
2	2061 Hz	2050 Hz	2061 Hz	0.0%
3	3542 Hz	3550 Hz	3478 Hz	1.8%
4	4494 Hz	4500 Hz	3950 Hz	12.1%

Table 5.1 - Measured and Simulated Compressor Rotor Blade Natural Frequencies

	2 mm Quasi Blade			3 mm Quasi Blade		
Mode	ESPI Measured Frequency	Simulation Frequency	Discrepancy	ESPI Measured Frequency	Simulation Frequency	Discrepancy
1	244 Hz	243 Hz	0.4%	338 Hz	353 Hz	4.4%
2	736 Hz	740 Hz	0.5%	1020 Hz	1075 Hz	5.4%
3	1471 Hz	1486 Hz	1.0%	1994 Hz	2146 Hz	2.6%

Table 5.2 - Measured and Simulated Quasi Blade Natural Frequencies

Holography was also used to capture the mode shapes of the compressor rotor blades and quasi blades. These results are illustrated in Figure D.4.1 and Figure D.4.2 for the compressor rotor blades and 2mm quasi blade respectively. These mode shapes show good agreement with the mode shapes obtained from FEA which are shown in Figure C.3.1 and Figure C.3.2 for the compressor rotor blades and Figure C.9.1 and Figure C.9.2 for the quasi blades.

5.4.3.2 Blade Tip Deflection to Strain Signal Calibration Using ESPI

The blades and quasi blades were again mounted on a V-block and excited on a crystal exciter vibration table. Blade tip deflections were measured using an optical system, while strain gauge signals were simultaneously captured. Deflections were measured at three points on the blade tip; at the leading edge, mid chord and at the trailing edge. This was done while exciting each blade and quasi blade at each of the first four natural frequencies of vibration in turn.

Calibration factors were thus established in terms of MPa/mm. Chosen example calibration factors for the compressor rotor blades and quasi blades are presented in Table 5.3.

Case	Calibration Factor	Error
Rotor Blade, Mode 1, Root Gauge	25.1 MPa/mm	±7 %
2mm Quasi Blade, Mode 1, Root Gauge	16.9 MPa/mm	±29 %
2mm Quasi Blade, Mode 1, Leading Edge Gauge	5.1 MPa/mm	±33 %

Table 5.3 - Strain Gauge to Blade Tip Mid Chord Deflection Calibration

The errors in the calibration factors arise from the signal to noise ratio of the strain signal generated during calibration and the number of fringes visible in the ESPI images. For the 2 mm quasi blade the errors are high at around 30%. This is due to the small strain level present during calibration (24 microstrain) and the sparsity of the fringes generated using ESPI, as illustrated in Figure D.4.2. The low number of fringes limits the accuracy with which the tip deflections can be determined to during calibration. The low strain level results in a low signal to noise ratio obtained during the calibration process. Both of these effects contribute to produce the large error bands associated with the 2 mm quasi blade calibration factors.

5.5 Optical Once Per Revolution Sensor

An essential factor in using tip timing to measure blade vibration is knowing the precise rotational speed of the compressor's rotor. This was achieved through the design of an optical once per revolution sensor. In order to make this sensor as accurate as possible three areas must be considered, namely; mechanical issues, optics and electronics.

Physically, the proposed system consisted of a statically mounted laser and receiver arrangement and a fin mounted on the rotor. The fin cuts the laser beam once per rotor revolution, hence with the use of some electronic circuitry a precise RPM speed is obtained.

To maximise the accuracy of the system it is desirable to cut the laser beam as quickly as possible at any given rotor RPM speed. This maximises the resolution with which the arrival time of the fin at the laser beam can be determined. To this end, the fin was mounted radially at as far out a position as possible, just below one of the blade roots. Thus, the tangential fin velocity for any given angular velocity is maximised. The position arrangement of the OPR sensor is illustrated in Figure D.6.9, while the laser and receiver arrangement are shown in Figure D.6.10.

The remaining factor in the speed at which the laser beam is cut is the diameter of the beam itself. Clearly, the smaller the diameter of the beam, the faster it will be completely cut at any given velocity. However, this factor must be balanced against the beam being large enough so that a signal of a sufficiently high power level reaches the receiver. This is discussed in detail in Section 5.5.2. Signal power is lost over distance due to the divergent conical nature of the laser beam. For this reason the end of the optical fibre carrying the signal from the laser is mounted as close as possible to the end of the fibre carrying the signal to the receiver. Therefore, the fibre ends were mounted 5 mm apart. This allowed enough clearance for the fin to pass safely in between the two fibres' ends.

5.5.1 Once Per Revolution Sensor Laser

The OPR sensor system's laser was specified in terms of physical size, power output, beam cone angle and wavelength. A 655 nm, 10 mW laser diode with a divergence cone angle of 16.4 degrees was chosen and purchased. This results in a signal of approximately 20 μW, considering the 5 mm separation between the emitter and receiver fibres, and based on the calculation in Appendix D.8. This represents a power level that a typical low-cost communications receiver can operate under.

The laser diode is of pigtail module type, which requires a +5V, 1A PSU to power the small PCB which the diode is connected to. The output is passed to an optical fibre terminated in an SMA type connector which can be screwed into the mounting shown in Figure D.6.9.

5.5.2 Once Per Revolution Sensor Receiver

A low-cost 125 MHz bandwidth optical receiver is used for the OPR sensor. Such a receiver is widely available and sees typical application in LANs. This type of receiver is PCB mountable and requires only a +5V supply and a load resistor to provide an output voltage signal. An additional receiving optical fibre is used to connect the PCB mounted receiver to the mounting illustrated in Figure D.6.9.

The recommended operating power range for this receiver is 1 to 125 μW. Therefore, this is compatible with the 20 μW signal provided to the receiver by the laser described in Section 5.5.1, given the mounting arrangement. The receiver is optimised for 850 nm signals, but still operates at 90% efficiency for 655 nm signals. The receiver circuit consequently provides a 400 mV voltage swing from this arrangement. The output voltage is 2.0 V in normal state, falling to 1.6 V when the laser shines on the end of the receiver fibre.

5.5.3 Once Per Revolution Sensor Digitiser

Due to the use of digital timer data acquisition with the OPR sensor, the output of the receiver circuit must be digitised. This was achieved by designing a custom digitiser circuit. The solution used a comparator based circuit, with one input to the comparator connected to the output of the receiver, while the other comparator input was held at a threshold voltage level. The principle of operation is that the digitiser output signal swings from 0 V (digital low) to 4 V (digital high) as the receiver signal crosses the threshold value.

Specifically, a comparator based circuit in Schmitt Trigger configuration is used. Thus, hysteresis effect is utilised to eliminate the comparator 'chattering' as the threshold value is crossed due to the high frequency noise on the receiver signal. A circuit diagram designed by the author is shown in Figure D.5.5. The circuit was realised by populating a matrix board which is then housed in a case, including a switch so that the digital output signal connection to the data acquisition can be enabled and disabled. This is useful when synchronising the data acquisition systems used for the strain signals, capacitance probe signals and the timer hardware used to capture the OPR signal itself.

5.5.4 Once Per Revolution Sensor Performance

A very short rise time for the OPR sensor signal is highly desirable. This maximises the accuracy with which the signal can be timed. There are two main factors limiting this, namely; the response speed of the Schmitt Trigger digitiser circuit, and the state change time of the receiver output signal.

The Schmitt Trigger has been designed to have as short a signal rise time as possible. This was achieved using a 'speed-up capacitor' in the feedback loop (see Figure D.5.5, component C2). The measured output signal rise times of the digitiser circuit designed by the author were typically 0.07 microseconds (maximum 0.1 microseconds, minimum 0.05 microseconds), as shown in Figure D.7.4.

The voltage fall time of the receiver output is dependant on the speed at which the fin cuts the laser beam. Measurements of the receiver output and comparator output were simultaneously taken over a range of rotor RPM speeds. To ensure that the bandwidth of the receiver was adequate, the shortest receiver output signal transition time that was experienced during compressor operation was considered. This occurred at the maximum operating speed of 1200 RPM. This fall time was found to be approximately 0.3 microseconds, representing a signal of frequency less than 4 MHz. Therefore, the 125 MHz bandwidth of the chosen receiver is clearly more than adequate. The pertinent results are presented in Table D.2.

Next, in order to assess the performance of the OPR sensor the state transition of the receiver output signal was considered. As the fin cuts the laser beam the receiver output signal falls from 2.0 V to 1.6 V. Therefore, a 2.0 V receiver output represents 0% of the beam being cut and a 1.6 V output represents so much of the beam being cut that the power level of the signal transmitted to the receiver falls below the minimum power level required to elicit any receiver output voltage change. Consequently, the consistency of the OPR signal triggering is considered. This was done over several revolutions and over a range of rotor RPM speeds.

The percentage position in the analogue receiver signal's fall time that the triggering of the digital output occurred at was investigated over several revolutions at each RPM speed. In this way the triggering positional error was assessed. An example case of the receiver output signal and digital output signal state changes is shown in Figure D.7.5. Table D.3 shows a triggering consistency assessment data set collected at the rotor speed of 938 RPM. The inconsistency of the triggering was calculated as 0.1 microseconds over the data set.

The overall uncertainty of the OPR sensor timing is therefore of the order of, and no worse than 0.1 microseconds. The uncertainty may in fact be considerably lower. However, in the absence of another, more accurate system to compare the OPR sensor against, this uncertainty is taken as the working value, erring on the side of caution. Further, this error level is expected to be at least an order of magnitude lower than that of the timing measurements taken from the capacitance probe system, thus a more precise definition of the OPR error is unnecessary for this application.

5.6 Data Acquisition

The acquisition of data from several signals is essential in performing the tip timing assessment of the commercially available capacitance probe based tip clearance measurement system. Three distinct data acquisition tasks can be identified to enable the assessment to be carried out.

Firstly, the signals from the blade mounted strain gauges must be captured. The solution used to achieve this is described Section 5.6.1. Secondly, the capacitance probe signals themselves must be acquired. The equipment put in place to enable this is described in Section 5.6.2. Thirdly, the optical OPR sensor's signal must be acquired. This was a digital signal, and the counter/timer hardware and custom written software used to achieve this is described in Section 5.6.3.

5.6.1 Strain Gauges Signals Acquisition

The testing programme used a maximum of two strain gauge instrumented blades on the compressor's rotor at any one time. Each instrumented blade had two surface mounted strain gauges. Therefore, provision was made to capture four signals. The bandwidth requirements for this acquisition must also be considered. The minimum acceptable limit of this stems from the highest frequency of the blade vibrations of interest. It was envisaged that frequencies no higher than 5 kHz would be required from the strain gauge signals. This was determined from FE analysis of the compressor rotor blade, where the fourth natural frequency was found to be less than 5 kHz (see Section 4.3).

The Nyquist theorem states that a sampling frequency of at least twice the frequency of the analogue signal is required. Provision was made to sample four channels at up to 20 kHz. A Microlink sixteen-channel, 100 kHz overall bandwidth data acquisition hardware and accompanying Windmill software solution was chosen to achieve this.

5.6.2 Capacitance Probes Signals Acquisition

Two capacitance probe based tip clearance measurement systems were available for the experimental investigation in this programme of research. Therefore, two-channel A/D conversion was required to sample these signals. The sampling rate associated with the capture of these signals was carefully considered.

The sampling period should be short enough such that it is not the factor limiting the resolution with which blade tip timing can be determined. National Instruments two-channel data acquisition hardware was chosen along with accompanying software. This hardware was capable of simultaneously sampling two channels at up to 20 MHz. In the tip timing tests, sampling events must last long enough to capture several consecutive rotor revolutions. Therefore, the highest practical useable sampling rate for the tip timing tests was in the region of 5 MHz, giving a sampling period of 0.2 microseconds. This was due to the limitations in the

size of the acquisition hardware's on-board memory and the speed with which the data could be transferred from the acquisition hardware to the PC.

With the blade tip speed at the compressor's designed operating speed of 850 RPM being approximately 50 m/s, the 5 MHz sampling rate used translated into a displacement measurement resolution of 10 microns. This is at least an order of magnitude lower than the tip deflections that can reasonably expected to be detected with the capacitance probe based system.

5.6.3 Optical Once Per Revolution Sensor Signal Acquisition

The optical OPR sensor's output was digitised using the electronics described in Section 5.5.3. Therefore, the best way to time this signal was to use digital counter/timer hardware. This hardware will also be used in a related optical tip timing research project [52].

A National Instruments ten-channel counter/timer card was chosen. One of these counters was used to time the rotor's period by timing the OPR sensor's signal. Custom software was written in Visual Basic so that the hardware could easily be used for both the capacitance probe and future optical probe tip timing investigations. A screenshot of the software's user interface is shown in Figure D.9.1

6. Experimental Investigations

6.1 Introduction

This chapter describes the experimental programme of work carried out to investigate the ability of capacitance probe based tip clearance measurement hardware to measure blade vibrations through tip timing.

Various off-rotor testing was done using a DC capacitance probe clearance measurement system. This testing produced mapping of capacitance probe characteristics as well as static blade vibration measurement assessment. This testing served as groundwork for the on-rotor testing programme. The on-rotor testing utilised a commercially available FM capacitance probe based turbomachinery tip clearance measurement system.

The static test programme set out to establish the characteristics of a DC capacitance probe tip clearance measurement system developed by Fylde Electronics Laboratories Ltd., UK. Characterisation of such a probe's response to interaction with blade tips was investigated by moving the probe in 3D space. This work is reported in Section 6.2.

The DC capacitance probe tip clearance measurement system described in Section 6.2.1 was used in a series of impulse response tests on a compressor rotor blade. Measurements were taken simultaneously using the capacitance probe and the blade mounted strain gauges. In this way the capacitance probe system's ability to detect small blade tip vibrations of statically mounted blades was investigated. This work is reported in Section 6.3.

On-rotor testing began by investigating the practicalities of using a commercially available FM capacitance probe based tip clearance measurement system to determine the time of arrival of a compressor rotor blade at a fixed point on the compressor case. The high stiffness compressor rotor blades were used in these tests. Consequently, these tests provided an assessment of tip timing of non-vibrating blades.

The nature of the capacitance blade passing signal was investigated and the accuracy with which blade time of arrival can be determined was assessed. In the absence of blade vibration the timing of the blade passing is entirely predictable from the rotor's rotational speed. The rotor's speed was measured using an optical once per revolution (OPR) sensor. Results of time of arrival were compared with those expected from the data gathered from the optical OPR sensor. This work is reported in Section 6.4.

Further on-rotor testing involved mounting a low stiffness, strain gauge instrumented quasi blade on the compressor's rotor. Blade tip deflections were measured using capacitance probe tip timing in conjunction with the optical OPR sensor. These deflections were compared to

deflections derived from an independent system using blade mounted strain gauges. The blade was forced to resonate in vibration mode one by running the compressor at 938 RPM.

The blade vibration measurement through tip timing was investigated in three ways. The first of these is single capacitance probe tip timing. This was used to establish instantaneous tip deflections as the instrumented blade passed the capacitance probe at it's fixed position mounted on the compressor casing. The second way was to use a single capacitance probe to measure instantaneous tip deflections as the rotor traversed the instrumented blade's first mode resonant frequency. The third method utilised dual capacitance probe tip timing to measure blade vibration amplitude. This was achieved by taking the two instantaneous tip deflections in sequence from the two probes at different circumferential positions on the compressor's casing in conjunction with the frequency of blade vibration calculated from the strain gauge signals. This information allowed a sine wave to be curve fitted to the two vibration measurements. Thus, the amplitude of blade vibration was calculated from capacitance probe tip timing.

In these ways the ability of the capacitance probe tip clearance system to measure blade vibration through tip timing was assessed. Errors associated with the vibration measurements made through both the tip timing and the blade mounted strain gauge based systems were quantified. Thus, the accuracy of the results was assessed. This work is reported in Section 6.5.

6.2 Capacitance Probe Response to Static Tests

The static test programme set out to establish the characteristics of a DC capacitance probe tip clearance measurement system. The ultimate aim was to assess the suitability to measure aero-engine blade tip timing of the FM capacitance probe tip clearance of the system described in Section 5.3. The FM system is unsuitable for off-rotor testing, and thus a DC system was used in these tests. These tests provide valuable initial information on how a capacitance transducer responds to movement in proximity to a blade tip. Therefore, the off-rotor test programme was a prelude to on-rotor testing.

Data is not readily available on the characteristics of such a probe's response to interaction with blade tips, other than manufacturer supplied data stating the linear operating ranges for tip clearance measurement purposes. However, to determine the equipment's performance in tip timing measurement the probe's response to movement in the circumferential direction as well as changes in clearance displacements was investigated.

Initial experiments were performed by using an actuator to position the capacitance probe head relative to a Aluminium block and relative to a compressor rotor blade tip. In this way the clearance measurement performance of the capacitance probe system was investigated. This was followed by an investigation into the probe's response to movement in the blade tip clearance and tip timing (circumferential) directions, again using an actuator for positioning.

6.2.1 Static Test Equipment Description

A commercially available capacitance displacement transducer (CDT) based clearance measurement system was investigated. The measurement hardware used in this investigation has been developed by Fylde Electronics Laboratories Ltd., UK (FE-411-OSC and FE-419-CDT) and is sold by Rotadata Ltd., UK for clearance measurement applications. The system consists of a capacitance displacement measurement probe connected by a cable to an electronics module. The electronics module provides a 0 V_{dc} to 10 V_{dc} output. This voltage was captured by a PC with data acquisition hardware and software installed.

The probe consists of a sensing head of 4 mm in diameter connected to a central sensing conductor. This conductor is surrounded by a driven guard conductor, which is itself surrounded by an earthed outer screen. The probe is connected to the electronics module via a tri-axial screened carbon-filled low-noise cable. The probe and cable assembly can be seen in Figure E.1.1.

The electronics module consists of a CDT amplifier and an oscillator. The oscillator produces a 16 kHz, 5 V_{rms} sine wave signal. The oscillator is interconnected with the amplifier to energise the probe head through the central sensing conductor. The electronics module also drives the guard conductor at the same voltage as the central sensing conductor, thus eliminating spurious cable capacitance. The system provides a 0 V_{dc} to 10 V_{dc} capacitance signal which is fed to a precision voltage inverter to output a linear clearance signal over the range 0.1 V_{dc} to 10 V_{dc}.

6.2.2 Clearance Test Experiment Method

An initial test was performed to assess the system's tip clearance measurement performance, before going on to perform tip timing characteristic measurements. A benchmark test was performed by measuring the clearance from the probe head to a large metal block. This was followed by clearance tests on a compressor rotor blade.

From the limitations of the electronics, the system should have a linear voltage-clearance response from 0.1 V_{dc}. The upper voltage-clearance linearity limit of the measurement system will be restricted by the probe head area. The manufacturer states that up to approximately 50% of the sensing head diameter will produce a linear voltage-clearance signal. This represents an expected linear tip clearance measurement range over approximately 0.2 mm to 2.0 mm.

The first clearance test was carried out by mounting the probe on an actuator so that it could be precision positioned in steps of as low as 10 microns. A block of Aluminium was positioned parallel to the probe head with zero clearance. The probe was retracted in steps to a clearance of 5 mm. System output voltage readings were taken between the retraction steps.

This procedure was repeated three times using a compressor rotor blade tip. Each time the capacitance probe was positioned over a different position chord-wise on the tip. Firstly over mid chord, then over the trailing edge, and finally over the leading edge.

6.2.3 Clearance Test Results and Analysis

The plot in Figure E.2.1 shows the results of the capacitance clearance measurement system clearance tests. From Figure E.2.1 it can be seen that the block, mid chord and leading edge clearance tests have very similar results, with their voltage-clearance curves closely matched. These three tests show fairly good linearity for clearances between 0.2 mm and 1.5 mm. Between 1.5 mm and 1.8 mm non-linearity is present and for clearances above 1.8 mm the output voltage-clearance relationship is clearly and increasingly non-linear. The small blade tip target area causes the non-linearity at lower clearances than stated by the probe manufacturer as the linear operating limitations of the system (0.2 mm to 2.0 mm). This is because the manufacturer's data stipulates a sufficiently large target area (at least 30% greater than that of the probe head area). The probe head is 4 mm in diameter, while the blade tip thickness varies from 6 mm to 1.3 mm.

The trailing edge test results apparently differ from the other three tests. Since the trailing edge presents a significantly smaller target area to the 4 mm diameter capacitance probe sensing head, the trailing edge test shows lower measured capacitances over the tested clearances. This produces the higher output voltages observed since the output voltage is derived from the capacitance signal through a voltage inverter. However, the trailing edge test results still show good linearity for clearances between 0.7 mm and 1.3 mm. Above 1.3 mm clearance the trailing edge voltage-clearance relationship shows increasing non-linearity.

With the establishment that the clearance measurement system is functioning as expected from manufacturer stated performance parameters, investigations next turn to tests to assess the system's potential for blade tip timing measurement.

6.2.4 Capacitance Probe Characteristic Mapping Experiment Method

The characteristic of the probe's interaction with a compressor rotor blade tip was investigated in three-dimensional space. As well as probe response to movement in the tip clearance direction, movement in the tip timing direction is also considered. This provides some insight into the capacitance tip clearance measurement system's ability to measure tip timing.

The capacitance probe was mounted on an actuator. The probe was moved in steps of 1 mm, to an accuracy of 10 microns, past the stationary blade tip in the timing direction with clearance held constant. The experiment set-up is illustrated in Figure E.1.2.

The voltage signal from the capacitance probe system was measured at each step position using a PC with data acquisition capability. Measurements were taken over the range of positions that the capacitance probe detected the presence of the blade tip, namely; from 20 mm either side of the blade tip centre.

The procedure was repeated for various clearances between the blade tip and the probe from 0.2 mm to 5 mm. This allowed a three dimensional plot of the characteristics of the capacitance probe's interaction with the blade tip to be visualised.

The whole procedure was repeated for three points on the blade tip, namely; mid chord, leading edge and trailing edge. This enabled comparisons to be made between different areas of blade tip, from a small area at the trailing edge to a much larger area at mid chord. The blade tip is 6 mm thick at mid chord, while only 1.3 mm thick at the trailing edge. Blade tip geometry is illustrated in Figure E.1.3.

6.2.5 Capacitance Probe Characteristic Mapping Results and Analysis

The characteristic of the capacitance displacement transducer system was mapped by measuring its voltage output at two hundred points in three dimensional space relative to a compressor blade tip. Mapping was carried out from 20 mm either side of the blade tip and at tip clearances from 0.2 mm to 5 mm. Three such maps were produced for three different points on the blade tip; leading edge, mid chord and trailing edge. Figure E.3.1, Figure E.3.2 and Figure E.3.3 show two dimensional representations of the maps by plotting multiple tip clearance traces over each 40 mm sweep. Figure E.3.4 shows a three dimensional surface plot of the probe characteristic mapped at the blade tip mid chord.

As the probe head passes the blade tip, the tip target area increases then decreases as a segment of the circular probe moves over. The target area used for the capacitance calculation is governed by the equation for the area of a segment of a circle (Equation 6.1), and is thus non-linear.

$$A_{seg} = r_p{}^2 \operatorname{acos}\left(\frac{h}{r_p}\right) - \sqrt{r_p{}^2 - h^2} \qquad 6.1$$

Where r_p is the radius of the probe head and h is the distance from the probe centre to the blade edge.

When the probe is centred over the blade tip, the system is relatively insensitive to movement in the timing direction. This is the desired condition for a tip clearance measurement system, but not ideal for measuring tip timing. This is illustrated by the flat troughs in Figure E.3.1 and Figure E.3.2.

The steep sides of the curves in the figures in Appendix E.3 represent a high resolution of voltage change to movement in the tip timing direction when the suction and pressure side edges of the blade tip are centred under the probe head. At these points, small movements in the timing direction result in relatively large changes in the probe's target area on the blade, and hence large signal changes.

The asymmetrical geometry of the rotor blade results in the traces in the figures in Appendix E.3 being slightly skewed. The probe's target area over the suction side edge of the blade tip is different from the target area over the pressure side edge. Hence the signals are not symmetrical about the tip centre (at Timing Direction 0 mm in the figures in Appendix E.3) as they would be for traces gathered from tests on a uniform beam. The skew effect is particularly apparent at the thick mid chord tip position. It is less apparent at the much thinner trailing edge where the probe head straddles both suction and pressure sides of the blade tip. The skew effect does not detract from the system's ability to measure timing since the effect remains constant and so timing consistency is maintained.

The effect of different blade tip geometries is also illustrated in the figures in Appendix E.3. The large probe target areas of the blade tip at mid chord and at leading edge positions show large voltage swings when the probe is swept past those positions. The smaller target area of the blade tip trailing edge produces a smaller voltage swing when the probe is swept past. The larger voltage swings constitute a higher signal to noise ratio. Therefore, this suggests it is possible to measure tip timing more accurately at the leading edge and at mid chord than at the trailing edge using the capacitance tip clearance probe.

6.2.6 Static Test Capacitance Probe Response Conclusions

The characteristics of a commercially available capacitance displacement transducer based clearance measurement system have been investigated. This was done with the alternative application of measuring aero-engine tip timing in mind. Off-rotor testing performed as a prelude to off-rotor vibration measurement tests and on-rotor investigations has been documented.

The characteristic of the system's response in three-dimensional space to movement in the proximity of a compressor rotor blade tip has been mapped. It was found that the position sensing of the blade tip was best achieved when the edge of the probe head was over the suction

side or pressure side edges of the blade tip. In these positions, small changes in displacement in the timing direction result in relatively large changes in the probe target area and hence signal level. When the circular probe head is centred over the blade tip, small changes in displacement in the timing direction result in small changes in target area and thus small changes in signal. This constitutes a high rate of signal change for the edge positioned case compared to the tip centred case. Thus a high signal to noise ratio is present in the tip edge positioned case. Therefore, this suggests that the edge of the blade can be detected more accurately than the centre of the blade tip. This does not have detrimental implications for tip timing with capacitance tip clearance probes since as long as timing of the edge is consistently measured, then this is just as valid as timing the blade tip centre.

The effect of measuring capacitance to derive blade tip timing over different areas of the blade tip has also been considered. The larger target areas of the tip mid chord and leading edge positions demonstrate a greater signal swing than the smaller target area of the trailing edge when moved past the capacitance probe. The larger voltage swings constitute a higher signal to noise ratio. This suggests that it is possible to measure tip timing more accurately at the leading edge and at mid chord than at the trailing edge using the capacitance tip clearance probe.

6.3 Impulse Tests Capacitance Probe Response

The DC capacitance probe tip clearance measurement system described in Section 6.2.1 was used in a series of impulse response tests on a compressor rotor blade. Measurements were taken simultaneously using the capacitance probe and the blade mounted strain gauges.

These off-rotor experiments set out to investigate the capacitance tip clearance measurement system's ability to measure static blade vibration. This was carried out by mounting the stationary blade and probe, while performing impulse response tests. Blade mounted strain gauges were used in a independent blade vibration monitoring system to assess the capacitance probe's performance by deriving tip deflections from the strain signal.

These static impulse tests constituted a prelude to dynamic on-rotor blade tip timing tests using the FM capacitance probe tip clearance measurement system described in Section 5.3.

6.3.1 Impulse Test Equipment Description

Impulse tests investigate the DC capacitance probe based clearance measurement system described in Section 6.2.1. The clearance measurement system is used here unaltered to investigate its ability to detect static blade vibrations. The system consists of a capacitance probe connected to an oscillator and CDT amplifier unit via a tri-axial cable.

The strain gauge mounted blade described in Section 5.4.1 is used in conjunction with the strain gauge energising and signal amplification circuit designed for on-rotor use, this is detailed in Section 5.4.2. In this case the circuit is used in off-rotor configuration as shown in the schematic diagram in Figure E.1.4. From this data blade tip deflections are derived.

6.3.2 Impulse Test Equipment Experiment Method

A strain gauge instrumented compressor rotor blade was mounted off-rotor fixed at the root. The strain gauges were energised and their signals amplified using the circuit described in Section 5.4.2. With the use of strain to blade tip deflection calibration data, provided by Rolls-Royce and reported in Section 5.4.3.2, these strain readings can be post processed to give blade tip deflections over time. The experiment set-up is illustrated in Figure E.1.5.

The capacitance probe head was positioned over the blade tip. Based on the findings reported in Section 6.2 the edge of the capacitance probe was positioned coincident with the plane of the suction side edge of the blade tip to ensure adequate sensitivity to detect the blade vibration.

An impulse force was applied at the blade tip at mid chord using a hammer. This provoked a response dominated by the first vibration mode. Results were simultaneously collected from the capacitance probe system and the strain gauge system using the data acquisition PC.

Tests were carried out with the probe head set at several clearances from 0.2 mm to 5 mm. The process was repeated at three points on the blade tip. These were the three points corresponding to the points for which the strain gauge tip displacement measurement system was calibrated, as described in Section 5.4.3. These points were at mid chord, the leading edge and the trailing edge as shown in Figure E.1.6.

6.3.3 Impulse Test Results and Analysis

Results from tests at the three considered points on the blade tip showed that the capacitance probe system's response was largely independent of the blade tip position measured. The results gathered with the probe head set at a clearance of 0.2 mm from blade tip mid chord are shown in Figure E.4.1. These results were mirrored with the probe head positioned at the same clearance from the blade tip, measured over the tip's leading and trailing edges.

The capacitance probe system showed decreasing amplitude of response signal as tip clearance increased. This was expected from the findings reported in Section 6.2. A response was still discernable up to clearances of approximately 3 mm, above which the blade tip vibration apparent from the strain gauge signal was not picked up by the capacitance probe system.

Figure E.4.2 shows the amplified impulse and vibration response strain signal voltage output from the strain gauge energising and amplification circuit. The strain signal shows the characteristic 'ski slope' response of the R-C filter in the energising and amplification circuit. The decay duration of the filter's step response is four times the R-C time constant, as expected from theory. Spectral analysis of the strain signal was performed using the Hanning window method FFT in order to reduce leakage effects [49]. The resulting PSD shows good agreement with the first natural frequency of the blade throughout the impulse response testing, as shown in Figure E.4.3. The same can be said of the PSD of the capacitance probe signal shown in Figure E.4.4. The strain derived voltage output can then be converted to tip deflection using Equation 6.2, which is derived in Appendix E.5.

$$d = \frac{E \cdot \Delta V_{out}}{cal \cdot GF \cdot R \cdot G \cdot I} \qquad 6.2$$

Figure E.4.5 and Figure E.4.6 show the tip deflection calculated from the strain signal using the calibration data for the blade tip leading edge. Also plotted on the same axes is a constantly scaled capacitance probe signal from the blade tip leading edge at 0.2 mm clearance. This signal has been normalised by removing the DC voltage level so that zero Volts equals zero tip displacement.

The capacitance signal in Figure E.4.5 shows a non-linear response to the vibration in the timing direction, as indicated would be the case from the probe characteristic tests reported in Section 6.2. The capacitance signal has been constantly scaled to have the same amplitude of free vibration as the linear strain signal. The non-linearity of the capacitance signal is clear at the impulse where the trough is much lower than that of the linear strain signal.

Figure E.4.6 shows that the capacitance probe system has successfully detected blade tip vibrations of amplitudes as low as 20 microns. This amplitude is derived from the strain gauge signal. The non-linear relationship between tip displacement and capacitance output in this configuration means that it is impractical to derive blade tip amplitudes from the capacitance probe signal alone in this configuration.

6.3.4 Impulse Tests Capacitance Probe Response Conclusions

The ability of a commercially available capacitance displacement transducer based clearance measurement system to measure static blade vibrations has been investigated. This has been done with the alternative application in mind for this equipment to measure aero-engine tip timing. Off-rotor testing performed as a prelude to on-rotor investigations has been reported.

Testing has been reported on an investigation into the capacitance probe tip clearance measurement system's performance in measuring vibration of the blade tip. By correlating capacitance probe signals with tip deflection values derived from calibrated blade mounted strain gauge signals, it was shown that the system in question detected blade impulse response vibrations of amplitudes of as small as 20 microns peak-to-peak. This was done by determining tip deflection amplitude from the strain gauge signals. The non-linear relationship between blade tip displacement and capacitance output in this configuration meant that in order to derive vibration amplitudes from the capacitance signal a calibration process would first have to be performed. Capacitance probe characteristic mapping tests such as those reported in Section 6.2 could provide calibration values to allow the relation between signal level and tip deflection to be established by accounting for probe head to blade tip clearance and lateral probe head to blade tip position. However, the frequency of vibration has been successfully detected through direct calculation with FFT using the capacitance probe.

The capacitance probe clearance measurement system's detection of static blade vibration at varying tip clearances has been investigated. Small vibrations were successfully detected by the capacitance probe at clearances up to 3 mm, above this the vibrations shown by the strain gauge based vibration measurement system were not detected by the capacitance probe based system. As clearance was reduced, capacitance signal strength increased. This was consistent with the findings presented in Section 6.2.

These investigations demonstrate blade vibration detection by the capacitance probe measurement and independent strain gauge systems in a static off-rotor environment. This serves as groundwork for the on-rotor testing presented in Section 6.4 and Section 6.5.

6.4 Compressor Rotor Blade Tip Timing Tests

The compressor rotor blade tip timing tests set out to investigate the practicalities of using a capacitance probe tip clearance measurement system to determine the time of arrival of a compressor rotor blade at a fixed point on the compressor case.

The nature of the capacitance blade passing signal was investigated and the accuracy with which blade time of arrival can be determined was assessed. In the absence of blade vibration the timing of the blade passing is entirely predictable from the rotor's rotational speed. However, with blade vibration present the timing of the blades passing the probe heads will differ from the time anticipated from the rotor's speed. The rotor's speed was measured using an optical once per revolution (OPR) sensor. It was anticipated from the blade FEA reported in Section 4.6 that the tip vibration amplitudes of the compressor rotor blade will be very low, of the order of 10 microns. In fact, insufficiently high to reasonably detect with the capacitance probes.

Therefore, the aim of these tests was to characterise the capacitance probe blade passing signal for the passing of a non-vibrating blade. Results of time of arrival were compared with those expected from the data gathered from the optical OPR sensor.

6.4.1 Tip Timing Test Equipment Description

The compressor rotor blade tip timing tests utilised six main pieces of equipment, namely; The one-and-a-half stage compressor test facility, an instrumented compressor rotor blade, strain gauge energising and amplification circuits, a capacitance tip clearance measurement system, an optical OPR sensor and two PCs with data acquisition hardware and software.

The one-and-a-half stage compressor test facility described in Section 5.2.1 was a full-sized, low speed compressor and is driven at speeds up to 1200 RPM during tip timing tests. On the compressor rotor is mounted 79 blades, one of which is an instrumented blade with mounted strain gauges, as described in Section 4.5. The strain gauges were energised and the resulting signals were amplified using the custom circuit developed for this project. These electronics were described in Section 5.4.2.

The commercially available FM capacitance probe based turbomachinery tip clearance measurement system was used. This system consists of a capacitance probe, oscillator and a demodulator and is described in detail in Section 5.3.

The optical OPR sensor developed and described in Section 5.5 was used in the tip timing tests to accurately establish the rotor's RPM. OPR and capacitance probe signals are captured using two-channel, high-speed data acquisition hardware at up to 20 MHz per channel sampling rate. This hardware was installed in a PC running data acquisition software. A second PC hosted additional data acquisition hardware and software to capture the strain gauge signals. This was multi-channel capable with an overall bandwidth of 100 kHz. The acquisition systems were synchronised by using the OPR signal to trigger all acquisition events.

6.4.2 Tip Timing Experiment Method

Initial on-rotor testing utilised a capacitance displacement transducer mounted on the one-and-a-half stage compressor test facility's rotor ring. The rotor ring comprises a ring surrounding the rotor, forming part of the compressor's case. The probe was positioned to study blades passing a fixed circumferential position on the rotor casing. The probes were mounted on the compressor case using the mounting arrangements described in Section 5.3. The capacitance probe was positioned over the paths where the mid-chord of the blade tips pass. The set-up is illustrated in Figure E.6.1.

A single strain gauge instrumented compressor rotor blade was mounted and its vibration was monitored using the electronics and acquisition equipment outlined in Section 6.4.1. Compressor rotor speed was measured using the optical OPR sensor described in Section 5.5. The capacitance probe, OPR and strain gauge signals were captured using data acquisition hardware and software. Two PC's were used running two different hardware and software combinations. Acquisition was synchronised using the OPR sensors signal.

The nature of the capacitance probe blade passing signal was investigated in this way. The determination of the time of arrival of the capacitance probe at a fixed point on the rotor ring was considered at various rotor RPM speeds.

The accuracy of the time of arrival determined from the capacitance probe was then be assessed. This was done by using the optical OPR sensor signal and the strain gauge signal data for comparison.

6.4.3 Tip Timing Test Results and Analysis

6.4.3.1 Levels of Compressor Rotor Blade Vibration

It was anticipated from the blade FE simulations reported in Section 4.6 that normal running of the low-speed compressor would not result in blade tip vibrations of sufficiently high amplitude to measure using capacitance probe based tip timing. Indeed, this proved to be the case during testing at all compressor operating speeds. However, these small vibrations were readily measured using the blade mounted strain gauges and associated electronics. A typical blade vibration trace generated during normal running conditions is shown in Figure E.7.1. This represents the voltage trace generated from the gauge mounted near the blade's root (see Figure C.5.1), which has been positioned to detect bending modes of vibration.

Spectral analysis of this signal shows that the vibrations detected are at the frequency of the blade's first mode of vibration. This is shown in Figure E.7.2, where the frequency of vibration can be seen to be 680 Hz. This is in good agreement with the frequency of the first mode of vibration reported as 687 Hz in Section 5.4.3.1, where ESPI tests on the compressor rotor blade are described.

Given this voltage trace, blade tip displacements can be calculated and plotted over time. This is achieved by using Equation 6.2, given the appropriate strain level to tip displacement calibration value (see Table 5.3) and electronic circuit properties (see Section 5.4.2). Typical blade vibration levels experienced during testing are shown in terms of tip displacement in Figure E.7.3. Tip deflection levels of vibration can thus be seen to be very small, of the order of a few microns.

The compressor rotor blade cannot readily be resonated to excite higher levels of vibration in mode one. This is due to the first natural frequency of vibration of the blade being out with the frequency bands of the forcing functions available from the compressor's engine orders. This is reported in detail in Section 4.6. Therefore, this section goes on to report and analyse tip timing of a non-vibrating compressor rotor blade using capacitance probes.

6.4.3.2 Determining Arrival Time

A typical blade arrival event detected by the capacitance probe is shown in Figure E.8.1. This illustrates a case with the compressor operating at its designed speed of 850 RPM.

The blade-passing peak shown in Figure E.8.2 has a flat spot at the 'peak' of the order of 20 microseconds. This severely limits the resolution with which the moment of blade arrival can be determined by looking for signal peaks. In order to achieve better arrival time accuracy the rising edge of the blade passing signal is instead considered. This is illustrated in Figure E.8.3.

Despite the noise levels present in the signal, the high rate of change on the leading edge allows the arrival time of the blade, relative to the previous arrival time of that blade, to be determined to approximately the nearest microsecond by considering a fixed voltage threshold on the signal's rising edge.

The fixed voltage threshold timing method is only used to time the arrivals of single blades relative to other arrival times of the same blade. Investigation of the arrival times of one blade relative to another blade would require multiple instrumented blades and a variable blade passing signal threshold to account for the different peak signal values of different blades of varying tip clearances.

A blade arrival event at the much lower rotor speed of 50 RPM is illustrated in Figure E.8.4. As expected from the FM system the signal levels are lower than those generated at 850 RPM. The signal to noise ratio is therefore lower than that at 850 RPM. Figure E.8.5 shows the rising edge of the blade passing signal. Here the lower rate of change of the signal means that the time of arrival determined by the voltage threshold has much greater uncertainty associated with it compared to the 850 RPM signal. In the 50 RPM case there is a period of approximately 200 microseconds where the signal oscillates above and below the one Volt threshold level due to the signal noise.

6.4.3.3 Time of Arrival Determination Consistency

Arrival times of the instrumented blade were determined using a fixed one Volt threshold on the blade passing signal leading edge. The arrival time of the instrumented blade was determined for several consecutive revolutions. These arrival times were compared to the expected arrival times anticipated from the optical OPR sensor.

Table 6.1 shows the period of several revolutions at 850 RPM as measured using the optical OPR sensor and the capacitance probe timing of blade arrival.

Revolution	Period of Revolution (s)		Difference (μs)
	OPR	Capacitance Probe	
1	0.070486	0.070485	-1
2	0.070486	0.070485	-1
3	0.070485	0.070485	0
4	0.070485	0.070487	+2
5	0.070484	0.070486	+2
6	0.070482	0.070482	0
7	0.070484	0.070485	+1
8	0.070484	0.070483	-1

Table 6.1 - Capacitance Probe and Optical OPR Timing Comparisons

The timing discrepancy between optical OPR sensor and capacitance probe over the data set can be seen to be no larger than 2 microseconds. The following section considers the sources of error in this timing method.

6.4.4 Tip Timing Results Error Analysis

Several factors contribute to the error in determining the time of arrival of the single instrumented non-vibrating compressor rotor blade. There is a digitising error associated with the acquisition of the capacitance probe and OPR signals. The noise level present in the capacitance probe signal is also a source of error. There is a small error associated with the small levels of blade vibration actually present. These are detected by the strain gauge based vibration monitoring system only. during the 'non-vibrating' tests. Time of arrival comparison between the capacitance probe and optical OPR sensor only is used in these particular investigations. hence the source of error.

The error associated with the OPR signal is very small, as reported in Section 5.5. Therefore, this does not contribute significantly to the overall error in determining blade time of arrival.

6.4.4.1 Discretisation Error

As with all analogue to digital (A/D) conversion processes, discretisation errors arise in the acquisition of the capacitance probe and OPR sensor signals. The A/D converters used in these investigations are of 8-bit word length type. Therefore, this corresponds to 256 discrete levels to which the voltage signal is discretised. Analogue inputs are possible over the range $\pm 5\,V$, the voltage resolution is thus 40 mV per digital level.

The time resolution is of course dependent on the sampling frequency. The data acquisition hardware is limited by the number of sample points it can hold in the on-board memory. The sampling rate is also limited by the maximum clock speed of the data acquisition hardware; namely 20 MHz.

During this set of tests, sampling was carried out for one second at a sampling rate of one million samples per second. This duration allowed several consecutive revolutions to be captured at the running speeds at which the tests were carried out. The resolution in time due to discretisation is therefore one microsecond.

The rotor speeds of interest for the tip timing tests are those at and around the rig's designed operating speed of 850 RPM. At these speeds the rising edge of the capacitance probe's voltage signal has a relatively high rate of change, as shown in Figure E.9.4. As a result the signal moves through several 40 mV discrete voltage levels from one sample to the next. Thus, the voltage level discretisation is not the critical source of uncertainty caused by signal digitisation. Therefore, the critical discretisation effect in terms of error in time of arrival is that determined by the sampling rate. In these tests this results in an uncertainty in time of arrival of not more than one microsecond per signal.

6.4.4.2 Error Due to Signal Noise

Significant levels of system noise are present in the commercially available capacitance probe based tip clearance measurement equipment. The noise signal present when the compressor is running at 850 RPM is illustrated in Figure E.9.1, where noise spikes of as high as $\pm 0.25\,V$ are observed. This signal can be seen to have higher voltage noise spikes than the noise trace captured when the compressor is at rest, shown in Figure E.9.2, where the noise spikes are $\pm 0.15\,V$ in magnitude.

The PSD of the capacitance probe signal shown in Figure E.9.3 illustrates that the noise is fairly evenly distributed over the spectrum. The blade passing frequency is a clear peak in the PSD, while the rest of the signal power is small and evenly spread across the spectrum. Therefore, the filtering out of this noise is impractical. Treatment could be investigated using more complex signal processing techniques, such as autocorrelation. However, this is beyond the scope of this investigation, which aims to characterise the capacitance probes response in terms of tip timing.

Clearly this system noise has detrimental implications for consistently determining the time of arrival of the blade at the capacitance probe's fixed position on the compressor case. An example of the entire rising edge of the blade passing signal at 850 RPM is shown in Figure E.9.4. This shows that small localised peaks can be present on the rising edge due to signal noise. This is clearly a potential source of error in determining the moment that the blade passes the capacitance probe by using the fixed threshold voltage method.

The typical blade passing signal rising edge illustrated in Figure E.9.4 shows that the rising edge has a rate of change of 20 microseconds per Volt. The typical noise level present in the capacitance probe signal is $\pm 0.1\,V$, as shown in Figure E.9.1. Typical error due to this noise level, based on capacitance probe signal rate of change is thus 2 microseconds.

6.4.4.3 Error Due to Blade Vibration Levels

Due to the fact that the compressor rotor blades show very small levels of vibration during normal running conditions, these tests are considered 'non-vibrating' blade tip timing tests. However, the actual levels of blade vibrations present introduce an error in the time of arrival comparison between the capacitance probe signal and the OPR signal.

Blade tip velocity at the compressor's operating speed of 850 RPM is approximately 55 m/s. The maximum tip displacements detected during testing was not more than 20 microns. The error in time of arrival from this level of vibration is therefore not more than 0.37 microseconds. This is the smallest of the three significant contributing factors to the overall error in determining time of arrival.

The blade tip speed at the designed operating rotational speed of 850 RPM is approximately 55 m/s, 2 microseconds therefore represents 110 microns. It is therefore necessary to excite the blade to at least a tenth of a millimetre in order to test the system's ability to detect the vibration.

6.4.5 Tip Timing Results Conclusions

Experimental investigations have been carried out to characterise a commercially available capacitance probe based tip clearance system's response to blade tip passing events. This has been done with the alternative application of measuring blade tip timing in mind. This has been achieved by characterising and assessing the practicalities of determining an instrumented blade`s time of arrival at a fixed point on the compressor casing.

Compressor rotor blade vibrations have been measured using blade mounted strain gauges in conjunction with energising signal amplification electronics. Vibration levels were found to result in very small amplitudes of blade tip deflections of not more than 20 microns. Hence, these tip timing investigations are essentially performed on non-vibrating blades.

The resolution with which the time of arrival of the blade can be determined with the capacitance probe based tip clearance system has been evaluated. This was done by measuring the blade passing period over several consecutive revolutions. This period was compared to the

period measured by the optical OPR sensor. The consistency of these measurements was assessed at the compressor's designed operating speed of 850 RPM.

The capacitance probe period was found to be consistent within two microseconds over the entire sample of data collected. This is within the expected error bands, as assessed in Section 6.4.4.

The capacitance probe signal has been characterised over differing rotor RPM speeds. As is the nature of the FM capacitance probe system, the signal power increased with increasing rotor speed. Thus, the signal to noise ratio is lower at lower RPM speeds. This has a detrimental effect on the accuracy with which the blade time of arrival can be determined from the capacitance probe signal.

The sources of error causing the inconsistencies in the time of arrival comparisons between the optical OPR sensor and capacitance probe have been investigated. Three significant sources of error were identified and each of their contributions to the overall error in the non-vibrating blade tip timing experiments was assessed. There are errors stemming from the noise level inherent in the commercially available capacitance probe based tip clearance measurement system's signal. There are also errors due to the discretisation of the capacitance probe and optical OPR sensor's acquisition. Finally there is a small error due to the small blade tip vibrations actually present in these 'non-vibrating' tip timing tests.

The most significant of these errors was found to be the noise level present in the capacitance probe system's signal. The signal to noise ratio was found to improve with increasing rotor RPM speed. At the designed operating speed of 850 RPM this noise caused an uncertainty in the determination of the time of arrival of the blade of not more than two microseconds.

The error associated with the process of digitising the capacitance probe and OPR sensor signals was also assessed. The discretisation of the voltage level was found not to contribute significantly to the error at the rotational speeds of interest, around 850 RPM. This is due to the relatively high rate of change of the voltage signal from the capacitance probe system. The critical discretising error comes from the time step between each sample. This was set at one microsecond in these tests due to hardware limitations. This results in a time of arrival determining uncertainty of not more than one microsecond for each signal. In the case of the optical OPR sensor signal, this could be greatly reduced by using high speed digital timer hardware. Since the OPR signal has been digitised by the electronics designed in Section 5.5, analogue to digital data acquisition is not the most efficient method to time this signal's period.

In the case of the optical OPR sensor the uncertainty could be significantly reduced simply by increasing the sampling rate. However, the noise level present in capacitance probe signal dictates that increasing the sampling rate of this signal will not in itself be enough to significantly reduce uncertainty. The accuracy of the system for blade tip timing purposes using this signal processing method is thus limited to about two microseconds. This translates to approximately 110 microns at the compressor's operating speed of 850 RPM. It is therefore concluded that blade tip deflections in excess of one tenth of a millimetre are required for the system to be able to successfully detect the vibrations.

6.5 Vibrating Blade Tip Timing Tests

The vibrating tip timing tests set out to establish the capacitance probe tip clearance measurement system's ability to detect blade vibration through tip timing measurement.

Blade tip deflections were measured using capacitance probe tip timing in conjunction with the optical OPR sensor to determine rotor speed. These deflections were compared to deflections derived from an independent system using blade mounted strain gauges.

The blade vibration measurement through tip timing was investigated in three ways. The first of these was single capacitance probe tip timing. This was performed to establish instantaneous tip deflections as the instrumented blade passes the capacitance probe. The probe was mounted at a fixed position on the compressor casing. The second way was to use a single capacitance probe to measure instantaneous tip deflections as the rotor traverses the speed that causes the instrumented blade to resonate in vibration mode one. The third method utilises dual capacitance probe tip timing to measure blade vibration amplitude. This was achieved by taking the two instantaneous tip deflections in sequence from the two probes at different circumferential positions on the compressor's casing in conjunction with the frequency of blade vibration calculated from the strain gauge signals. This information allows a sine wave to be curve fitted to the two vibration measurements. Thus the amplitude of blade vibration was calculated from capacitance probe tip timing.

In these ways the ability of the capacitance probe tip clearance system to measure blade vibration through tip timing was assessed. Errors associated with the vibration measurements made through both the tip timing and the blade mounted strain gauge based systems were quantified. Thus, the accuracy of the results was assessed.

6.5.1 Vibrating Blade Tip Timing Test Equipment Description

The vibrating blade tip timing tests utilised the same six pieces of equipment used in the non-vibrating blade tip timing tests reported in Section 6.4, namely; the one-and-a-half stage compressor test facility, an instrumented compressor rotor blade, the strain gauge energising and amplification circuits, a capacitance tip clearance measurement system, the optical OPR sensor and three PCs with data acquisition hardware and software. For a description of this equipment, refer to Section 6.4.1.

An additional data acquisition system was used in the vibrating blade tests. This was the counter/timer hardware and custom written software used to time the OPR sensor's signal. This equipment is described in detail in Section 5.6.3. This freed up an additional channel on the high speed A/D hardware so that dual capacitance probe tip timing could be performed.

6.5.2 Vibrating Blade Tip Timing Experiment Method

A strain gauge instrumented quasi rotor blade was mounted on the compressor's rotor and its vibration was measured using the electronics and acquisition equipment described in Section 5.4.2 and Section 5.6.1 respectively. Blade vibration measurement was also performed through tip timing using single and then dual capacitance probes. These probes are mounted on the compressor's rotor ring. The rotor ring comprises a ring surrounding the rotor, forming part of the compressor's case. There are five circumferential positions available to mount the capacitance probes on the compressor's rotor ring. These positions are illustrated in Figure E.6.2. The probes were positioned to study blades passing fixed circumferential positions on the rotor casing. The probes were mounted on the compressor case using the mounting arrangements described in Section 5.3. The capacitance probes were positioned over the paths where the mid-chord of the blade tips pass. The set-up is illustrated in Figure E.6.3.

Compressor rotor speed was measured using the optical OPR sensor described in Section 5.5. The capacitance probe, OPR and strain gauge signals were captured using data acquisition hardware and software. Three PC's were used running three different hardware and software combinations, as described in Section 5.6. Acquisition is synchronised using the OPR sensor's signal.

The time of OPR signal's arrival was measured by digital timer acquisition hardware and was taken as when the OPR digitiser output crosses the +2V level (goes digital high). This was clocked by the timer hardware at 80 MHz.

The precise rotor speed was measured using the optical OPR sensor. The distance that the instrumented blade travels from the triggering of the OPR sensor until detection of the blade by the capacitance probe can then be calculated by measuring tip timing. This distance was measured in the absence of blade vibration. This value was then compared to the distance measured when the blade is vibrating. The difference between these distances is the instantaneous blade tip vibration displacement level. The concept is illustrated in Figure E.6.4.

This method was first used to detect instantaneous blade vibration using a single capacitance probe. Secondly, blade vibration across mode one resonance condition was investigated by measuring tip timing and calculating blade vibration levels as the rotor speed traverses resonant speed. Finally, dual capacitance probe tip timing was used to measure two instantaneous tip deflections in sequence at the two capacitance probes. The spacing between the two capacitance probes was measured. Given the frequency of blade vibration measured from the blade mounted strain gauges' signals, a sine wave was curve fitted to these two tip deflection values. Thus, the amplitude of blade tip vibration was calculated from the amplitude of this sine wave.

In all cases, vibration levels measured through tip timing were compared to those measured by the blade mounted strain gauges. In this way, the ability of the capacitance probe based system's ability to detect blade vibration through tip timing measurement was investigated.

6.5.3 Vibrating Blade Tip Timing Test Results and Analysis

6.5.3.1 Quasi Blade Vibration

The thinner of the quasi rotor blades described in Section 4.7 showed the greatest level of tip deflections during testing. At the rotor speed of 938 RPM the blade was observed to resonate in the first mode of vibration. This was the expected result since the 16 engine order frequency at this rotor speed coincides with the first natural frequency of the blade. The source of the 16 engine order is the 16 compressor intake struts. The voltage trace captured from the strain gauge energising and signal amplification circuit is shown in Figure E.10.1. This is the voltage trace generated from the gauge mounted near the blade's root (see Figure C.5.1), which has been positioned to detect bending modes of vibration. Figure E.10.2 shows the voltage trace generated simultaneously from the strain gauge mounted at the blade's leading edge.

The PSD of the root strain gauge voltage signal, illustrated in Figure E.10.3, shows that the frequency of vibration is 253 Hz. This is in good agreement (within 4%) with the frequency of the first mode of vibration reported from simulations in Section 4.7 and from ESPI tests in Section 5.4.3. Spectrally, this is also true for the voltage trace from the leading edge mounted strain gauge.

Given this single frequency of vibration content of the voltage signal, the tip displacements may be directly calculated from both strain signals. This is done by using the appropriate strain level to tip deflection calibration values (see Table 5.3) and electronic circuit properties (see Section 5.4.2) in conjunction with Equation 6.2.

Figure E.10.4 and Figure E.10.5 show the tip displacement vibration levels present with the compressor running at 938 RPM. These traces have been derived from the root strain gauge and leading edge strain gauge respectively by using the method described in the preceding paragraph. The amplitudes of tip deflection shown in Figure E.10.4 and Figure E.10.5 are not in good agreement, being 1.5 mm and 0.9 mm respectively. However, this is consistent with the large errors associated with the strain to tip deflection calibration values, as described in Section 5.4.3.2.

The root mounted gauge consistently measures higher tip deflections than the leading edge mounted gauge. To mitigate the large errors, the average of the two tip deflections derived is taken as the definitive strain derived tip deflection. Therefore, this results in a tip deflection amplitude of 1.2 mm for the example data presented in Figure E.10.4 and Figure E.10.5. This is some 100 times the vibration levels of the compressor rotor blades used for the 'non-vibrating' tip timing tests reported in Section 6.4. The previous findings in this chapter suggested that the capacitance probe based tip clearance measurement system would be able to detect vibrations of this amplitude.

6.5.3.2 Blade Vibration Measurement Through Single Probe Tip Timing

The ability of a single capacitance probe to measure blade vibration has been investigated. This has been done with the instrumented blade vibrating in mode one.

The distance that the instrumented blade travels through from the moment that the OPR sensor is triggered until the tip arrives at the capacitance probe has been measured. This has been done by timing the interval between the OPR sensor triggering and the blade's arrival at the capacitance probe. This timing, in conjunction with the precise rotor RPM speed measured using the OPR sensor, allows the distance travelled by the blade tip to be calculated. Clearly, in the absence of blade vibration, this distance is constant. However, with blade vibration present, this distance will differ from the expected distance due to the blade tip displacement caused by blade vibration. The concept is depicted graphically in Figure E.6.4.

Before the tip deflection detected through tip timing can be established, it is first necessary to measure, in the absence of vibration, the distance that the blade travels between the OPR sensor triggering and the moment it is detected passing the capacitance probe.

This is achieved by using the blade mounted strain gauges and associated electronics to monitor blade vibration levels, and consequently derive blade tip deflections using the method described in Section 6.4.3.1. The blade's distance travelled is then measured using the capacitance probe at several different RPM speeds where the blade vibration levels are very small.

The blade's time of arrival at the capacitance probe is established using the method described in Section 6.4.3.2. The instrumented blade was mounted such that it was fractionally longer than the other blades. This simplified post processing of the capacitance probe signals since the instrumented blade then produced a higher signal level when passing the capacitance probe than the other blades. This made it easy to distinguish from the other 78 blades when processing the data gathered from the capacitance probe signals. Figure E.10.6 shows one revolution period of capacitance probe blade passing signals. In real engine testing this method would not be possible since all the blades are more or less the same length. Consequently, more sophisticated post processing would be required.

FORTRAN programmes were used to establish the blade passing times by retrieving the time index when the chosen constant voltage threshold was crossed. This threshold voltage was chosen on the rising edge of the blade passing signal, where there is a high rate of voltage change. This was the method of determining time of arrival of the blade at the capacitance probe found to be most accurate from the investigations in Section 6.4.

In these vibrating blade tests the additional threshold criteria was used to ensure that only the instrumented blade passing signal peaks above this threshold voltage value. For example this would be 1.5 V for the data set illustrated in Figure E.10.6. In this way the time of arrival determination of the blade of interest was automated, thus greatly speeding up the data analysis process.

Figure E.10.7 illustrates the OPR triggering to capacitance probe blade detection distances calculated by averaging measurements over several revolutions at several different rotor RPM speeds. This represents a test case with a capacitance probe mounted in socket number two (refer to Figure E.6.2). The distance is not constant over the speed range, even at blade non-vibrating conditions. There is a clear trend of decreasing distance measured with increasing rotor RPM speed. This is to be expected and is due to the use of the constant voltage threshold method used to determine time of arrival (described in Section 6.4.3.2). Since signal strength increases with frequency, then as rotor RPM increases the blade passing signal peaks get higher. Thus the measured distance becomes shorter as RPM increases. The measured distance can be seen to decrease by 0.2 mm over the speed range 800 RPM to 1050 RPM. The error bars on the non-vibrating blade trace in Figure E.10.7 represent the uncertainty in the distance measured. This error is dominated by the small vibration levels actually present when calculating the distance in the 'non-vibrating' condition. The error bars on the vibrating blade data point are determined by the accuracy by which the blade passing timing is established. This was assessed as two microseconds in Section 6.4. This translates to an uncertainty of 0.12 mm at 938 RPM, where the blade tip speed is 60 m/s.

With these distances plotted, the expected distance at the blade resonant condition rotor speed of 938 RPM can be interpolated. This non-vibrating distance must be interpolated since it cannot be measured directly at 938 RPM due to the large vibration amplitudes present. In the test case shown in Figure E.10.7 this corresponds to 1526.2 mm. The actual measured distance at 938 RPM is 1527.1 mm. This is also illustrated in Figure E.10.7. Thus, an instantaneous blade tip deflection of 0.9 mm is inferred. This is consistent with the levels of tip deflection calculated from the independent vibration measurement system using blade mounted strain gauges. As described in section Section 6.5.3.1 tip deflections of between -1.2 mm and +1.2 mm are expected. Therefore, the 0.9 mm deflection measured through single capacitance probe tip timing is consistent with some point on the 1.2 mm amplitude sine wave.

To calculate the amplitude of the vibration sine wave through tip timing, dual probe techniques are considered in Section 6.5.3.4. However, next the single capacitance probe is used to measure vibration across blade resonance condition.

6.5.3.3 Investigation of Blade Vibration Across Resonance

The ability of a single capacitance probe based tip clearance measurement system to measure vibration across blade vibration mode one resonance through tip timing has been investigated. Tip timing was performed over various different rotor RPM speeds. The constant voltage threshold method for determining blade time of arrival is used. This method is described in Section 6.4.3.2. Tip timing was measured at various speeds above and below resonance, in the absence of vibration. This was done to establish the distance that the instrumented blade travels from the moment the OPR sensor is triggered until its arrival is detected by the capacitance probe. The concept is illustrated in Figure E.6.4.

Several tip timing tests were carried out at speeds close to and across the rotor speed that causes mode one resonant vibration in the instrumented quasi blade. Figure E.10.8 represents a test case carried out with the capacitance probe mounted in socket number four (see Figure E.6.2), over the path at which the mid chord positions of the blade tips pass.

From the non-vibrating blade timing data illustrated in Figure E.10.8 the expected distance at and around the 938 RPM blade resonance speed can be seen to be 349.6 mm, in the absence of blade vibration. Figure E.10.8 also illustrates the marked change in measured distances as the rotor speed moves across the blade's mode one resonance speed. The error bars in Figure E.10.8 are the same as those in Figure E.10.7, which are explained in Section 6.5.3.2.

Figure E.10.9 shows the tip deflections calculated from the tip timing results presented in Figure E.10.8. A tip deflection phase change is clear from Figure E.10.9. The level of blade tip deflection detected varies from -0.5 mm to +0.5 mm as the rotor speed traverses the resonance speed of 938 RPM. This is the expected result from theory of forced harmonic vibration of a single degree of freedom, lightly damped system, of which the blade can be considered [53].

6.5.3.4 Blade Vibration Measurement Through Dual Probe Tip Timing

The commercially available capacitance probe based tip clearance measurement system's ability to measure blade vibration amplitude through tip timing has been assessed. This has been achieved by using two capacitance probes and associated oscillator and demodulator electronics.

Two capacitance probes were positioned on the compressor case at different circumferential positions. Both were positioned protruding into the flow over the path at which the mid chord positions on the blade's tips pass.

As with the single probe tests reported in Section 6.5.3.2, the distance that the instrumented blade travels through from the moment that the OPR sensor is triggered until the tip arrives at the capacitance probe has been measured. This has been done by timing the interval between the OPR sensor triggering and the blade's arrival at the capacitance probe. This timing, in conjunction with the precise rotor RPM speed measured using the OPR sensor, allows the distance travelled by the blade tip to be calculated.

Figure E.10.10 and Figure E.10.11 show these distances as measured through tip timing. Both of these figures show the distances measured in cases where the blade is not vibrating. The measured distance in the presence of blade vibration is also shown. The difference between these two values represents the blade tip deflection measured through tip timing. In the example data illustrated in Figure E.10.10 and Figure E.10.11 this can be seen to be -0.4 mm at capacitance probe number one and +0.6 mm at capacitance probe number two.

The distance between the two capacitance probes has also been measured using tip timing in conjunction with the precise rotor RPM speed measured by the optical OPR sensor. Figure E.10.12 shows the expected non-vibrating blade condition distance to be 48.1 mm at 938 RPM. The actual physical separation between the capacitance probe mountings is 48.0 $\pm$0.1 mm, as can be seen from the engineering drawing of their mounting in Figure D.6.4. As well as the machining tolerances, discrepancies between the distance measured using tip timing and the actual distance stem from capacitance probe clearance setting differences. Small differences in the clearance setting between each probe mean that different peak voltages will be produces when the instrumented blade passes. This fact, in conjunction with the same constant arbitrary

threshold voltage value being used to determine blade time of arrival at both of the probes, causes an absolute distance error. Therefore, this distance measurement is most useful as a relative one, used to compare with the distance measurement in the presence of blade vibration. This does not have a detrimental effect on the tip timing measurements, since measurements are relative ones, and as such consistency is the important factor.

Figure E.10.12 shows a measured distance of 47.0 mm in the presence of blade vibration. Thus indicating that the blade has travelled 1.1 mm in its vibration cycle between detections by the two capacitance probes (for example from -0.5 mm to +0.6 mm). This measurement, in conjunction with the times of arrival at both capacitance probes can then be used to calculate the blade tip vibration amplitude.

This amplitude is calculated from the time difference between the blade's arrival at the capacitance probes, the tip deflection calculated through tip timing at both capacitance probes and the frequency of vibration calculated from the strain signal using FFT. How this is achieved is shown in Appendix E.11, where the appropriate system of equations and method of solution is described.

Example data for the vibration measured through tip timing are shown in Table 6.2 for six consecutive revolutions with the compressor running at 938 RPM. The tip deflection measured at each probe can be seen to change with each revolution. This indicates that the phase of the blade vibration sine wave is not locked with rotor revolution.

The overall vibration amplitude can be seen to be relatively constant (within 15%). This is expected from experience gained with the strain gauge derived blade tip deflections, as illustrated in the strain gauge vibration tests detailed in Section 6.4.4.3. Small drifts in rotor RPM speed that are present from one revolution to the next, even when the rotor speed is set 'constant' by the controller, result in changes in vibration amplitudes over time.

The blade tip vibration amplitudes measured through dual capacitance probe tip timing can be compared with those determined from the blade mounted strain gauge signals. Figure E.10.13 shows the tip deflection amplitudes calculated from tip timing and those calculated from the blade mounted strain gauges. The error bars in Figure E.10.13 show that the deflection measurement by tip timing is more accurate than the strain derived measurement. The strain derived amplitude is the average value calculated from the two amplitudes derived from the two gauges. The amplitudes of blade tip deflection are plotted from the same data set presented in Table 6.2. The results can be seen to agree within the calculated error bands, as illustrated in Figure E.10.13.

Revolution	Distances in Millimetres Measured Through Tip Timing		
	Tip Deflection at Cap. Probe 1	Tip Deflection at Cap. Probe 2	Vibration Amplitude
1	0.55	-0.55	0.94
2	0.58	-0.52	0.94
3	0.40	-0.69	0.94
4	0.29	-0.81	0.99
5	0.19	-0.85	0.97
6	0.04	-1.07	1.14

Table 6.2 - Dual Capacitance Probe Blade Tip Timing Vibration Measurements

The discrepancy between the strain derived and tip timing calculated amplitudes can be seen to decrease as the strain derived amplitude decreases. In general, the amplitude calculated from tip timing is lower than that derived from the strain gauges. The discrepancy reduces as the phase position on the vibration cycle that is detected by the tip timing approaches a peak or trough. This is apparent from the example data presented in Table 6.2, and was also present in other data sets collected during the experimental programme. Thus, it can be seen to be desirable to calculate vibration amplitudes from tip timing over several rotor revolutions when using this timing and amplitude calculation method. The highest of the calculated amplitudes from the data set will then be closest to the strain derived amplitude measurement.

6.5.4 Vibrating Blade Tip Timing Results Error Analysis

The errors associated with the vibrating blade tip timing results are largely the same as those associated with the non-vibrating blade tip timing results. These are analysed in Section 6.4.4. There is a digitising error as described in Section 6.4.4.1. In the case of the vibrating blade tip timing results, the digitising applies only to the capacitance probe signals. This is since that during this programme of testing the optical OPR sensor signal was timed using digital counter hardware.

There is also error arising from the noise level present on the capacitance probe based tip clearance measurement system's signal. This error was analysed in Section 6.4.4.2. The error associated with the optical OPR sensor signal was very small, as described in Section 5.5.4. Therefore, this does not make a significant contribution to the overall error in determining blade time of arrival.

The comparison between the tip deflections determined through capacitance probe tip timing and the strain gauge derived tip deflections have significant errors associated with them. The errors in tip timing were assessed in Section 6.4.4. in the example data set presented in Section

6.5.3.4 and are illustrated by error bars in Figure E.10.13. The errors associated with the strain derived tip vibration amplitudes are detailed in Section 5.4.3.2 and are also represented by error bars in the data set shown in Figure E.10.13.

6.5.5 Vibrating Blade Tip Timing Conclusions

Blade vibration measurement through capacitance probe tip timing with a tip clearance measurement system has been investigated in three ways. Single capacitance probe tip timing has been performed to measure instantaneous tip deflection. This was followed by an investigation into measuring blade vibration across resonance using single capacitance probe tip timing. Finally, dual capacitance probe tip timing was carried out to measure blade vibration amplitude with the use of curve fitting.

Blade vibration was investigated using blade mounted strain gauges. A low stiffness quasi blade was mounted on the compressor rotor. It was found that this blade could be resonated in vibration mode one at a rotor speed of 938 RPM. This is due to the 16 engine order coinciding with the blade's first natural frequency of vibration. Blade tip vibration amplitudes of up to 1.2 mm were measured.

The vibration was successfully detected through single capacitance probe tip timing over several rotor revolutions. The method used to achieve this was to measure the distance that the instrumented blade travels through from the moment that the OPR sensor is triggered until the tip arrives at the capacitance probe. This was done by timing the interval between the OPR sensor triggering and the blade's arrival at the capacitance probe. This timing, in conjunction with the precise rotor RPM speed measured using the OPR sensor, allows the distance travelled by the blade tip to be calculated. Clearly, in the absence of blade vibration, this distance is constant. However, with blade vibration present, this distance will differ from the expected distance due to the blade tip displacement caused by blade vibration.

The ability of capacitance probe tip timing to detect blade vibration across resonance was then investigated. The compressor was accelerated through the instrumented blade's mode one resonance speed of 938 RPM. During this, tip timing was performed using a capacitance probe. The blade vibration phase change over resonance expected from theory was detected by the capacitance probe tip timing.

Finally, dual capacitance probe tip timing was used to measure blade vibration amplitude. This was again done with the instrumented blade vibrating in mode one. Two capacitance probes were mounted over the blade tip mid chord paths at different circumferential positions. Capacitance probe tip timing was used to measure instantaneous tip deflections at both capacitance probes. The frequency of blade vibration was obtained from spectral analysis of the blade mounted strain gauges' signals. This frequency information was used in conjunction with the measured capacitance probe separation to curve fit a sine wave to the two tip timing measured tip deflections. In this way the blade tip deflection amplitude was calculated. This amplitude was compared to the tip vibration amplitude calculated from the blade mounted strain gauge signals.

The vibration amplitudes measured through capacitance probe tip timing agreed with those derived from the blade mounted strain gauges within the associated error bands. The amplitude derived from tip timing was consistently lower than that derived from the blade mounted strain gauges. The discrepancy between the two derived amplitudes was found to decrease as the strain derived amplitude decreased. This was because the rate of change of the vibration magnitude was lowest at the maxima and minima. Hence, errors in the timing measurement resulted in smaller differences in amplitudes calculated at the vibration cycle's maxima and minima than at high rates of change points on the vibration cycle. The discrepancy was also found to fall as the point in the vibration cycle detected by tip timing neared a signal maximum or a minimum. This can be attributed to the fact that the error in the strain derived deflection was directly proportional to the vibration amplitude. This was due to the error in the strain to tip deflection calibration factor.

The error in the amplitudes derived from the independent tip deflection measurement system using blade mounted strain gauges was assessed. The errors associated with the strain to tip deflection calibration factors dominate this, and are reported in Section 5.4.3. In order to mitigate this error the average of the tip deflections derived from the two blade mounted strain gauges was taken as the definitive strain derived tip deflection.

The uncertainty in determining blade vibration levels through tip timing was also assessed, and found to be around two microseconds in the non-vibrating blade tip timing tests reported in Section 6.4. This translates to a tip deflection uncertainty of approximately 0.12 mm for the vibrating blade tests conducted at 938 RPM.

7. Discussion

This section looks at what the results of the investigations reported in this thesis mean, in terms of the rigour by which capacitance probe tip timing using the commercially available tip clearance measurement system has been assessed. It also considers what implications the findings have in terms of taking the system from the laboratory and applying it to a rig or to a real engine.

The capacitance probe tip timing method used to measure blade vibration has been assessed for accuracy. This has been done using an independent blade vibration measurement system to provide comparison with the tip timing results. While results from both systems were found to agree within the error bands, further investigations are desirable before the capacitance probe tip timing system could realistically be taken from the laboratory and used on a rig. This is due to the large error bands (thirty percent) associated with the strain derived vibration measurements.

In order to take the assessment of the capacitance tip clearance system's performance in tip timing measurement forward, further laboratory work would involve testing the capacitance probe tip timing system against a more accurate system than the strain gauge based system reported in this thesis. This could be achieved by performing a more accurate strain to tip deflection calibration. The high uncertainty in the calibration factors relating strain levels to blade tip deflections used in these investigations was due to the low strain level and low number of fringes present during calibration tests at Rolls-Royce. However, the errors in calibration factors are likely to still be of the order of ten percent, even when recalibrating using ESPI with more fringes and higher strain levels present than those present during the calibration used for the investigations reported in this thesis. Although this would be a significant improvement, it would not be entirely satisfactory either. An optical tip timing system would be more accurate than a strain derived method to establish blade tip deflections. Optical systems exist capable of detecting blade tip vibrations of a few tens of microns. In contrast, the strain gauge vibration measurement system used in the investigations reported in this thesis would have errors of the order of one hundred microns in tip deflection, even once recalibrated, for the vibration levels present on the low-speed compressor test facility used in these investigations. Therefore, an optical tip timing system would be the most suitable type with which to test the capacitance probe tip timing system against in proposed further work. The initial stage in further work would be to take the capacitance probe based tip clearance measurement system and test it's tip timing accuracy against an optical probe based tip timing system using the low-speed compressor test facility.

The evaluation of the capacitance probe tip timing measurement method reported here was limited by the small number of case mounted capacitance probes used. The maximum of two probes available for the investigations reported here meant that in order to derive vibration amplitudes from tip timing, it was necessary to calculate the frequencies of vibration from the strain signals. Mounting four probes would allow vibration amplitudes and frequencies to be measured through tip timing. This would allow four instantaneous vibration level values to be obtained per vibration cycle, rather than the maximum of two measured in the investigations

reported in this thesis. From these four values, both amplitude and frequency of vibration could be calculated using the equations shown in Appendix E.11. Using larger numbers of probes would also open the possibility to use more sophisticated signal processing techniques than the sine wave curve fitting used in these investigations. Averaging signal processing techniques such as autocorrelation may be employed in an attempt to improve signal to noise ratio.

Although the investigations reported in this thesis were performed on a low-speed compressor, with blade passing frequencies of up to 1.5 kHz, the capacitance probe tip clearance system is successfully used to measure tip clearance on high-speed turbomachinery. As such, it would be able to measure tip timing at the high blade passing frequencies present on a high-speed machine of 20 kHz and above. Additional further testing would involve assessing the tip timing measurement accuracy against an optical probe based tip timing measurement system on a high-speed turbomachine. Again, as many probes would be used as possible, and no fewer than four should be used.

The results of the investigations reported in this thesis showed that the FM capacitance probe system's response was frequency dependant, this is as expected. This means that blade passing signal peak levels are dependant upon both probe-to-blade tip clearance and blade tip velocity. This implies that calibration considering tip velocity and clearance would be required to achieve a fully operational dual use tip clearance and tip timing measurement system using the FM capacitance probe based system. The blade passing frequencies present in the investigations on the low-speed compressor test facility were 1 kHz. This is close to the lower end of the capacitance probe based tip clearance measurement system's operating bandwidth of 0.1 kHz to 70 kHz. Consequently, the frequency dependency effect observed here may be less apparent with test carried out at higher blade passing frequencies, closer to the centre of the operating frequency envelope.

In the tests carried out to assess the accuracy of the capacitance probe system when applied to tip timing, a precision laser one per revolution sensor was used. However, on a real engine such a sensor is unlikely to be available. This has the implication that when using a standard engine speed sensor's signal on an in-service engine, the accuracy of the tip timing results obtained would be lower than those achieved using the specially designed once per revolution sensor. It remains to be seen if this would be a significant deterrent to the system being installed on in-service turbomachinery. Next, the capacitance probe's accuracy would have to be assessed continuing to use a precision once per revolution sensor, using multiple capacitance probes, eventually on a high-speed turbomachine, before the drawback of using a normal engine speed sensor could be usefully quantified.

In conclusion, the results reported in this thesis have tested the accuracy of the capacitance probe based tip clearance measurement system in measuring tip timing down to a level of one microsecond for the assessment of timing non-vibrating blades passing. This represents 0.12 mm at the blade tip speeds present on the test rig used. Due to the large errors (thirty percent) associated with the strain gauge based blade tip deflection measurement system, the capacitance probe tip timing measurement method of measuring blade tip vibration amplitude has been assessed to an accuracy of 0.4 mm. This represents thirty percent of the 1.2 mm blade tip deflection amplitudes present on the test rig when resonating the instrumented blade in vibration mode one. Clearly, it is also desirable to assess the capacitance probe blade tip deflection amplitude measurement to an accuracy of at least 0.12 mm. Further work utilising more

capacitance probes and an optical tip timing system, as outlined previously in this chapter, could reasonably assess the blade tip vibration amplitude measurement accuracy of the capacitance probe based system to this level. This work would be the next logical step towards the development of a dual use tip clearance and tip timing measurement capacitance probe based system suitable for use on an in-service rig or engine.

8. Conclusions

The characteristics of a commercially available capacitance displacement transducer based turbomachinery tip clearance measurement system have been investigated. This has been done with the alternative application in mind for this equipment to measure aero-engine tip timing. Various off-rotor and on-rotor experimental investigations have been completed. Findings from these testing programmes have been reported. As a result, a commercially available capacitance probe tip clearance measurement system's response in terms of tip timing measurement has been characterised.

Through on-rotor testing the practicalities of using the system as a tip timing measurement device have been investigated. Blade vibration has been measured through capacitance probe tip timing and the accuracy of the measurements has been assessed. Such a characterisation and assessment of such a system has not previously been available in open literature. The publication of this work constitutes an addition to the state of the art.

8.1 Experimental Results Conclusions

8.1.1 Capacitance Probe Response to Static Tests

Off-rotor testing performed as a prelude to off-rotor vibration measurement tests and on-rotor investigations has been documented. The characteristic of the system's response in three-dimensional space to movement in the proximity of a compressor rotor blade tip has been mapped. It was found that the position sensing of the blade tip was best achieved when the edge of the probe head is over the edge of the blade tip. In this position small changes in displacement in the timing direction result in relatively large changes in probe target area and hence signal level. When the circular probe head is centred over the blade tip small changes in displacement in the timing direction result in small changes in target area and thus small changes in signal. This suggests that the edge of the blade can be detected more accurately than the centre of the blade tip. This does not have detrimental implications for tip timing with capacitance tip clearance probes since as long as timing of the edge is consistently measured, then this is just as valid as timing the blade tip centre.

The effect of measuring capacitance to derive blade tip timing over different areas of the blade tip has also been considered. The larger target areas of the tip mid chord and leading edge positions demonstrate a greater signal swing than the smaller target area of the trailing edge when moved past the capacitance probe. This suggests it is possible to measure tip timing more accurately at the leading edge and at mid chord than at the trailing edge using the capacitance tip clearance probe.

8.1.2 Impulse Tests Capacitance Probe Response

Testing has been reported on an investigation into the capacitance probe tip clearance measurement system's performance in measuring vibration of the blade tip. By correlating capacitance probe signals with tip deflection values derived from calibrated blade mounted strain gauge signals, it was shown that the system in question detected blade impulse response vibrations of amplitudes of as small as twenty microns peak-to-peak.

The capacitance probe clearance measurement system's detection of static blade vibration at varying tip clearances has been investigated. Small vibrations were successfully detected by the capacitance probe at clearances up to 3 mm, above this the vibrations shown by the strain gauge based vibration measurement system were not detected by the capacitance probe based system. As clearance was reduced, capacitance signal strength increased. This is consistent with the findings presented in Section 6.2.

These investigations demonstrate blade vibration detection by the capacitance probe measurement and independent strain gauge systems in a static off-rotor environment. This serves as groundwork for the on-rotor testing presented in Section 6.4 and Section 6.5.

8.1.3 Compressor Rotor Blade Tip Timing Tests

Experimental investigations have been carried out to characterise a commercially available FM capacitance probe based tip clearance system's response to blade tip passing events. This has been done with the alternative application for this system in mind to measure blade tip timing. This has been achieved by characterising and assessing the practicalities of determining an instrumented blade's time of arrival at a fixed point on the compressor casing.

Compressor rotor blade vibrations have been measured using blade mounted strain gauges in conjunction with energising and signal amplification electronics. Vibration levels were found to result in very small amplitudes of blade tip deflections of not more than twenty microns. Hence, these initial on-rotor tip timing investigations are essentially performed on non-vibrating blades.

The resolution with which the time of arrival of the blade can be determined with the capacitance probe based tip clearance system has been evaluated. This was done by measuring the blade passing period over several consecutive revolutions. This period was compared to the period measured by the optical OPR sensor. The consistency of these measurements was assessed at the compressor's designed operating speed of 850 RPM. The capacitance probe period was found to be consistent within two microseconds over the entire sample of data collected. This is within the expected error bands, as assessed in Section 6.4.4.

The capacitance probe signal has been characterised over differing rotor RPM speeds. As is the nature of the FM capacitance probe system, the signal power increased with increasing rotor speed. Thus, the signal to noise ratio is lower at lower RPM speeds. This has a detrimental effect on the accuracy with which the blade time of arrival can be determined from the capacitance probe signal at low RPM speeds.

The sources of error causing the inconsistencies in the time of arrival comparisons between the optical OPR sensor and capacitance probe have been investigated. Three significant sources of error were identified and each of their contributions to the overall error in the non-vibrating blade tip timing experiments was assessed. There are errors stemming from the noise level inherent in the commercially available capacitance probe based tip clearance measurement system's signal. There are also errors due to the discretisation of the capacitance probe and optical OPR sensor's acquisition. Finally there is a small error due to the small blade tip vibrations actually present in these 'non-vibrating' tip timing tests.

The most significant of these errors was found to be the noise level present in the capacitance probe system's signal. The signal to noise ratio was found to improve with increasing rotor RPM speed. At the designed operating speed of 850 RPM this noise caused an uncertainty in the determination of the time of arrival of the blade of not more than two microseconds.

The error associated with the process of digitising the capacitance probe and OPR sensor signals was also assessed. The discretisation of the voltage level was found not to contribute significantly to the error at the rotational speeds of interest, around 850 RPM. This is due to the relatively high rate of change of the voltage signal from the capacitance probe system. The critical discretising error comes from the time step between each sample. This was set at one microsecond in these tests due to hardware limitations. This results in a time of arrival determining uncertainty of not more than one microsecond for each signal. In the case of the optical OPR sensor signal, this could be greatly reduced by using high speed digital timer hardware. Since the OPR signal has been digitised by the electronics designed in Section 5.5, analogue to digital data acquisition is not the most efficient method to time this signal's period.

In the case of the optical OPR sensor the uncertainty could be significantly reduced simply by increasing the sampling rate. However, the noise level present in the capacitance probe signal dictates that increasing the sampling rate of this signal will not in itself be enough to significantly reduce uncertainty. The accuracy of the system for blade tip timing purposes using this signal processing method is thus limited to about two microseconds. This translates to approximately 110 microns at the compressor's operating speed of 850 RPM. It is therefore concluded that blade tip deflections in excess of one tenth of a millimetre are required for the system to be able to successfully detect the vibrations.

8.1.4 Vibrating Blade Tip Timing Tests

Blade vibration measurement through capacitance probe tip timing with a tip clearance measurement system has been investigated in three ways. Single capacitance probe tip timing has been performed to measure instantaneous tip deflection. This was followed by an investigation into blade vibration across resonance using single capacitance probe tip timing. Finally, dual capacitance probe tip timing was carried out to measure blade vibration amplitude.

Blade vibration was investigated using blade mounted strain gauges. A low stiffness quasi blade was mounted on the compressor rotor. It was found that this blade could be resonated in vibration mode one at a rotor speed of 938 RPM. This is due to the sixteen engine order

coinciding with the blade's first natural frequency of vibration. Blade tip vibration amplitudes of up to 1.2 mm were measured.

This vibration was successfully detected through single capacitance probe tip timing over several rotor revolutions. The method used to achieve this was to measure the distance that the instrumented blade travels through from the moment that the OPR sensor is triggered until the tip arrives at the capacitance probe. This has been done by timing the interval between the OPR sensor triggering and the blade's arrival at the capacitance probe. This timing, in conjunction with the precise rotor RPM speed measured using the OPR sensor, allows the distance travelled by the blade tip to be calculated. Clearly, in the absence of blade vibration, this distance is constant. However, with blade vibration present, this distance will differ from the expected distance due to the blade tip displacement caused by blade vibration.

The ability of capacitance probe tip timing to detect blade vibration across resonance was then investigated. The compressor was accelerated through the instrumented blade's mode one resonance speed of 938 RPM. During this, tip timing was performed using a capacitance probe. The blade vibration phase change over resonance expected from theory was detected by the capacitance probe tip timing.

Finally, dual capacitance probe tip timing was used to measure blade vibration amplitude. This was again done with the instrumented blade vibrating in mode one. Two capacitance probes were mounted over the blade tip mid chord paths at different circumferential positions. Capacitance probe tip timing was used to measure instantaneous tip deflections at both capacitance probes. The frequency of blade vibration was obtained from spectral analysis of the blade mounted strain gauges' signals. This frequency information was used in conjunction with the measured capacitance probe separation to curve fit a sine wave to the two tip timing measured tip deflections. In this way the blade tip deflection amplitude was calculated. This amplitude was compared to the tip vibration amplitude calculated from the blade mounted strain gauge signals.

The vibration amplitudes measured through capacitance probe tip timing agreed with those derived from the blade mounted strain gauges within the associated error bands. The amplitude derived from tip timing was consistently lower than that derived from the blade mounted strain gauges. The discrepancy between the two derived amplitudes was found to decrease as the strain derived amplitude decreased. The discrepancy was also found to fall as the point in the vibration cycle detected by tip timing neared a peak or a trough.

The error in the amplitudes derived from the independent tip deflection measurement system using blade mounted strain gauges was assessed. The errors associated with the strain to tip deflection calibration factors dominate this, and are reported in Section 5.4.3. In order to mitigate this error the average of the tip deflections derived from the two blade mounted strain gauges is taken as the definitive strain derived tip deflection.

The uncertainty in determining blade vibration levels through tip timing was also assessed, and found to be around two microseconds in the non-vibrating blade tip timing tests reported in Section 6.4. This translates to a tip deflection uncertainty of approximately 0.12 mm for the vibrating blade tests conducted at 938 RPM.

8.2 Original Contribution

The work documented in this thesis has led to findings being reported that have not previously been available in open literature.

A commercially available turbomachinery blade tip clearance measurement system has been used to measure blade tip timing. Through an extensive body of experimental work the practicalities in this alternate use of the tip clearance measurement equipment have been assessed. System responses pertaining to tip timing measurement have been investigated and documented. The accuracy by which tip timing can be measured using the system has been reported through the findings of an experimental programme carried out on a full-sized, low-speed compressor.

Specifically, this has been achieved through the following original contributions:

1. A commercially available FM capacitance probe based turbomachinery blade tip clearance measurement system has been used to measure on-rotor compressor blade vibration through dual probe tip timing. Vibration amplitudes obtained through this dual capacitance probe tip timing have been compared to those amplitudes derived from an independent blade mounted strain gauge based vibration measurement system.

2. The ability of this tip clearance measurement system to detect blade vibrations across resonance has been demonstrated. This was achieved by using single capacitance probe tip timing to measure instantaneous tip deflections as the rotor was accelerated through resonant blade vibration speed. The vibration phase change across resonance expected from theory was detected and explicitly demonstrated.

3. The FM capacitance probe tip clearance measurement system has been used to measure instantaneous tip deflections through single probe tip timing. These deflections were compared to those derived from an independent strain gauge based blade vibration measurement system.

4. The uncertainty associated with the blade vibration measurements through capacitance probe tip timing has been investigated, explained and quantified. The errors associated with the independent strain gauge based blade vibration measurement system have also been explained and quantified.

5. The FM capacitance probe tip clearance measurement system's ability to determine blade time of arrival has been investigated. By using an optical OPR sensor and blade mounted strain gauges to ensure non-vibrating conditions, the capacitance probe blade passing signal was analysed at various rotor speeds and the accuracy by which time of arrival could be determined was established.

6. A DC capacitance probe clearance measurement system has been used in static, off-rotor, impulse tests to investigate the system's ability to detect small blade tip vibrations. These vibrations were also measured using an independent strain gauge based blade vibration

measurement system. Impulse tests were carried out with the capacitance probe head placed at various positions relative to the blade tip.

7. The DC capacitance probe clearance measurement system's response to movement in 3D space in close proximity to a compressor rotor blade tip has been mapped.

8. A full-sized, low-speed compressor test facility has been commissioned at Cranfield University. This is a unique facility dedicated to instrumentation. HCF monitoring instrumentation systems have been designed, built and installed on the facility. These systems take the form of strain gauge based blade vibration measurement, a precision optical OPR sensor and provision to mount non-intrusive blade tip timing devices.

The increasing importance of tip timing has been reported. The issues in practically mounting a blade condition monitoring system on a flying engine have been discussed. The case for working towards a dual use sensor system using capacitance probes to measure both blade tip clearance and tip timing has been made. Therefore, the findings in terms of the practicality and accuracy in using a commercially available capacitance probe based turbomachinery blade tip clearance measurement system to measure blade tip timing constitutes a valuable original contribution in advancing the state of the art.

8.3 Publications List

8.3.1 Technical Papers

Lawson, C.P., Ivey, P.C., 2003, "Compressor Blade Tip Timing Using Capacitance Tip Clearance Probes". ASME GT-2003-38284. (Presented at ASME Turbo. Expo. 06/03).

Lawson, C.P., Ivey, P.C., 2002, "The Use of Commercially Available Capacitance Tip-Clearance Probes for Tip-Timing of Aero-Engine Compressor Blades". AIAA-2002-3070. (Presented at AIAA/ASME Joint Propulsion Conference 07/02).

Ivey, P.C., Grant, K.R., Lawson, C.P., 2002, "Tip Timing Techniques for Turbomachinery HCF Condition Monitoring". The 16th Symposium on Measuring Techniques in Transonic and Supersonic Flow in Cascades and Turbomachines. Cambridge.

Lawson, C.P., Ivey, P.C., 2003, "The Use of Capacitance Tip-Clearance Probes for Tip-Timing of Aero-Engine Compressor Blades". AIAA Journal. (Submitted).

Lawson, C.P., Ivey, P.C., 2004, "The Measurement of Turbomachinery Blade Vibration Through Tip Timing with Capacitance Tip Clearance Probes". ASME GT-2004-53563. (Submitted).

8.3.2 Management Papers

Coldrick, S., Lawson, C.P., Ivey, P.C., Lockwood, C., 2002, "A Decision Framework for R&D Project Selection". IEEE 2002-IEMC-2002.

Lawson, C.P., Longhurst, P.J., Ivey, P.C., 2003, "The Application of a New Research and Development Project Selection Model in SMEs". R&D Management Journal. (Submitted).

8.4 Further Work

The findings of the experimental investigations reported in this thesis point to several avenues of further work in using the commercially available capacitance tip clearance probe based turbomachinery blade tip clearance system to measure tip timing.

8.4.1 Improved Accuracy Determination

The assessment of the accuracy by which blade time of arrival and consequently tip vibration levels are determined by the capacitance probe could be improved by employing an independent vibration measurement system of greater accuracy than that used in the investigations reported in this thesis.

The errors associated with determining blade tip deflections using the blade mounted strain gauge technique could be reduced with improved strain to tip deflection calibration. Alternatively, or in parallel, a different independent blade vibration measurement system could be utilised to test the capacitance probe based system against. The leading candidate would be an optical probe based tip timing measurement system. Such systems are the most mature non-intrusive blade vibration measurement system type. This work would also open the possibility of a comparative assessment between capacitance probe tip timing and optical probe tip timing.

8.4.2 Multi Capacitance Probe Blade Tip Timing Tests

The testing reported in this thesis culminates in using two capacitance probes to perform tip timing and derive blade vibration amplitudes. Further work could involve measuring blade tip vibration amplitude and frequency through four probe tip timing. This could be achieved by mounting four capacitance probes on the compressor's casing at different circumferential positions within one blade vibration cycle. These four instantaneous vibration measurements could then be used to establish vibration amplitude and frequency.

8.4.3 Blade Vibration Control

Greater control over blade vibration would also open an avenue for future experimental investigations. In the tests reported in this thesis, blade vibration has been forced by resonating the instrumented blade in mode one. This was achieved by setting rotor speed, thus making an engine order frequency coincide with the blade's first natural frequency of vibration.

Control could be exercised over the amplitudes and frequencies of the blade tip's vibrations to investigate, in particular, how well smaller vibration amplitudes are detected through capacitance probe tip timing. This could be achieved by using an independent blade excitation system to control the forcing functions that the blades are subjected to. Such a system could perhaps consist of an electromagnet mounted on the compressor casing. Also, mounting blades with different dynamic properties would also provide a variety of vibration frequencies and amplitudes.

8.4.4 Dual Use Capacitance Probe Based Sensor Development

In order to work towards the development of a dual use capacitance probe based system to measure both tip clearance and blade tip timing, alternative probe head designs could be investigated. Reducing probe head size and changing the head's geometry from circular to, for example, rectangular could be studied. This would be done with the aim of increasing the resolution by which time of arrival may be determined by the capacitance probe based system.

The investigations reported in this thesis are based on experimental work carried out on a low-speed compressor. Further work could involve investigations performed on a high-speed turbomachine. This would provide insight into the practicalities in using this instrumentation on an in-service engine.

References

[1] D. Müller, A. G. Sheard, S. Mozumdar, E. Johann. "Capacitive Measurement of Compressor and Turbine Blade Tip to Casing Running Clearance" *Transactions of the ASME: Journal Of Engineering For Gas Turbines And Power*. Vol. 119 No. 4, October 1997.

[2] J. Chivers. "A Technique for the Measurement of Blade Tip Clearance in a Gas Turbine". AIAA 89-2916. 1989.

[3] I. Zablotsky, K. Ye, A. Yu and L. B. Sviblov. "Contactless Measuring of Vibrations in the Rotor Blades of Turbines". *Technical Translations* FTD-HT-23-673-74. 1974.

[4] M. Zielinski, G. Ziller. "Optical Blade Vibration Measurement at MTU". *Symposium - Advanced Non-intrusive Instrumentation for Propulsion Engines*. 1997.

[5] M. Zielinski, G. Ziller. "Noncontact Vibration Measurement on Compressor Rotor Blades". *Measurement and Science Technology*. 2000.

[6] M. Drumm, W. Hasse. "High Performance Rotor Health Monitoring". *IEEE* 0-7803-6395-7, June 2000.

[7] R. G. Cooper, S. J. Edgett, E. J. Kleinschmidt. "Portfolio Management for New Product Development: Results of an Industry Practices Study". *R&D Management*. Vol. 31, Issue 4. October 2001.

[8] D. Ferguson. "The Development of Air-Cooling Techniques for Fast Response Pressure Transducers in High Temperature Environments". *Cranfield University Ph.D. Thesis*. 1997.

[9] C. Lockwood. "Comparison of Average-Passage Equation Closures Through Simulation of Single and Multi-Row Axial Compressors; The Limitations of Using A Commercial CFD Code". *Cranfield University Ph.D. Thesis*. 1999.

[10] R. G. Cooper, S. J. Edgett, E. J. Kleinschmidt. "Portfolio Management in New Product Development: Lessons from the Leaders-I". *Research Technology Management*. Vol. 40, Issue 5. 1997.

[11] R. G. Cooper, S. J. Edgett, E. J. Kleinschmidt. "Portfolio Management in New Product Development: Lessons from the Leaders-II". *Research Technology Management*. Vol. 40, Issue 6. 1997.

[12] R. G. Cooper, S. J. Edgett, E. J. Kleinschmidt. "Best Practices for Managing R&D Portfolios". *Research Technology Management*. Vol. 41, Issue 4. 1998.

[13] R. G. Cooper, S. J. Edgett, E. J. Kleinschmidt. "New Product Portfolio Management: Practices and Performance". *Journal of Product Innovation Management*. Vol. 16, pp 333-351. 1999

[14] R. G. Cooper, S. J. Edgett, E. J. Kleinschmidt. "New Problems, New Solutions: Making Portfolio Management More Effective". *Research Technology Management*. Vol. 43, Issue 2. 2000.

[15] D. Matheson, J. E. Matheson, M. M. Menke. "Making Excellent R&D Decisions". *Research Technology Management*. Vol. 37, Issue 6. 1994.

[16] M. M. Menke. "Essentials of R&D Strategic Excellence". *Research Technology Management*. Vol. 40, Issue 5. 1997.

[17] M. M. Menke. "Managing R&D for Competitive Advantage". *Research Technology Management*. Vol. 40, Issue 6. 1997

[18] Y. Osawa, M. Murakami. "Development and Application of a New Methodology of Evaluating Industrial R&D Projects". *R&D Management*. Vol. 32, Issue 1. 2002.

[19] H. M. Stillman. "How ABB Decides on the Right Technology Investments". *Research Technology Management*. Vol. 40, Issue 6. 1997.

[20] J. R. Moore Jr., N. R. Baker. "An Analytical Approach to Scoring Model Design-Application to Research and Development Project Selection" *IEEE Transactions on Engineering Management*. Vol. EM-16, No. 3. 1969.

[21] I. Fradley. "Improved Methods of Determining Turbine Blade Vibration Levels". *Cranfield University M.Sc. Thesis*. 1995.

[22] C. D. Hsiao-Wei, Chen Chi-Chih, Hsu Chih-Neng. "An Investigation of Turbomachinery Shrouded Rotor Blade Flutter". *Transactions of the ASME*. GT2003-38311. 2003.

[23] X. Wu, M. Vahdati, A. Sayma, M. Imregun. "A Numerical Investigation of Aeroacoustic Fan Blade Flutter". *Transactions of the ASME*. GT2003-38454. 2003.

[24] D. H. Buffum. "Blade Row Interaction Effects on Flutter and Forced Response". *Transactions of the AIAA*. AIAA-93-2084. 1993.

[25] N. Sarigul-Klijn, S. Oguz. "Influence of Chordwise Vibration Modes on Compressor Blade Flutter Predictions". *Transactions of the AIAA.* AIAA-95-2485. 1995.

[26] H. Stagardter. "Optical Determination of Rotating Fan Blade Deflections". *ASME Journal of Engineering for Power*. Vol. 99. 1977.

[27] P. Nava. "Design and Experimental Characterization of a Nonintrusive Measurement System of Rotating Blade Vibration". *ASME Journal of Engineering for Gas Turbines and Power*. Vol. 116, No. 3. July 1994.

[28] W. B. Watkins, R. M. Chi. "A Noninterference Blade Vibration Measurement System for Gas Turbine Engines". *Transactions of the AIAA.* AIAA-87-1758. 1987.

[29] R. M. Chi, H. T. Jones. "Demonstration Testing of a Noninterference Technique for Measuring Turbine Engine Rotor Blade Stresses". *Transactions of the AIAA.* AIAA-88-3143. 1988.

[30] H. R. Simmons, D. L. Michalsky, K. E. Brewer, A. J. Smalley. "Measuring Rotor and Blade Dynamics Using an Optical Blade Tip Sensor". *Transactions of the ASME*. 90-GT-91. 1990.

[31] W. W. Robinson, R. S. Washburn. "A Real Time Non-Interference Stress Measurement System (NSMS) for Determining Aero Engine Blade Stresses". *Transactions of the ISA*. Paper #91-103. 1991.

[32] N. Paone, G. Rossi. "Large-Bandwidth Reflection Fiber-Optic Sensors for Turbomachinery Rotor Blade Diagnostics". *Sensors and Actuators A*. Vol. 32. 1992.

[33] S. Heath, M Imregun. "An Improved Single-Parameter Tip-Timing Method for Turbomachinery Blade Vibration Measurements Using Optical Laser Probes". *Int. J. Mech. Sci.* Vol. 38, No. 10. 1996.

[34] S. Heath, M Imregun. "A Review of Analysis Techniques for Blade Tip-Timing Measurements". *Transactions of the ASME*. 97-GT-213. 1997.

[35] S. Heath. "A New Technique for Identifying Synchronous Resonances Using Tip-Timing". *ASME Journal of Engineering for Gas Turbines and Power*. Vol. 122, No. 2. April 2000.

[36] I. B. Carrington, J. R. Wright, J.E. Cooper, G. Dimitriadis. "A Comparison of Blade Tip Timing Data Analysis Methods". *Proc. Instn. Mech. Engrs.* Vol. 215. Part G. 2001.

[37] Henry Jones. "A Nonintrusive Blade Vibration Monitoring System". *Transactions of the ASME*. 96-GT-84. 1996.

[38] W. A. Strange. "Advanced Instrumentation Development for the High Cycle Fatigue (HCF) Program and the National Turbine Engine Durability (NTED) Initiative". *Transactions of the ASME*. 2000-GT-652. 2000.

[39] W. C. Hasse, J. K. Roberge, M. J. Drumm. "High Bandwidth, Capacitive Sensing Preamplifier for Engine Health Monitoring". *ExSell Inc. Technical Paper*. January 2000.

[40] W. C. Hasse, M. J. Drumm. "Capacitive Multi-Element Blade Vibration Sensor". *ExSell Inc. Technical Paper*. February 2000.

[41] D. C. Wisler. "Loss Reduction in Axial-Flow Compressors Through Model Testing". *ASME Journal of Engineering for Gas Turbines and Power*. Vol. 107, No. 2. April 1985.

[42] N. Grice, I. Sherrington, E. H. Smith, S. G. O'Donnell, J. F. Stringfellow. "A Capacitance Based System For High Resolution Measurement of Lubricant Film Thickness". *Proceedings of Nordtrib*. 1990.

[43] A. Sheard, S. G. O'Donnell, J. F. Stringfellow. "High Temperature Proximity Measurement in Aero and Industrial Turbomachinery". *Transactions of the ASME*. 97-GT-198. 1997.

[44] A. Sheard, B. Killeen. "A Blade-by-Blade Tip Clearance Measurement System for Gas Turbine Applications". *ASME Journal of Engineering for Gas Turbines and Power*. Vol. 117, No. 2. April 1995.

[45] A. Sheard. "The Aerodynamic and Mechanical Performance of a High-Pressure Turbine Stage in a Transient Wind Tunnel". *ASME Journal of Engineering for Gas Turbines and Power*. Vol. 114, No. 1. January 1992.

[46] A. Howard, P. Ivey, J. P. Barton, K. F. Young. "Endwall Effects at Two Tip Clearances in a Multistage Axial Flow Compressor With Controlled Diffusion Blading". *Transactions of the ASME*. 93-GT-299. 1993.

[47] J. Brown. "Characterization of MSC/NASTRAN & MSC/ABAQUS Elements for Turbine Engine Blade Frequency Analysis". *Journal*. Year.

[48] M. A. Lawry. *I-DEAS Master Series: Student Guide*. SDRC. 1999.

[49] L. Balmer. *Signals and Systems: An Introduction*. 2nd Edition. Prentice Hall. 1997.

[50] S. Coldrick, P. Ivey, R. Wells. "Considerations for Using 3D Pneumatic Probes in High Speed Axial Compressors". *Transactions of the ASME*. GT-2002-30045. 2002.

[51] P. Lyes. "Low Speed Axial Compressor Design and Evaluation: High Speed Representation and Endwall Flow Control Studies". *Cranfield University Ph.D. Thesis*. 1999.

[52] K. Grant and P. Ivey. "The Experimental Validation of Tip-Timing Techniques for Condition Monitoring of HCF in Gas Turbine Aero-Engines". *Transactions of the AIAA*. AIAA 2002-4305. 2002.

[53] W. T. Thomson. *The Theory of Vibrations with Applications*. 4th Edition. Chapman and Hall. 1997.

[54] S. Coldrick, C. P. Lawson, P. C. Ivey, C. Lockwood. "A Decision Framework for R&D Project Selection". IEEE 2002-IEMC-2002. 2002.

[55] C. P. Lawson, P. C. Ivey. "Compressor Blade Tip Timing Using Capacitance Tip Clearance Probes". *Transactions of the ASME*. ASME GT-2003-38284. 2003.

[56] C. P. Lawson, P. C. Ivey. "The Use of Commercially Available Capacitance Tip-Clearance Probes for Tip-Timing of Aero-Engine Compressor Blades". *Transactions of the AIAA*. AIAA-2002-3070. 2002.

[57] P. C. Ivey, K. R. Grant, C. P. Lawson. "Tip Timing Techniques for Turbomachinery HCF Condition Monitoring". The 16th Symposium on Measuring Techniques in Transonic and Supersonic Flow in Cascades and Turbomachines. Cambridge. 2002.

Appendix A - Research Project Selection Model Application

Appendix A.1 - Step-by-step Model Application

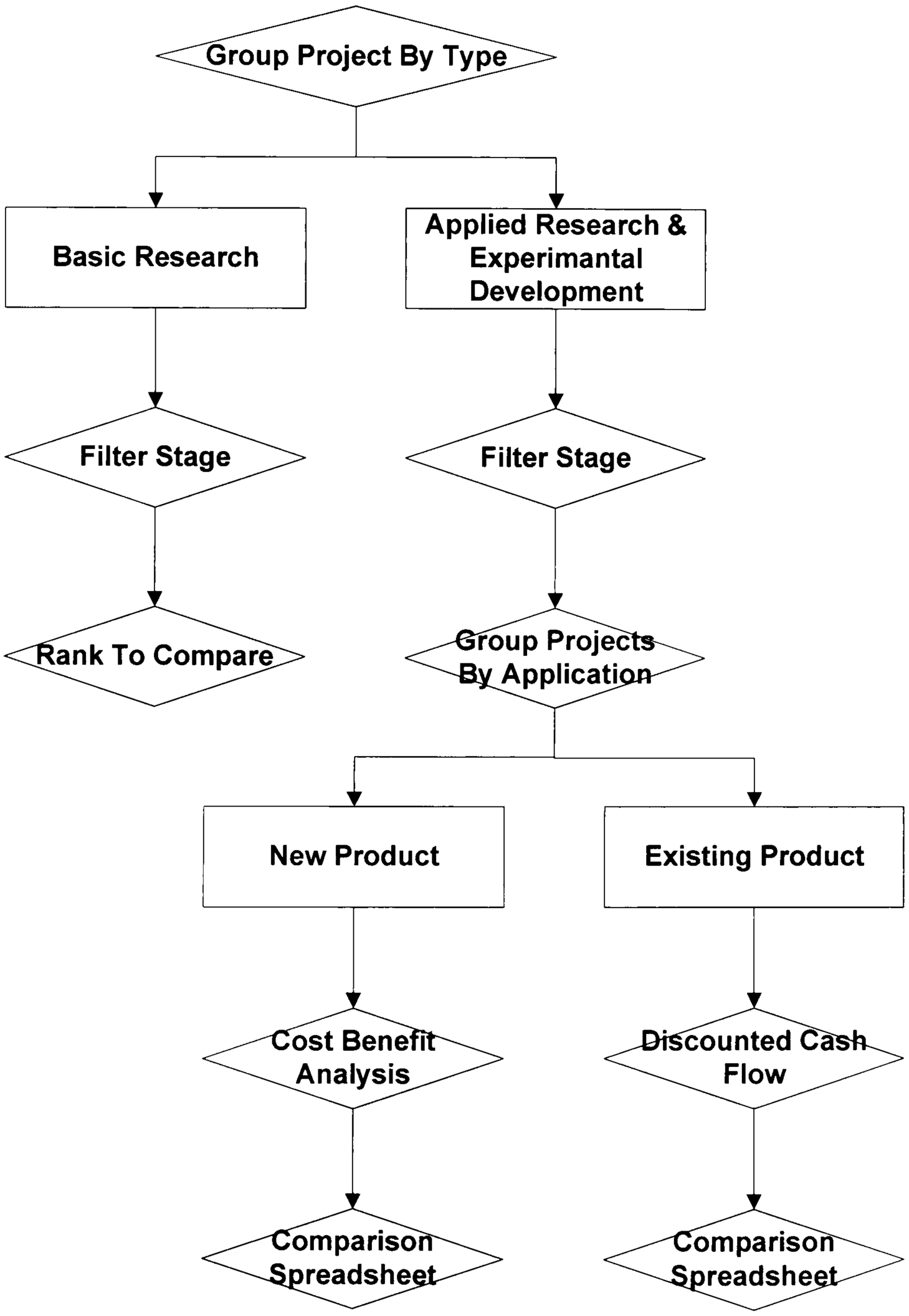

Figure A.1.1 - Project Selection Model Step-By-Step Flow Chart

Step 1 - Group Project by Type

Project types
1a) Basic Research
1b) Applied Research and Experimental Development

Definitions:
Basic Research - where knowledge is acquired.
Applied Research - where knowledge is acquired, leading to a practical aim.
Experimental Development - where knowledge is acquired, leading to a practical aim, leading to a new product or material.

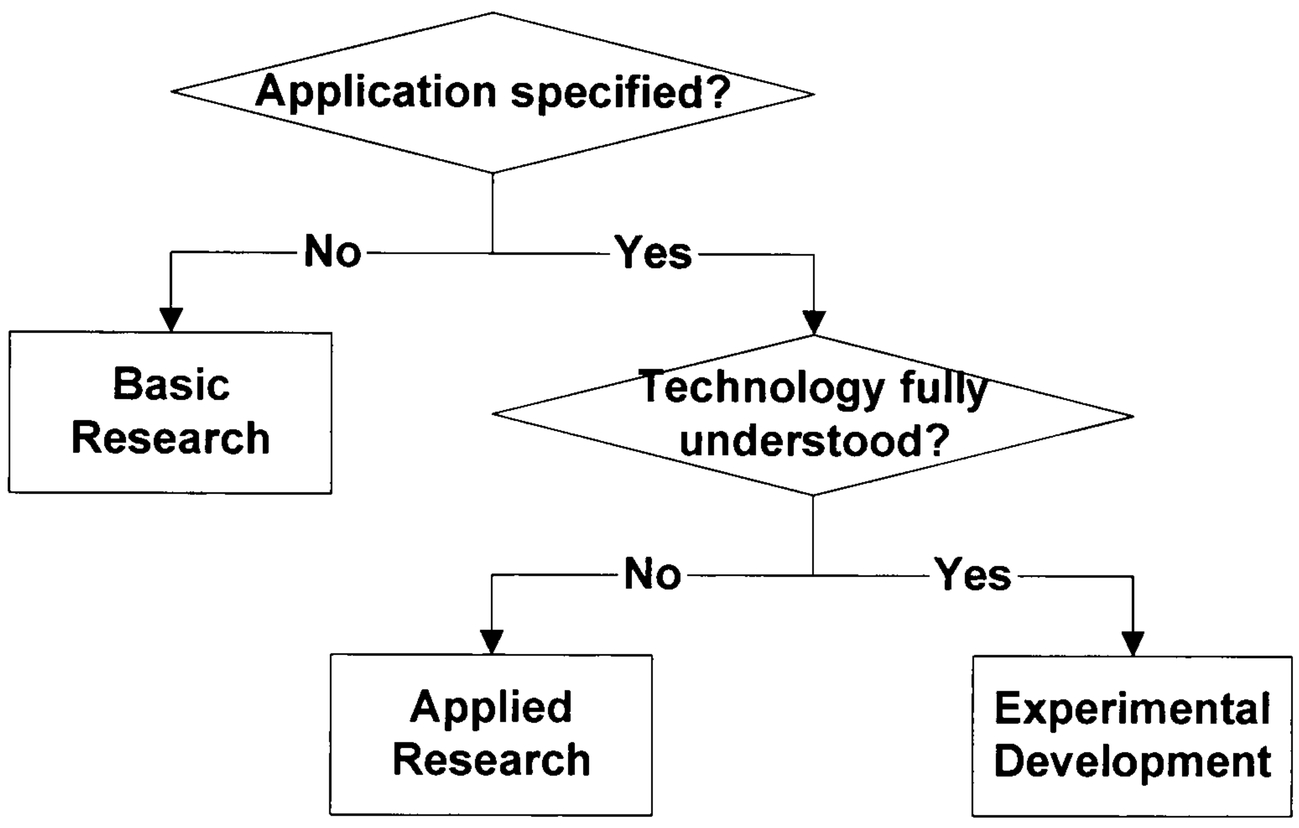

Figure A.1.2 - Project Type Grouping Flow Chart

Step 2 - Filter

A simple analysis to reject unpromising projects. Table A.1 shows such an analysis suitable for projects identified as type 1b), Applied Research and Experimental Development. For projects of type 1a), basic research, only the first three categories are considered.

Step 3 - Group Promising Projects by Application

Consider further those projects that were not rejected at Step 2. The following assumes that projects were classified 1b), as is expected by the nature of the field test company's business. Step 3 is different for type 1a) basic research projects.

Group Project by Application
3a) New product - Generally applied research projects
3b) Existing product - Generally experimental development projects

Projects identified as type 3a cannot be compared directly with those defined as type 3b. Thus for further assessment projects are divided into these two groups.

Step 4a - For Projects Classified as Type 3a

- Rank projects by scores derived in Step 2.
- Conduct Risk Assessment and Analysis.
- Conduct Cost Benefit Analysis.
- Comparison Spreadsheet.

Step 4b - For Projects Classified as Type 3a

- Rank projects by scores derived in Step 2.
- Conduct Risk Assessment and Analysis.
- Conduct Discounted Cash Flow study.
- Comparison Spreadsheet.

Project Evaluation Filter	Criteria		Category		Project
	Score 1-5	Weight	Score 1-5	Weight	Score 1-5
1. Technical					
Technical risk to project completion	?	?	Multiply		
Technical resource availability	?	?	Multiply		
		SumCrW	SumCaS/SumCrW	?	Multiply
2. Corporate and Strategic					
Fit with company business plan	?	?	Multiply		
Product range growth potential	?	?	Multiply		
Synergy with other products/processes	?	?	Multiply		
		SumCrW	SumCaS/SumCrW	?	Multiply
3. Regulatory					
Risk in obtaining regulatory clearance	?	?	Multiply		
Ability to meet likely future regulations	?	?	Multiply		
		SumCrW	SumCaS/SumCrW	?	Multiply
4. Market					
Effect on existing market share	?	?	Multiply		
Effect on existing market outlook	?	?	Multiply		
New market potential	?	?	Multiply		
		SumCrW	SumCaS/SumCrW	?	Multiply
5. Financial					
Commercial risk of application	?	?	Multiply		
Potential return on investment	?	?	Multiply		
		SumCrW	SumCaS/SumCrW	?	Multiply
6. Application					
Ability to implement production/process	?	?	Multiply		
Patentability/design protection	?	?	Multiply		
		SumCrW	SumCaS/SumCrW	?	Multiply
NB: Use Categories 1-3 only for projects classified as Basic Research.				**Total**	Sum

Table A.1 - Project Evaluation Filter Stage

Filter Use Guidelines

Score Assignment

Integer values between 1 and 5 inclusive should be assigned to each criterion. The following provides guidance on assigning scores to each criteria.

Technical

Technical risk to project completion.

Score	Description
5	Technical objectives straight-forward to achieve.
1	Technical aspects difficult to achieve, even when bringing in outside expertise.

Technical resource availability.

Score	Description
5	Resource readily available within the company.
1	Resources not available within the company, and would be difficult to bring in.

Corporate and Strategic

Fit with company business plan.

Score	Description
5	Central to company business plan.
1	Inconsistent with company business plan.

Product range growth potential.

Score	Description
5	Adds to company's product range.
1	Replaces an existing company product, making it obsolete.

Synergy with other products/processes.

Score	Description
5	Directly supports other company product(s).
1	No relation to any other company products.

Regulatory

Risk in obtaining regulatory clearance.

Score	Description
5	Laws encourage product.
1	Laws prohibit product.

Technical resource availability.

Score	Description
5	Future laws will encourage product sales.
1	Future laws will prohibit product.

Market

Effect on existing market share.

Score	Description
5	Enhances existing product.
1	Competes with existing product.

Effect on existing market outlook.

Score	Description
5	Wide market, innovative, high-tech. product.
1	Limited market product that doesn't add to company's technological image.

New market potential.

Score	Description
5	Opens new wide markets to the company.
1	In existing market sector only.

Financial

Commercial risk of application.

Score	Description
5	No detrimental effect on the financial viability of the company's other product productions.
1	Possibly seriously detrimental effect on the financial viability of the company's ability to continue trading.

Potential return on investment.

Score	Description
5	Many times return on the investment.
1	Very small return on the investment.

Application

Ability to implement production/process.

Score	Description
5	Company already has in place equipment/knowledge to implement.
1	Extremely difficult for the company to gain equipment/knowledge.

Patentability/design protection.

Score	Description
5	Difficult for others to copy the design, and easy to obtain a patent.
1	Easy for others to copy the product, and difficult to obtain a patent.

Criteria Weightings

Assign values between 1.0 and 0.0, inclusive to weight the relative importance of each criterion in each category in turn.

The most important/significant criteria in each category should be assigned a weighting of 1.0. The other criteria should then be assigned values between 1.0 and 0.0, inclusive, reflecting their relative importance compared to the most important criteria in each category.

Special Case
In the Regulatory category, where regulations are of no importance (i.e. pose no obstacle) to the project, criteria should both be scored 1.0.

Category Weightings

Assign values between 1.0 and 0.0, inclusive to weight the relative importance of each category.

The most important/significant category should be assigned a weighting of 1.0. The other categories should then be assigned values between 1.0 and 0.0, inclusive, reflecting their relative importance compared to the most important category.

Appendix A.3 - Risk Assessment and Analysis

Risk Assessment

Equations to determine the appropriate level of risk analysis:

$$x = R \cdot r + B \cdot b + \frac{a}{BCR} \qquad \text{A.1}$$

$$r + b = 1 \qquad \text{A.2}$$

Where: R is manpower resource. (1-5)
r is the resource weighting factor.
B is the project budget. (1-5)
b is the budget weighting factor
BCR is the Benefit Cost Ratio
$a = 0.01$. A weighting factor to reduce the importance of BCR
BCR = (Benefits - Total Cost) / Total Cost

The value, x indicates the type of risk analysis that should be carried out. This is shown in the table below.

x value	Risk analysis type
$x \leq 2$	None - very low risk project
$x > 2$	Likelihood/Consequence Analysis
$x > 3$	Event Tree Analysis
$x > 4$	Analytical Modelling
$x > 5$	Simulation Modelling

Table A.2 - Risk Analysis Level

Deriving *x*

Choosing values of *B* and *R*

A table should be constructed from which values of *B* and *R* can be read for the projects being considered. Table values will depend on the company involved and the range of proposed projects.

An example of assignments of *B* and *R* values is shown in the table below.

Project Budget		Manpower Resource	
Ranges £1000's	B value	Ranges Hours	R value
0 - 0.4	1	0 - 40	1
0.4 - 1.0	2	40 - 100	2
1.0 - 4.0	3	100 - 400	3
4.0 - 10	4	400 - 1000	4
10 - 40	5	1000 - 4000	5

Table A.3 - Budget and Manpower Values

Choosing values of *b* and *r*

b and *r* shift emphasis between projects' man power and budget. For example, a project for which funding has already been secured may have a greater risk emphasis towards manpower resources. $r + b = 1$.

Risk Analysis Levels

Likelihood/Consequence

Likelihood

Likelihood	Probability
Low	< 10%
Medium	Between 10% and 33%
High	> 33%

Table A.4 - Likelihood Analysis

Consequence

	Time	Cost	Specification
Low	< 1 extra day	< 1% over budget	Insignificant change
Medium	1 day to 1 week extra	1 to 5% over budget	Small non-recoverable change
High	> 1 week extra	> 5% over budget	Many non-recoverable changes

Table A.5 - Consequence Analysis

Event Trees

Event trees are an extension of likelihood/consequence analysis suitable for processes that depend on sequential events. This can be applied to the cost, time and specification.

Analytical Modelling

Perform an analytical analysis of each identified risk. For example a Gaussian probability distribution could be used to describe each risk. This can be applied to the cost, time and specification.

Simulation Modelling

Software packages, such as those based on Monte Carlo technique.

Risk Mitigation

When retrospectively analysing projects, risks will tend just to be accepted. However, when performing a risk analysis before the project is undertaken, risk mitigation will be an important process.

Appendix A.4 - Cost Benefit Analysis and Discounted Cash Flow

CBA and DCF are well established and widely used financial techniques for evaluating a project's worth. Although there is no standard way of presenting the results the method always involves comparing project costs with the expected benefits derived from undertaking the project.

CBA and DCF are very similar, and sometimes indistinguishable. However CBA does not necessarily include discounting, while DCF does. Since including a discount rate gives a more accurate project assessment it is often included in CBA.

Net Present Value (NPV) is a quantifiable measure considered when using DCF. NPV calculations reveal the current value of a sum of money received at some point in the future. This is called discounting and is achieved by choosing a discounting rate and using the compound interest formula to calculate the discounting factor. Thus:

$$P = \frac{A}{(1+r)^t} \qquad \text{A.3}$$

Where: P = amount invested (current amount)
A = final amount (in the future)
r = annual interest rate
t = time (in years)

Another value calculated when performing DCF is Internal Rate of Return (IRR). This reveals at what discount rate, or annual interest rate the project ceases to be profitable.

Present Value Index (PVI) is the third and final value that can be used to rank projects using DCF. PVI is a ratio of the operational net cash flows over the present value of the project investments.

Examples of conducting CBA and DCF are shown in Table A.6 and Table A.7 respectively.

Cost Benefit Analysis

Cost	Year			
	0	1	2	3
Labour				
Materials				
Fixed Overheads				
Total				
Benefits	**Year**			
Sales	0	1	2	3
Total				

Table A.6 - Example Cost Benefit Analysis

Discounted Cash Flow

Benefits	Year				Totals
	0	1	2	3	
Outflow					
Inflow					
Discount Rate					
Present Value Outflow					
Present Value Inflow					
				PV Index	
Total (Net Present Value)					

Table A.7 - Example Discounted Cash Flow

PV Index = PV Inflow / PV Outflow.

Table A.8 - Discounted Cash Flow: Example Project 1

Calendar Year Project Year	1990 1	1991 2	1992 3	1993 4	1994 5	1995 6	1996 7	1997 8	1998 9	1999 10
Capital Investment										
Research Costs	0.7	8.3	4.5	4.0	0	0	0	0	0	0
Student Sponsorship	2.0	2.0	2.0	2.0	0	0	0	0	0	0
University Fees	1.5	1.5	1.5	1.5	0	0	0	0	0	0
Labour Resource	0	2.0	2.0	2.0	0	0	0	0	0	0
Rig Investment										
Instrumentation	0	0	0	0	230.4	230.4	230.4	230.4	230.4	230.4
Re-building	0	0	0	0	60.0	60.0	60.0	60.0	60.0	60.0
Re-running	0	0	0	0	128.0	128.0	128.0	128.0	128.0	128.0
Total Investment	4.2	13.8	10.0	9.5	418.4	418.4	418.4	418.4	418.4	418.4
Capital Return										
Preventing damage to test rigs	0	0	0	0	768.0	768.0	768.0	768.0	768.0	768.0
Total Return	0	0	0	0	768.0	768.0	768.0	768.0	768.0	768.0
Net Cash Flow	-4.2	-13.8	-10.0	-9.5	349.6	349.6	349.6	349.6	349.6	349.6
Tax Effect @33%	1.4	4.6	3.3	3.1	-115.4	-115.4	-115.4	-115.4	-115.4	-115.4
Effective Cash Flow	-2.8	-9.2	-6.7	-6.4	234.2	234.2	234.2	234.2	234.2	234.2
Cumulative Cash Flow	-2.8	-12.1	-18.8	-25.1	209.1	443.3	677.6	911.8	1146.0	1380.3
Discount Factor @16%	1.000	0.862	0.743	0.641	0.552	0.476	0.410	0.354	0.305	0.263
Net Present Value (real)	-2.8	-8.0	-5.0	-4.1	129.4	111.5	96.1	82.9	71.4	61.6

Table A.9 - Discounted Cash Flow: Example Project 2

Calendar Year Project Year	1998 1	1999 2	2000 3	2001 4	2002 5	2003 6	2004 7	2005 8	2006 9	2007 10
Capital Investment										
Research Costs	1.4	8.0	6.5	0	0	0	0	0	0	0
Consultancy Fees	10.0	10.0	0	0	0	0	0	0	0	0
Labour Resource	4.0	4.0	4.0	0	0	0	0	0	0	0
Test Facility Investment										
Build	200	50	40	0	0	0	0	0	0	0
Instrumentation	0	0	0	2.0	2.0	2.0	2.0	2.0	2.0	2.0
Maintenance	0	0	0	40.0	40.0	40.0	40.0	40.0	40.0	40.0
Total Investment	215.4	72.0	50.5	42.0	42.0	42.0	42.0	42.0	42.0	42.0
Capital Return										
Testing Contracts	0	0	0	0	0	250.0	250.0	250.0	250.0	250.0
Outsourced Testing Saving	0	0	0	0	60.0	60.0	60.0	60.0	60.0	60.0
Total Return	0	0	0	0	60.0	310.0	310.0	310.0	310.0	310.0
Net Cash Flow	-215.4	-72.0	-50.5	18.0	268.0	268.0	268.0	268.0	268.0	268.0
Tax Effect @33%	71.1	23.8	16.7	-5.9	-88.4	-88.4	-88.4	-88.4	-88.4	-88.4
Effective Cash Flow	-144.3	-48.2	-33.8	12.1	179.6	179.6	179.6	179.6	179.6	179.6
Cumulative Cash Flow	-144.3	-192.6	-226.4	-214.3	-34.8	144.8	324.3	503.9	683.5	863.0
Discount Factor @16%	1.000	0.862	0.743	0.641	0.552	0.476	0.410	0.354	0.305	0.263
Net Present Value (real)	-144.3	-41.6	-25.1	7.7	99.2	85.5	73.7	63.5	54.8	47.2

Table A.10 - Discounted Cash Flow: Example Project 3

Calendar Year Project Year	2003 1	2004 2	2005 3	2006 4	2007 5	2008 6	2009 7	2010 8	2011 9	2012 10
Capital Investment										
Research Costs	9.2	9.8	0.4	0	0	0	0	0	0	0
Labour Resource	4.0	4.0	2.0	0	0	0	0	0	0	0
Test Facility Investment										
Test and Development Machine	200	0	40	0	0	0	0	0	0	0
Manufacturing Machine	0	400.0	0	2	2	2	2	2	2	2
Maintenance	0	6.0	0	14	14	14	14	14	14	14
Total Investment	213.2	411.8	50.5	16	16	16	16	16	16	16
Capital Return										
Testing Contracts	0	0	40.0	80.0	80.0	80.0	80.0	80.0	80.0	80.0
New Product Sales	0	0	0	200.0	400.0	700.0	600.0	500.0	300.0	200.0
Total Return	0	0	40.0	280.0	480.0	780.0	680.0	580.0	380.0	280.0
Net Cash Flow	-215.4	-72.0	-50.5	18.0	268.0	268.0	268.0	268.0	268.0	268.0
Tax Effect @33%	71.1	23.8	16.7	-5.9	-88.4	-88.4	-88.4	-88.4	-88.4	-88.4
Effective Cash Flow	-144.3	-48.2	-33.8	12.1	179.6	179.6	179.6	179.6	179.6	179.6
Cumulative Cash Flow	-144.3	-192.6	-226.4	-214.3	-34.8	144.8	324.3	503.9	683.5	863.0
Discount Factor @16%	1.000	0.862	0.743	0.641	0.552	0.476	0.410	0.354	0.305	0.263
Net Present Value (real)	-144.3	-41.6	-25.1	7.7	99.2	85.5	73.7	63.5	54.8	47.2

Appendix B - Gas Turbine Tip Timing and Tip Clearance Systems

Appendix B.1 - Capacitance Tip Clearance Probes

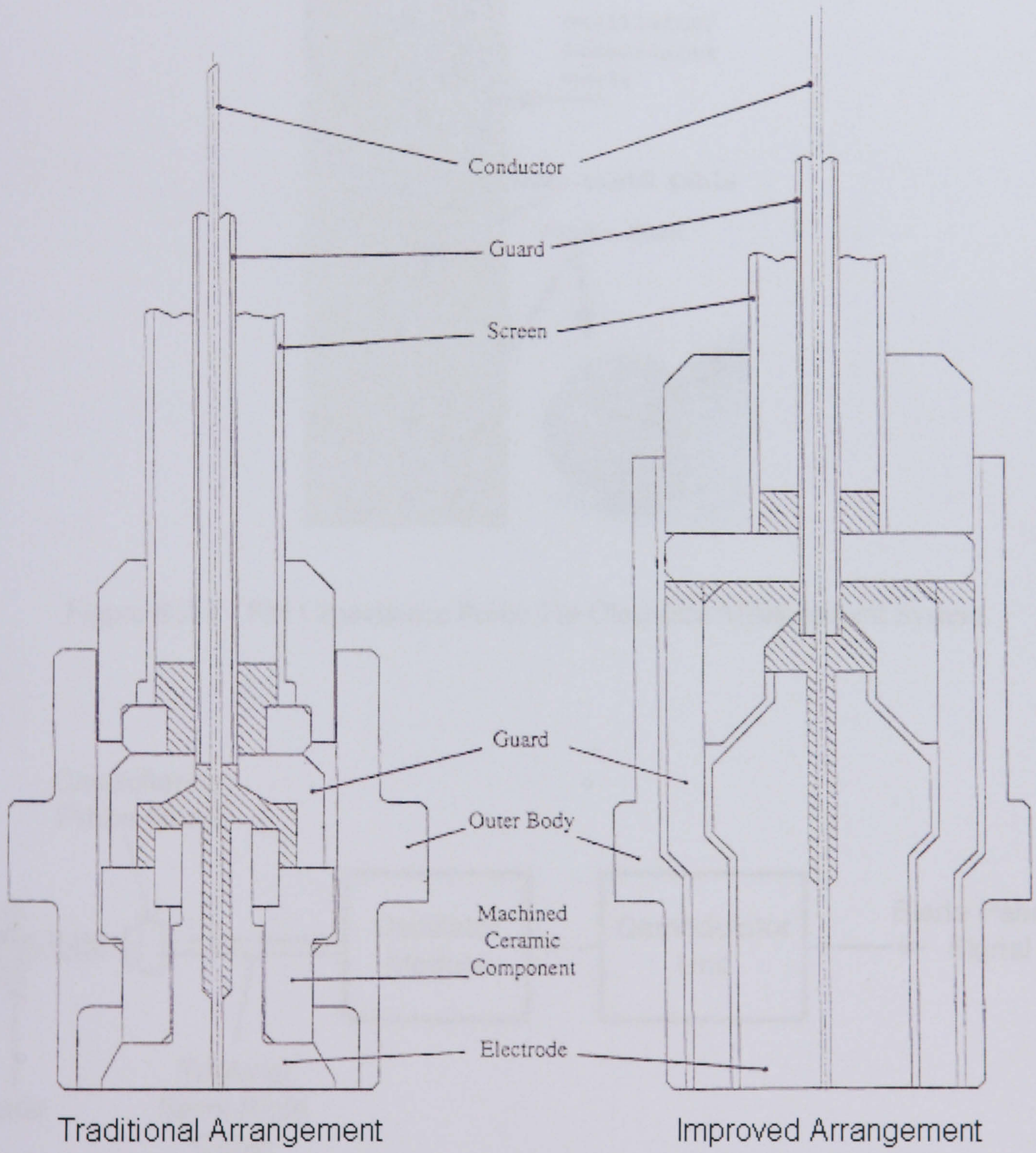

Figure B.1.1 - Tri-Axial Capacitance Probes

Source: [43].

Appendix B.2 - RotaCap Tip Clearance Measurement System

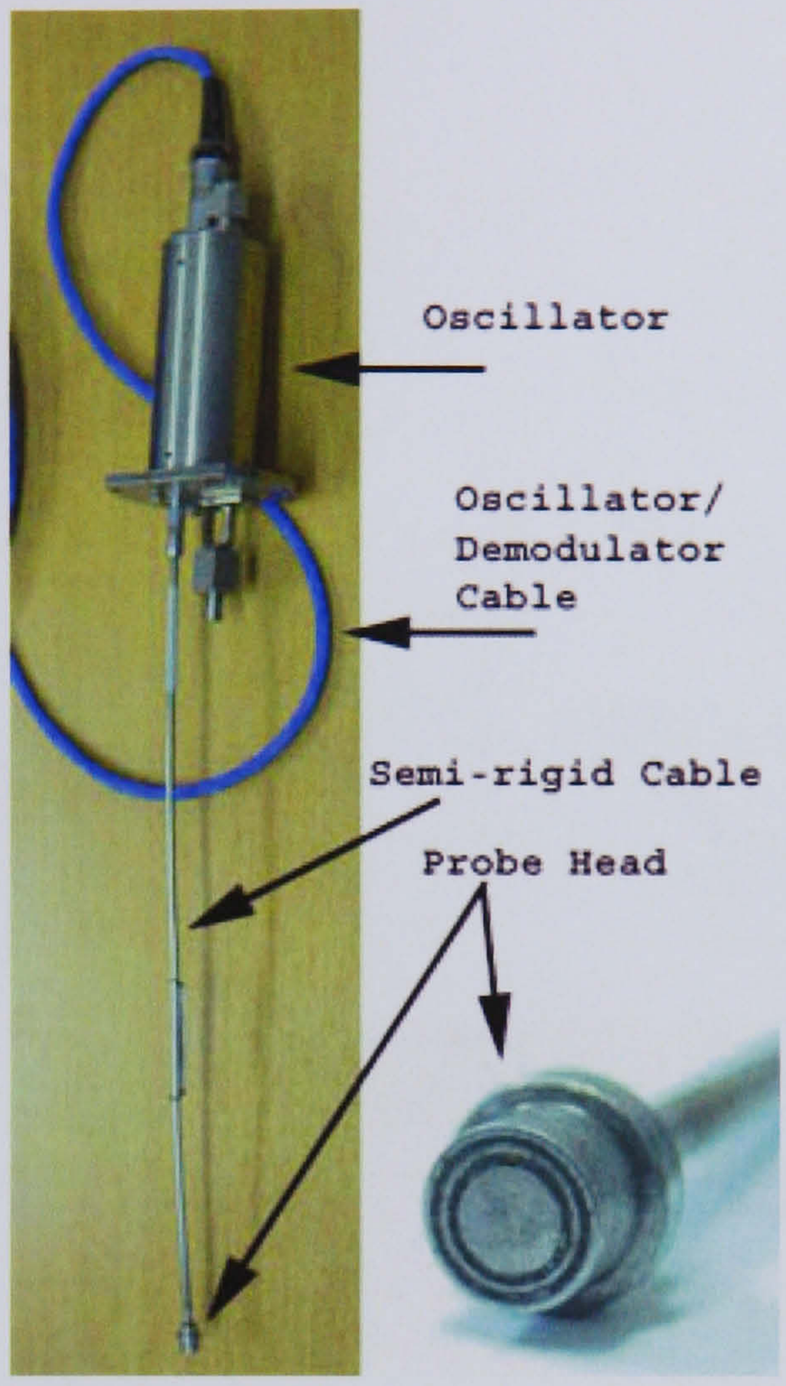

Figure B.2.1 - FM Capacitance Probe Tip Clearance Measurement System

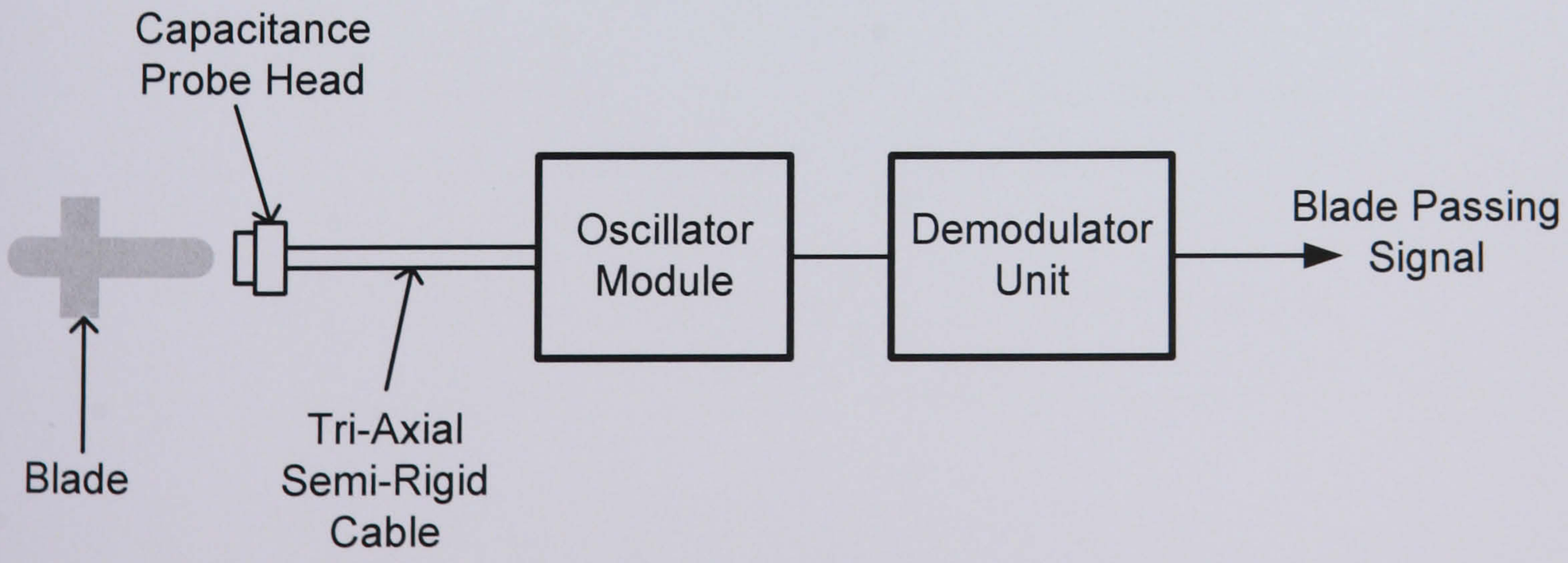

Figure B.2.2 - Tip Clearance Measurement System Schematic

Appendix B.3 - Optical Tip Timing Measurement Systems

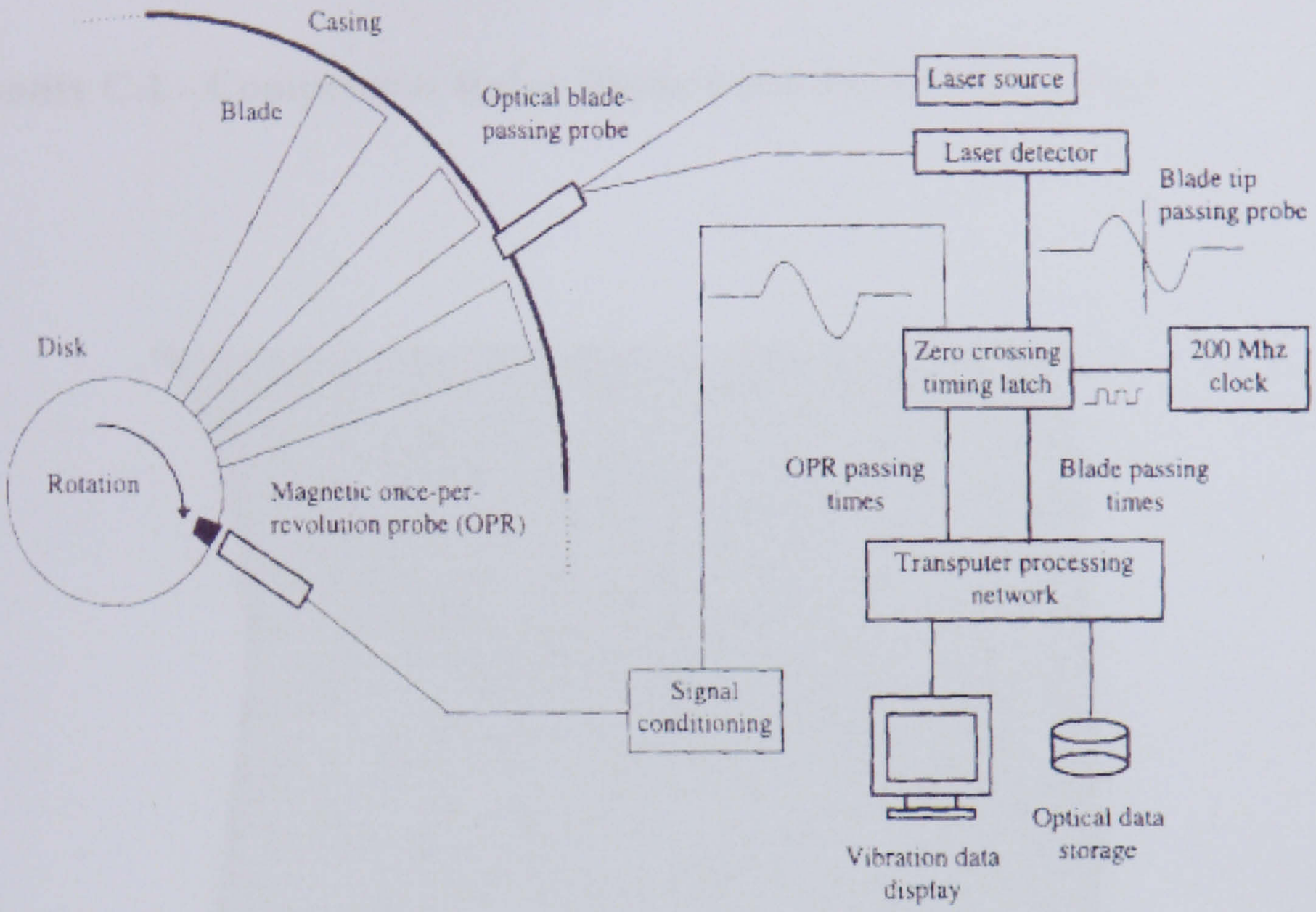

Figure B.3.1 - Optical Tip Timing System Diagram

Source: [27].

Appendix C - Turbomachinery Blade Solid Modelling and FEA

Appendix C.1 - Compressor Rotor Blade Solid Model Generation

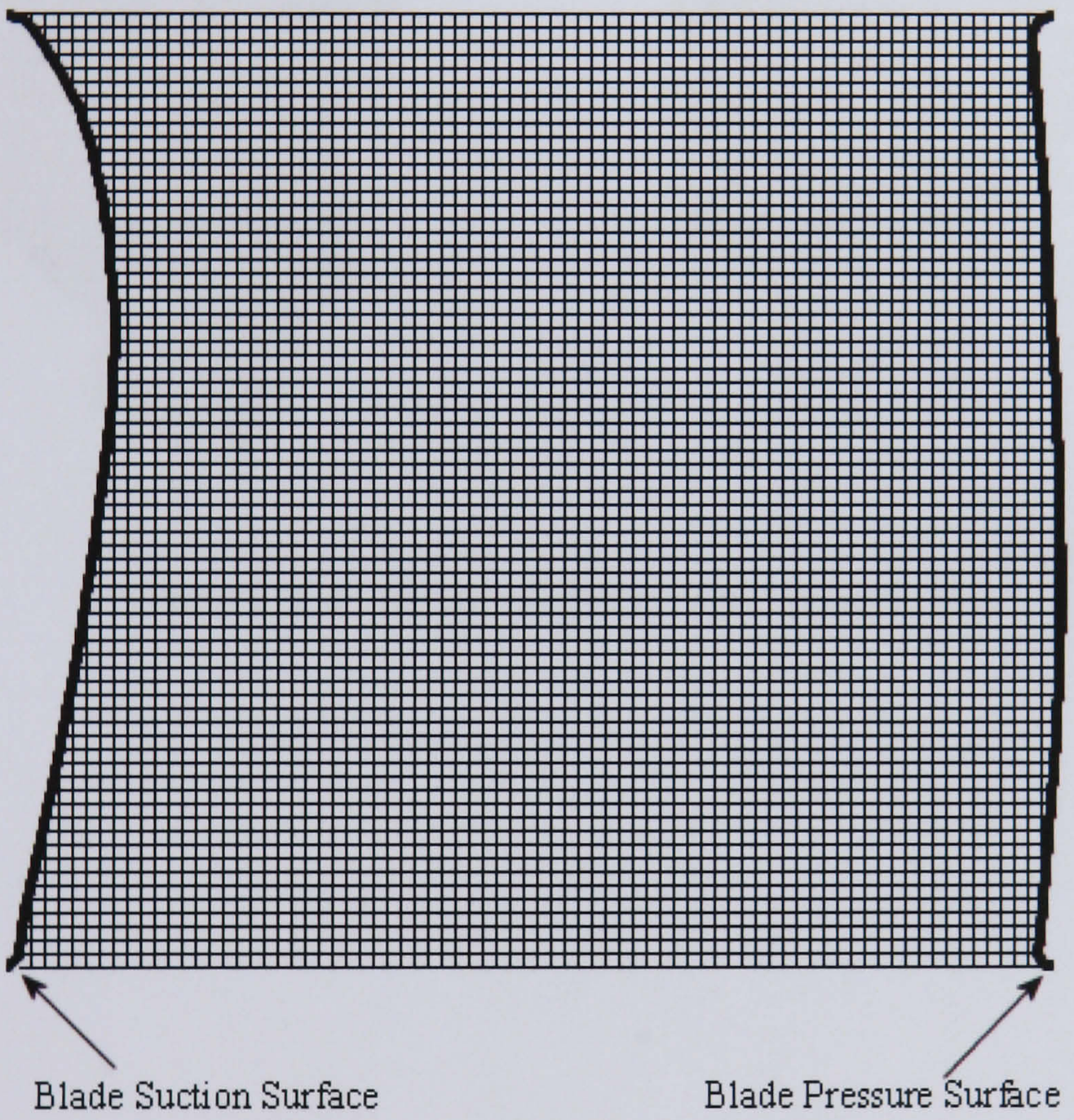

Figure C.1.1 - Physical Representation of CFD Calculation Grid

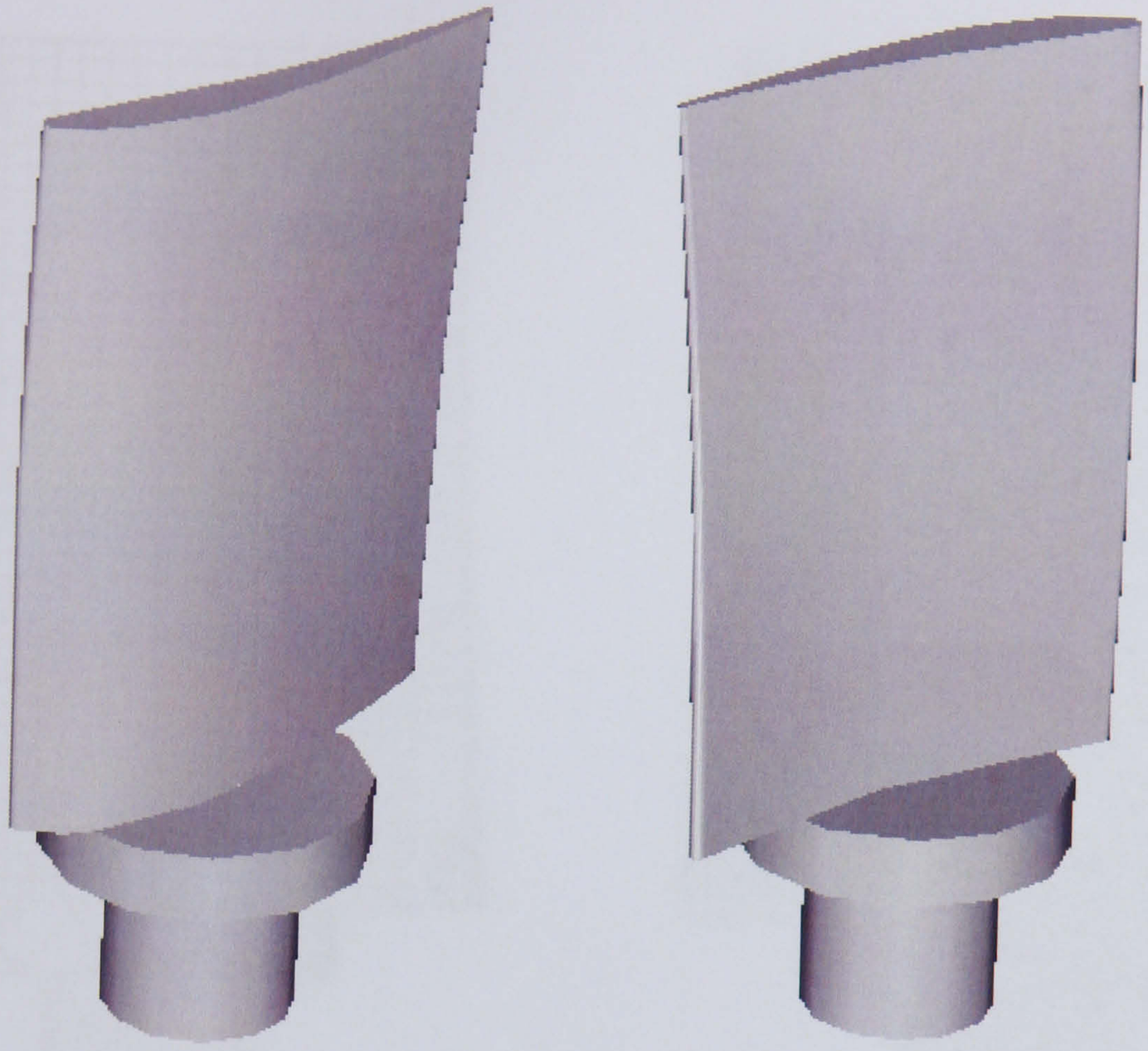

Figure C.1.2 - Rendered Compressor Rotor Blade

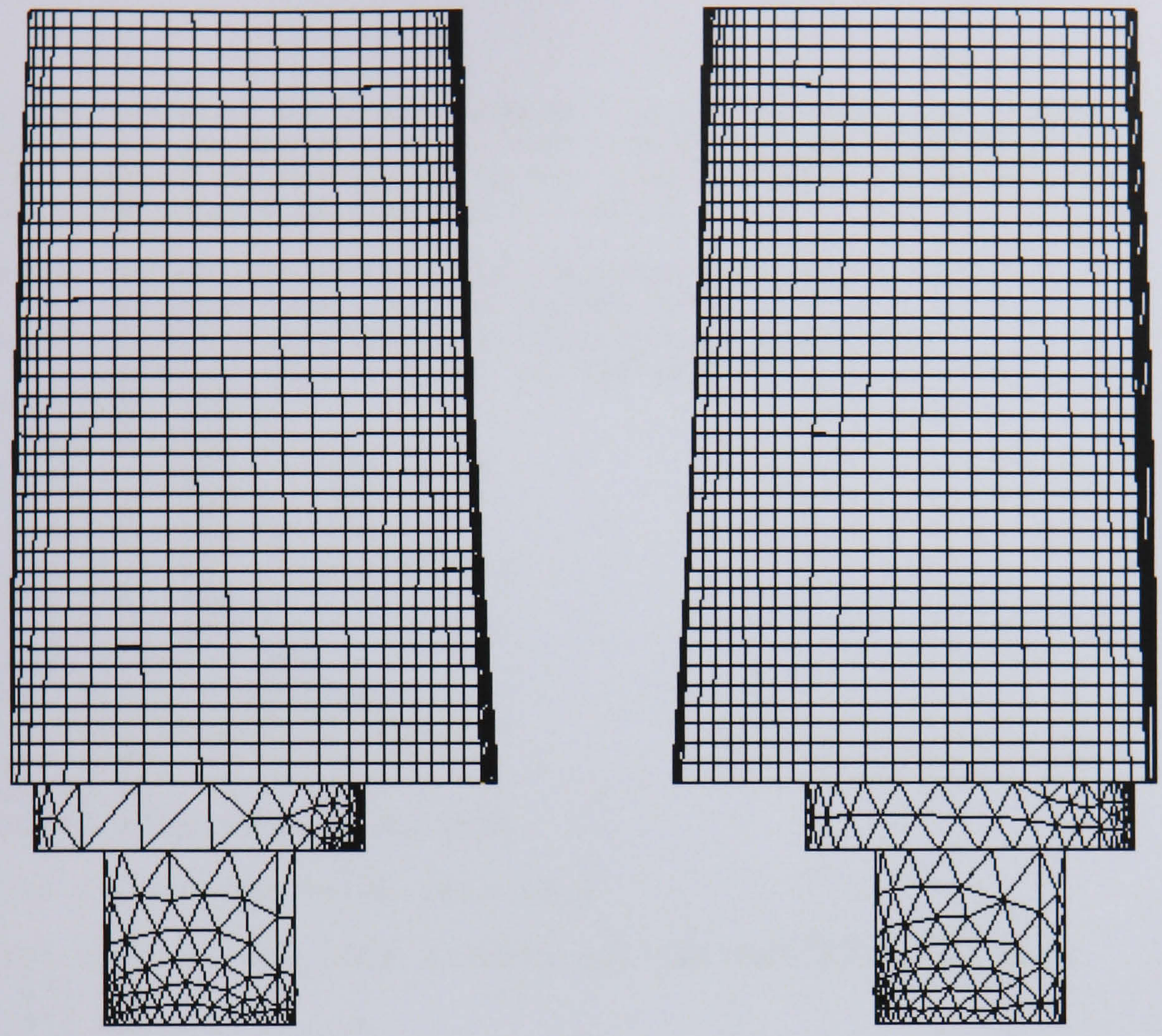

Figure C.1.3 - Compressor Rotor Blade Mesh

Density	2700 kg/m^3
Young's Modulus	71 GPa
Poisson's Ratio	0.33

Table C.1 - LM24 Aluminium Material Properties

Appendix C.2 - Blade Solid Model Generation Fortran Programs

```
C     Fortran program by Craig Lawson. Copyright 2001. All rights reserved.
C     Program to generate a file that can be run as a program in I-DEAS.
C     Reads points on the rotor blade from CFD grid in file grCU_3D.
C     Generates points on the rotor blade.

      open(6, file='rotor79main_blade_pressure_points.txt',
     +     status='new', form='formatted')
      open(7, file='rotor79main_blade_suction_points.txt',
     +     status='new', form='formatted')
      write ( 6, 240 )
      write ( 7, 240 )
240   format ( 12hK : $ return )
      write ( 6, 340 )
      write ( 7, 340 )
340   format ( 14hK : $ /cr m3 p )
      write ( 6, 440 )
      write ( 7, 440 )
440   format ( 7hK : KEY )
      open(13,file='grCITmain')
C     Read file header (3 lines)
      read(13,*)
      read(13,*)
      read(13,*)nz,ny,nx,izin,izot

C     write (6, 550)nz,ny,nx,izin,izot

C     Start nested 'do' loop to read all co-ords from CFD grid
      do i=1,nz
      do j=1,ny
      do k=1,nx
      read(13,*) x_coord,y_coord,z_coord

C     write ( 6, 550 ) x_coord,y_coord,z_coord,i,j,k


C     if statement to select only points on the blade pressure surface
      if (    ( izin .LE. i ) .AND.
     +        ( izot .GE. i ) .AND.
     +        ( k .EQ. nx ) ) write ( 6, 540 ) x_coord,y_coord,z_coord

C     if statement to select only points on the blade suction surface
      if (    ( izin .LE. i ) .AND.
     +        ( izot .GE. i ) .AND.
     +        ( k .EQ. 1 ) ) write ( 7, 540 ) x_coord,y_coord,z_coord


C     Write points to file in format suitable to be read by I-DEAS
540   format ( 3hK :, 2x, F10.7, 1h,, 2x, F10.7, 1h,, 2x, F10.7 )
550   format ( 3hK :, 2x, F11.9, 1h,, 2x, F11.9, 1h,, 2x, F11.9, I5, I5,
     + I5 )

C     End triple nested 'do' loop
      enddo
      enddo
      enddo

C     Write I-DEAS program termination commands
      write ( 6, 640 )
      write ( 7, 640 )
640   format ( 22hK : $ mpos :; /F PR E )
      write ( 6, 740 )
      write ( 7, 740 )
740   format ( 29hE : **** END OF SESSION **** )
      close(6)
      close(7)
      END
```

```
C     Fortran program by Craig Lawson. Copyright 2001. All rights reserved
C     Program to generate a file that can be run as a program in I-DEAS.
C     Reads points on the rotor blade from CFD grid in file grCU_3D.
C     Generates blade SPAN-WISE SPLINES on the SUCTION surface of the
C     rotor blade.

C     Define a variable to count the span-wise position of the data point
      INTEGER ROWS = 0

      open(6, file='rotor79s_blade_suction_spanwise_splines.txt',
     +           status='new', form='formatted')

C     Write I-DEAS spline-from-points creation commands to the output file
      write ( 6, 240 )
240   format ( 12hK : $ return )
      write ( 6, 340 )
340   format ( 15hK : $ /cr m3 sp )
      write ( 6, 440 )
440   format ( 7hK : KEY )

C     Open and read CFD grid file
      open(13,file='grCIT-18-main')
      read(13,*)
      read(13,*)
      read(13,*)nz,ny,nx,izin,izot
C     Start nested 'do' loop to read all the co-ords from the CFD grid
      do i=1,nz
      do j=1,ny
      do k=1,nx
      read(13,*) x_coord,y_coord,z_coord

C     if end of span-wise row is reached (45th point) write I-DEAS command
C     to end current spline
      if ( ROWS .GE. ny ) write ( 6, 500 )
500   format ( 4hK :  )
C     if end of span-wise row is reached (45th point) write I-DEAS command
C     to start new spline
      if ( ROWS .GE. ny ) write ( 6, 520 )
520   format ( 8hK : OKAY )
C     Reset row counter
      if ( ROWS .GE. ny )  ROWS = 0
C     if statement to select only points on the blade pressure surface
      if (    ( izin .LE. i ) .AND.
     +        ( izot .GE. i ) .AND.
     +        ( k .EQ. 1 ) ) write ( 6, 540 ) x_coord,y_coord,z_coord
540   format ( 3hK :, 2x, F10.7, 1h,, 2x, F10.7, 1h,, 2x, F10.7 )

C     After each suction side point is writen to output file increment
C     span-wise counter
      if (    ( izin .LE. i ) .AND.
     +        ( izot .GE. i ) .AND.
     +        ( k .EQ. 1 ) ) ROWS = ROWS + 1

C     End nested 'do' loop
      enddo
      enddo
      enddo

C     Write I-DEAS program termination commands to the output file
      write ( 6, 640 )
640   format ( 22hK : $ mpos :; /F PR E )
      write ( 6, 740 )
740   format ( 29hE : **** END OF SESSION **** )
      close(6)
      END
```

Appendix C.3 - Rotor Blade FEA Natural Frequency and Mode Shapes

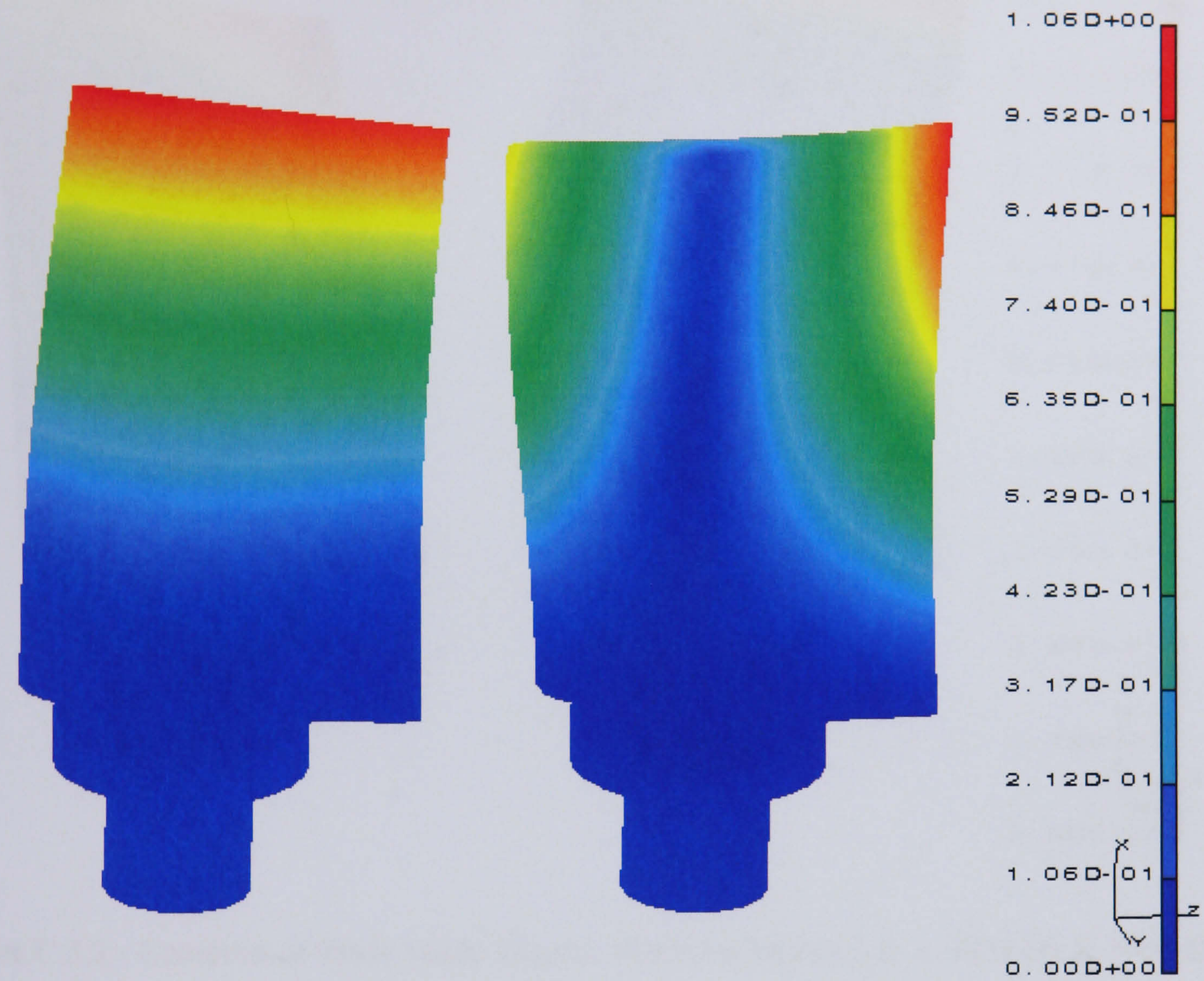

Figure C.3.1 - Compressor Blade Mode Shapes: Vibration Modes 1 & 2, 725 Hz & 2061 Hz

NB: The scale shows normalised displacement in meters.

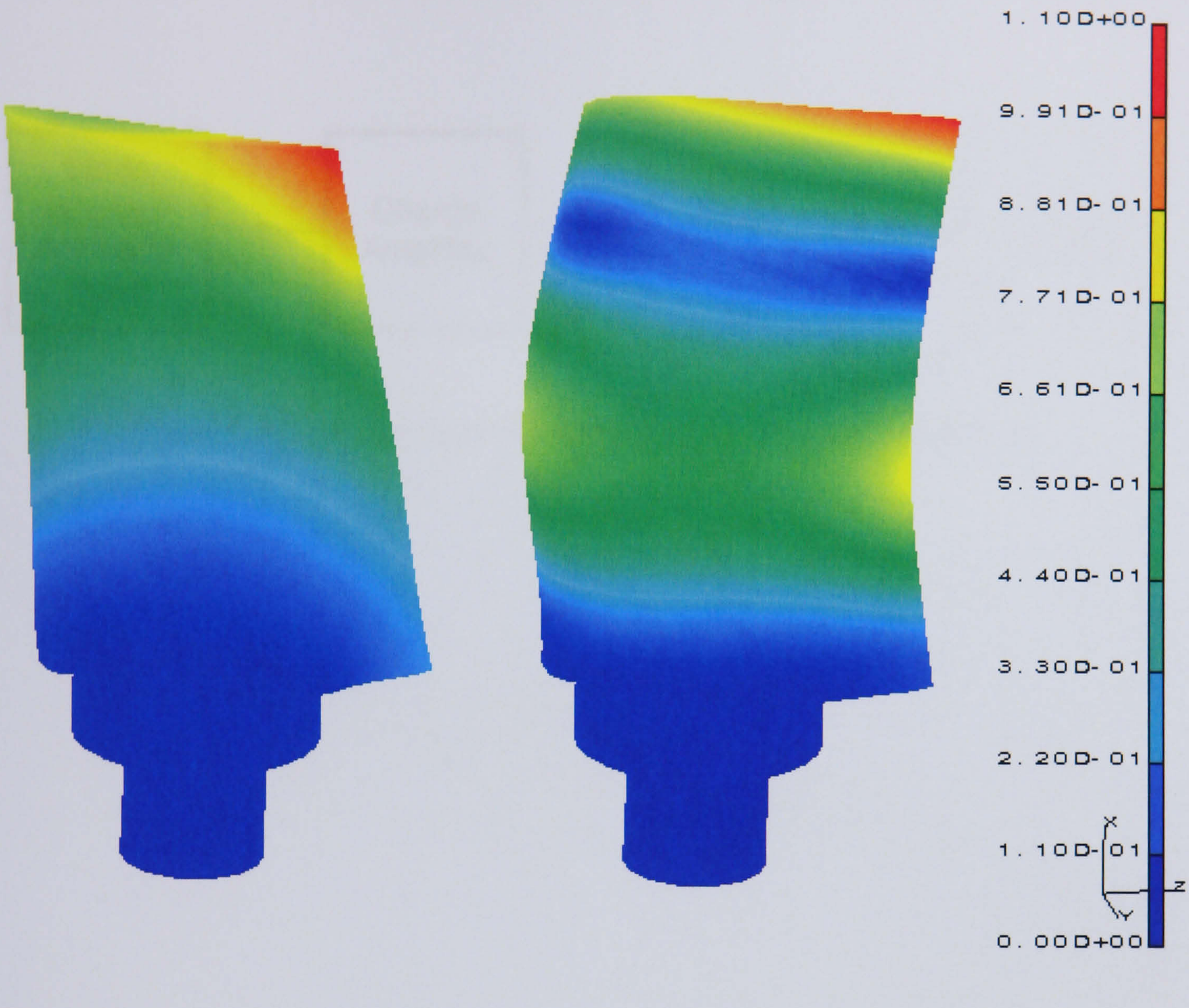

Figure C.3.2 - Compressor Blade Mode Shapes: Vibration Modes 3 & 4, 3478 Hz & 3950 Hz

NB: The scale shows normalised displacement in meters.

Appendix C.4 - Finite Element Analysis Simulation Verification Experiment

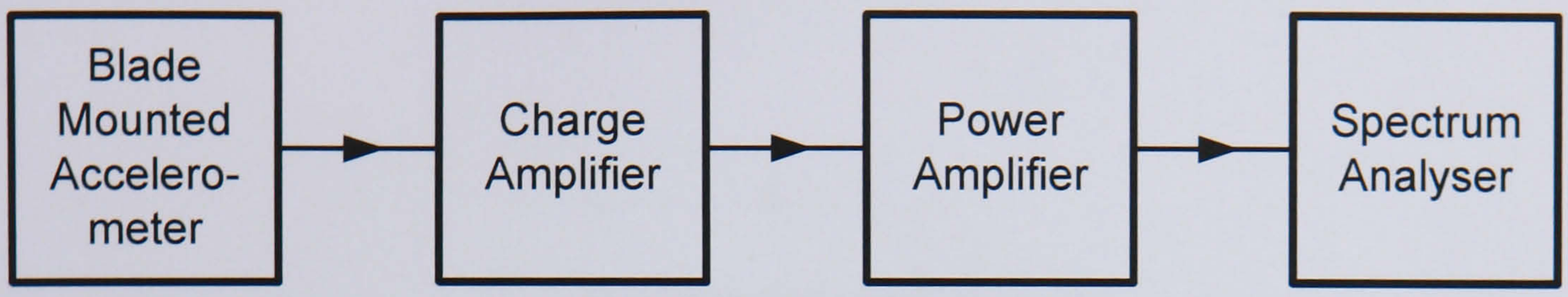

Figure C.4.1 - Rotor Blade Natural Frequency Accelerometer Tests

Appendix C.5 - Blade Mounted Strain Gauge Locations

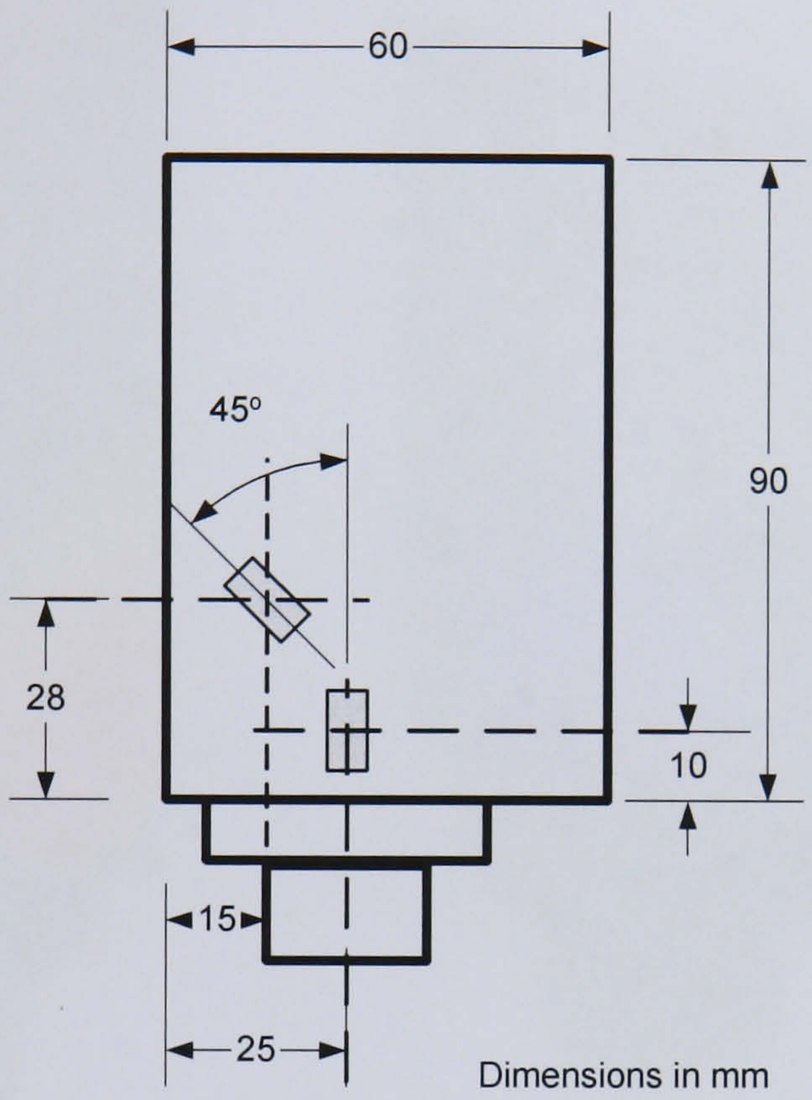

Figure C.5.1 - Blade Mounted Strain Gauge Locations

Appendix C.6 - Rotor Blade FEA Strain Results

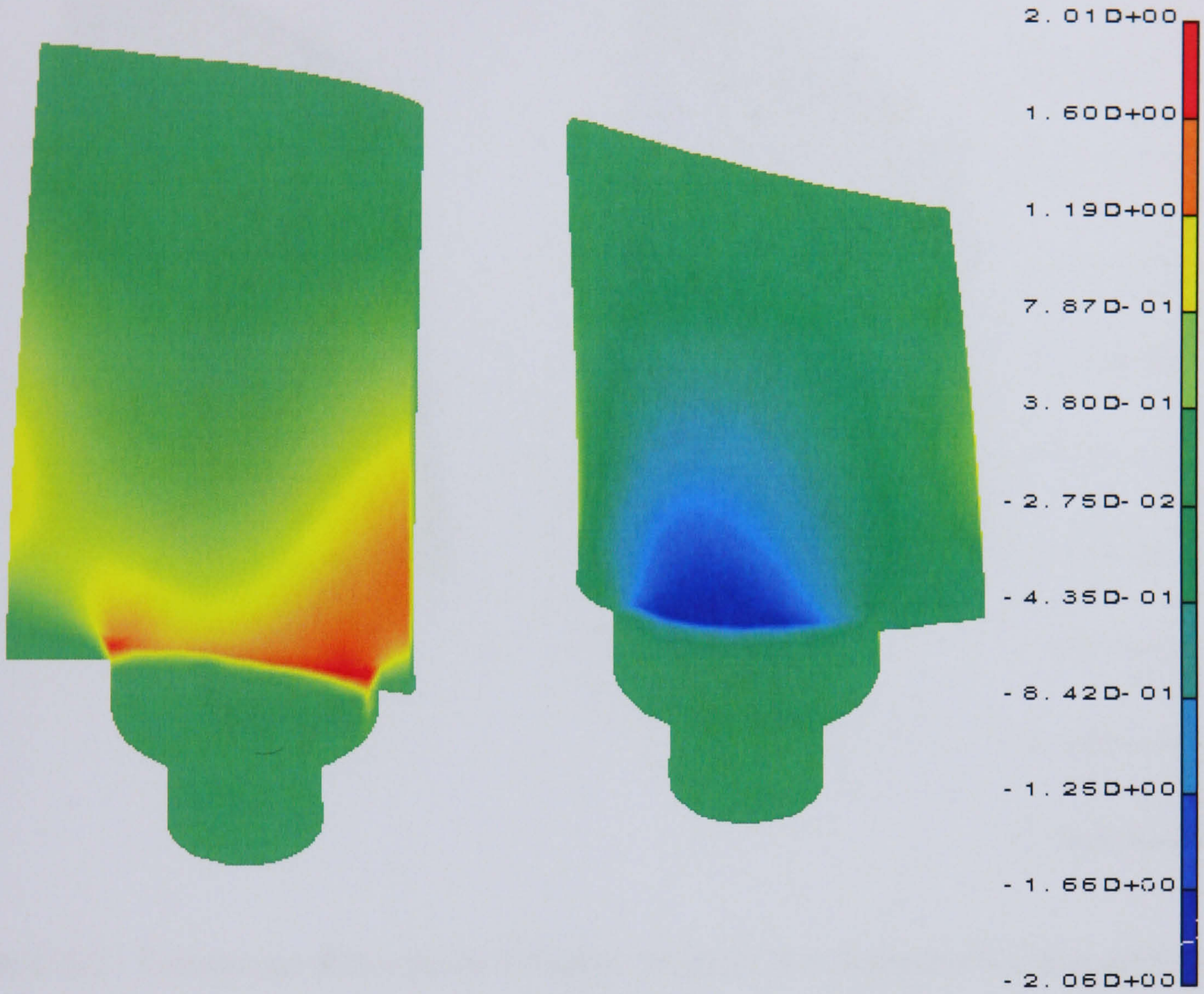

Figure C.6.1 - Compressor Rotor Blade Vibration Mode 1: X Direction Normalised Strain

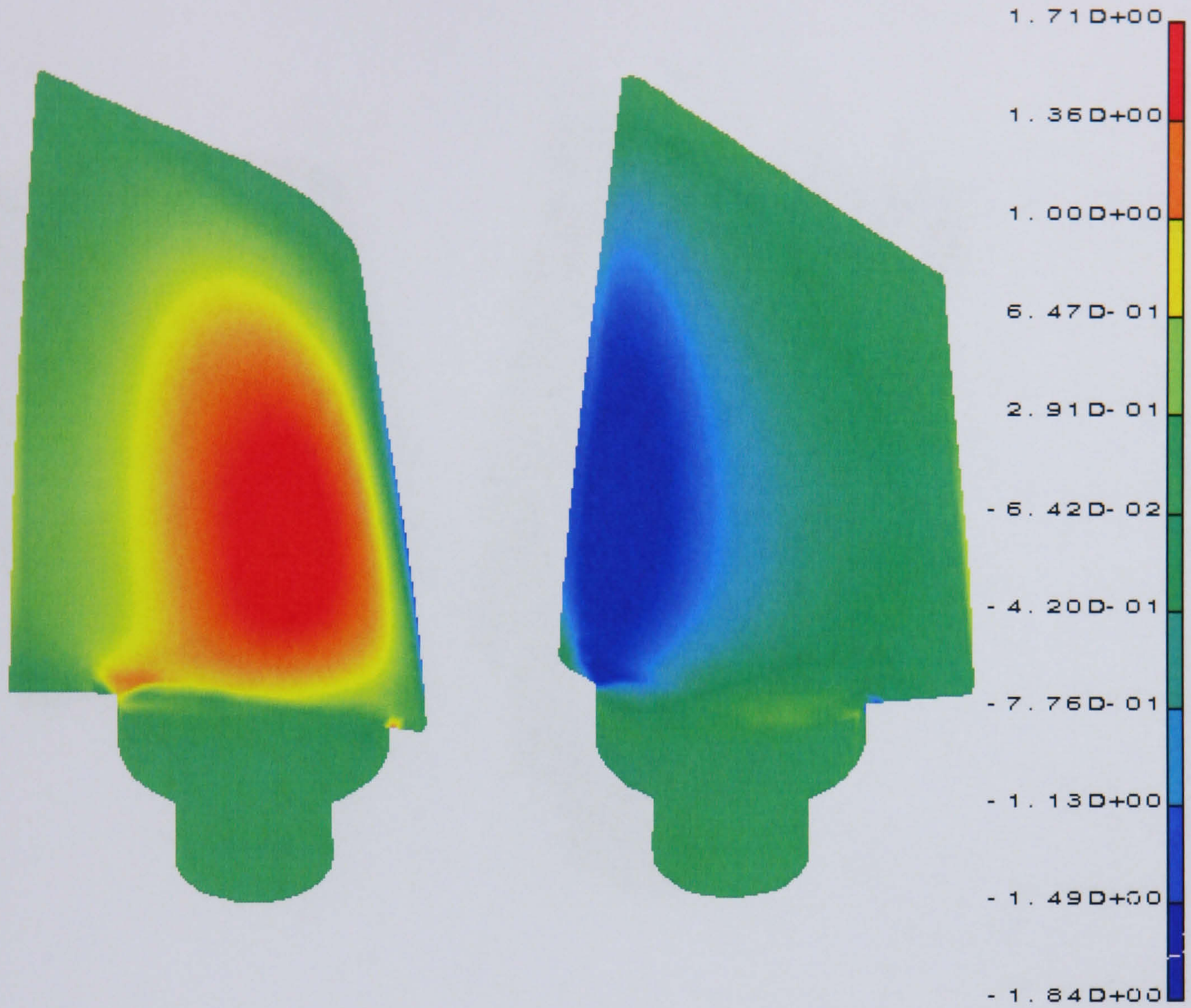

Figure C.6.2 - Compressor Rotor Blade Vibration Mode 2: X-Y Direction Normalised Strain

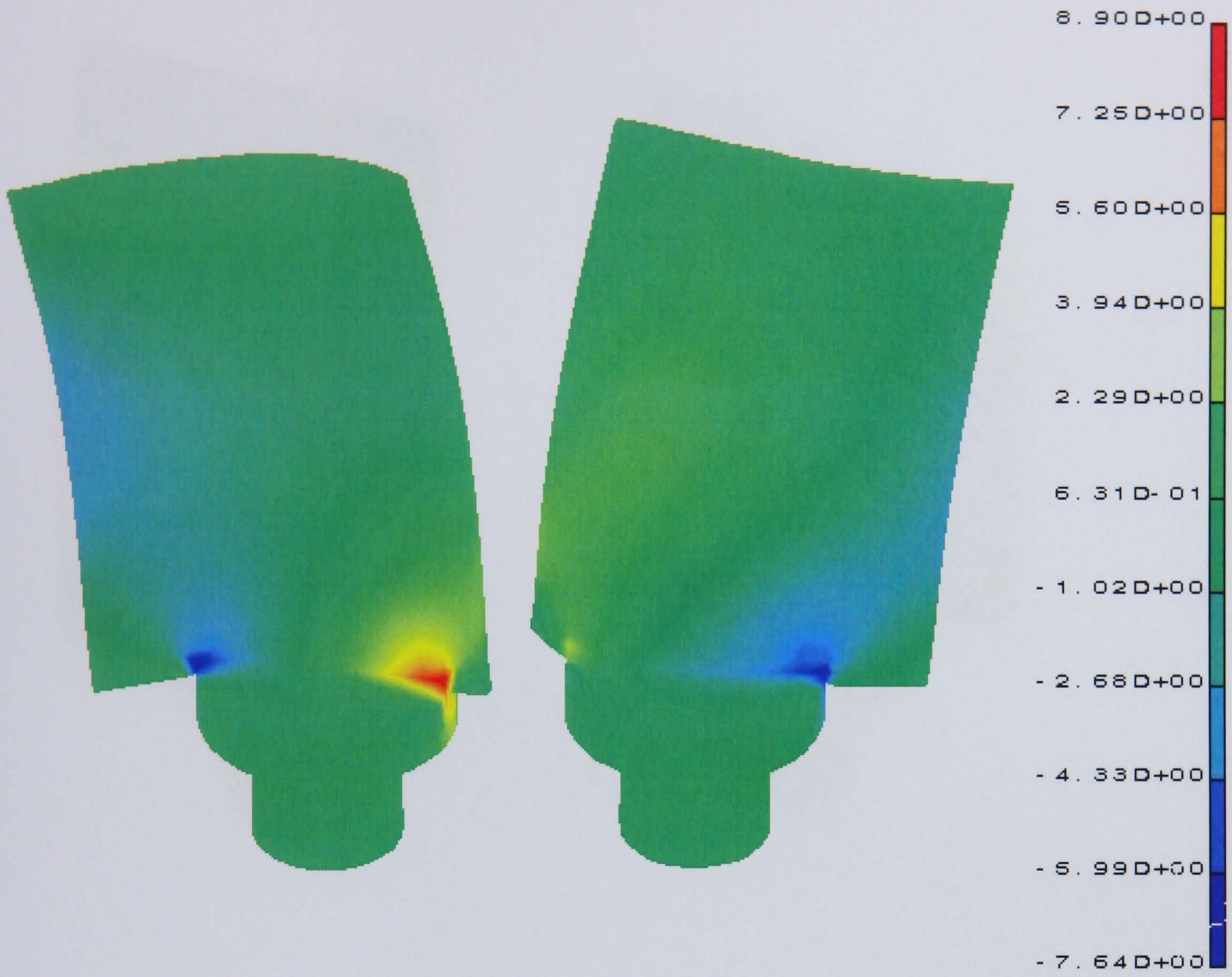

Figure C.6.3 - Compressor Rotor Blade Vibration Mode 3: X-Direction Normalised Strain

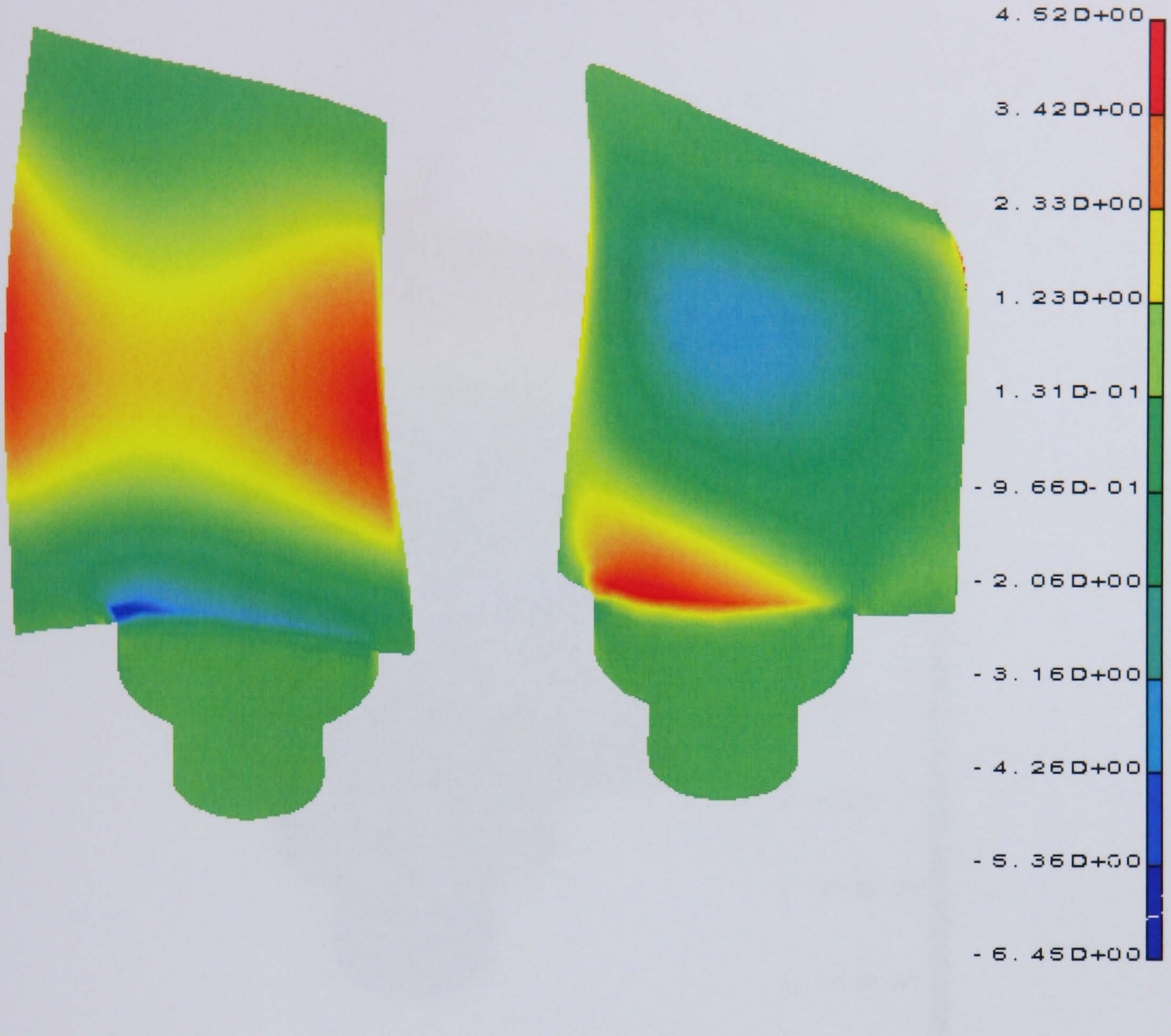

Figure C.6.4 - Compressor Rotor Blade Vibration Mode 4: X-Direction Normalised Strain

Appendix C.7 - Rotor Blade FEA Deflection Results

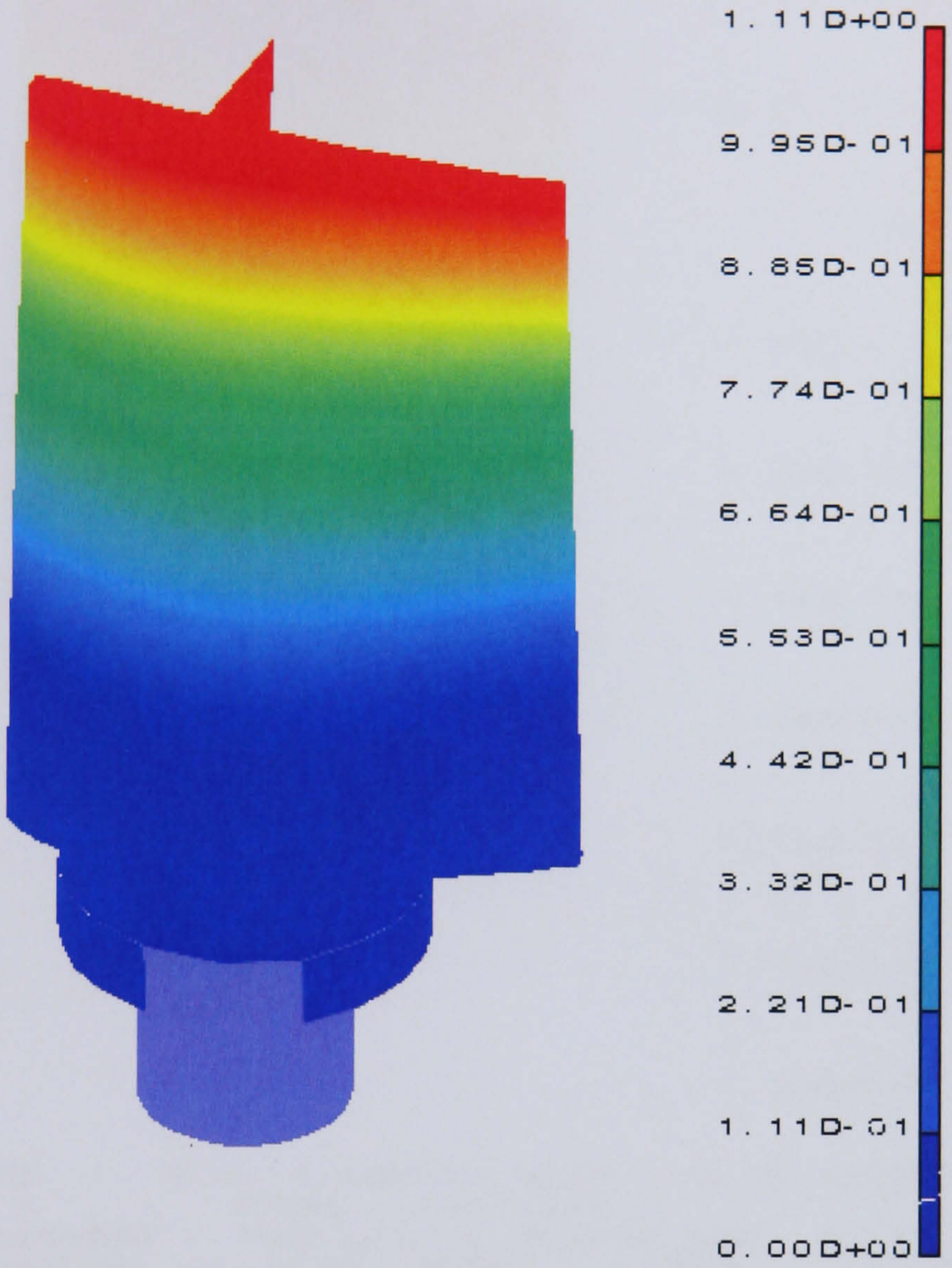

Figure C.7.1 - Compressor Rotor Blade 930Hz Forced Response

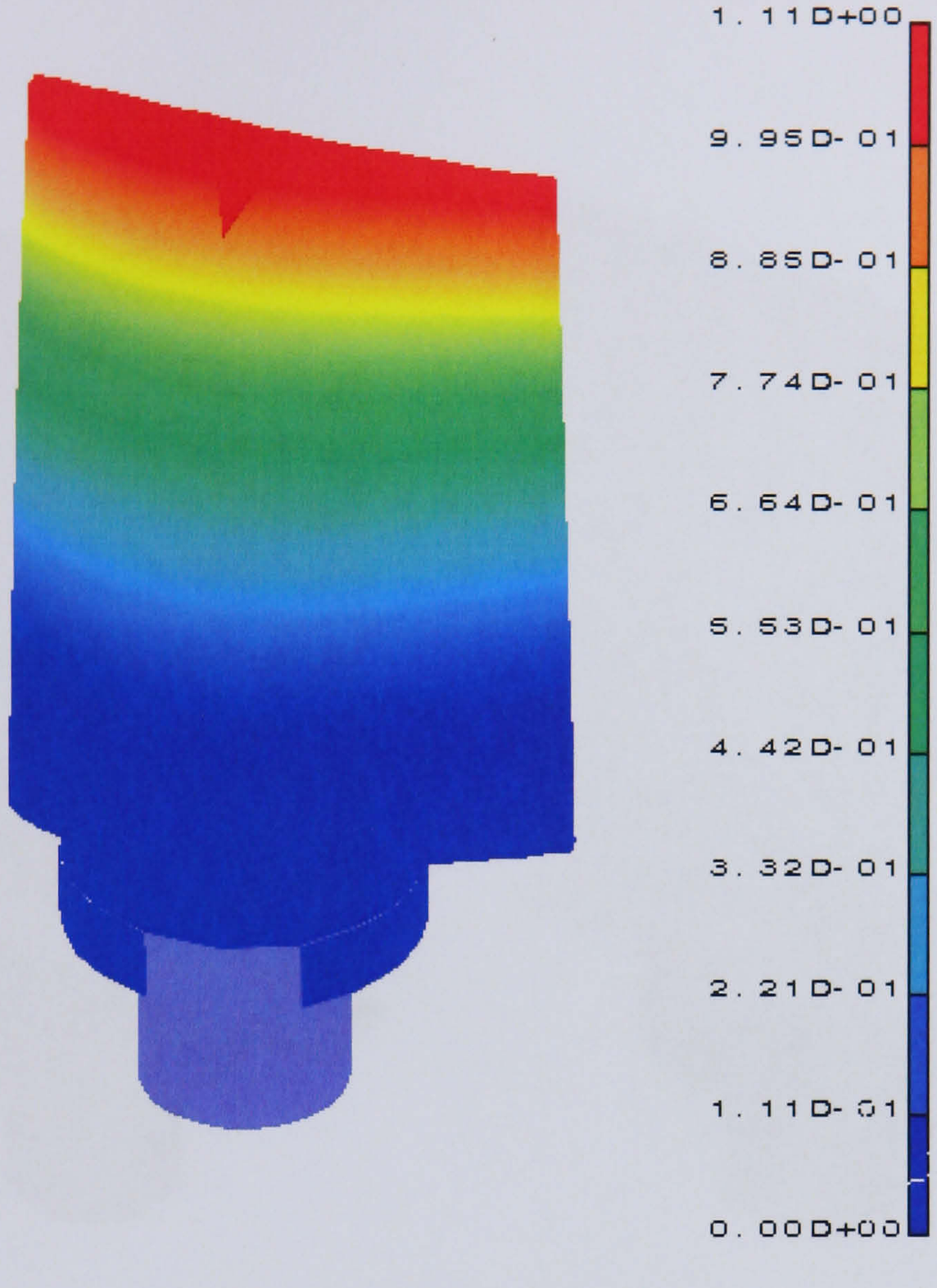

Figure C.7.2 - Compressor Rotor Blade Vibration Mode 1 Resonance Forced Response

Appendix C.8 - Quasi Blade Geometry

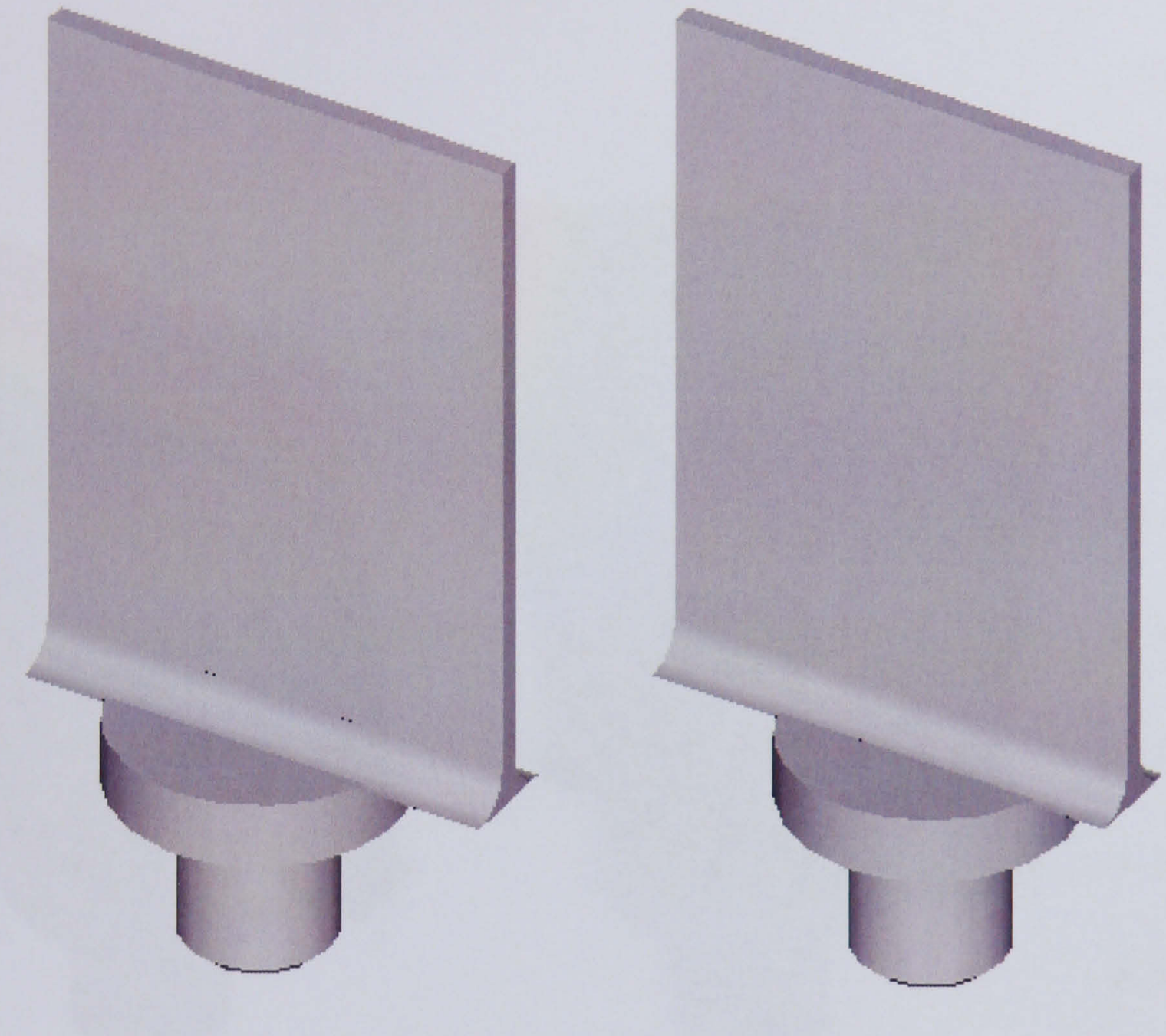

Figure C.8.1 - Rendered Quasi Blade

Appendix C.9 - Quasi Rotor Blade FEA Natural Frequencies and Mode Shapes

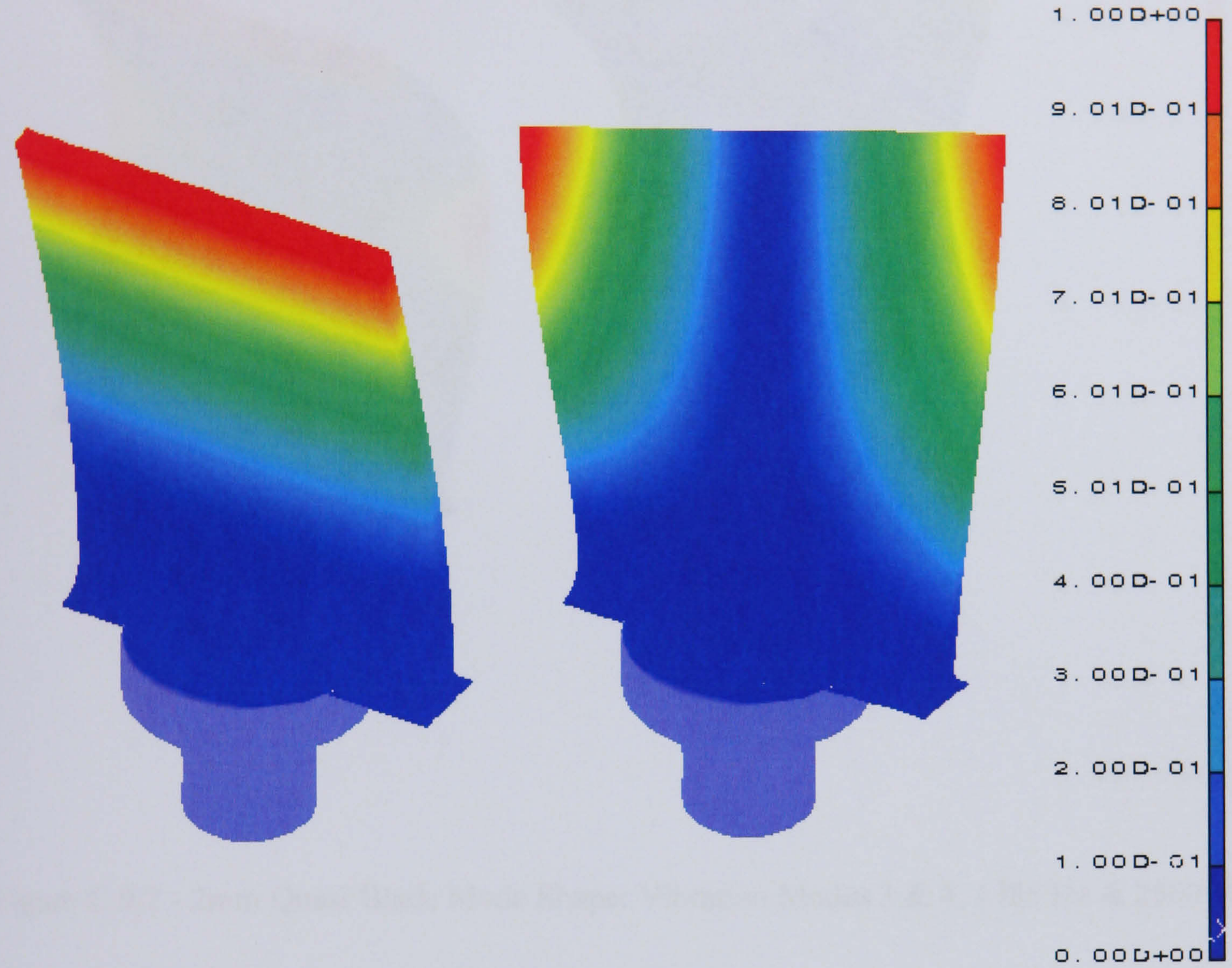

Figure C.9.1 - 2mm Quasi Blade Mode Shape: Vibration Modes 1 & 2, 243 Hz & 740 Hz

NB: The scale shows normalised displacement in meters.

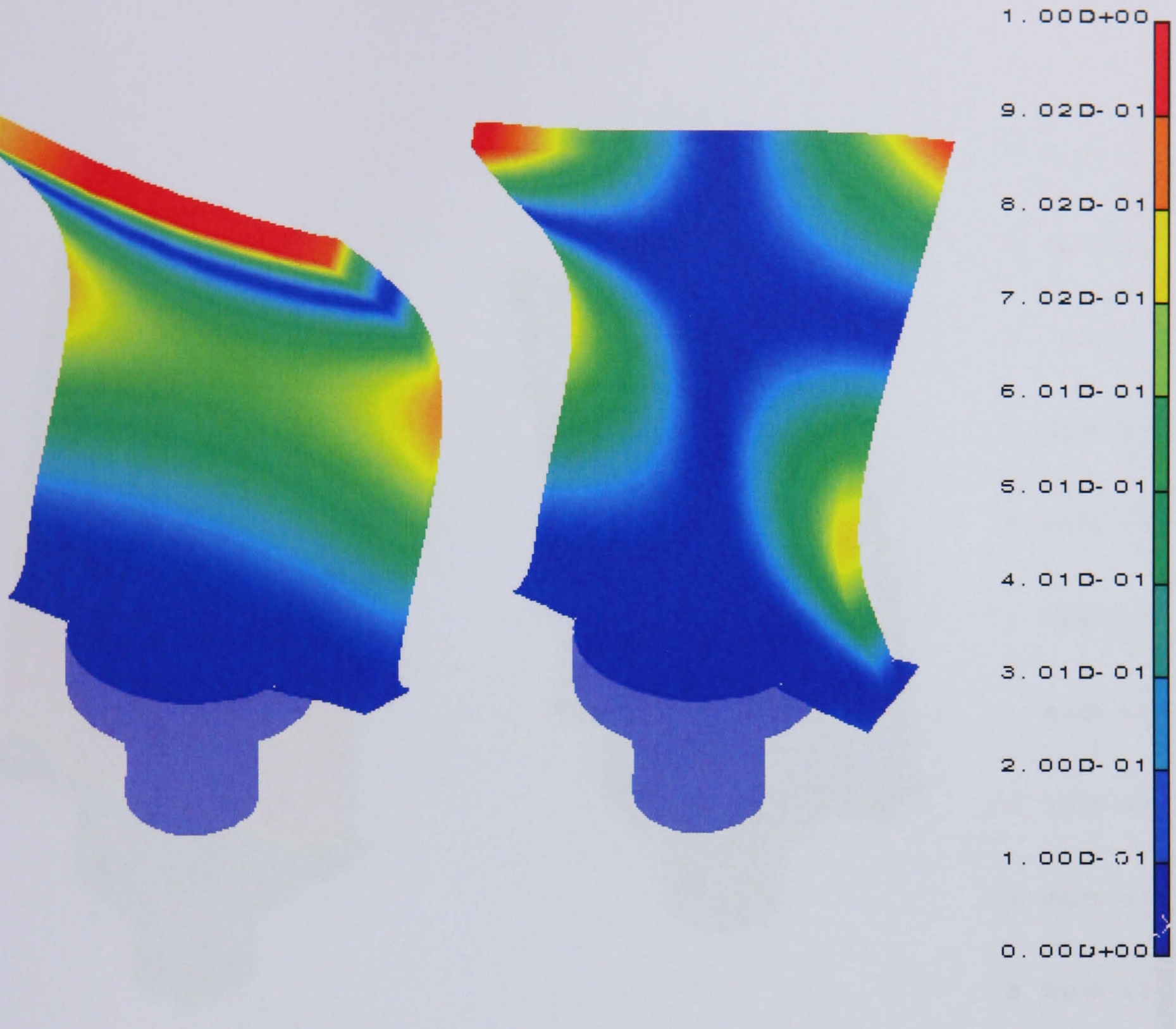

Figure C.9.2 - 2mm Quasi Blade Mode Shape: Vibration Modes 3 & 4, 1486 Hz & 2540 Hz

NB: The scale shows normalised displacement in meters.

Appendix C.10 - Quasi Rotor Blade FEA Strain Results

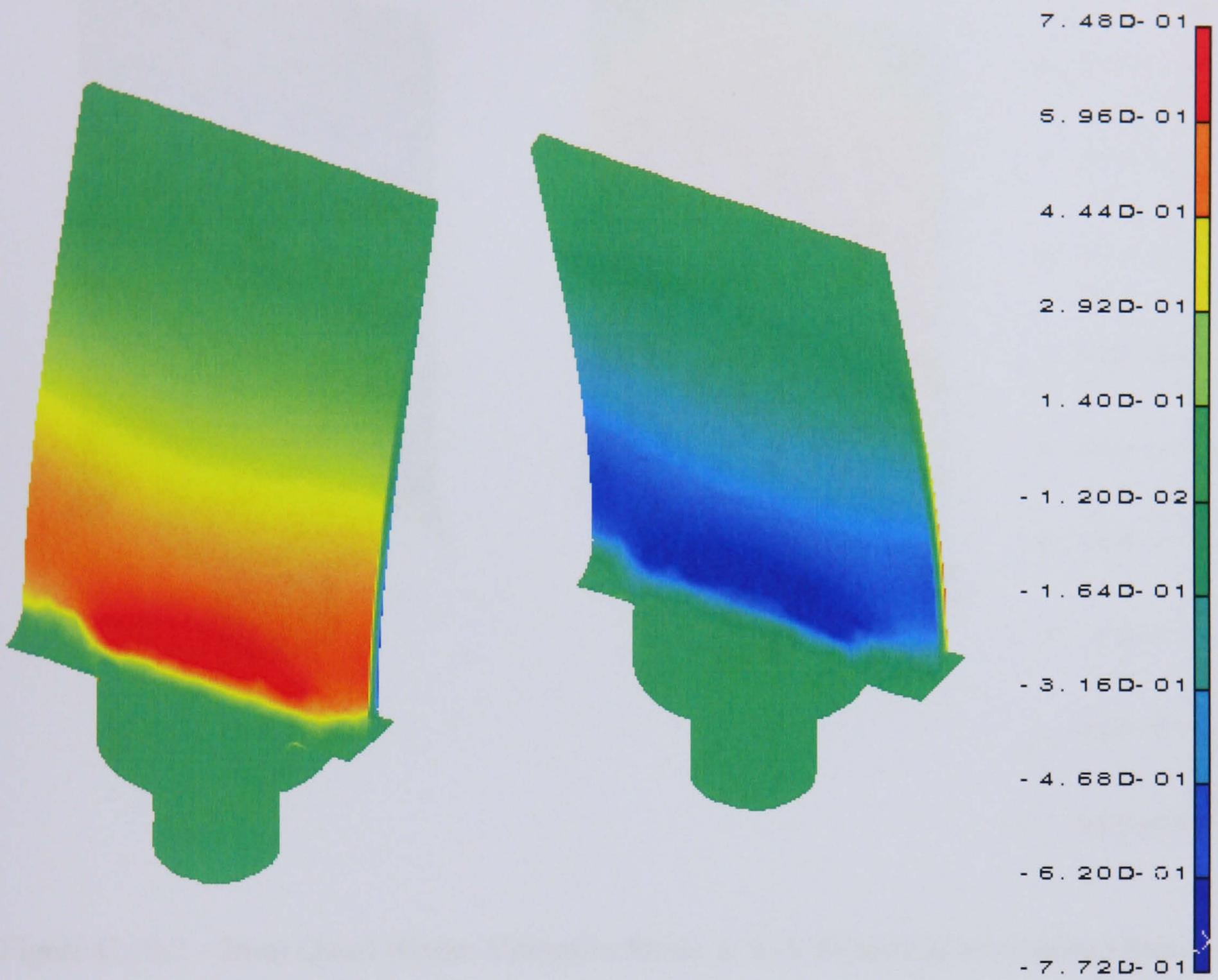

Figure C.10.1 - 2mm Quasi Blade: Vibration Mode 1, X Direction Normalised Strain

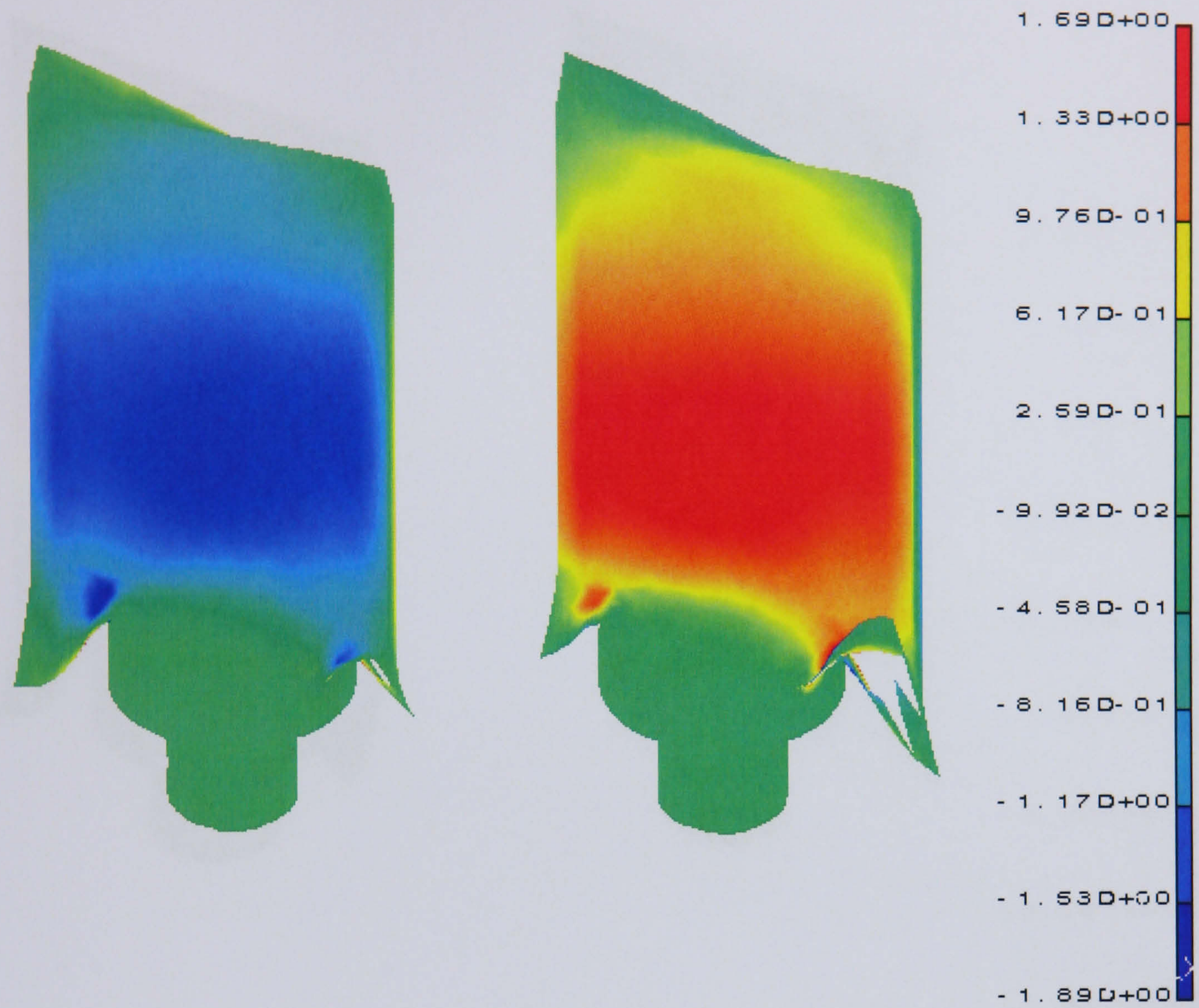

Figure C.10.2 - 2mm Quasi Blade: Vibration Mode 2, X-Y Direction Normalised Strain

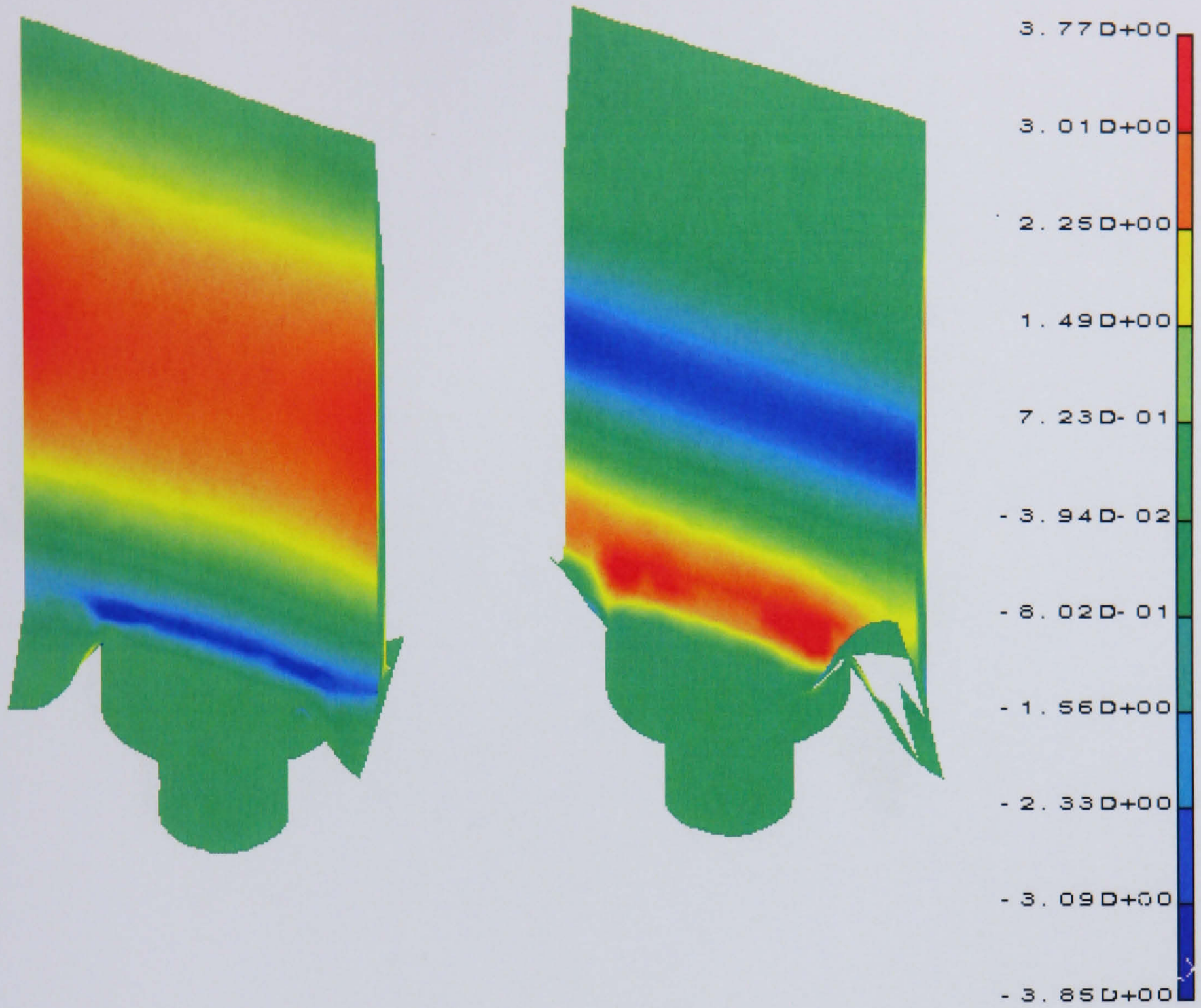

Figure C.10.3 - 2mm Quasi Blade: Vibration Mode 3, X Direction Normalised Strain

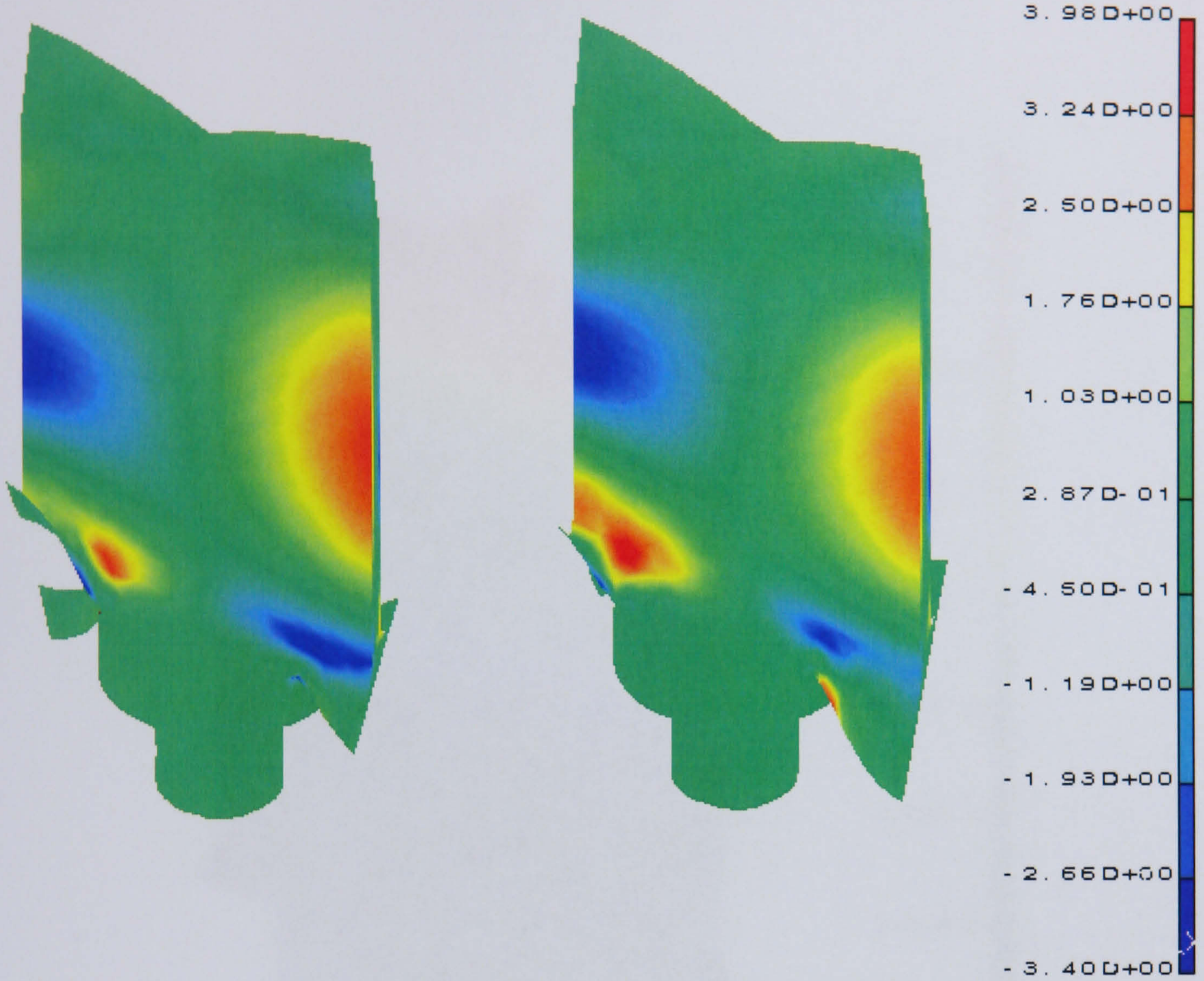

Figure C.10.4 - 2mm Quasi Blade: Vibration Mode 4, X Direction Normalised Strain

Appendix C.11 - Quasi Rotor Blade FEA Deflection Results

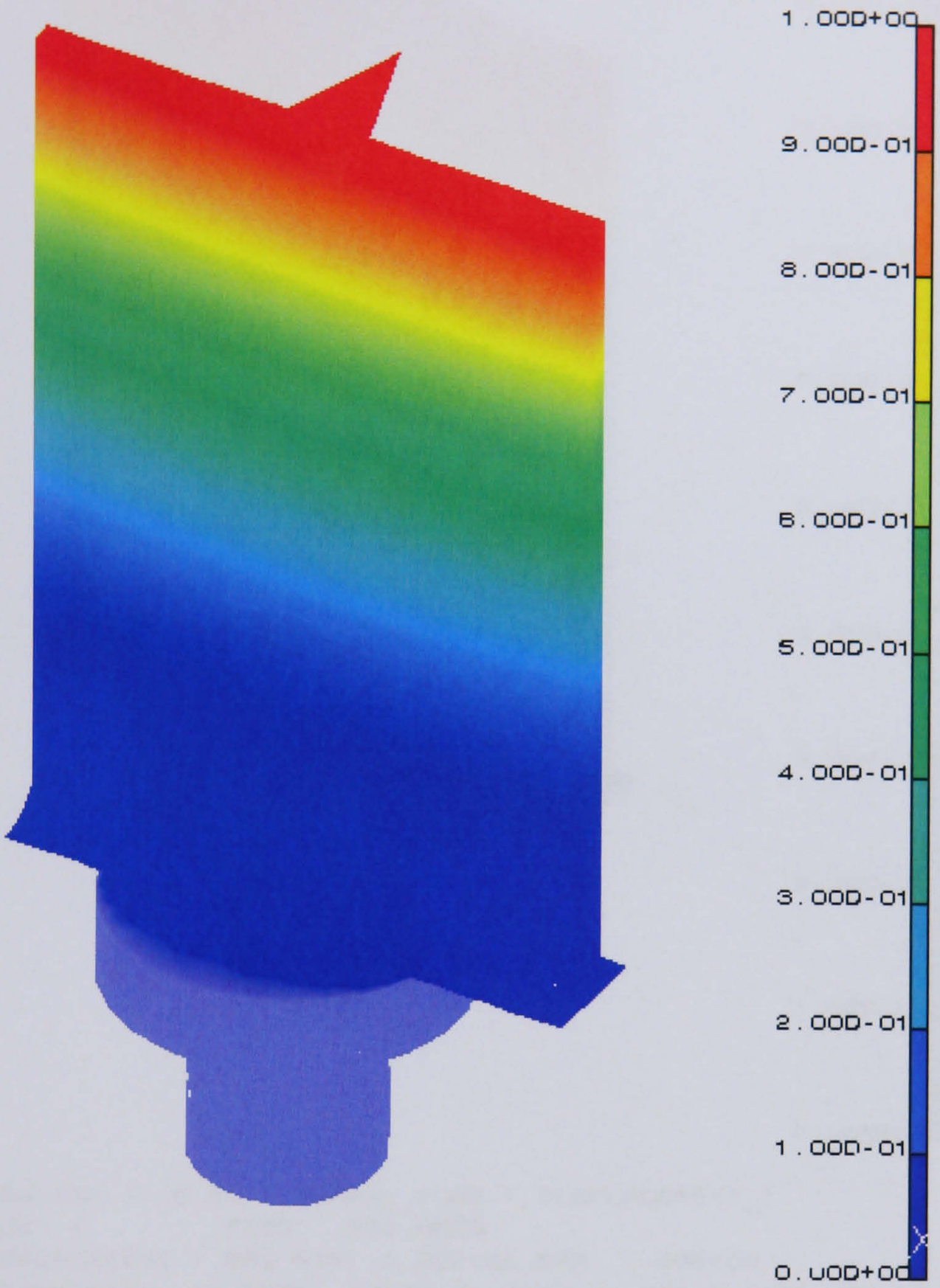

RESULTS: 1- B.C. 1,NORMAL_MODE 1,DISPLACEMENT_1
MODE: 1 FREQ: 242.9051
DISPLACEMENT - MAG MIN: 0.00E+00 MAX: 1.00E+00
DEFORMATION: 16-RESP, EVENT 5, FREQ = 250.0,DISPLACE_16
FREQSTEP: 26 FREQ: 250.0
DISPLACEMENT - MAG MIN: 0.00E+00 MAX: 1.76E-03
FRAME OF REF: PART

Figure C.11.1 - 2mm Quasi Blade: Vibration Mode 1 Resonance Forced Response

NB: The text in the red box shows the maximum tip deflection in meters at mid chord.

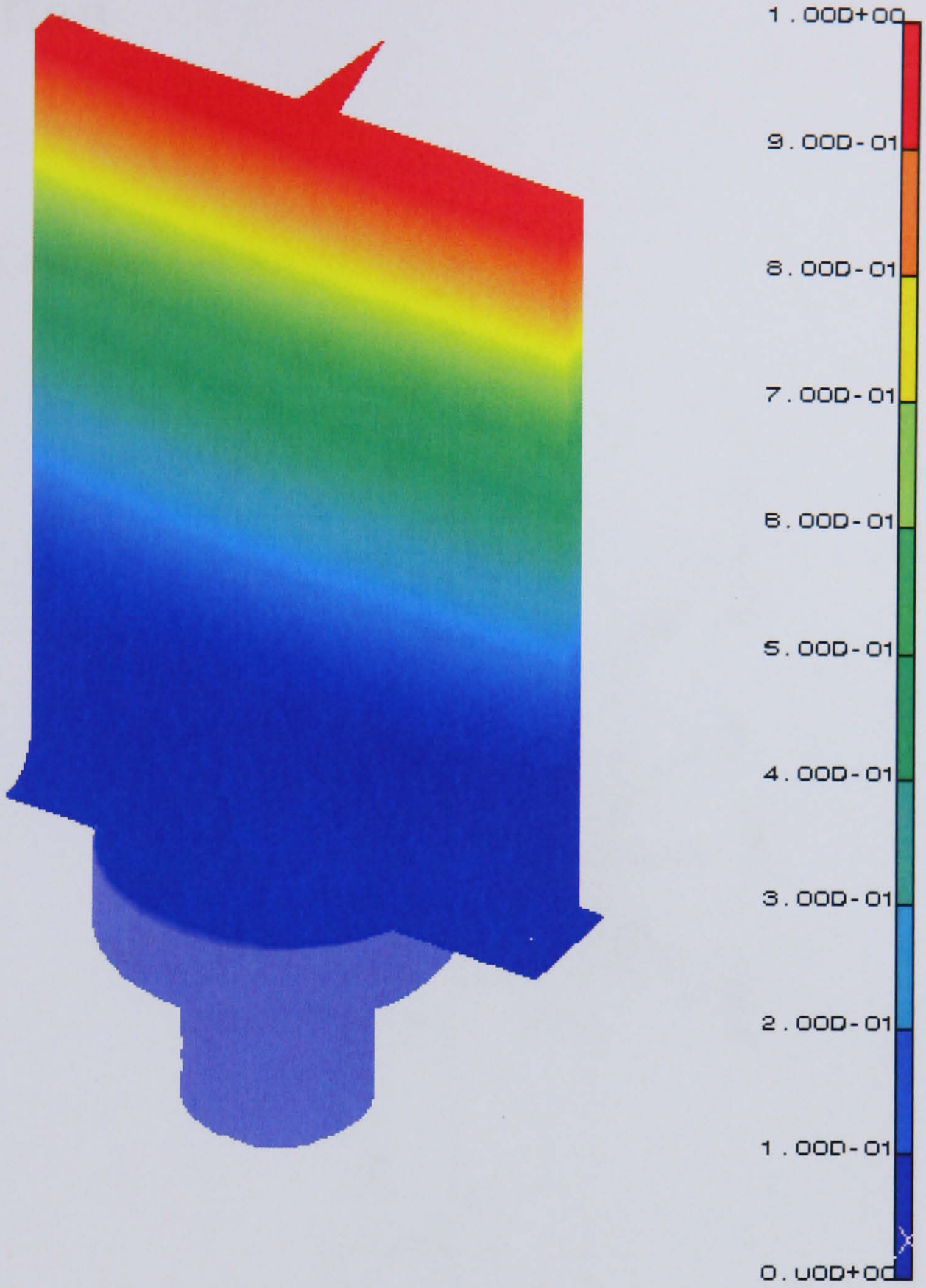

Figure C.11.2 - 3mm Quasi Blade: Vibration Mode 1 Resonance Forced Response

NB: The text in the red box shows the maximum tip deflection in meters at mid chord.

Appendix D - Experiment Equipment and Instumentation

Appendix D.1 - Compressor Test Facility

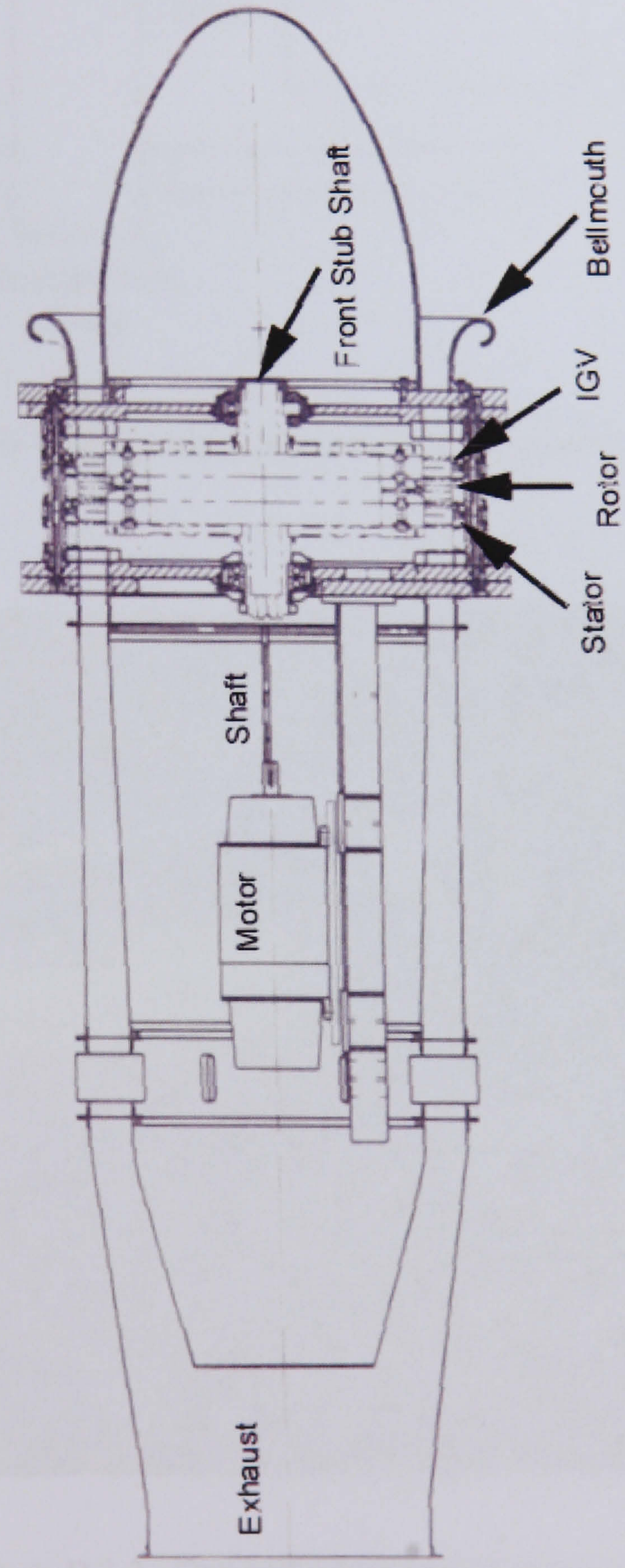

Figure D.1.1 - Compressor Test Facility Schematic

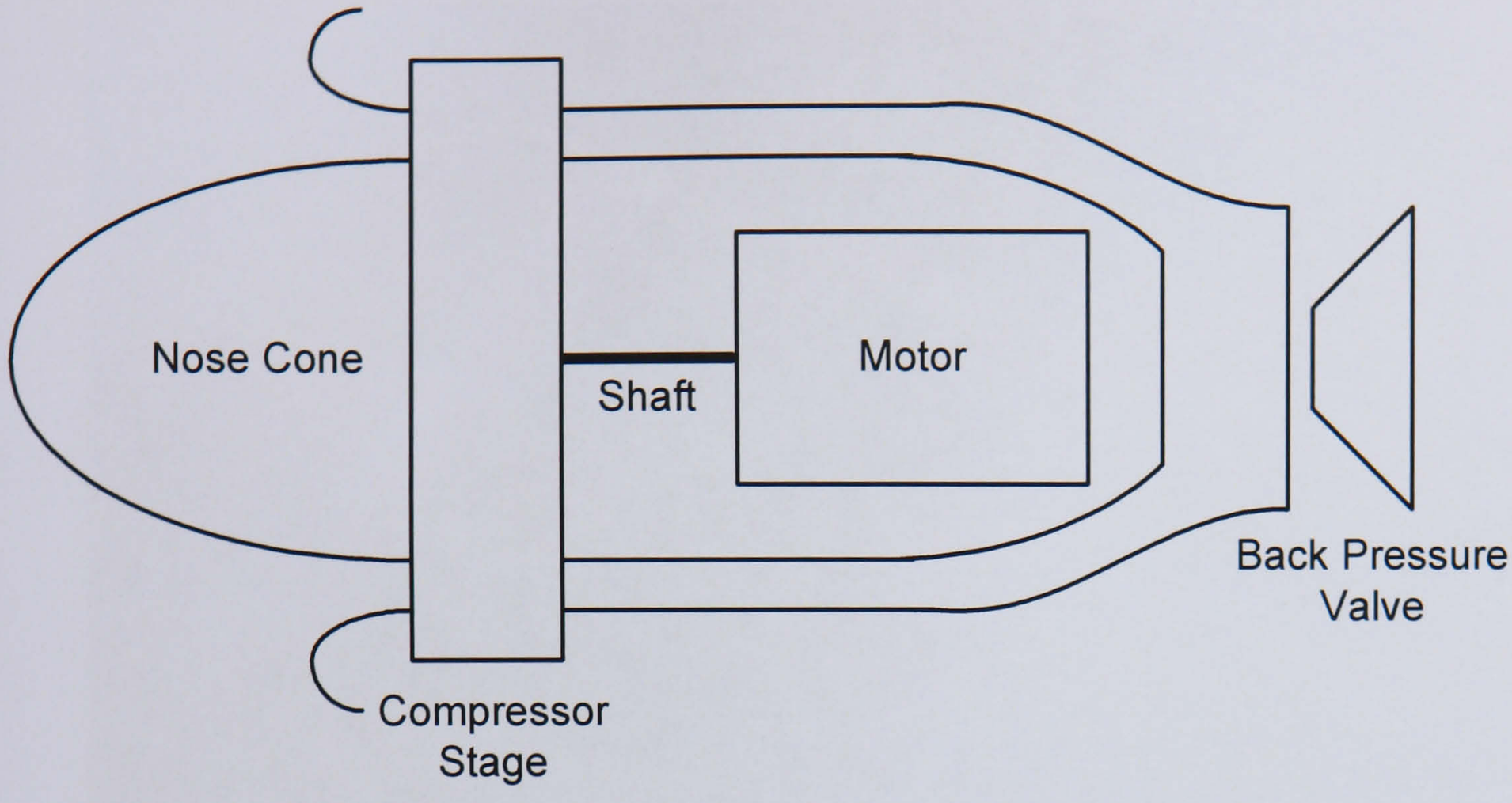

Figure D.1.2 - Compressor Test Facility Schematic Illustrating the Electric Motor Positioning

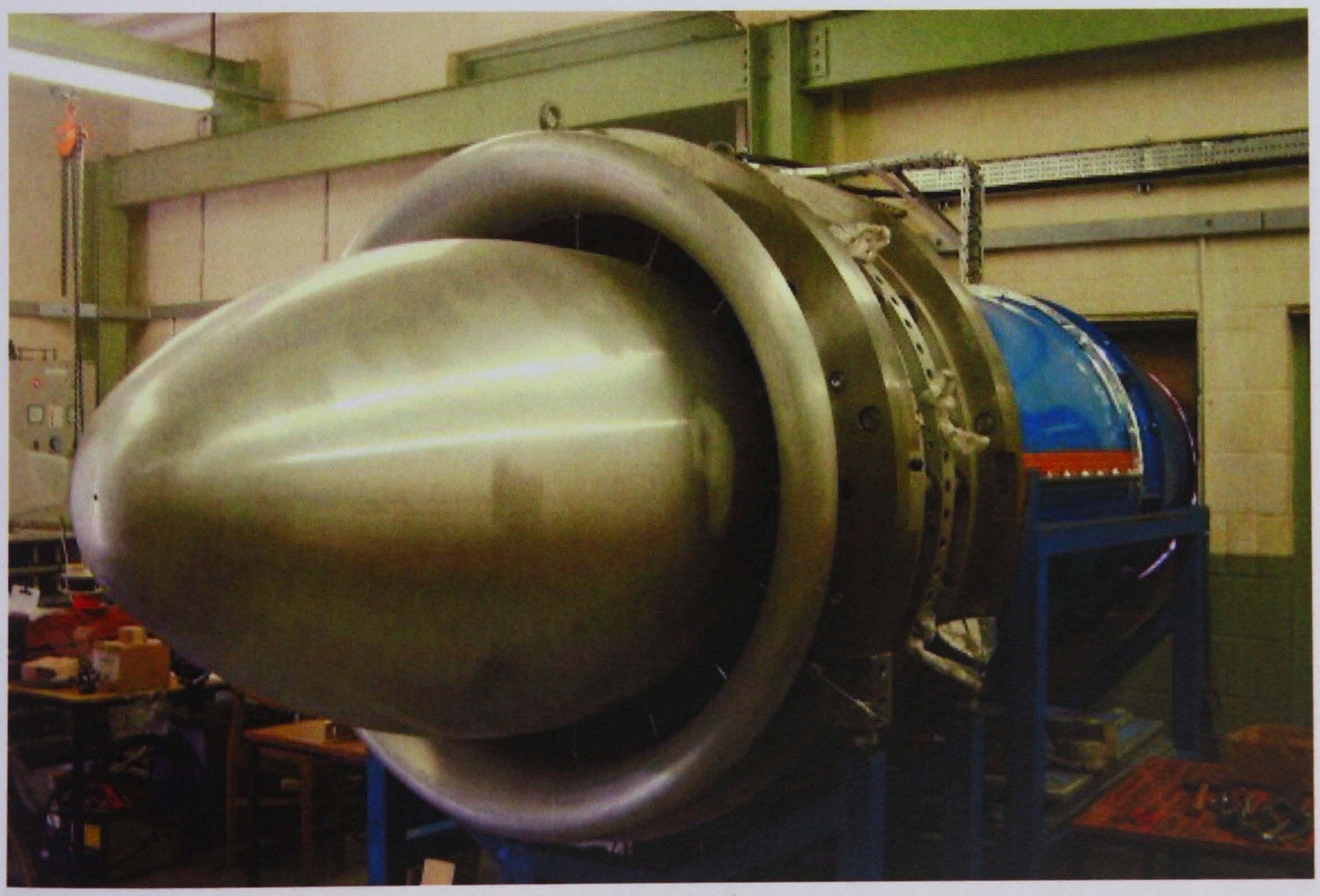

Figure D.1.3 - One-and-a-half Stage Compressor

Figure D.1.4 - One-and-a-half Stage Compressor Intake

Figure D.1.5 - One-and-a-half Stage Compressor Back Pressure Valve

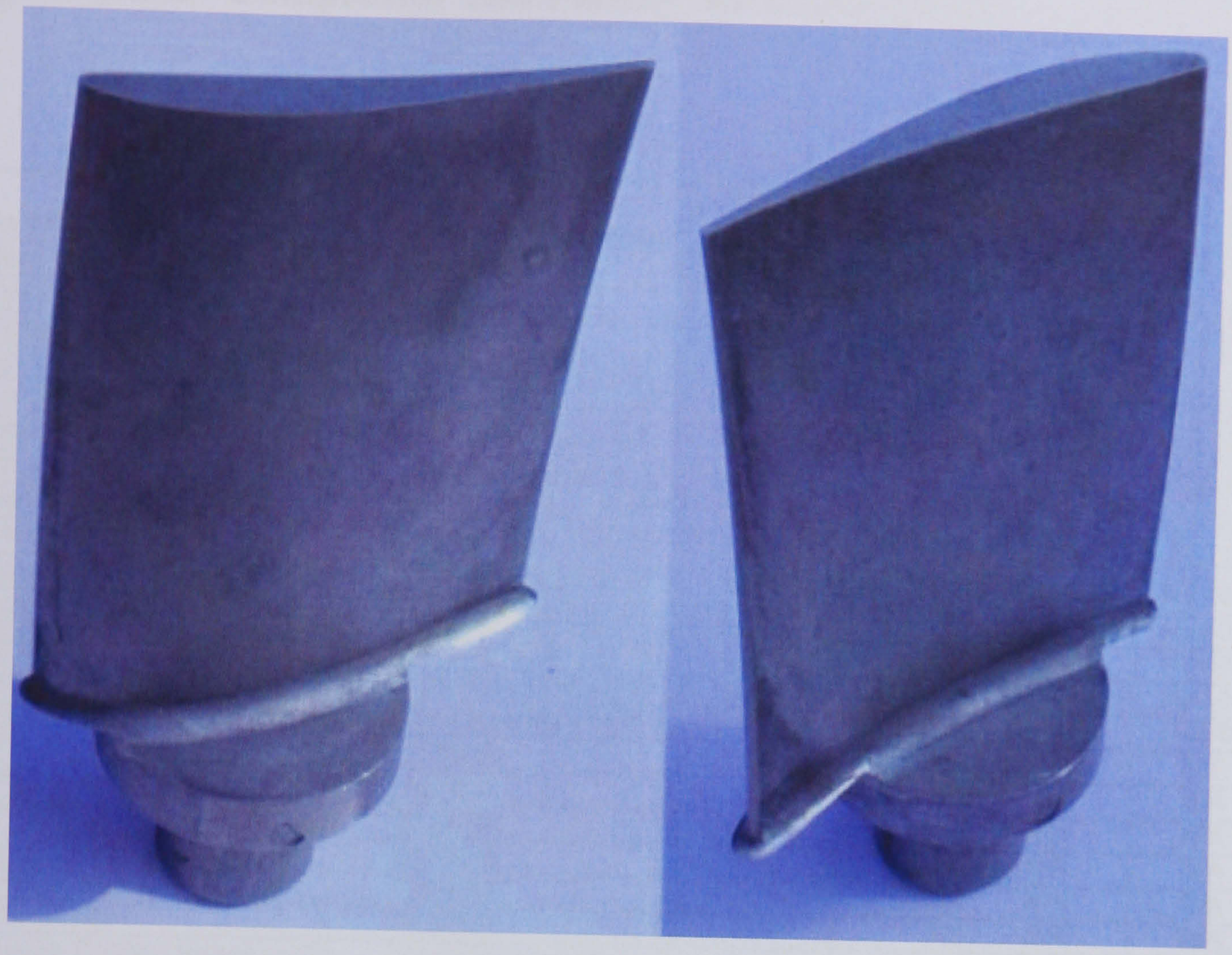

Figure D.1.6 - Compressor Rotor Blade

Appendix D.2 - Compressor Test Facility Build and Budget

Part Description	Made/Modified By	Quote Received	Price	Scheduled Delivery	Part Received
Central Section					
Rotor Plate (Front)	In Stock	N/A	£0	N/A	N/A
Rotor Plate (Rear)	In Stock	N/A	£0	N/A	N/A
Lip Contact Seal (Front)	Stainless Metalcraft	Oct-00	£1,350	Dec-00	Jan-01
Lip Contact Seal (Rear)	Stainless Metalcraft	Oct-00	£1,350	Dec-00	Jan-01
Exhaust Plate #1	Stainless Metalcraft	Aug-00	£5,718	Nov-00	Nov-00
Exhaust Plate #2	Stainless Metalcraft	Aug-00	£4,802	Nov-00	Nov-00
Intake Plate #1	Stainless Metalcraft	Aug-00	£5,718	Nov-00	Jan-01
Intake Plate #2	Stainless Metalcraft	Aug-00	£4,802	Nov-00	Jan-01
Rotor Spacer (Front) (Modify)	Stainless Metalcraft	Aug-00	£2,837	Nov-00	Nov-00
Rotor Spacer (Rear) (Modify)	Stainless Metalcraft	Aug-00	£2,837	Nov-00	Nov-00
Stator Spacer Ring (Modify)	Stainless Metalcraft	Aug-00	£3,391	Nov-00	Nov-00
Lip Contact Seal Ring (Back)	Stainless Metalcraft	Sep-00	£2,236	Dec-00	Dec-00
Lip Contact Seal Ring (Front)	Stainless Metalcraft	Sep-00	£2,236	Dec-00	Dec-00
IGVs (NEB 1D)	In Stock	N/A	£0	N/A	N/A
Rotor (NEB 1D)	In Stock	N/A	£0	N/A	N/A
Rotor Ring	In Stock	N/A	£0	N/A	N/A
Stator (NEB 1D)	In Stock	N/A	£0	N/A	N/A
Stator Rings	In Stock	N/A	£0	N/A	N/A
Stub Shafts	In Stock	N/A	£0	N/A	N/A
Angular Contact Bearings (2)	Direct Engineering	Jul-00	£800	Oct-00	Oct-00
Roller Bearing	Direct Engineering	Jul-00	£332	Oct-00	Oct-00
Stands					
Stand for Exhaust	Stainless Metalcraft	Aug-00	£385	Nov-00	Nov-00
Stand for Main Rig	Stainless Metalcraft	Aug-00	£565	Nov-00	Nov-00
Stand for Outlet	Stainless Metalcraft	Aug-00	£456	Nov-00	Nov-00
Inlet Components					
Inlet Centre Nose Cone	Stainless Metalcraft	Jul-00	£4,670	Nov-00	Nov-00
Inlet Outer Flair	Stainless Metalcraft	Jul-00	£3,394	Nov-00	Nov-00
Outlet Components					
Exhaust Section (Inner)	Stainless Metalcraft	Aug-00	£2,727	Nov-00	Nov-00
Exhaust Section (Outer)	Stainless Metalcraft	Aug-00	£3,012	Nov-00	Nov-00
Exhaust Cone	Stainless Metalcraft	Aug-00	£3,939	Nov-00	Nov-00
Exhaust Duct	Stainless Metalcraft	Aug-00	£3,436	Nov-00	Nov-00
Motor Frame	Stainless Metalcraft	Sep-00	£1,128	Nov-00	Nov-00
Back Pressurising Valve	Stainless Metalcraft	Sep-00	£1,583	Nov-00	Nov-00
Electrical Components					
60kW Motor	Polaron Cortina	Jun-00	£12,776	Nov-00	Nov-00
Instrumentation					
Back Pressure Valve Control	In Stock	N/A	£0	N/A	N/A
Probe Traverses (3)	In Stock	N/A	£0	N/A	N/A
Probe Traverses Controllers (3)	National Instruments	N/A	£3,896	Dec-00	Dec-00
Torque Meter	In Stock	N/A	£0	N/A	N/A
Bearing Temperature Monitor	RS Components	Sep-00	£126	Dec-00	Dec-00
Inlet Temperature Measurement	Pico	Sep-00	£369	Dec-00	Dec-00
Slip Ring (24 way)	In Stock	N/A	£0	N/A	N/A
Water Manometer	In Stock	N/A	£0	N/A	N/A
		Net Cost	£80,871		
		VAT	£14,152		
		Total Cost	£95,023		

Table D.1 - Compressor Test Facility Build Inventory, Schedule and Costing

Figure D.2.1 - Compressor Test Facility Build Gantt Chart

Appendix D.3 - Compressor Test Facility Commissioning

$$\dot{m} = C_D \cdot A_{inlet} \sqrt{\frac{2(P_T - P_0)}{R \cdot T_0}} \qquad \text{D.1}$$

$$D_m = \dot{m} \frac{\sqrt{T_0}}{P_T} \qquad \text{D.2}$$

$$\eta_{isentropic} = \frac{\dot{m} \cdot C_p \cdot T_0 \left[\left(\frac{P_4}{P_2} \right)^{\frac{\gamma - 1}{\gamma}} - 1 \right]}{\omega \cdot \tau} \qquad \text{D.3}$$

$$CW = \frac{\tau}{4 \cdot \dot{m} \cdot d_u^2 \cdot \omega} \qquad \text{D.4}$$

$$Va = \frac{\dot{m}}{U} \qquad \text{D.5}$$

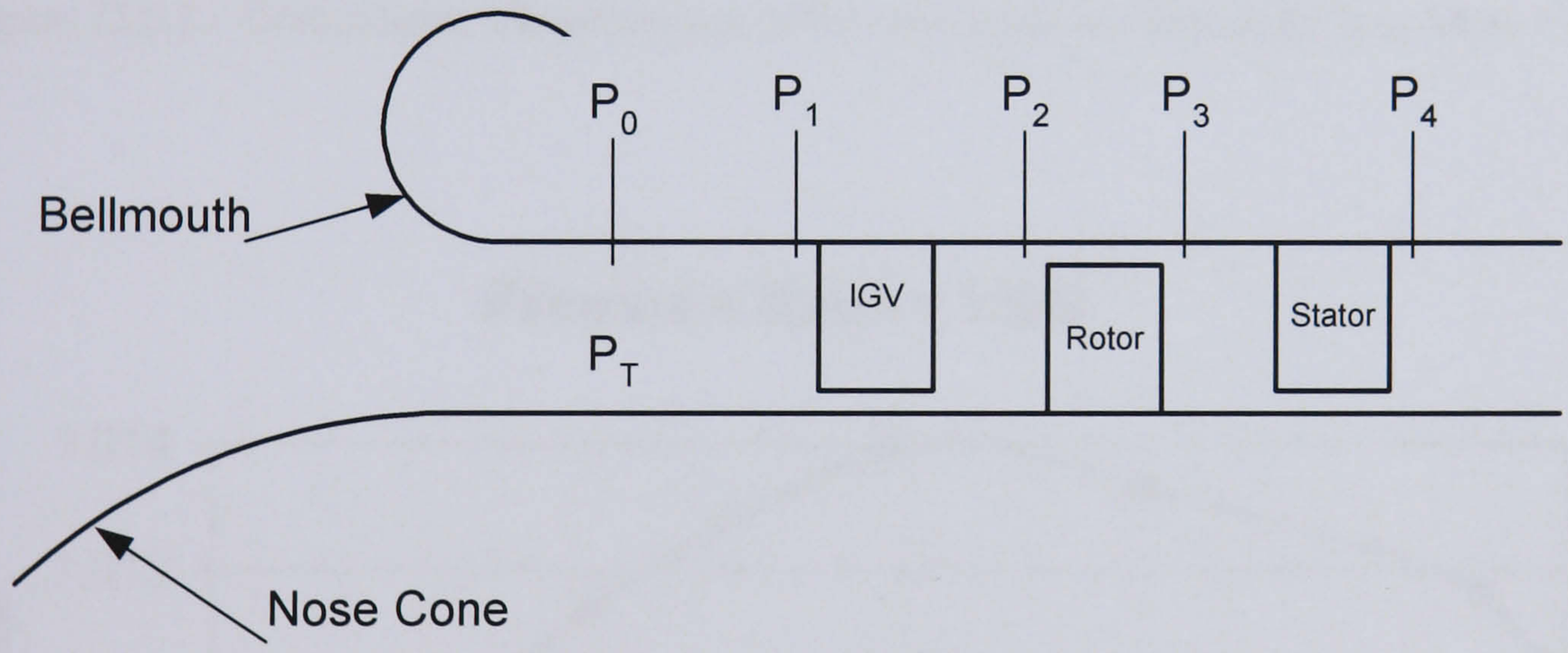

Figure D.3.1 - Compressor Flow Passage

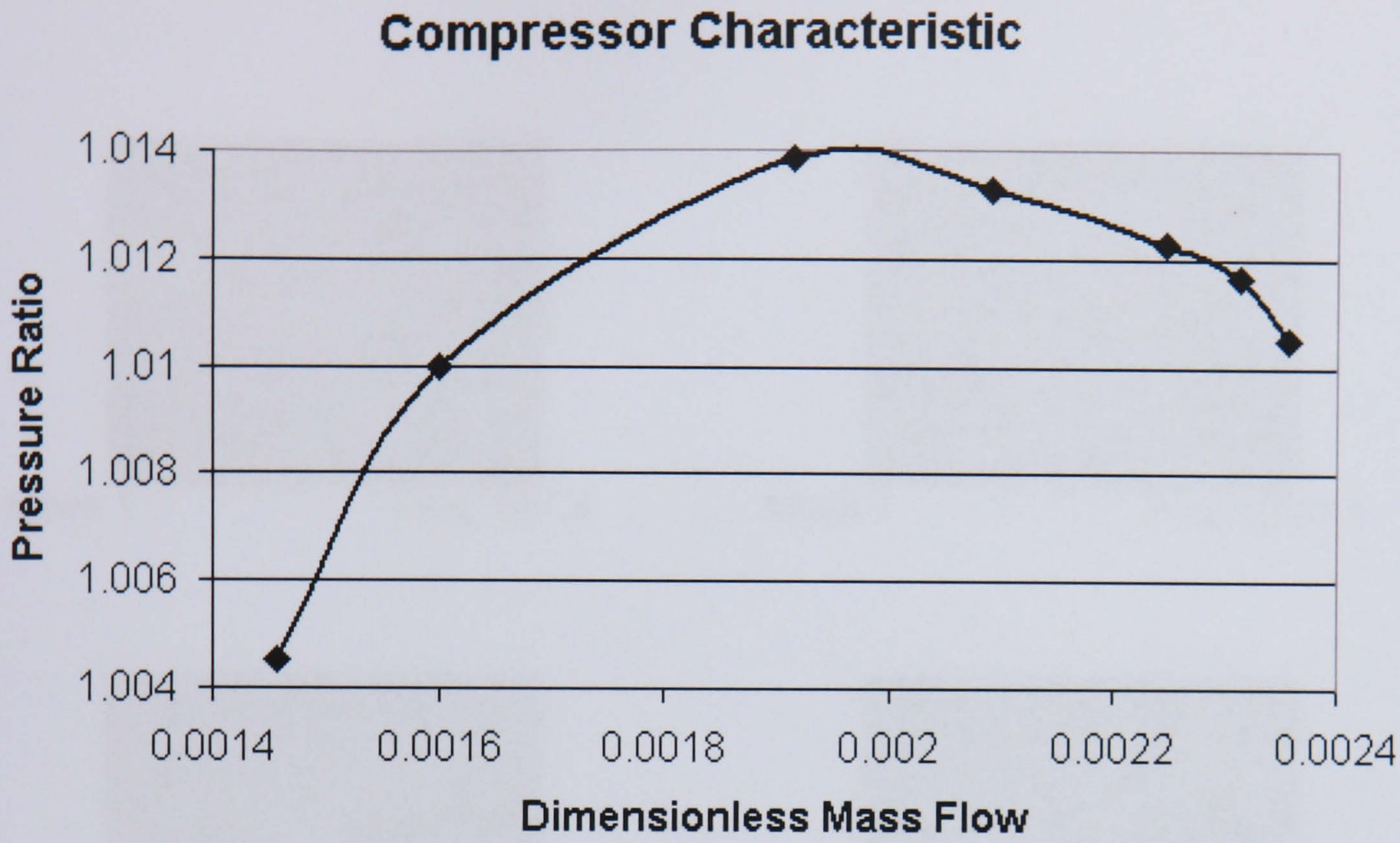

Figure D.3.2 - Compressor Characteristic: Pressure Ratio v. Dimensionless Mass Flow

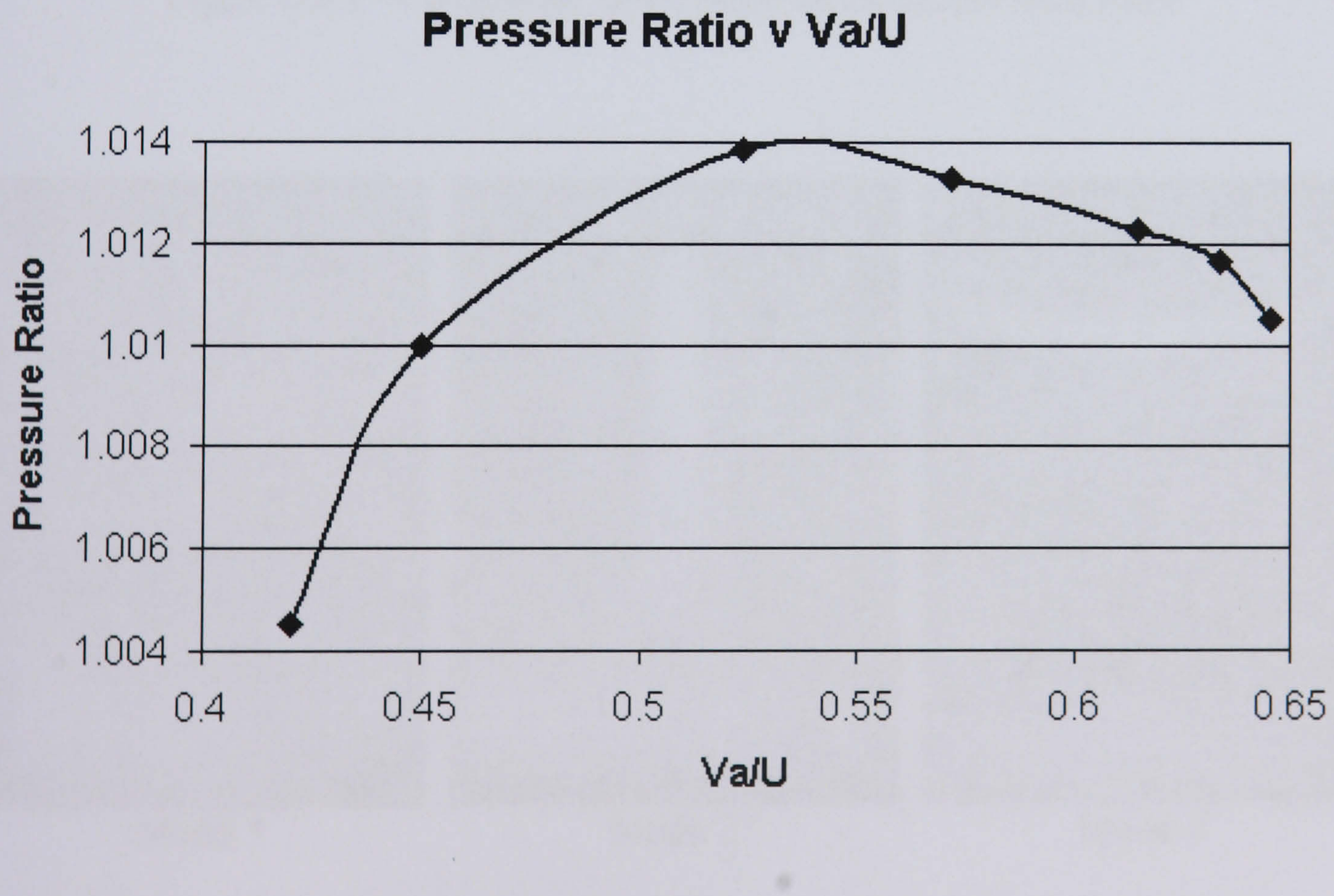

Figure D.3.3 - Compressor Characteristic: Pressure Ratio v. Va/U

Appendix D.4 - ESPI Blade Vibration and Calibration Results

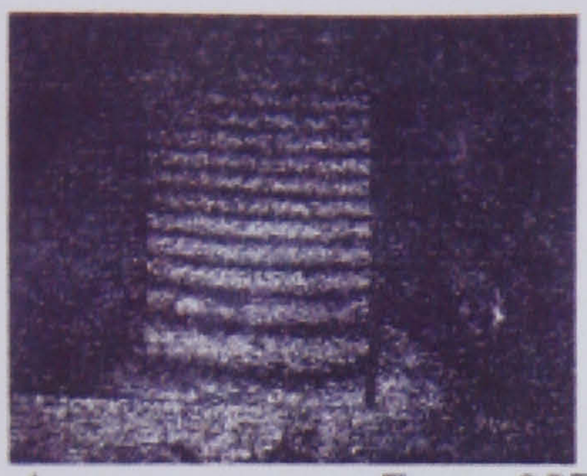

Mode 1 Freq. 687.4

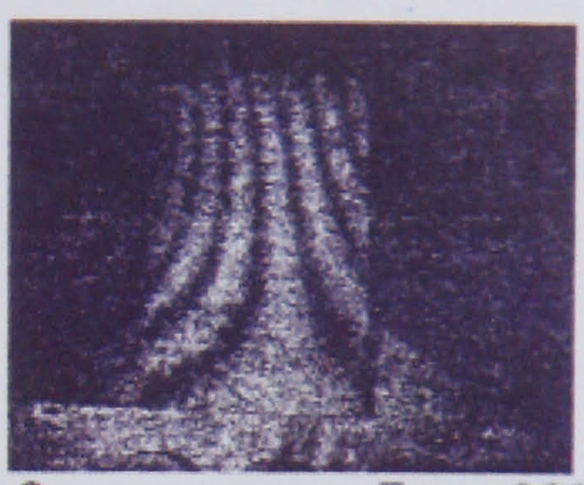

Mode 2 Freq. 2061.1

Mode 3 Freq. 3542.1

Mode 4 Freq. 4494

Figure D.4.1 - Compressor Rotor Blade Mode Shapes from ESPI

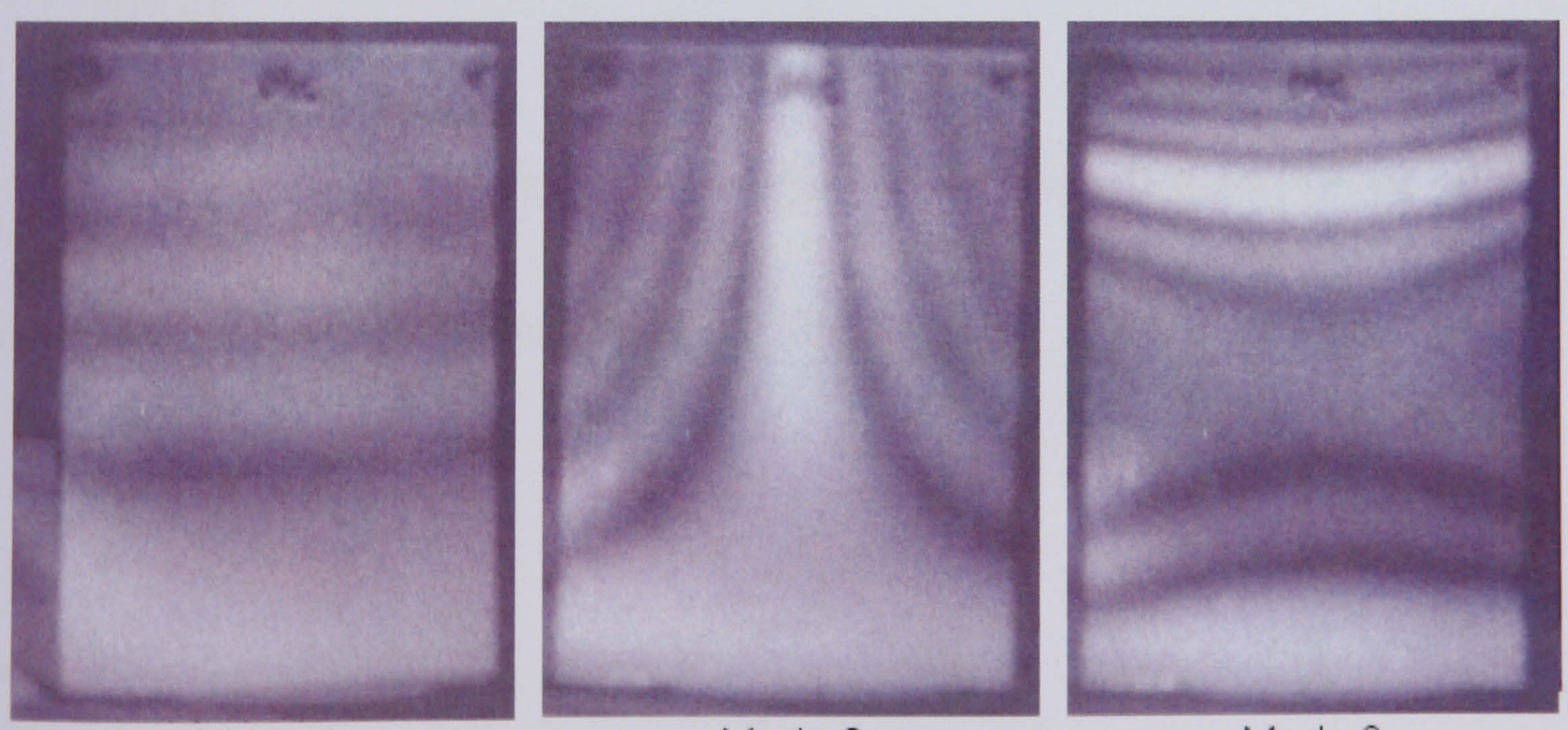

Mode 1 Mode 2 Mode 3

Figure D.4.2 - 2 mm Quasi Blade Mode Shapes from ESPI

Appendix D.5 - Instrumentation Electronic Circuit Schematic Diagrams

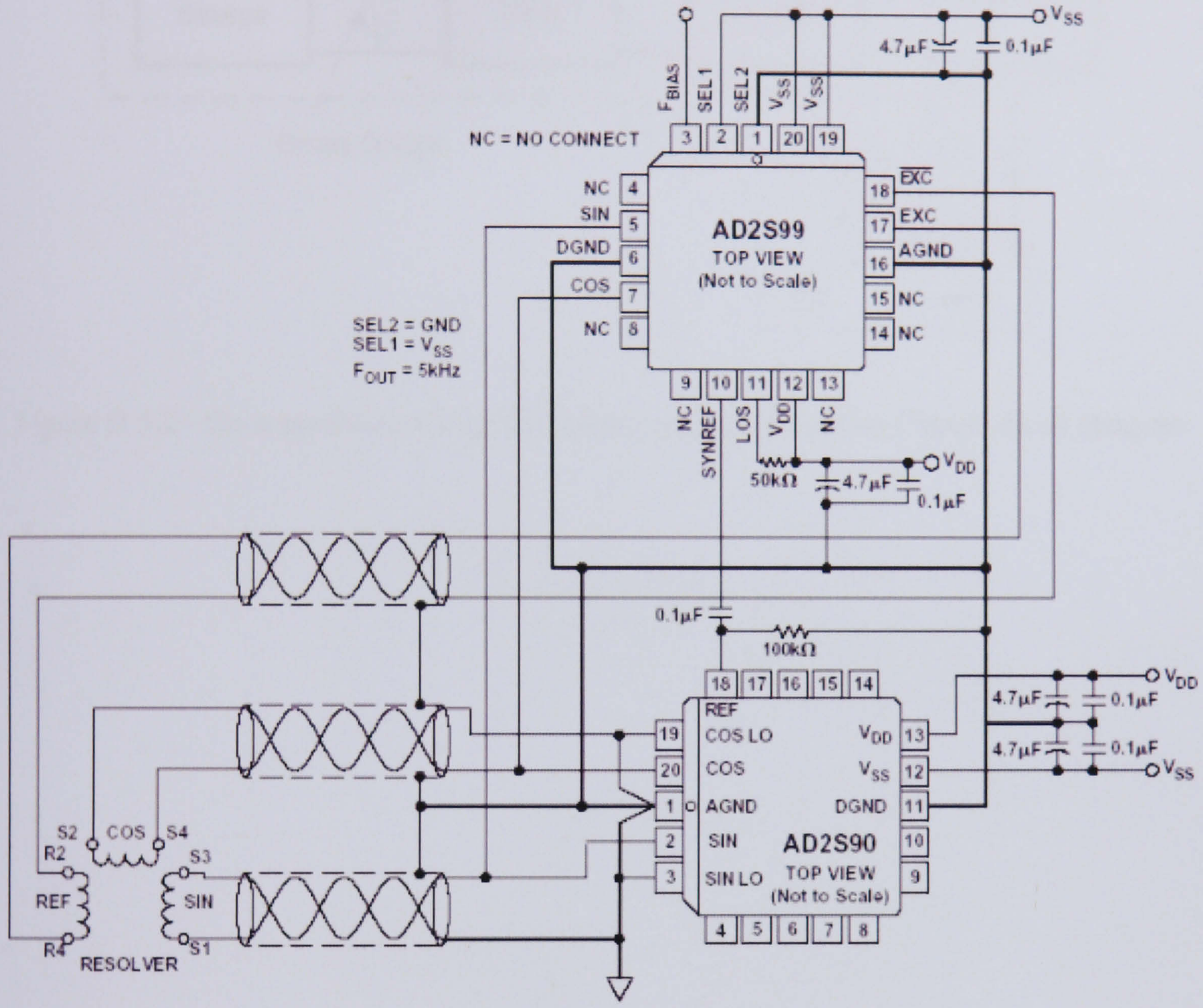

Figure D.5.1 - Actuator Yaw Axis Resolver-to-Digital Converter Circuit

Source: Analog Devices AD2S90 Data Sheet.

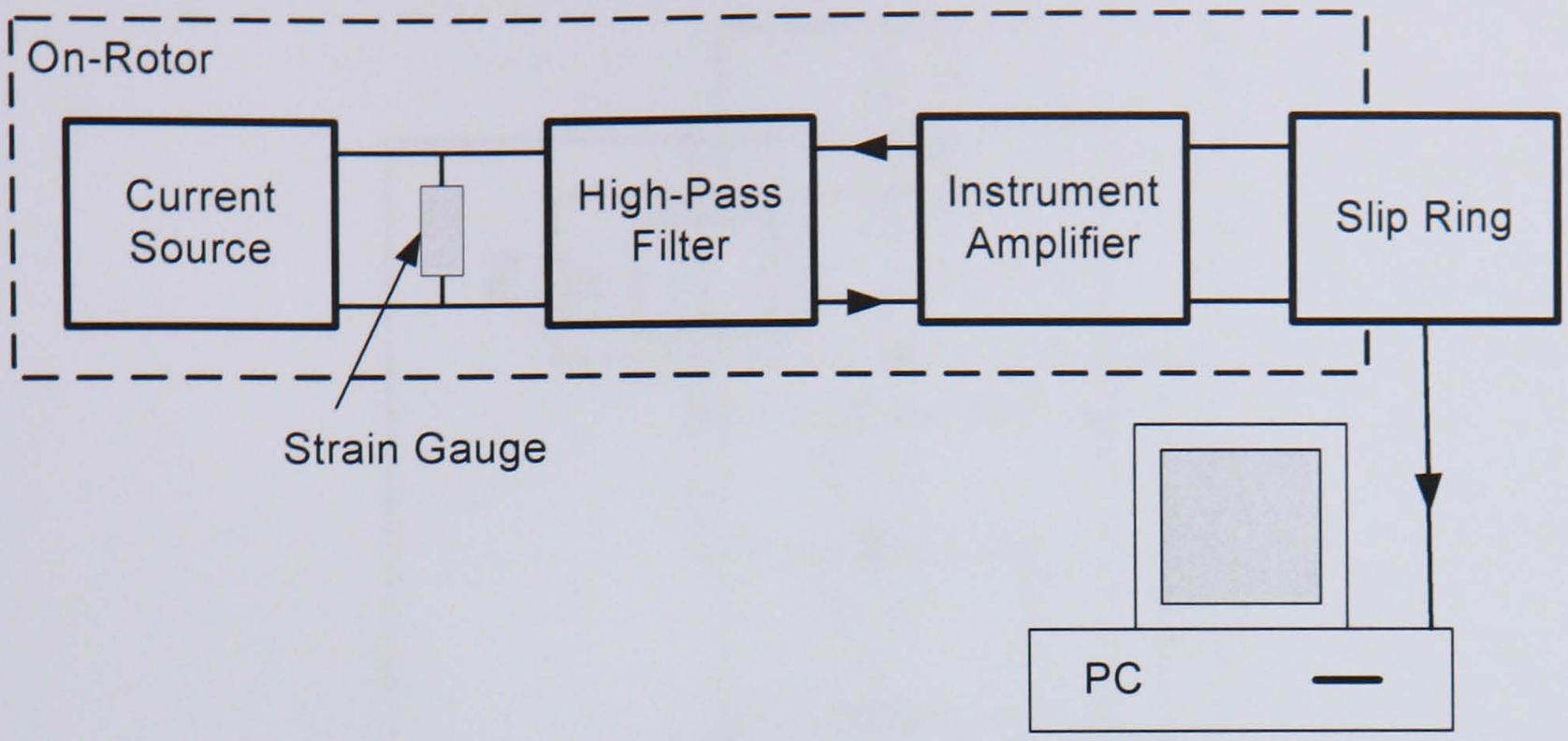

Figure D.5.2 - On-rotor Strain Gauge Energising and Amplification Circuit Block Diagram

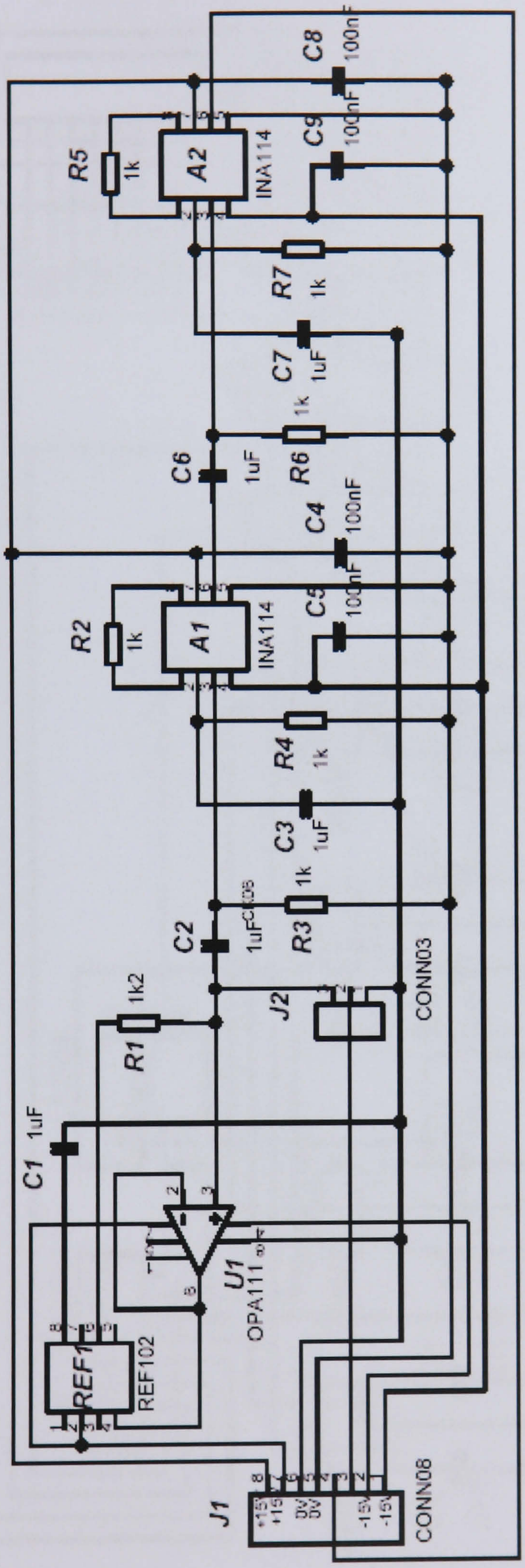

Figure D.5.3 - Strain Gauge Energising and Signal Amplification Circuit Schematic Diagram

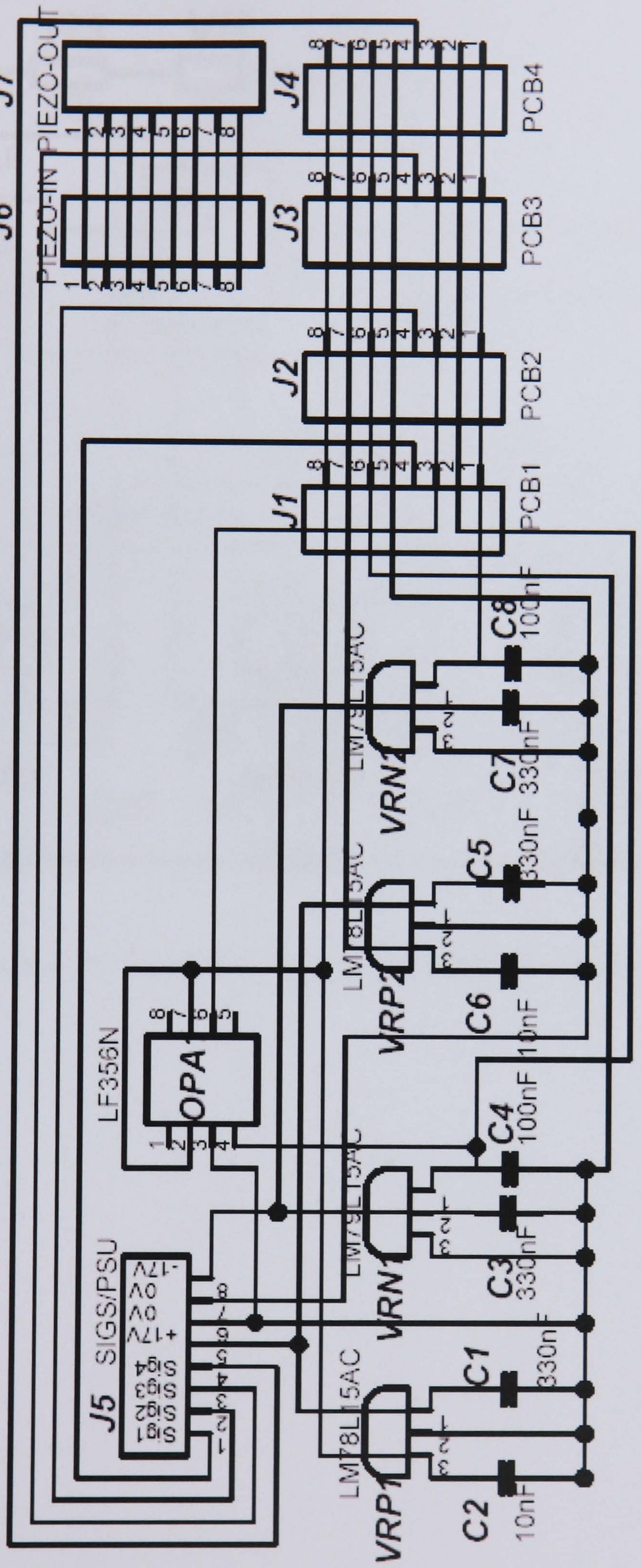

Figure D.5.4 - Junction and Power Board Circuit Schematic

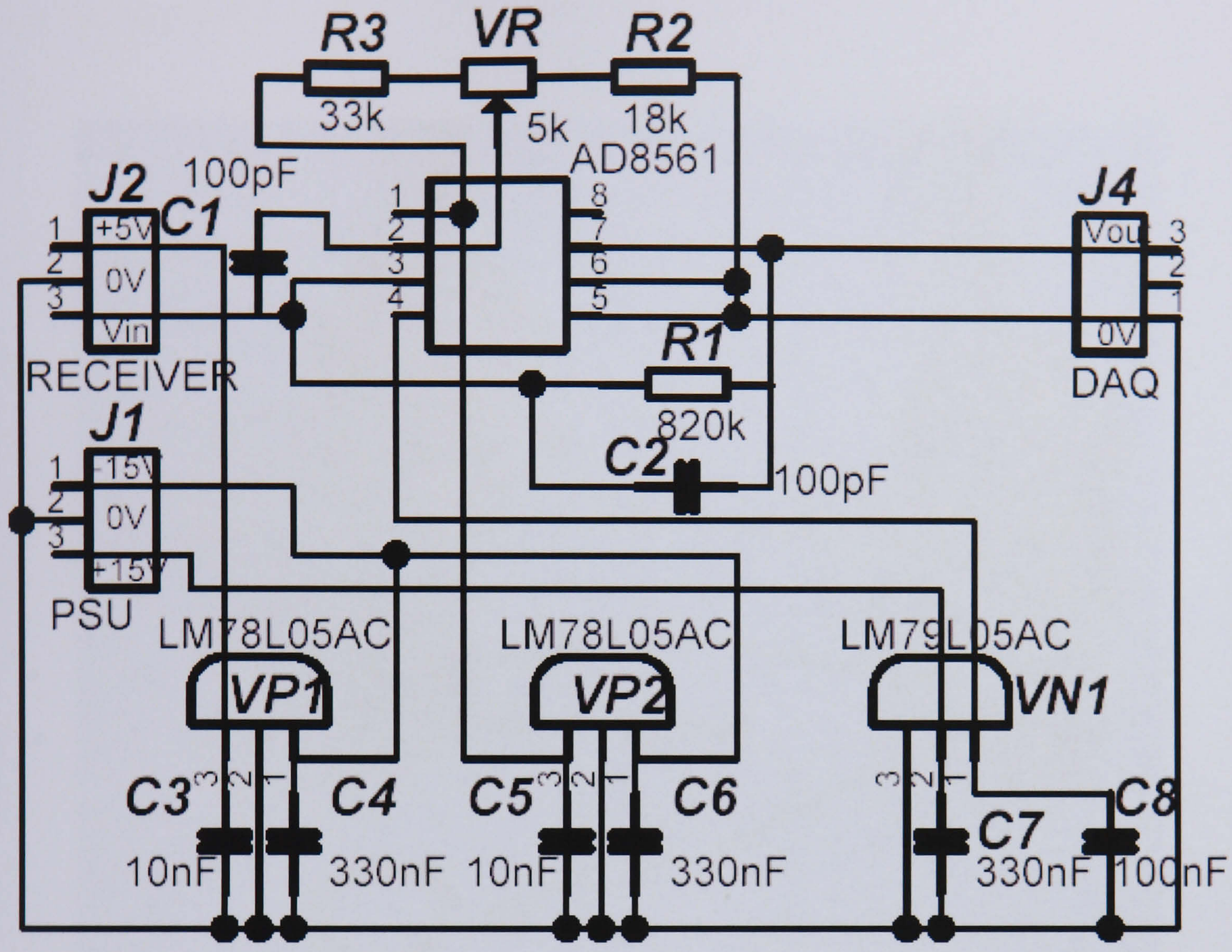

Figure D.5.5 - Once Per Revolution Sensor Digitiser Circuit Schematic Diagram

Appendix D.6 - Instrumentation Illustrations

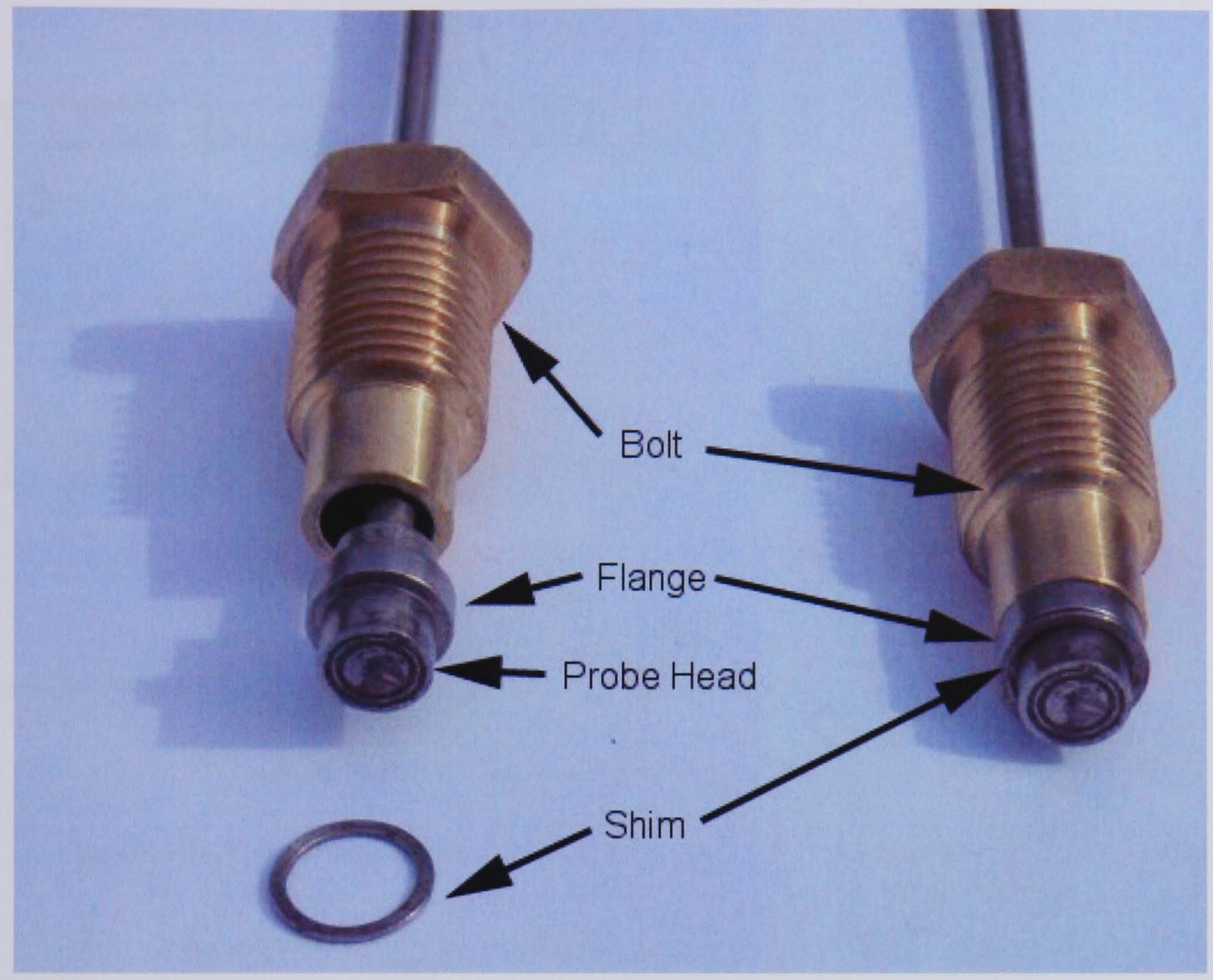

Figure D.6.1 - Capacitance Probe Head Securing Arrangement

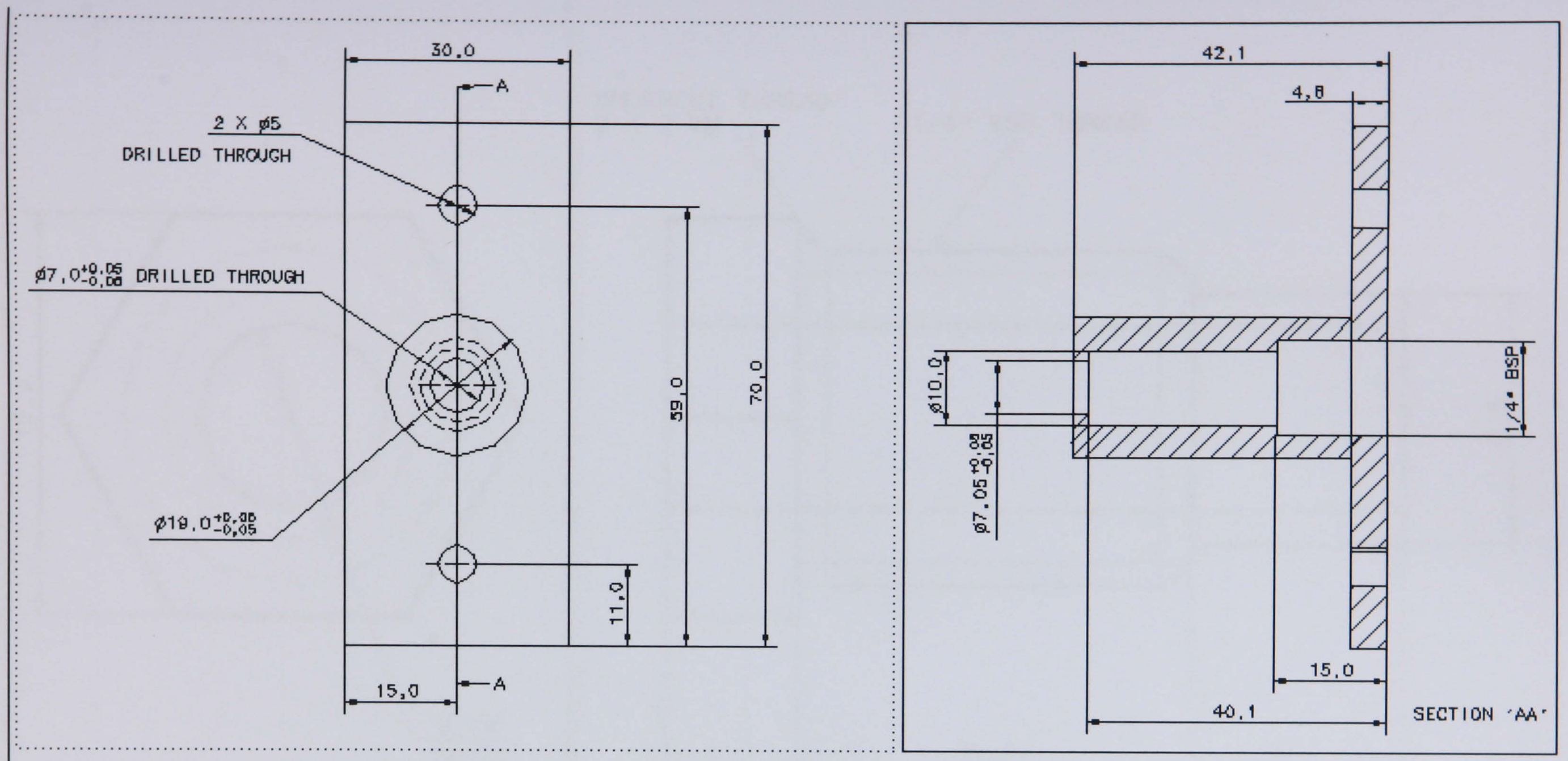

NOTE: 2 OFF REQUIRED

TITLE: 1.5 STAGE COMPRESSOR ROTOR - CAPACITANCE PROBE MOUNTING		
MATERIAL: ALUMINIUM ALLOY		
DRAWN BY: CRAIG LAWSON	DATE: 25-09-02	SIZE: A3
DIMENSIONS ARE IN MILLIMETERS UNLESS OTHERWISE SPECIFIED TOLERANCES ARE +/- 0,1 MM UNLESS OTHERWISE SPECIFIED		

Figure D.6.2 - Capacitance Probe Socket Engineering Drawing

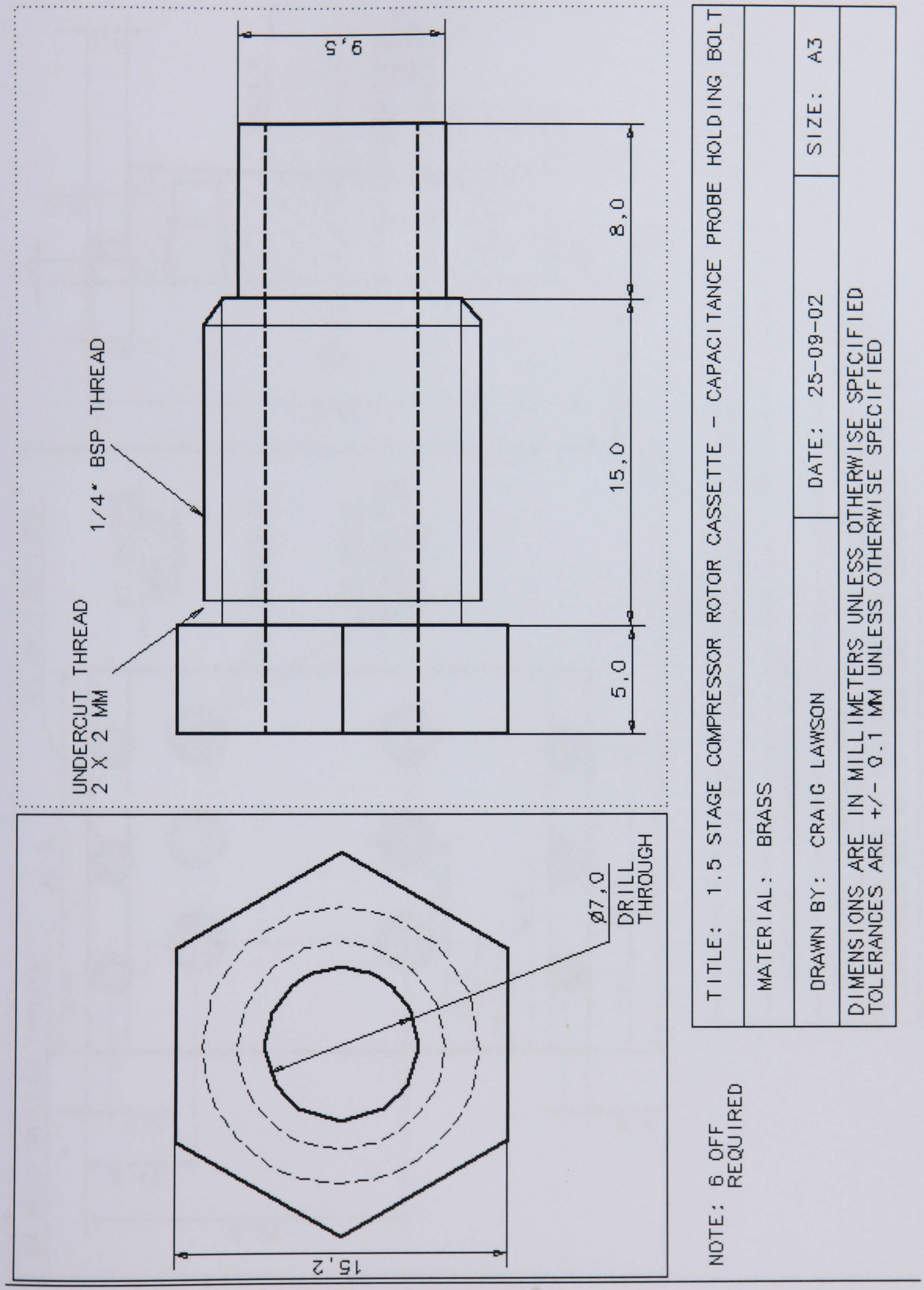

Figure D.6.3 - Capacitance Probe Securing Bolt Engineering Drawing

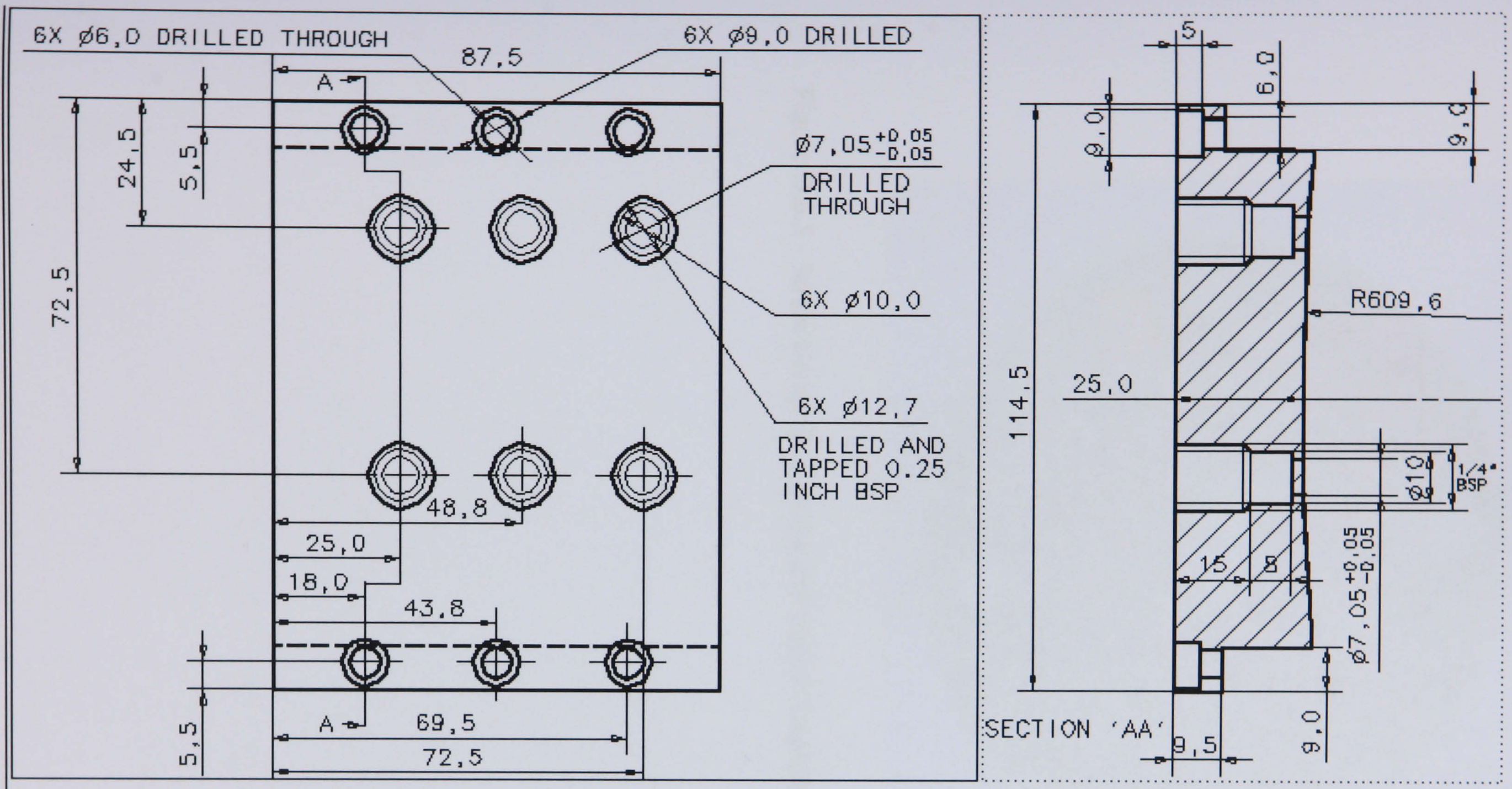

TITLE: 1.5 STAGE COMPRESSOR ROTOR CASSETTE - CAPACITANCE PROBE MOUNTING		
MATERIAL: ALUMINIUM ALLOY		
DRAWN BY: CRAIG LAWSON	DATE: 25-09-02	SIZE: A3
DIMENSIONS ARE IN MILLIMETERS UNLESS OTHERWISE SPECIFIED TOLERANCES ARE +/- 0.1 MM UNLESS OTHERWISE SPECIFIED		

Figure D.6.4 - Capacitance Probe Cassette Engineering Drawing

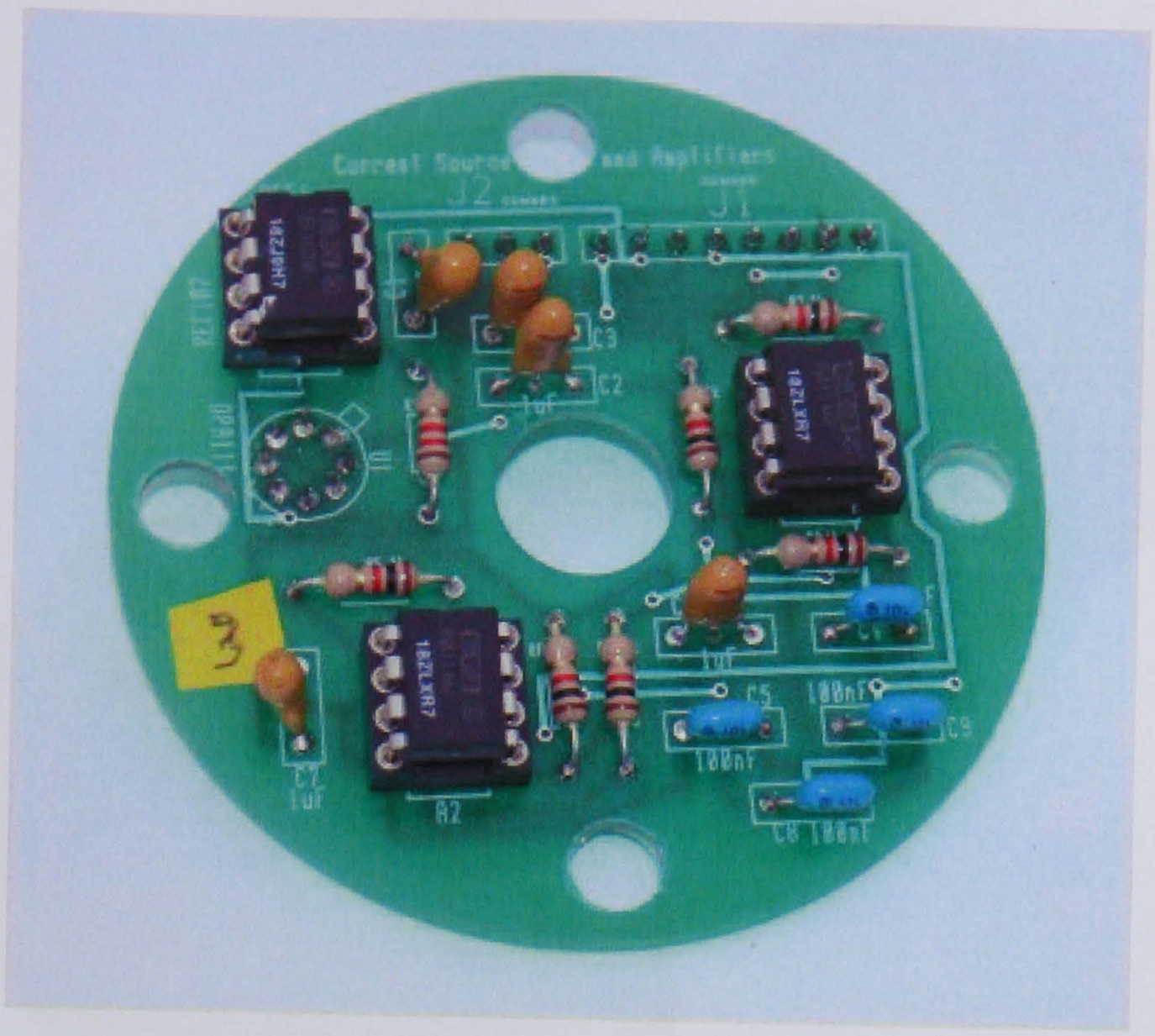

Figure D.6.5 - Strain Gauge Energising and Signal Amplification Circuit PCB

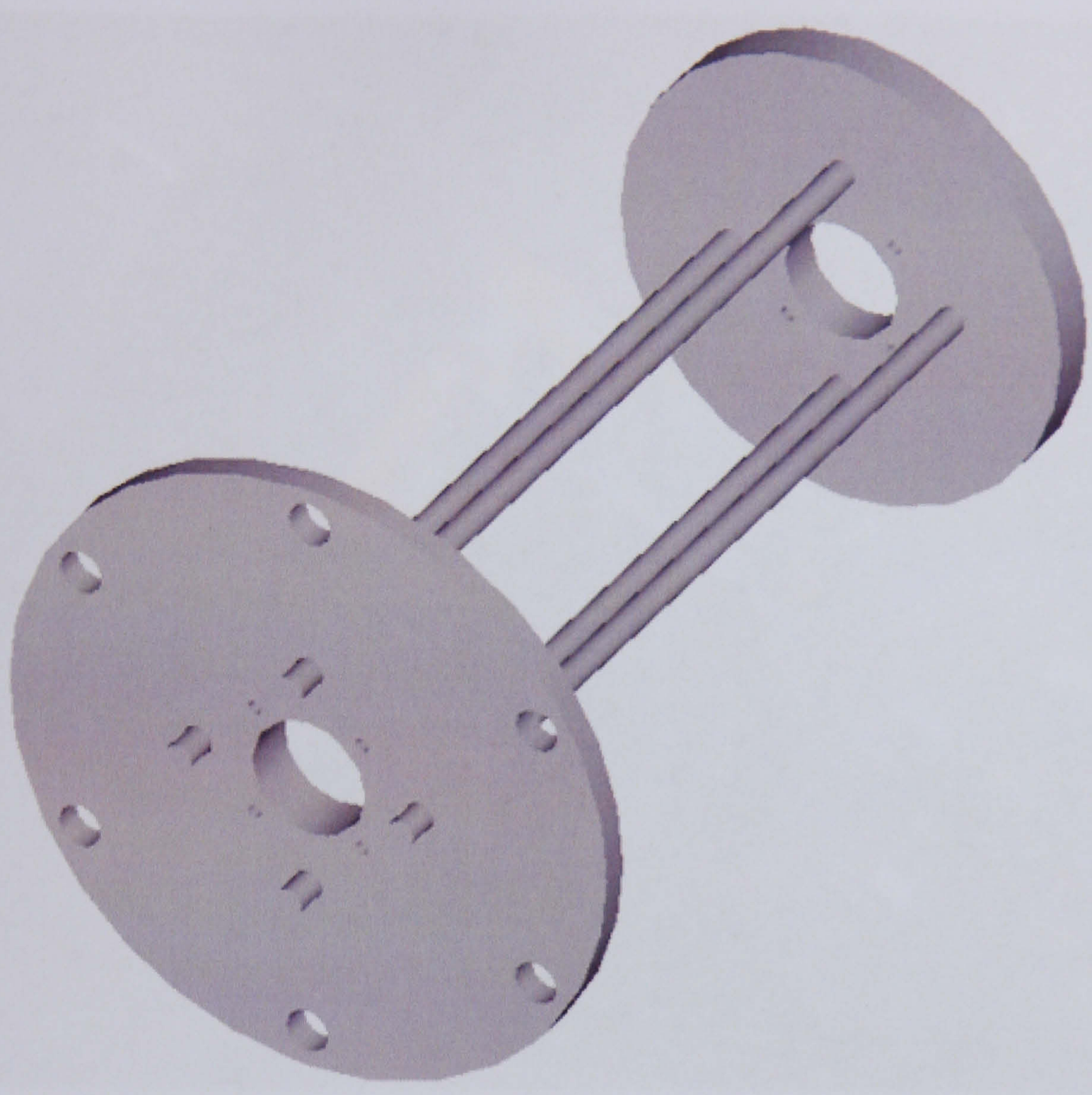

Figure D.6.6 - PCB Mounting Cage Assembly: Isometric View

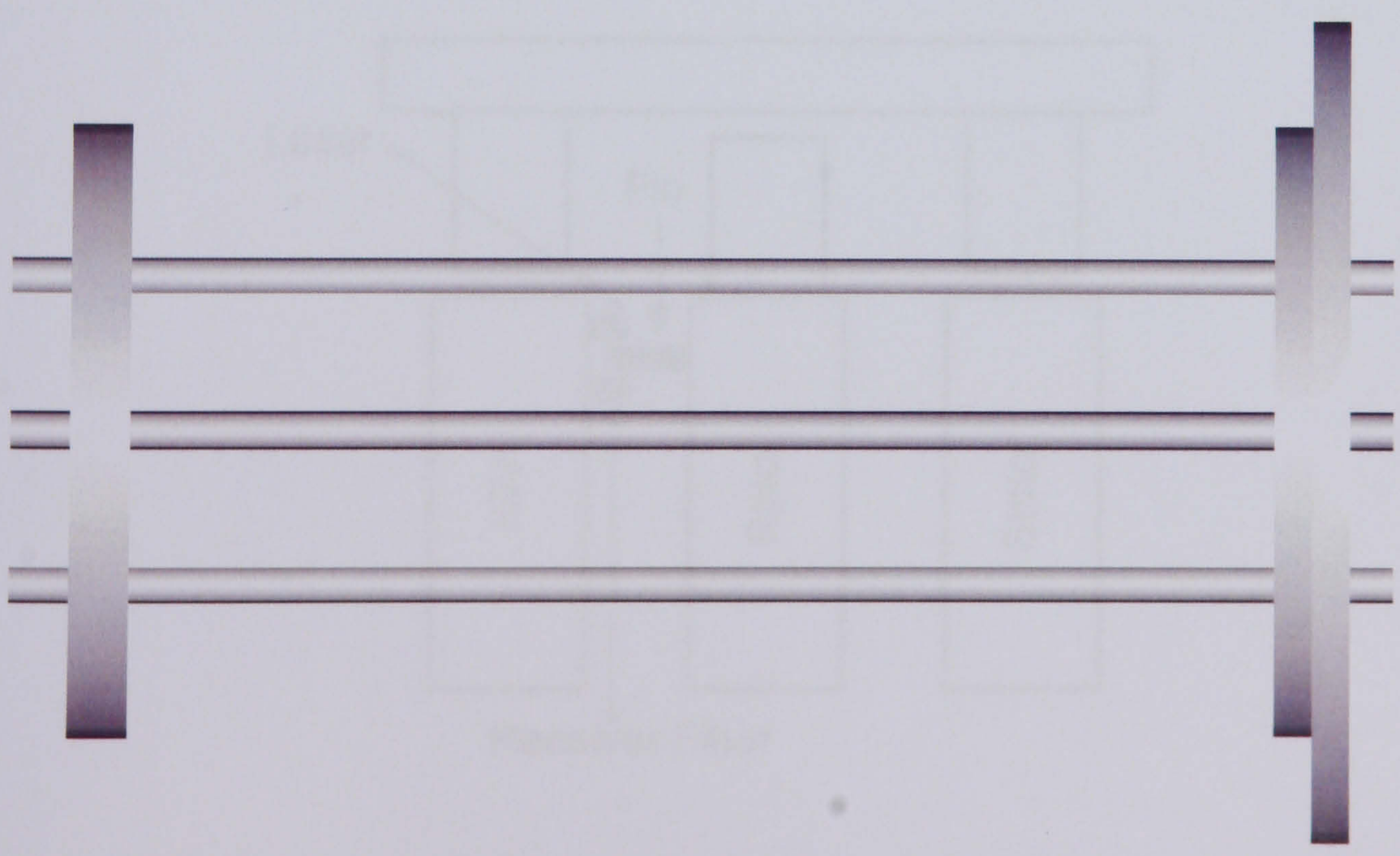

Figure D.6.7 - PCB Mounting Cage Assembly: Plan View

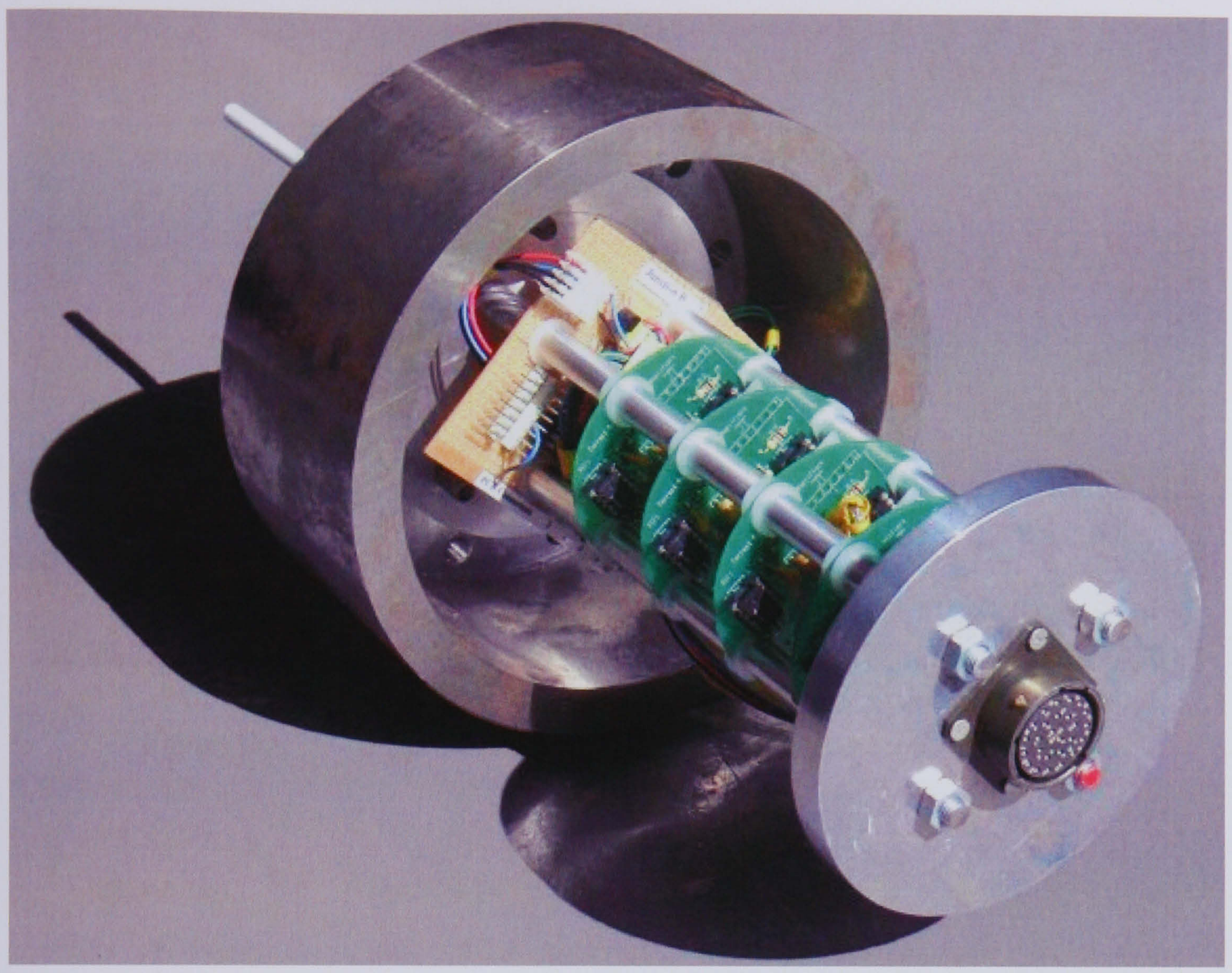

Figure D.6.8 - PCB Mounting Cage with PCBs in Place: Assembly Illustration

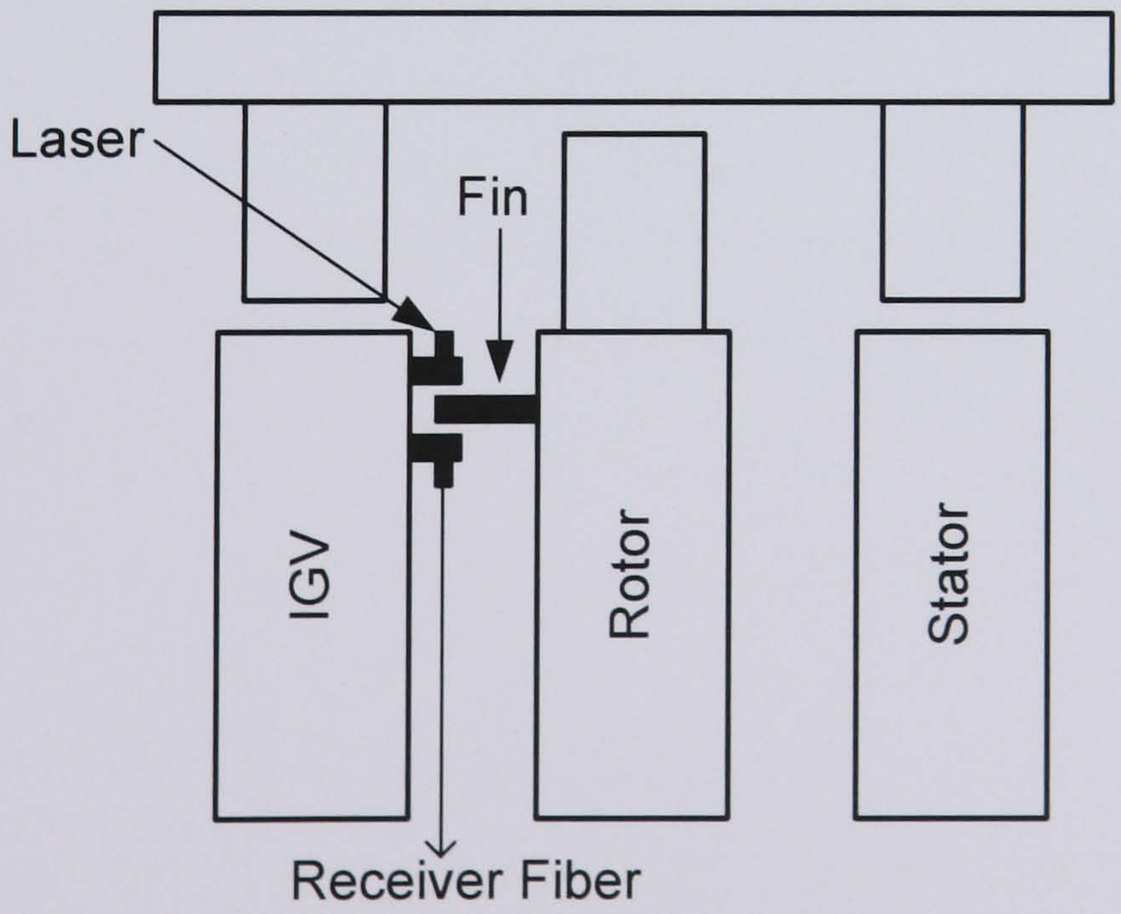

Figure D.6.9 - Once Per Revolution Sensor Positioning

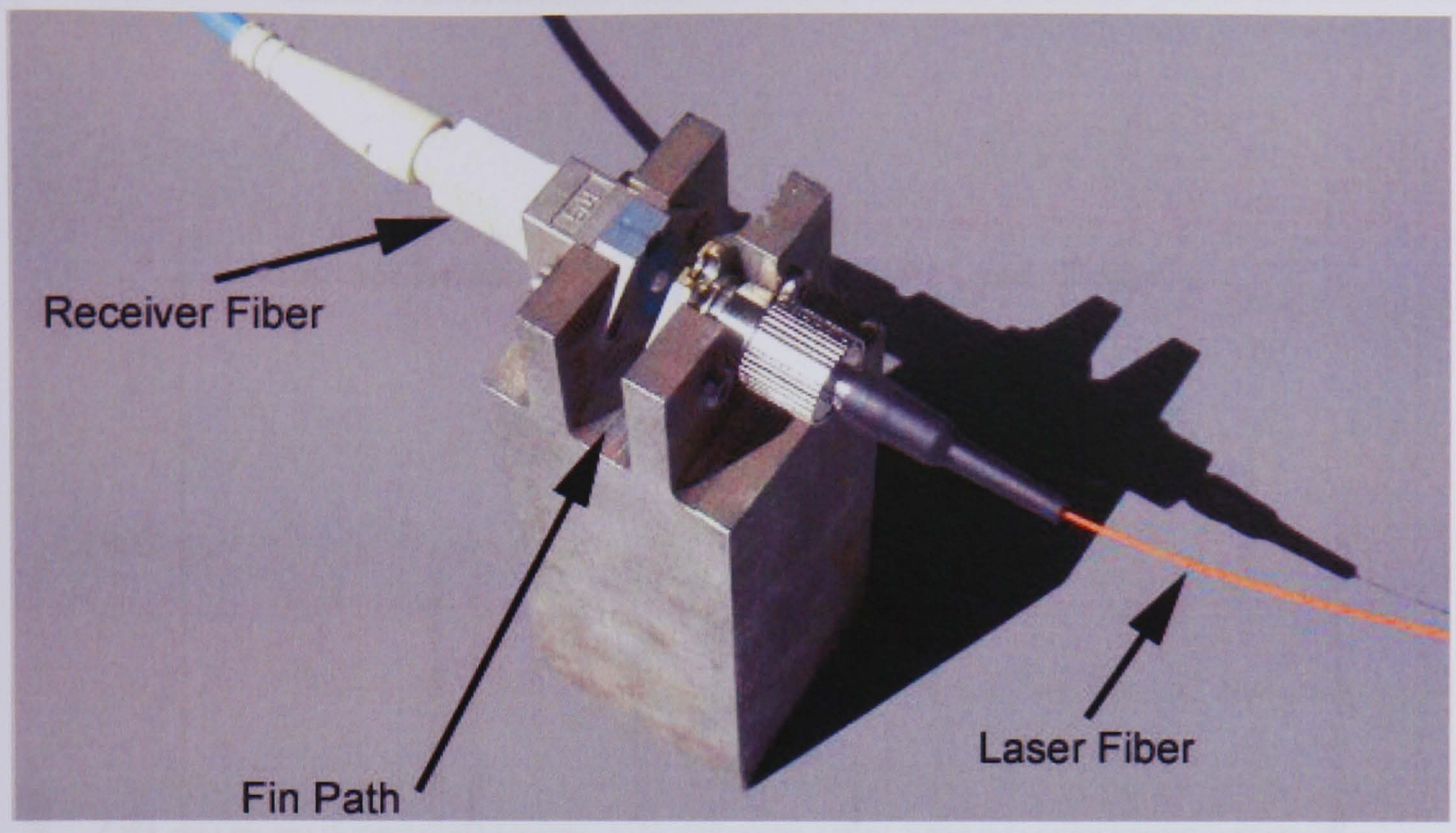

Figure D.6.10 - Once Per Revolution Laser and Receiver Arrangement

Appendix D.7 - Instrumentation Electronics Performance Characteristics

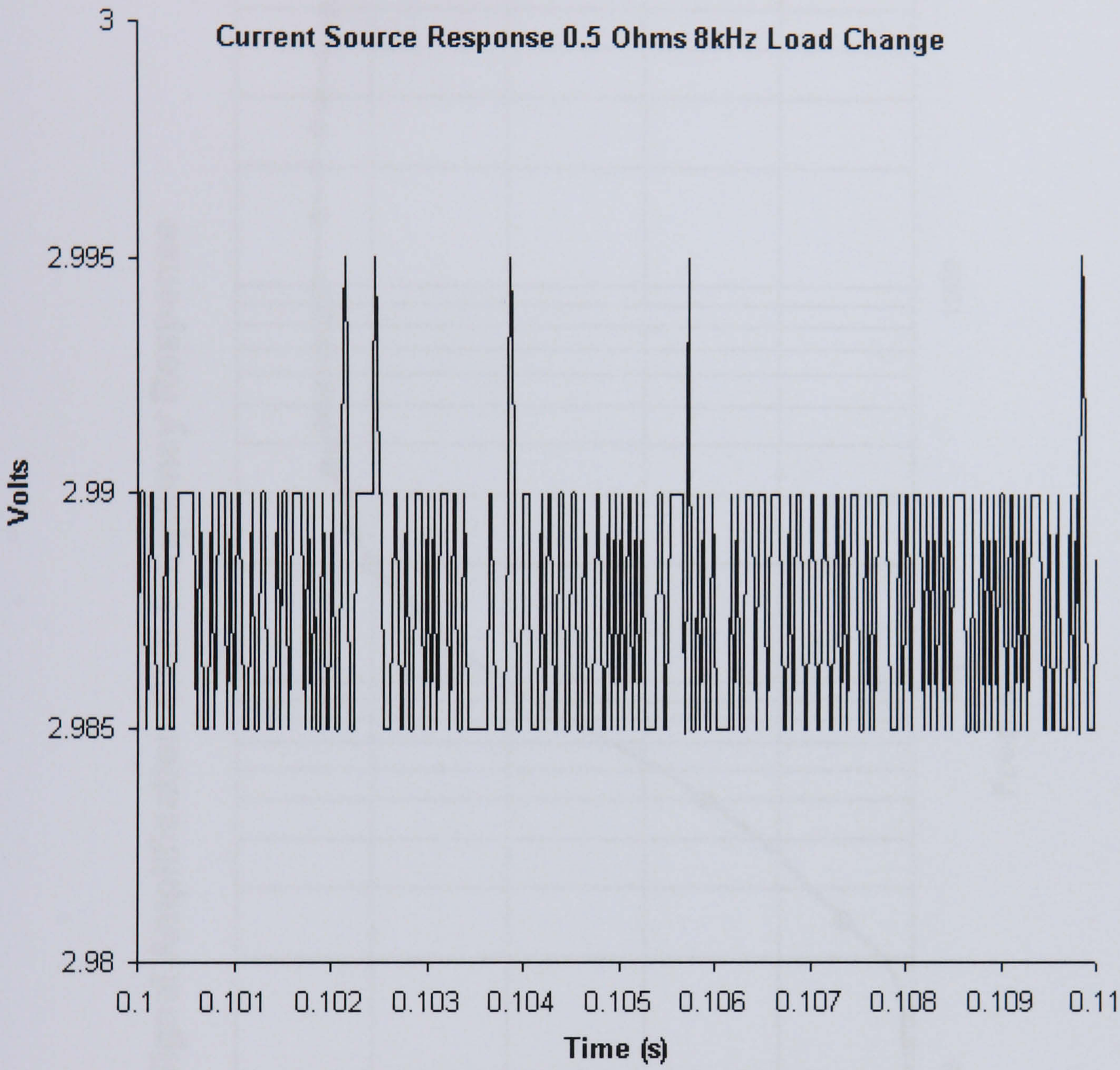

Figure D.7.1 - Current Source Performance Characteristic

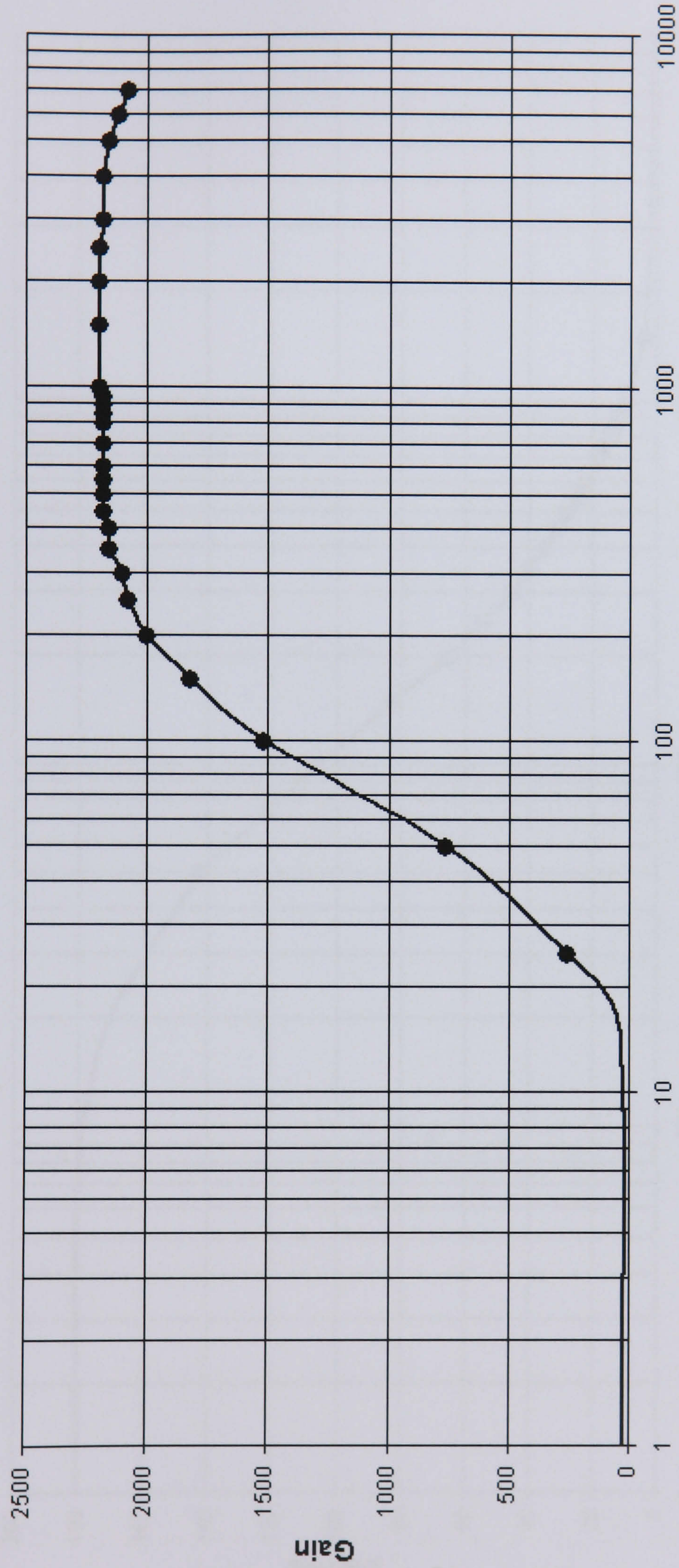

Figure D.7.2 - Strain Signal Amplification Gain-Frequency Response Characteristic

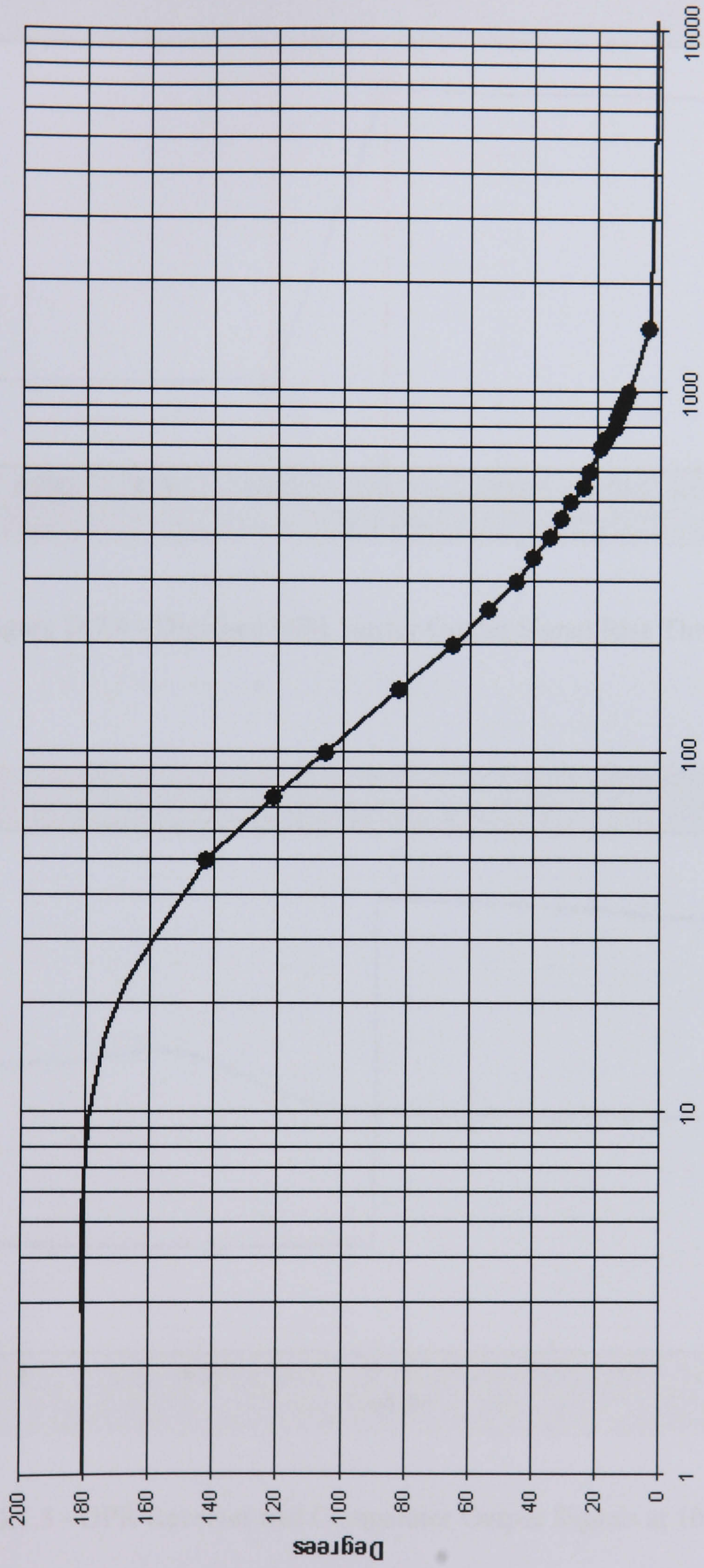

Figure D.7.3 - Strain Signal Amplification Phase-Frequency Response Characteristic

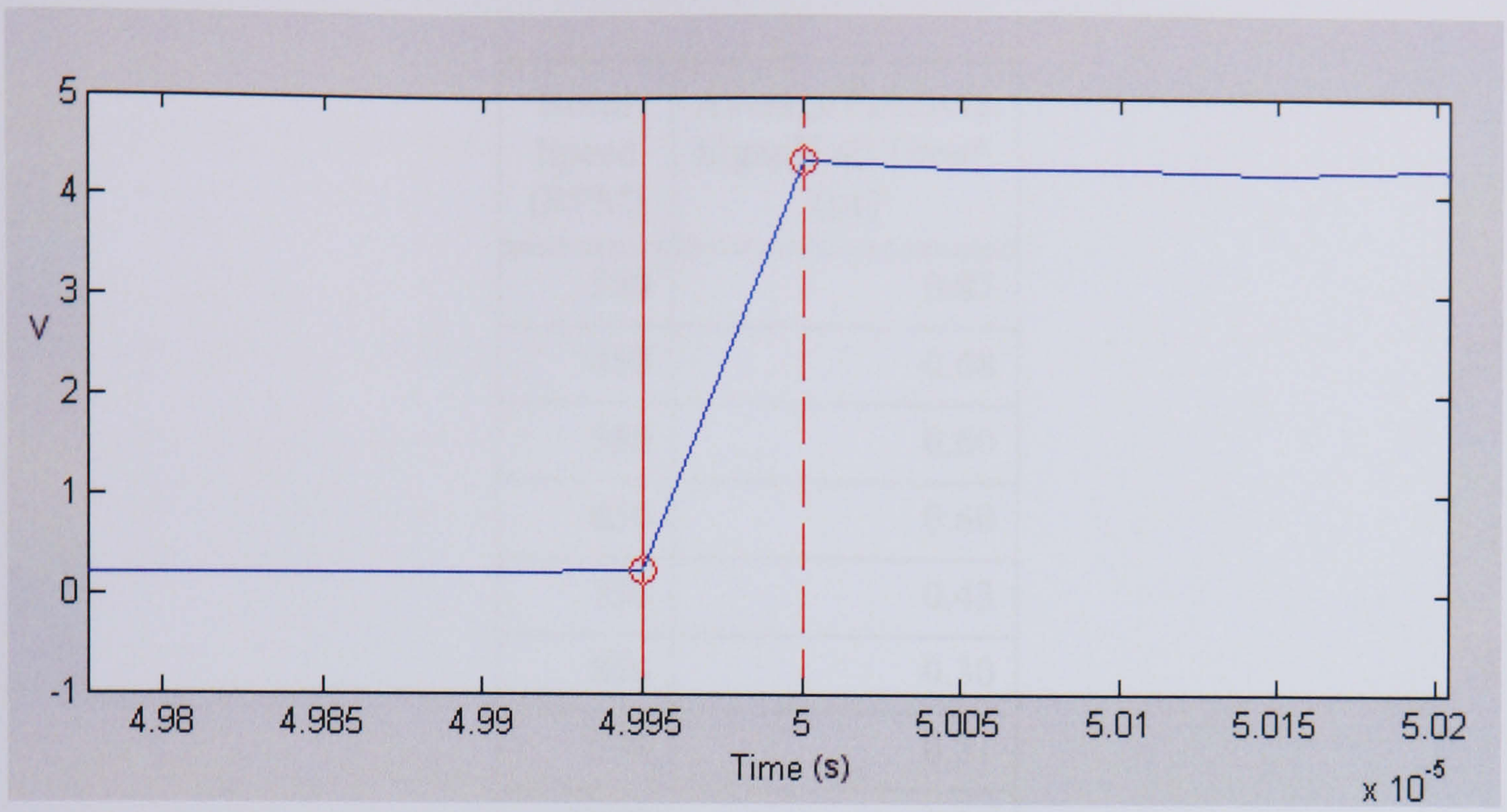

Figure D.7.4 - Digitised OPR Sensor Output Signal Rise Time

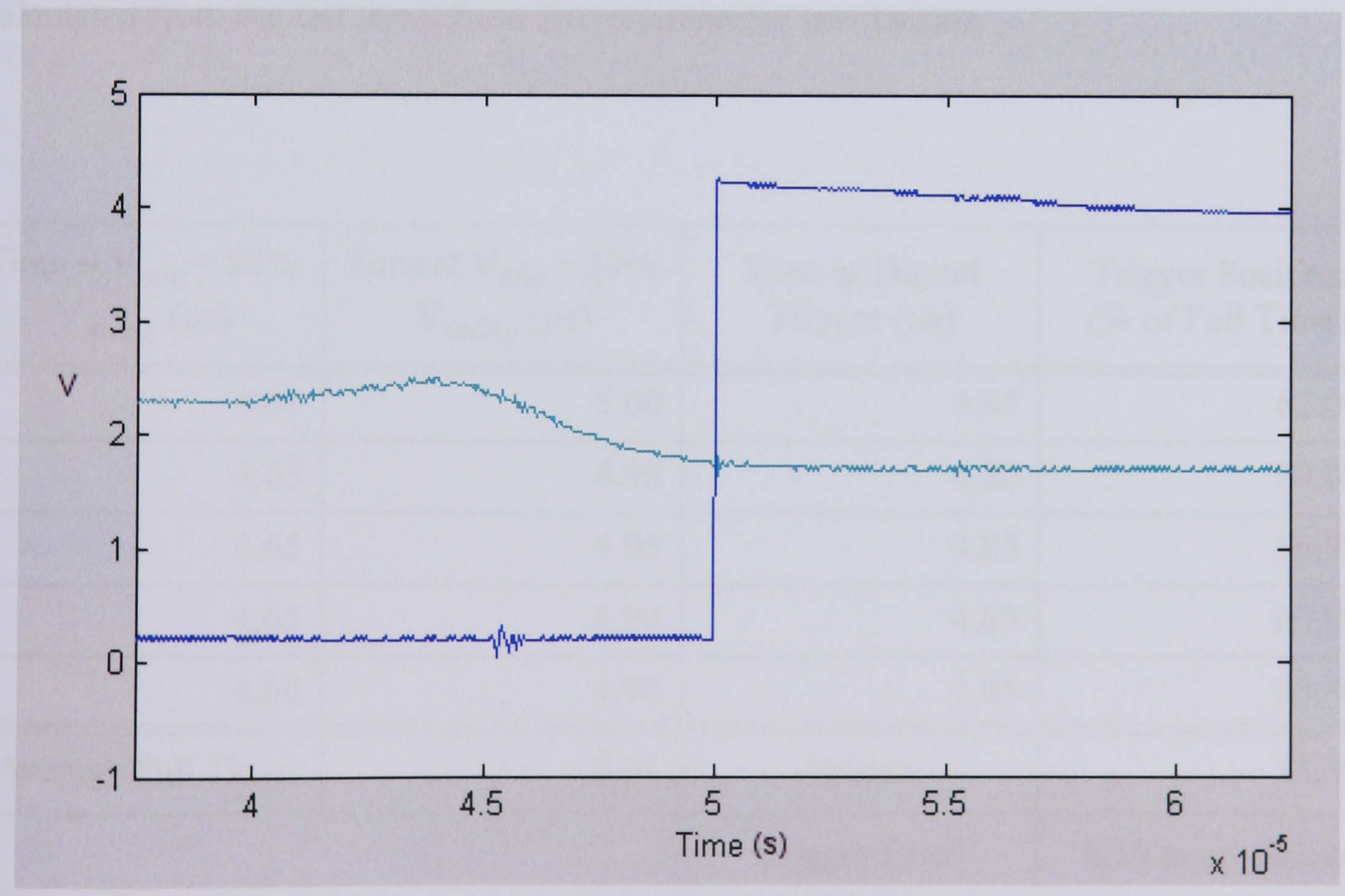

Figure D.7.5 - OPR Receiver and Comparator Output Signals at 100 RPM

Rotor Speed (RPM)	Average Receiver Signal Fall Time* (μs)
350	0.87
450	0.68
550	0.60
650	0.60
750	0.43
850	0.30
938	0.31
1050	0.30
1150	0.32

Table D.2 - OPR Receiver Signal Fall Times at Various Rotor RPM Speeds

* Calculated from the fall times from five consecutive revolutions.

Time at V_{min} + 80% V_{swing} (μs)	Time at V_{min} + 20% V_{swing} (μs)	Time at Digital Trigger (μs)	Trigger Position (% of Fall Time)
4.60	5.00	4.85	62.0%
4.65	4.95	4.80	50.0%
4.65	4.95	4.85	66.7%
4.65	4.90	4.80	60.0%
4.60	4.90	4.85	83.3%
Average Fall Time	0.31	Spread	33.3%
		Trigger Error	0.10 microseconds

Table D.3 - OPR Triggering Consistency at 938 RPM

Appendix D.8 - Once Per Revolution Sensor Calculations

Receiver Power Calculation

Emitter Fibre: 9/125 μm,
Laser Beam Divergence Cone Angle = 16.4°

$$\therefore A_{5mm} = \pi\left(\frac{9\times10^{-3}}{2} + 5\tan\frac{16.4°}{2}\right) = 1.65mm^2$$

Laser Power = $10mW$

Power at Emitter Fibre, assuming 4% glass/air loss: $10mW \times 0.96 = 9.6mW$

Receiver Fibre: $62.5/125\mu m$

$$\therefore A_{receiver} = \pi\left(\frac{62.5}{2}\right)^2$$

Emitter Fibre to Receiver Fibre Power Loss Ratio = $A_{5mm} : A_{receiver} \Rightarrow 538 : 1$

Power at Receiver Fibre: $\frac{9.6mW}{538} = 17.8\mu W$

Power at Receiver, assuming 4% glass/air loss: $17.8\mu W \cdot 0.96 = 17.1\mu W$

Appendix D.9 - Data Acquisition Software

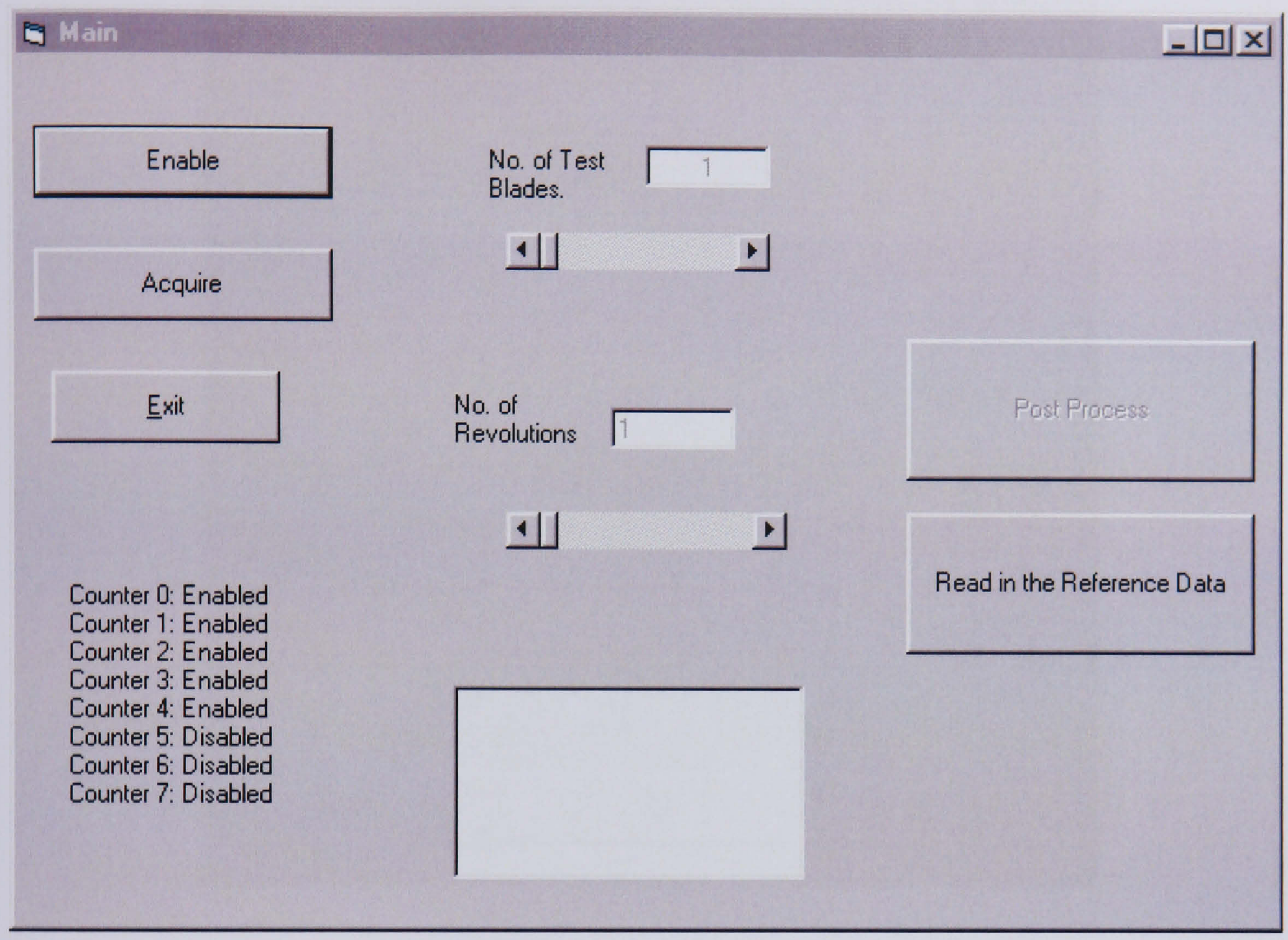

Figure D.9.1 - Custom Counter/Timer Hardware Control Software Screenshot 1

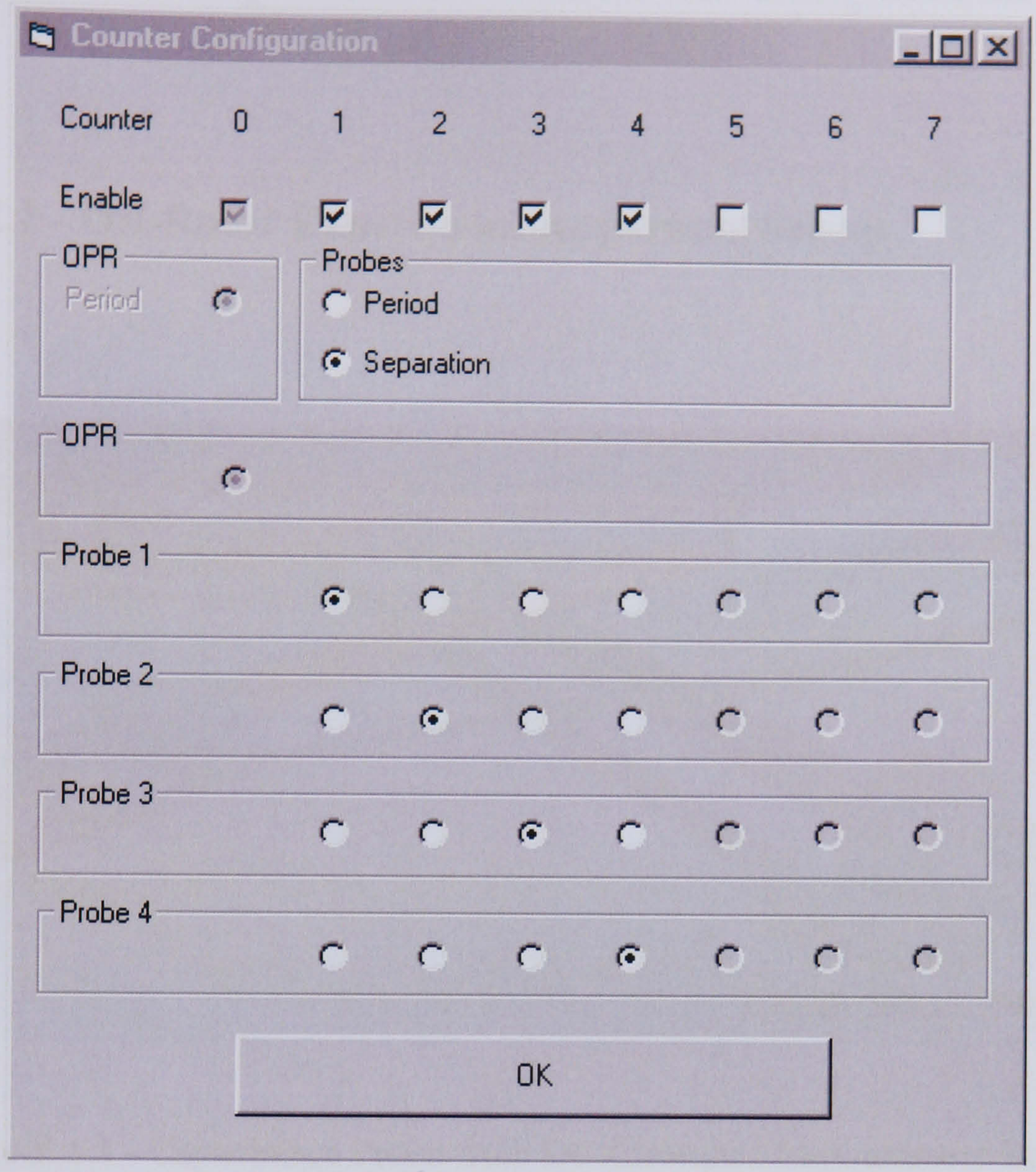

Figure D.9.2 - Custom Counter/Timer Hardware Control Software Screenshot 2

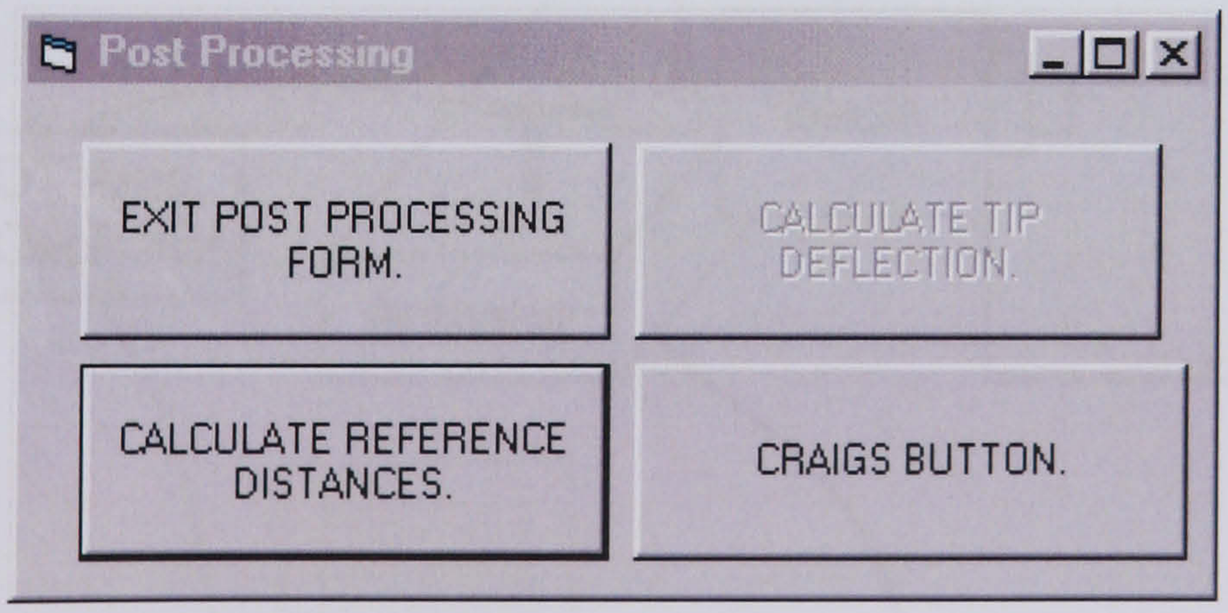

Figure D.9.3 - Custom Counter/Timer Hardware Control Software Screenshot 3

Appendix E - Experiment Method and Results

Appendix E.1 - Off-Rotor Experiment Apparatus Set-up

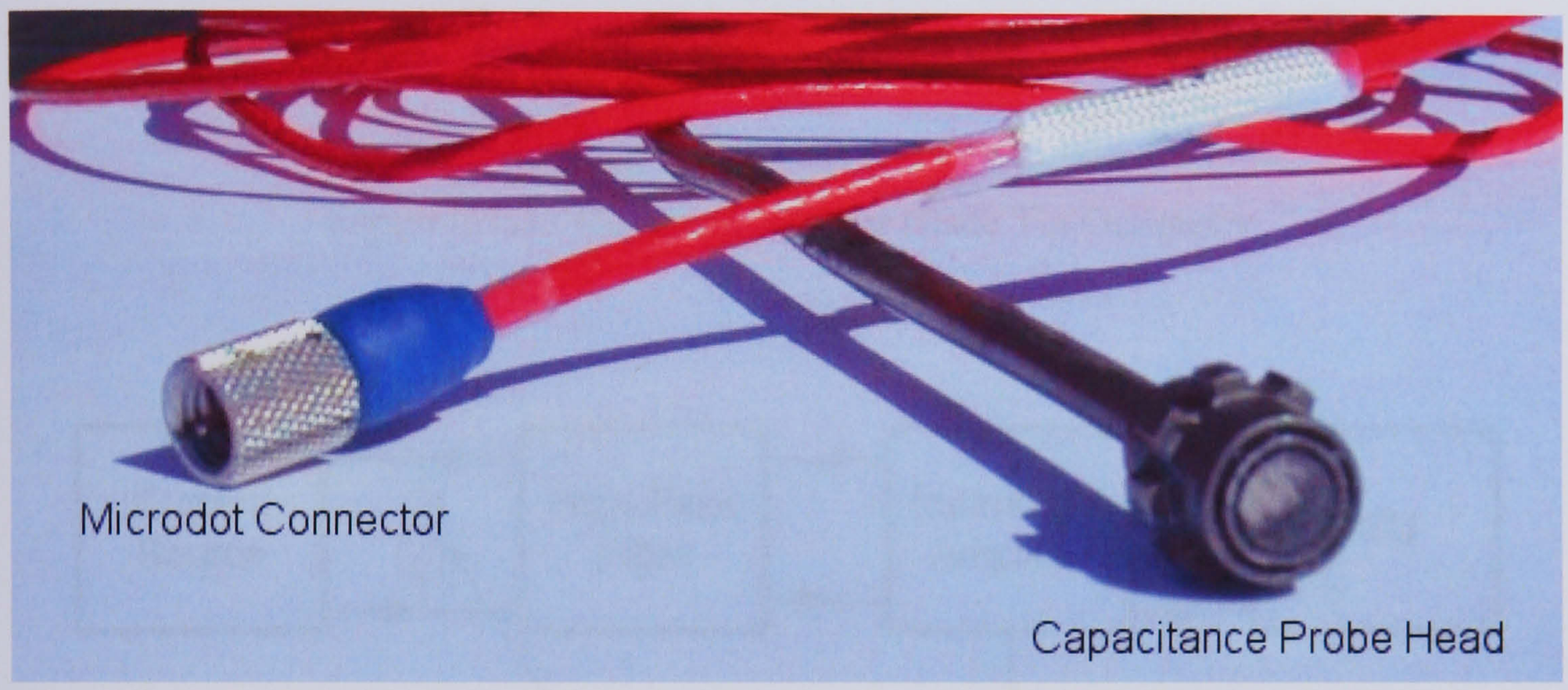

Figure E.1.1 - Capacitance Probe from DC Clearance Measurement System

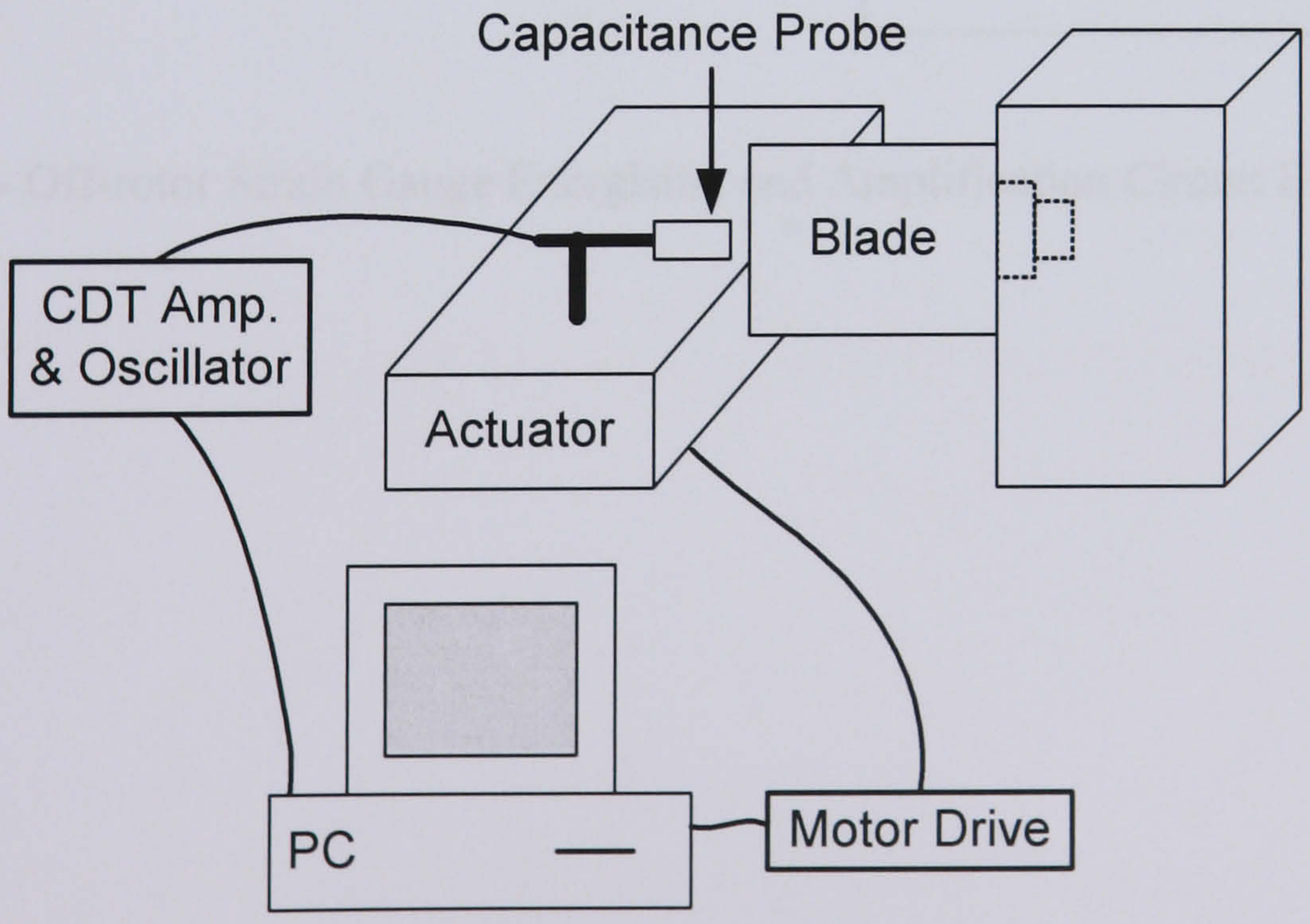

Figure E.1.2 - Capacitance Probe Characteristic Test Experiment Set-up

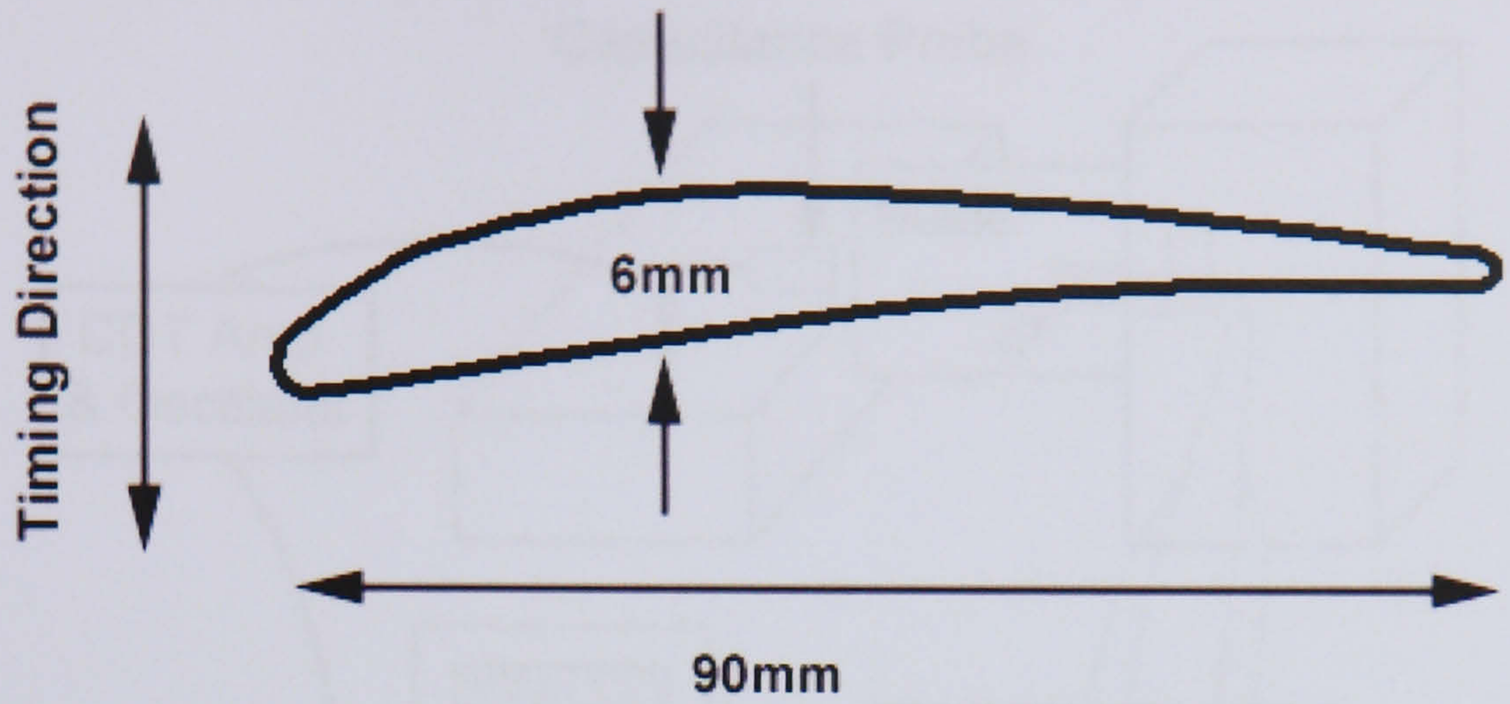

Figure E.1.3 - Compressor Rotor Blade Tip Geometry

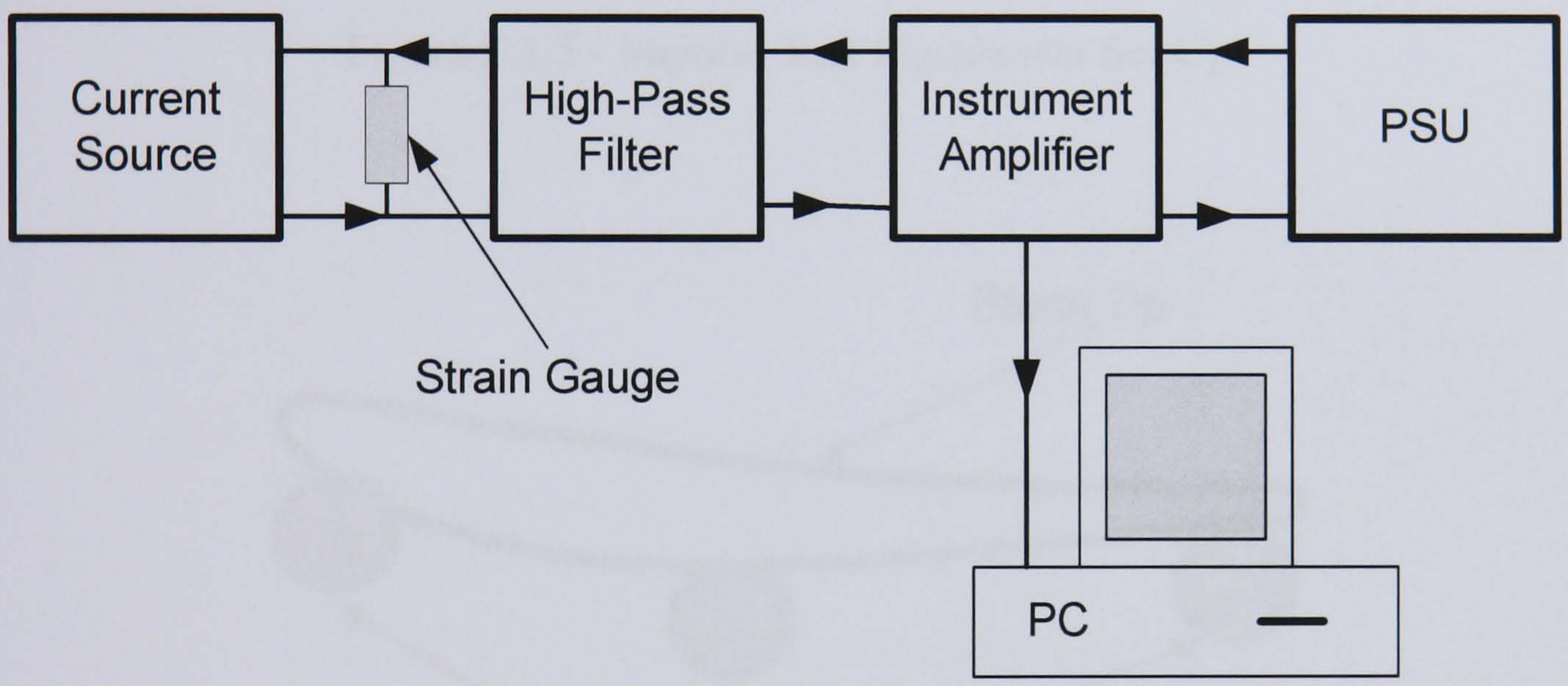

Figure E.1.4 - Off-rotor Strain Gauge Energising and Amplification Circuit Block Diagram

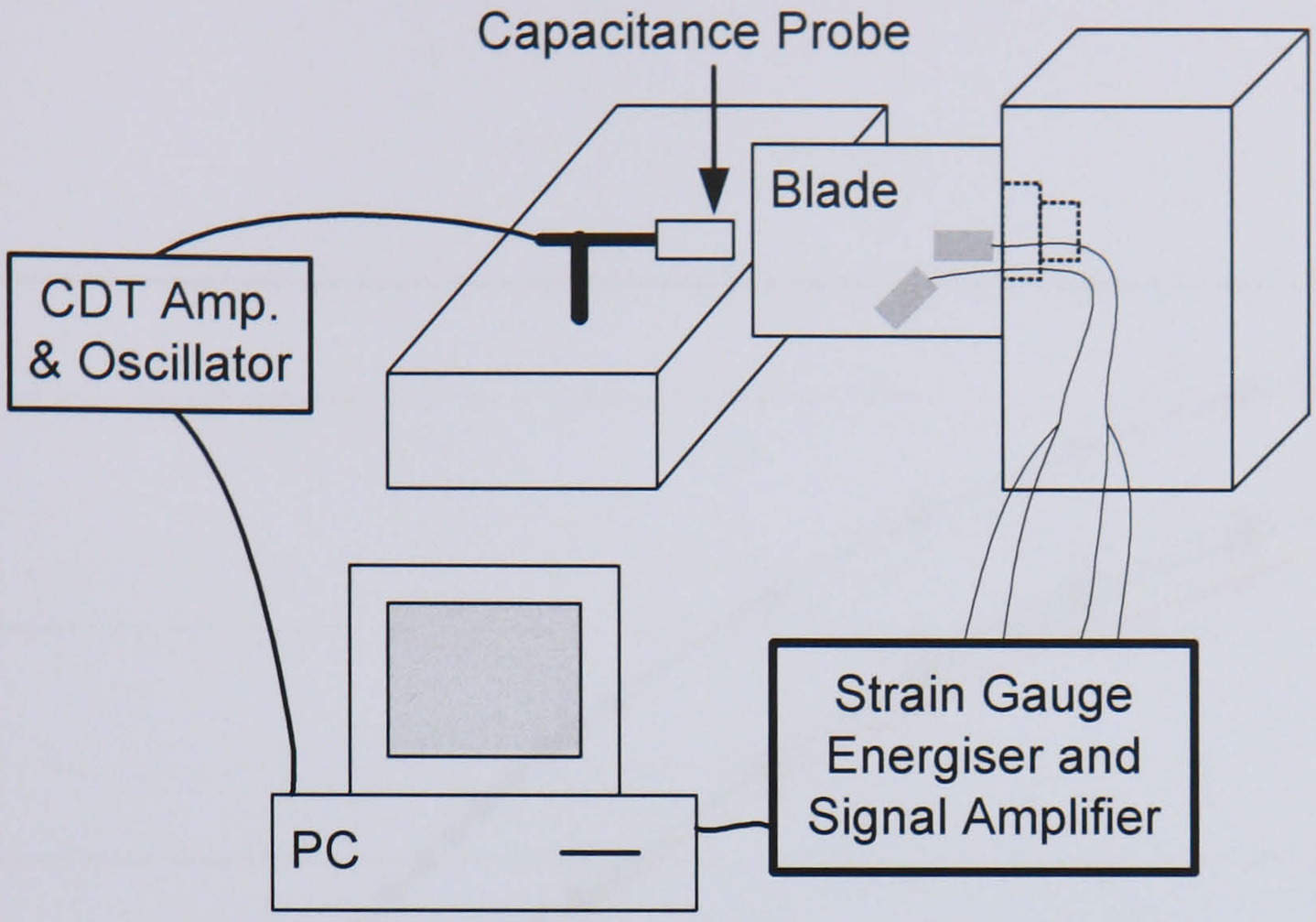

Figure E.1.5 - Impulse Test Experiment Set-Up

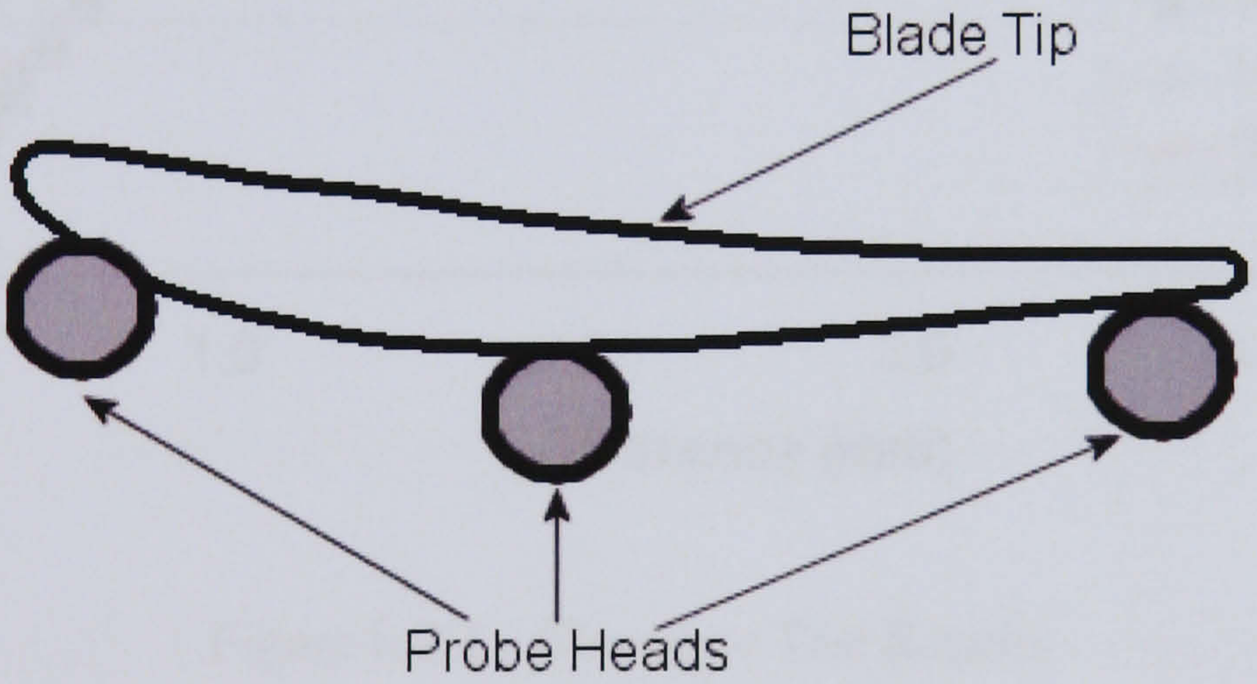

Figure E.1.6 - Impulse Test Capacitance Probe Head Positioning

Appendix E.2 - Clearance Test Results

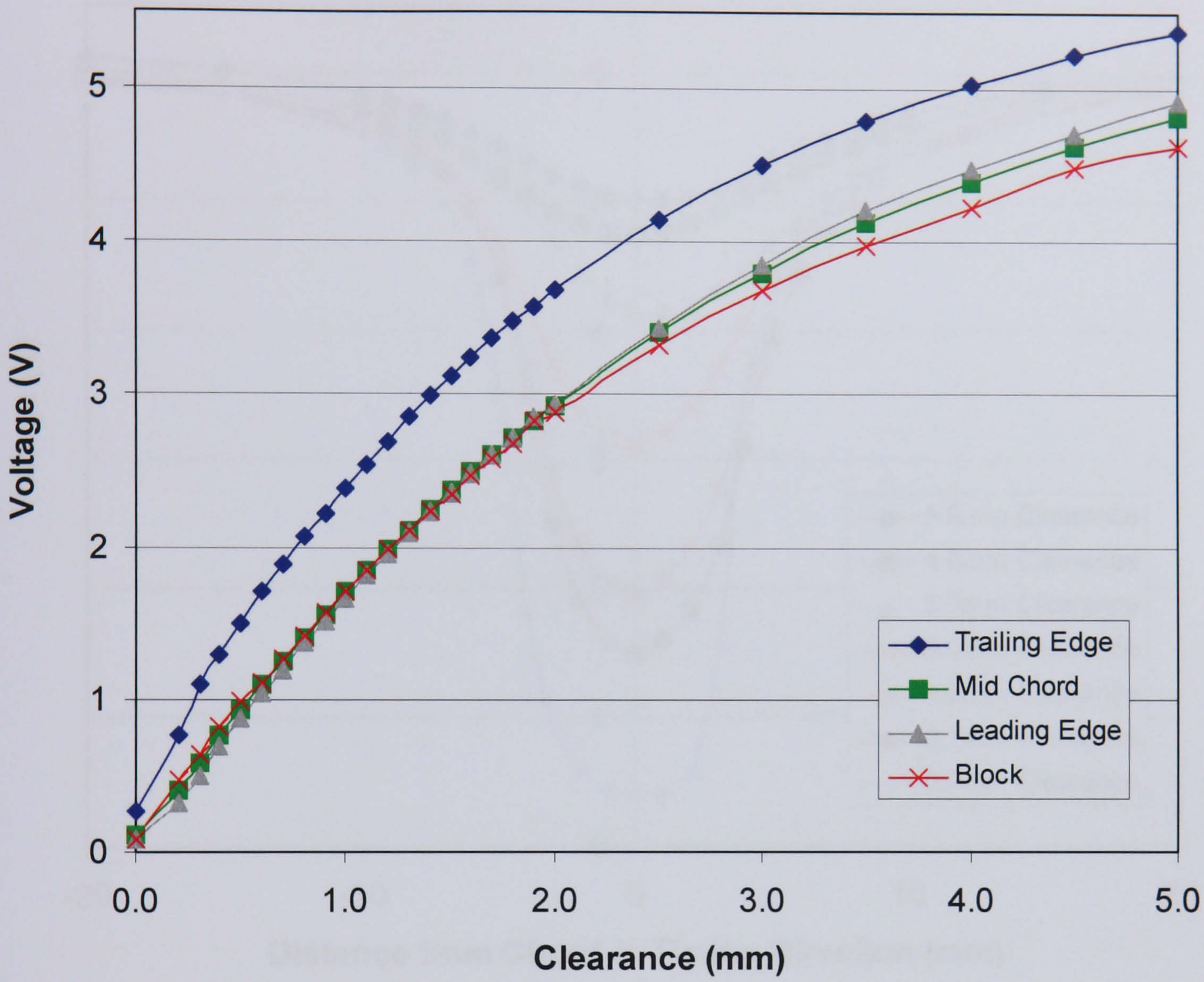

Figure E.2.1 - Clearance Test Results

Appendix E.3 - Capacitance Probe Characteristic Mapping Test Results

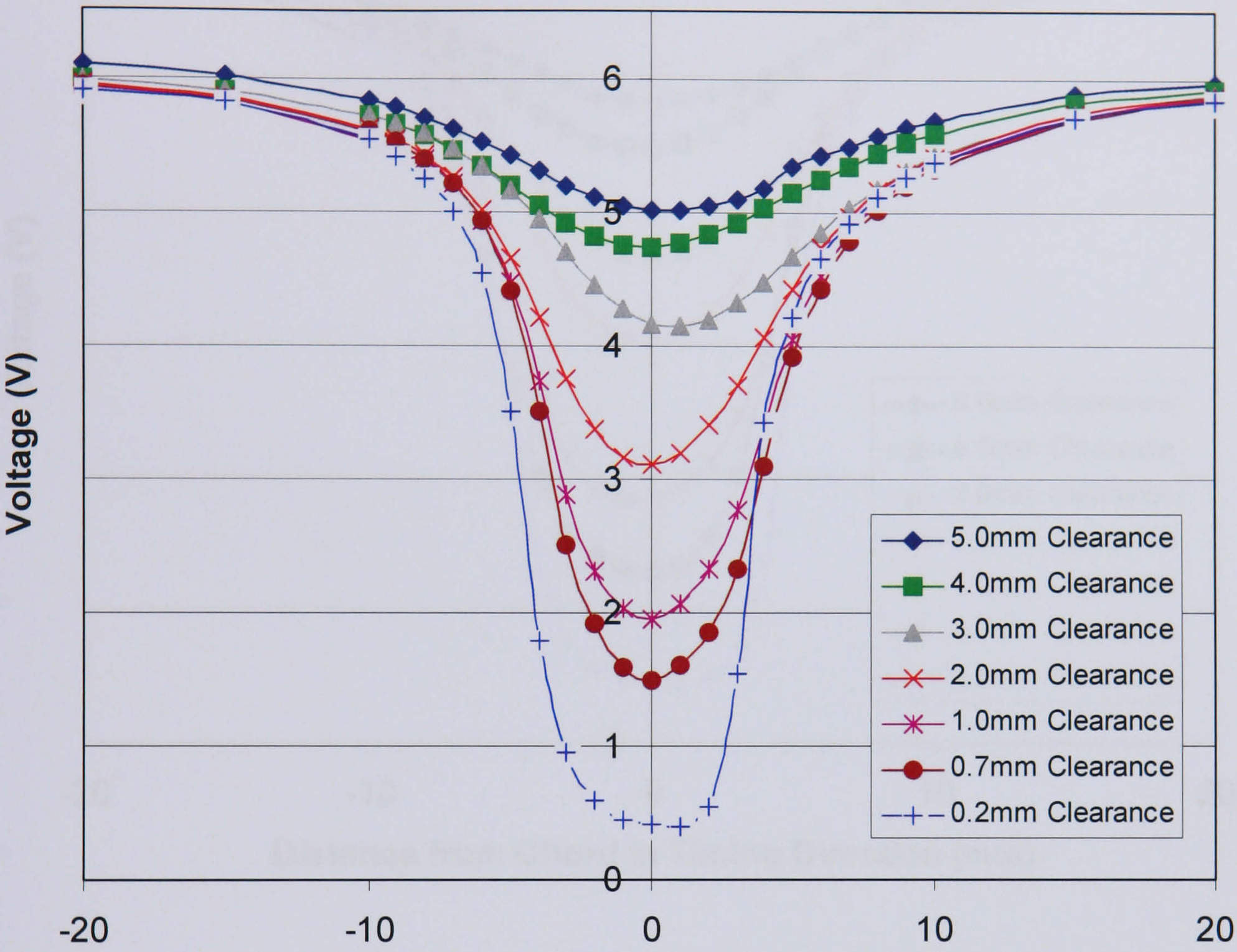

Figure E.3.1 - Capacitance Probe Characteristic Mapping Test Blade Leading Edge

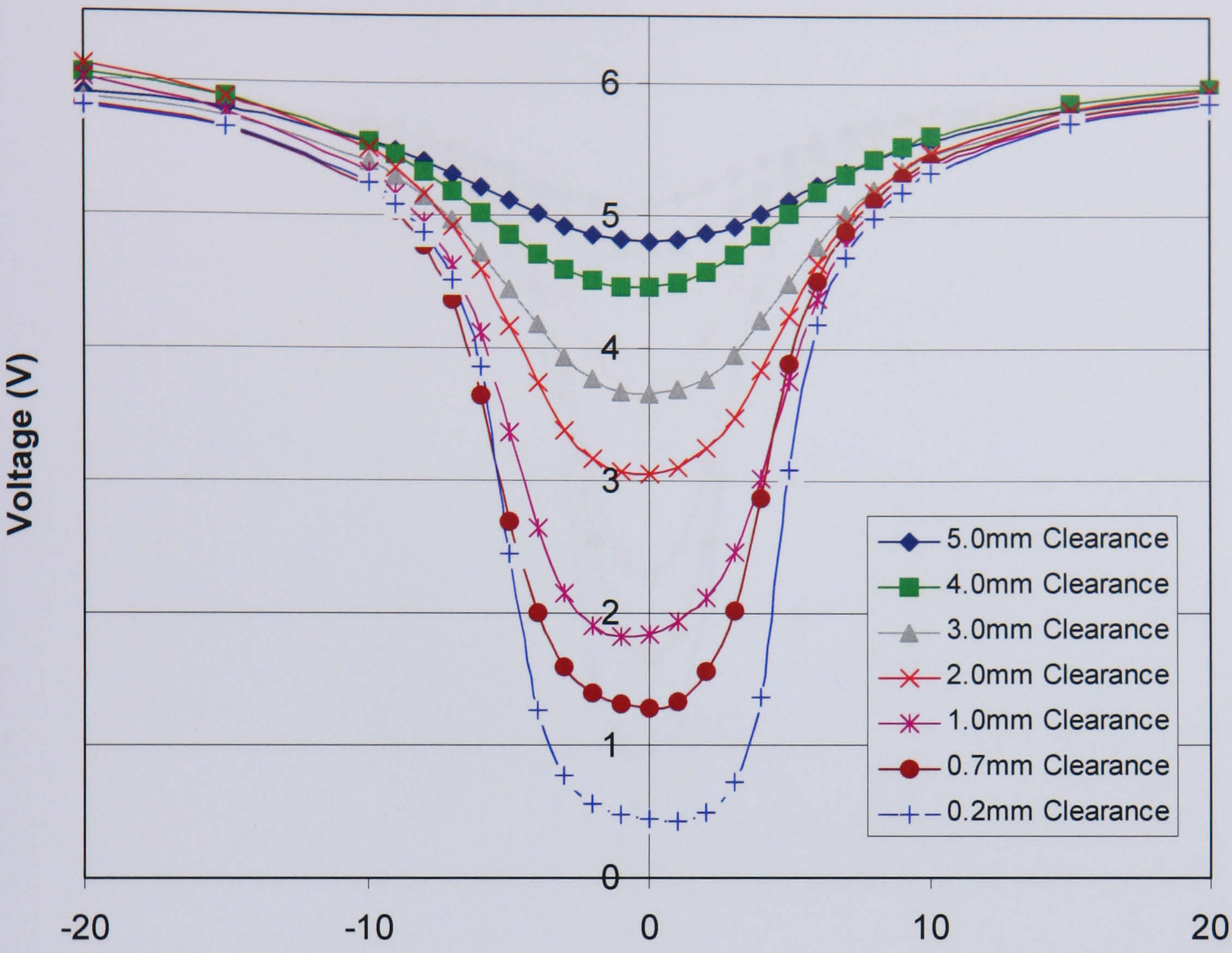

Figure E.3.2 - Capacitance Probe Characteristic Mapping Test Blade Mid Chord

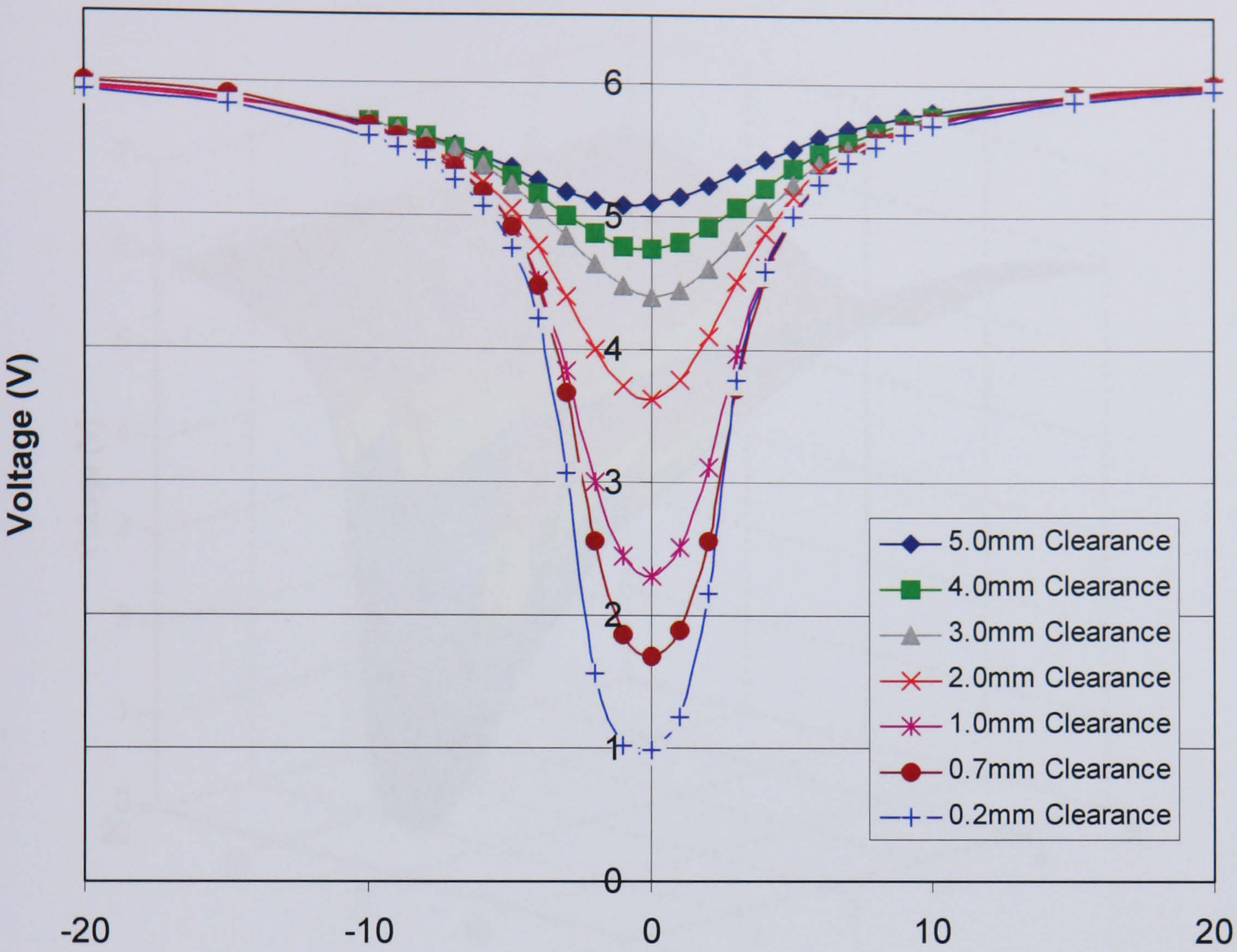

Figure E.3.3 - Capacitance Probe Characteristic Mapping Test Blade Trailing Edge

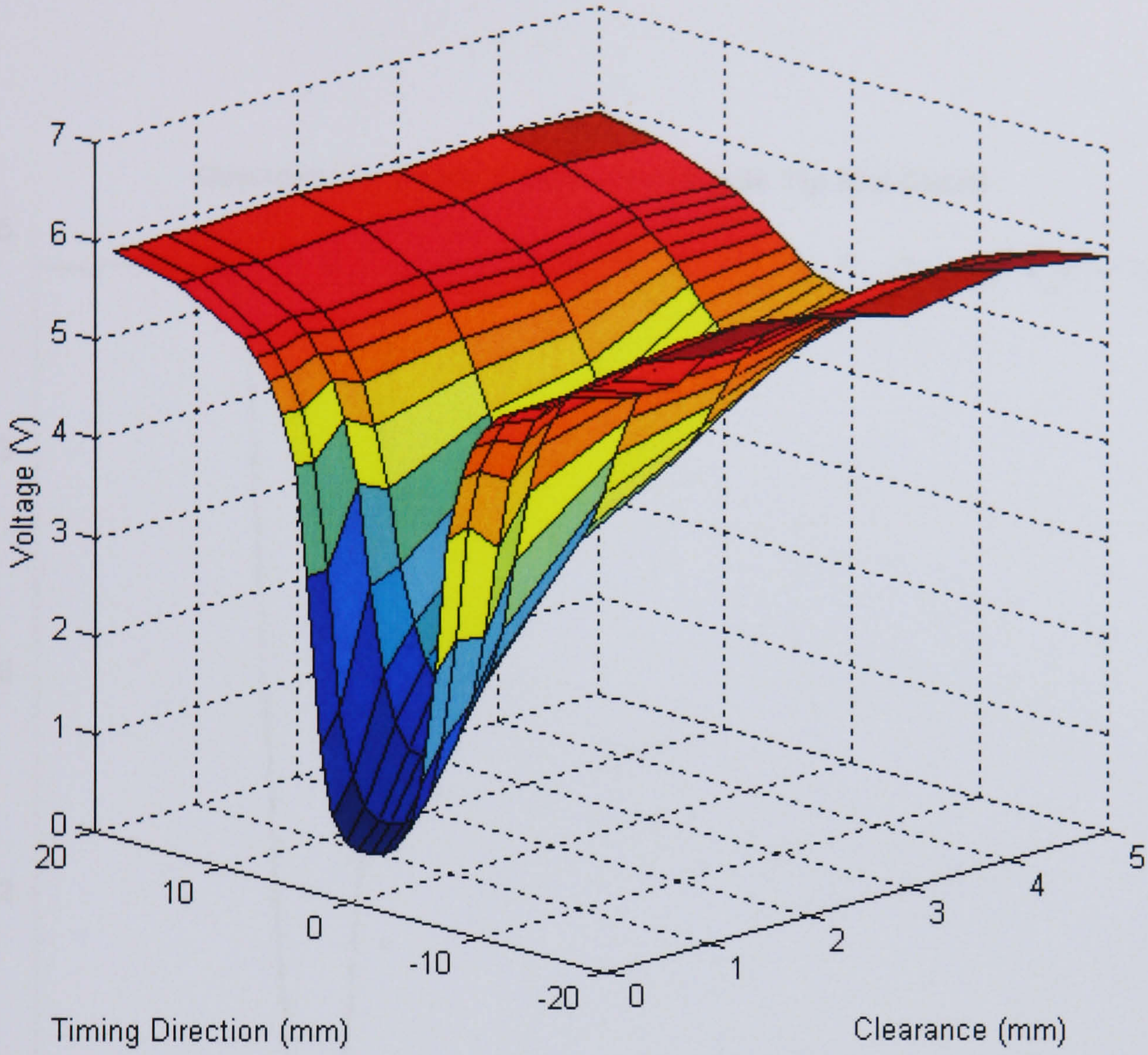

Figure E.3.4 - Capacitance Probe Characteristic 3-D Map Blade Mid Chord

Appendix E.4 - Impulse Test Results

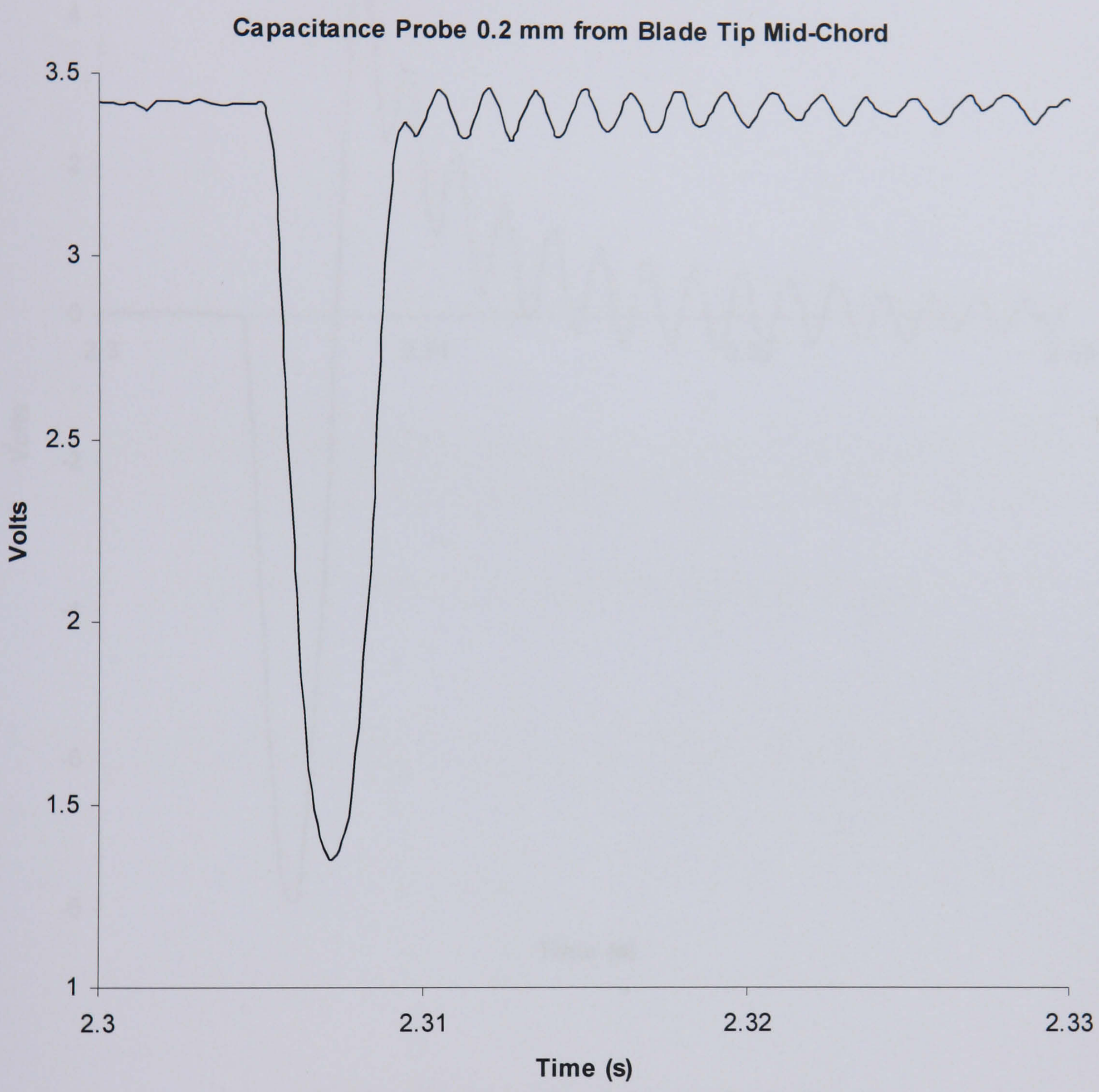

Figure E.4.1 - Capacitance Probe at 0.2 mm Clearance From Blade Tip Mid Chord

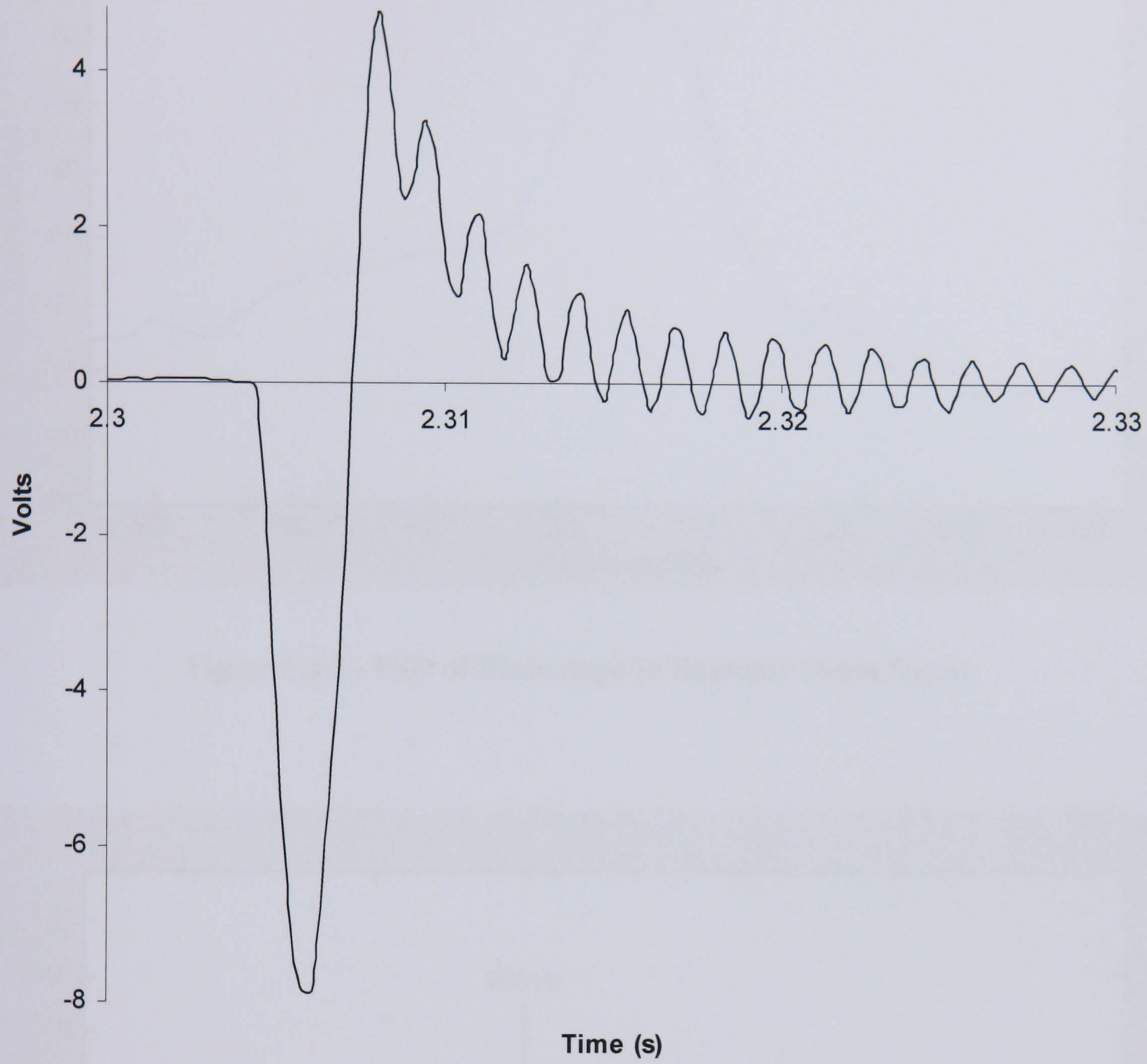

Figure E.4.2 - Blade Impulse Response Strain Signal

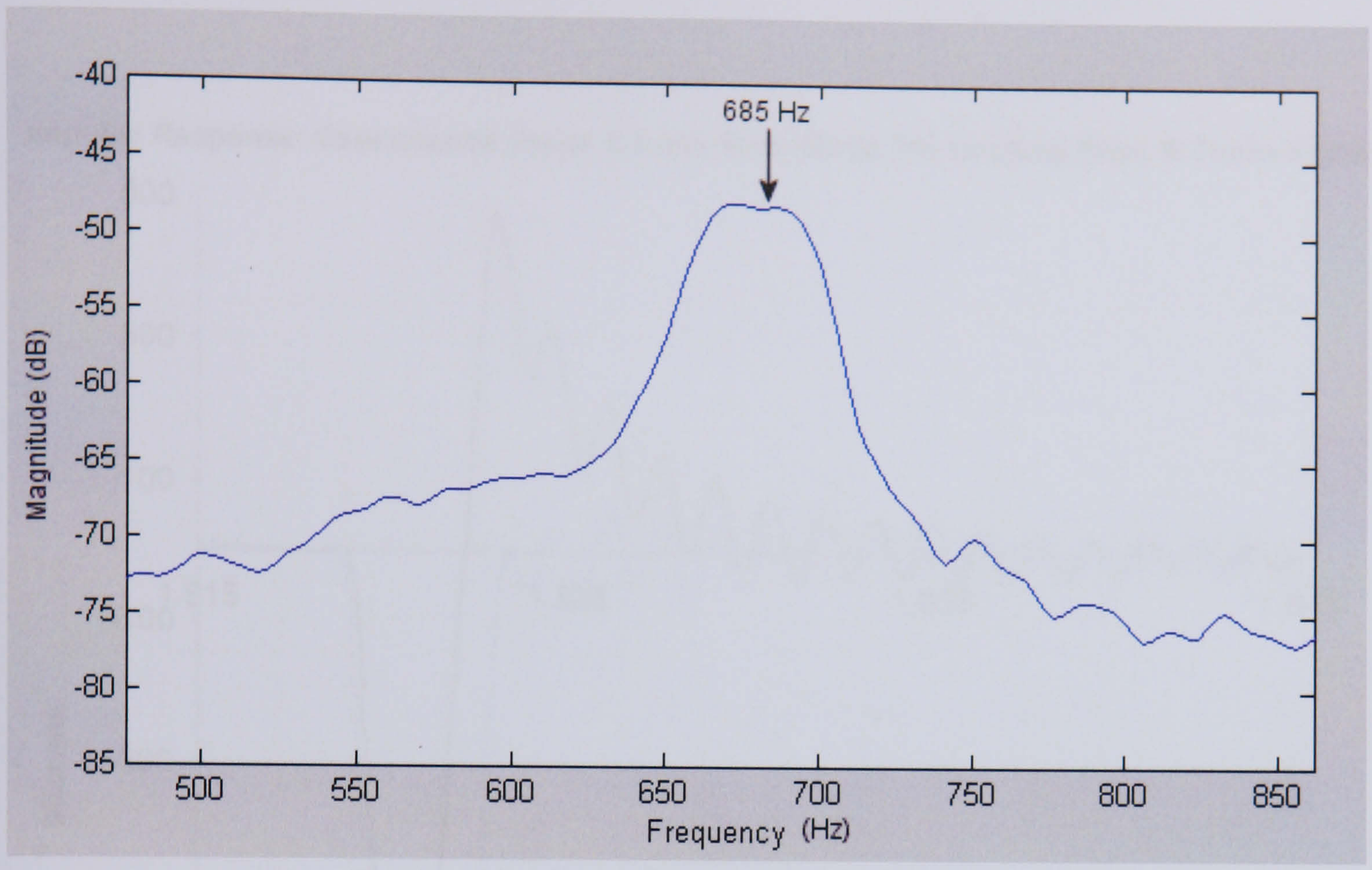

Figure E.4.3 - PSD of Blade Impulse Response Strain Signal

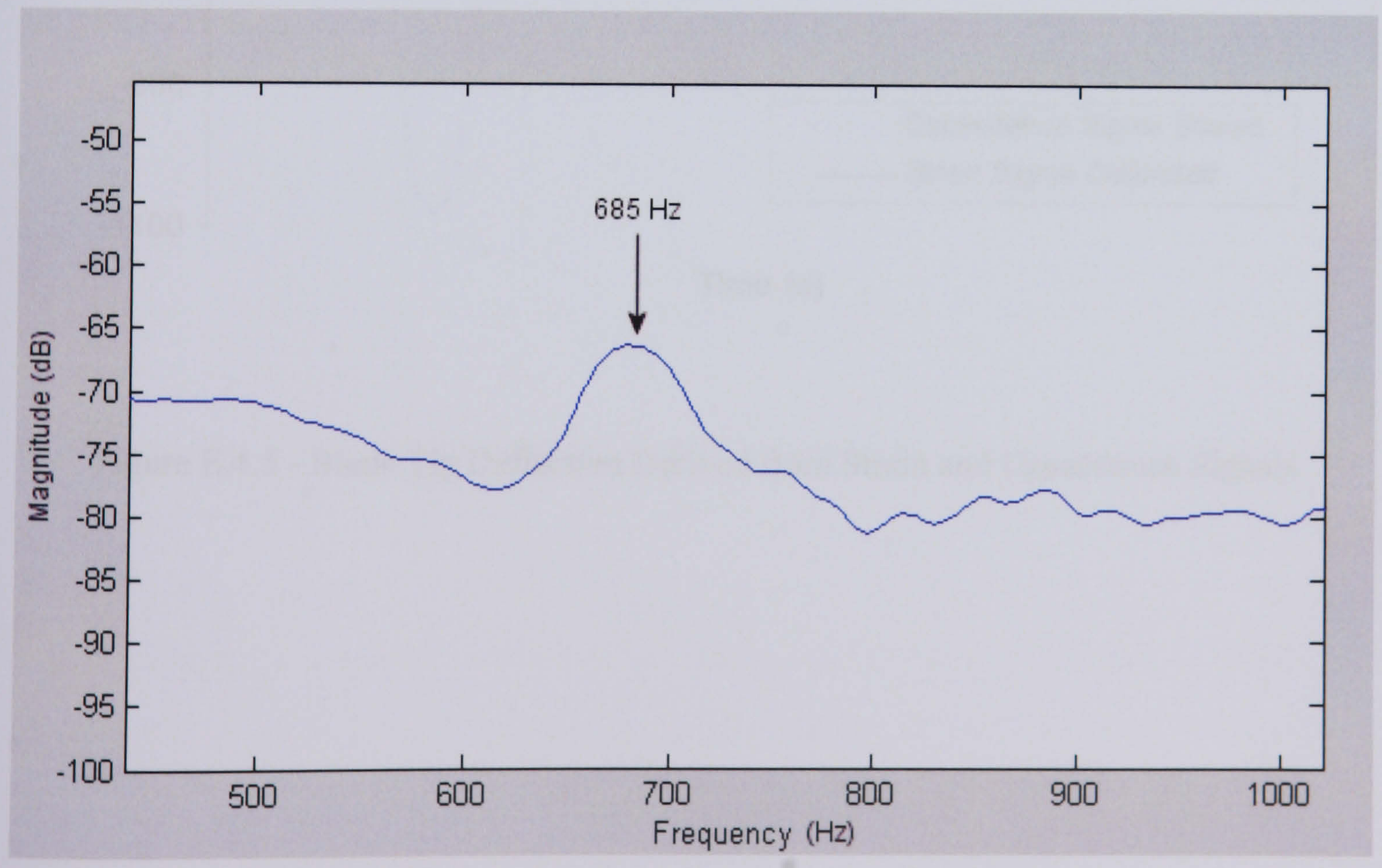

Figure E.4.4 - PSD of Blade Impulse Response Capacitance Probe Signal

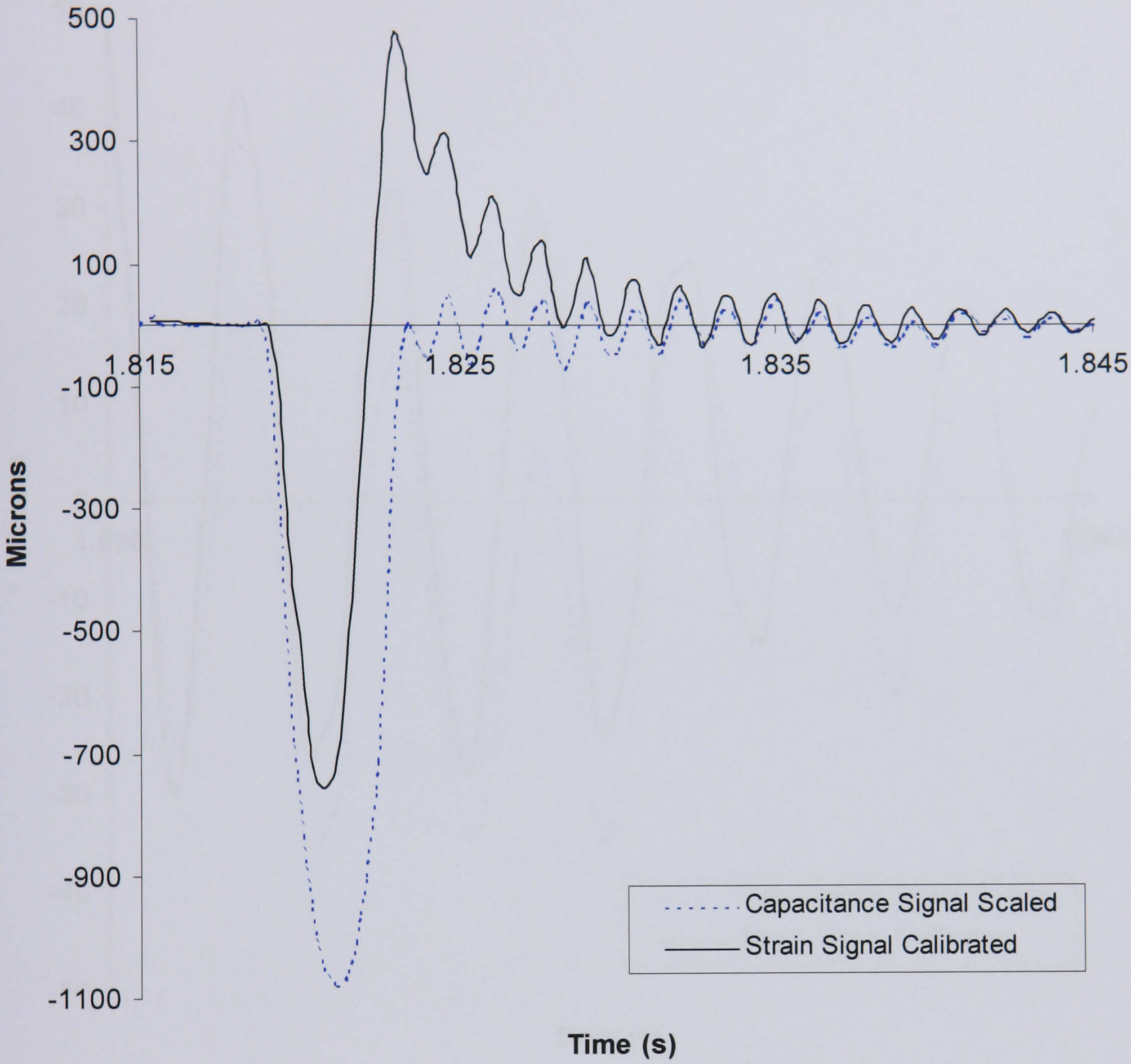

Figure E.4.5 - Blade Tip Deflection Derived from Strain and Capacitance Signals

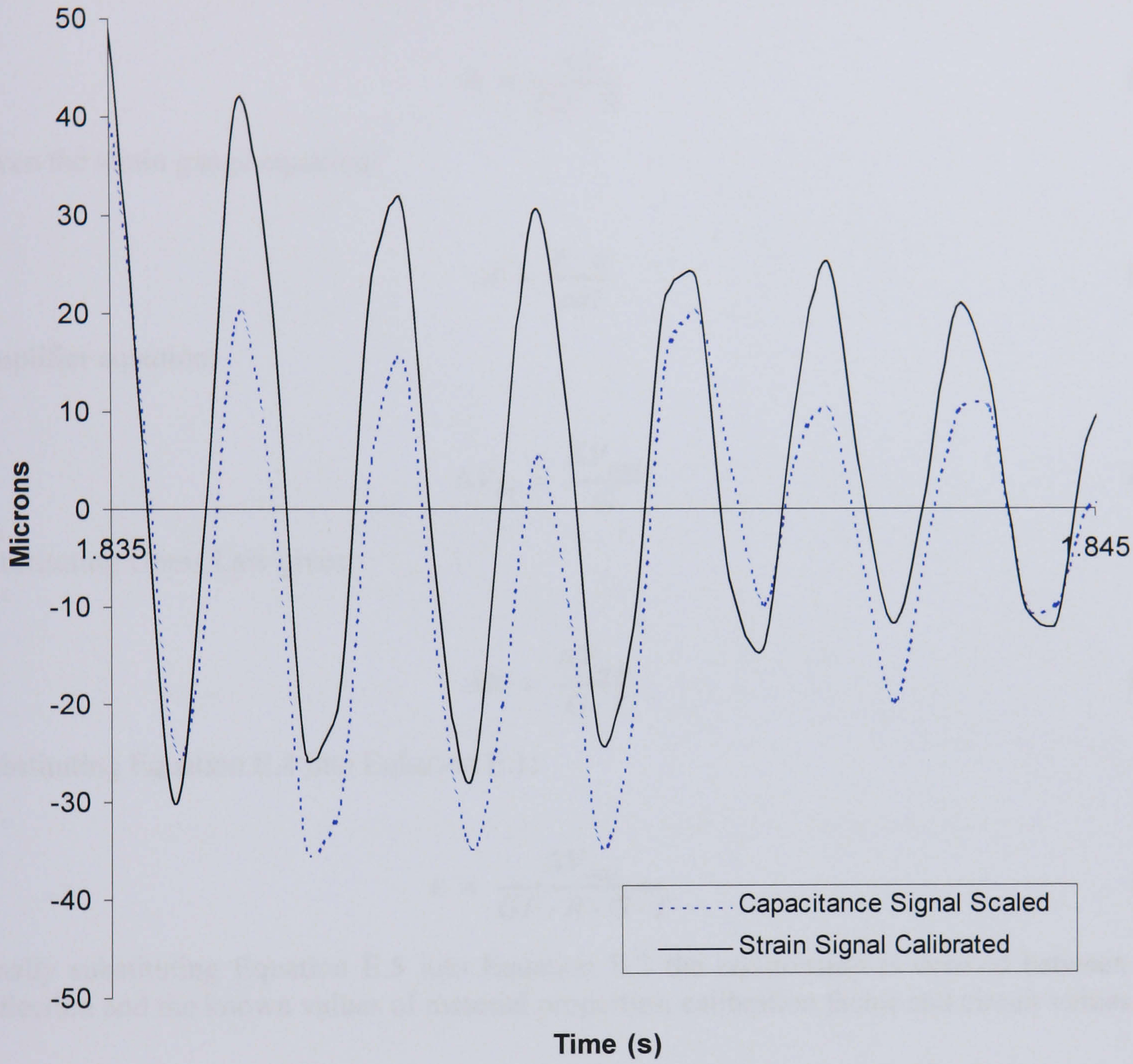

Figure E.4.6 - Blade Tip Deflection Derived from Strain and Capacitance Signals

Appendix E.5 - Strain to Tip Deflection Derivation

Calibration data is in m/Pa, therefore the following equation is used:

$$\varepsilon = \frac{\Delta R}{GF \cdot R} \qquad \text{E.1}$$

Given the strain gauge equation:

$$d = \frac{E \cdot \varepsilon}{cal} \qquad \text{E.2}$$

Amplifier equation:

$$\Delta V_{in} = \frac{\Delta V_{out}}{G} \qquad \text{E.3}$$

Substituting Ohms Law gives:

$$\Delta R = \frac{\Delta V_{out}}{G \cdot I} \qquad \text{E.4}$$

Substituting Equation E.4 into Equation E.1:

$$\varepsilon = \frac{\Delta V_{out}}{GF \cdot R \cdot G \cdot I} \qquad \text{E.5}$$

Finally substituting Equation E.5 into Equation E.2 the relationship is derived between tip deflection and the known values of material properties, calibration factor and circuit values.

$$d = \frac{E \cdot \Delta V_{out}}{cal \cdot GF \cdot R \cdot G \cdot I} \qquad \text{E.6}$$

Appendix E.6 - On-Rotor Testing Experiment Apparatus Set-up

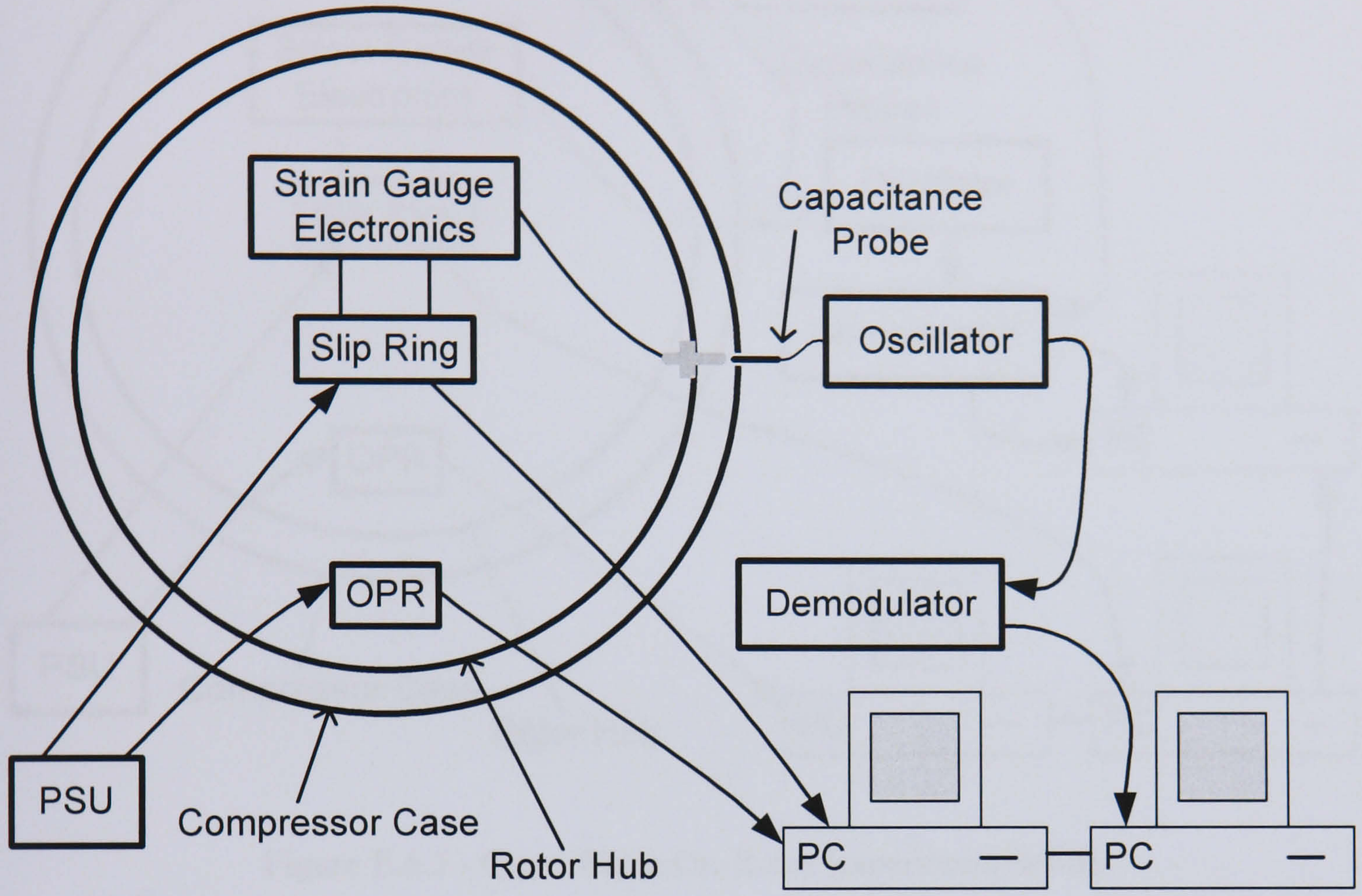

Figure E.6.1 - Compressor Rotor Blade On-Rotor Experiment Set-up

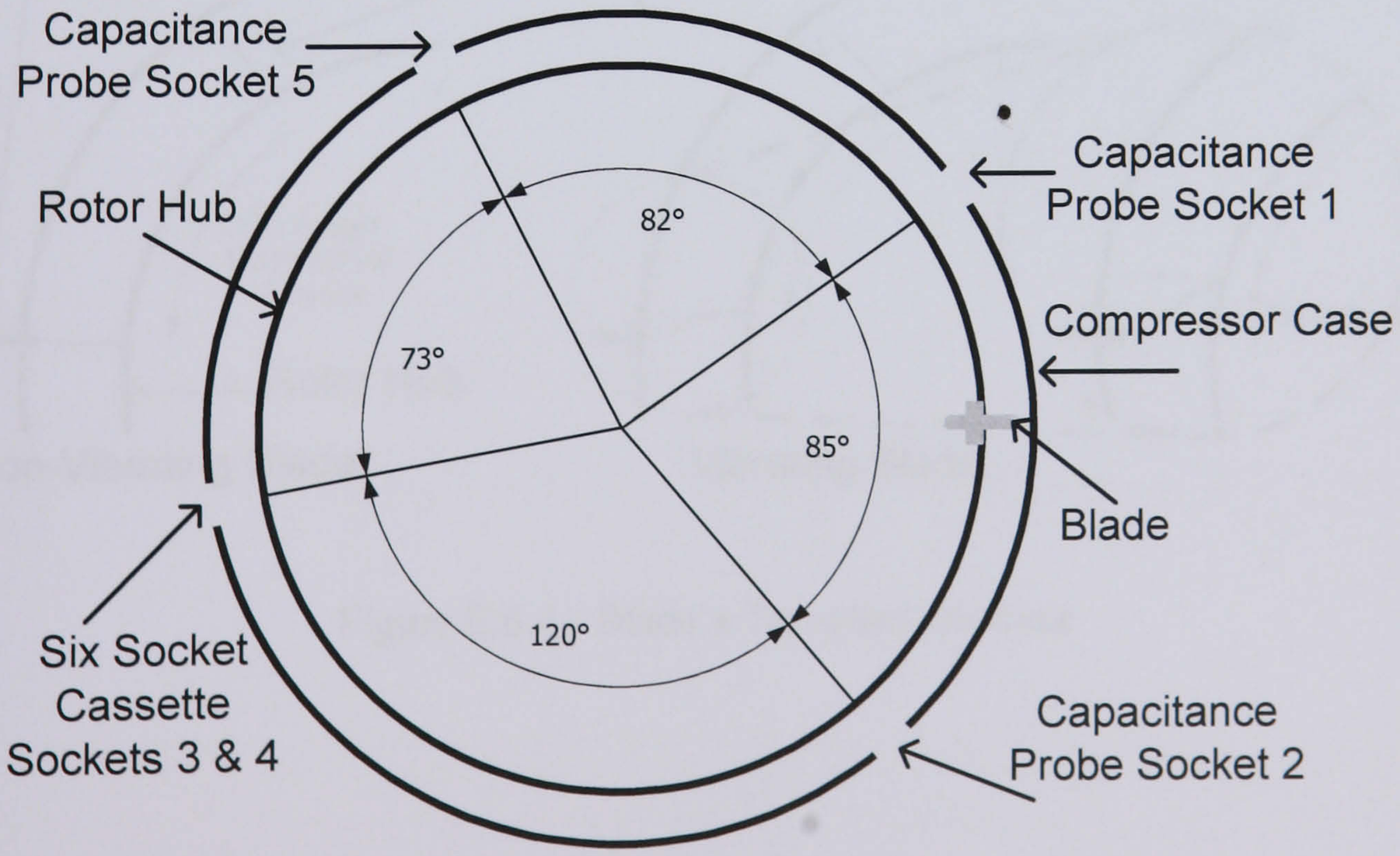

Figure E.6.2 - Capacitance Probe Mounting Positions

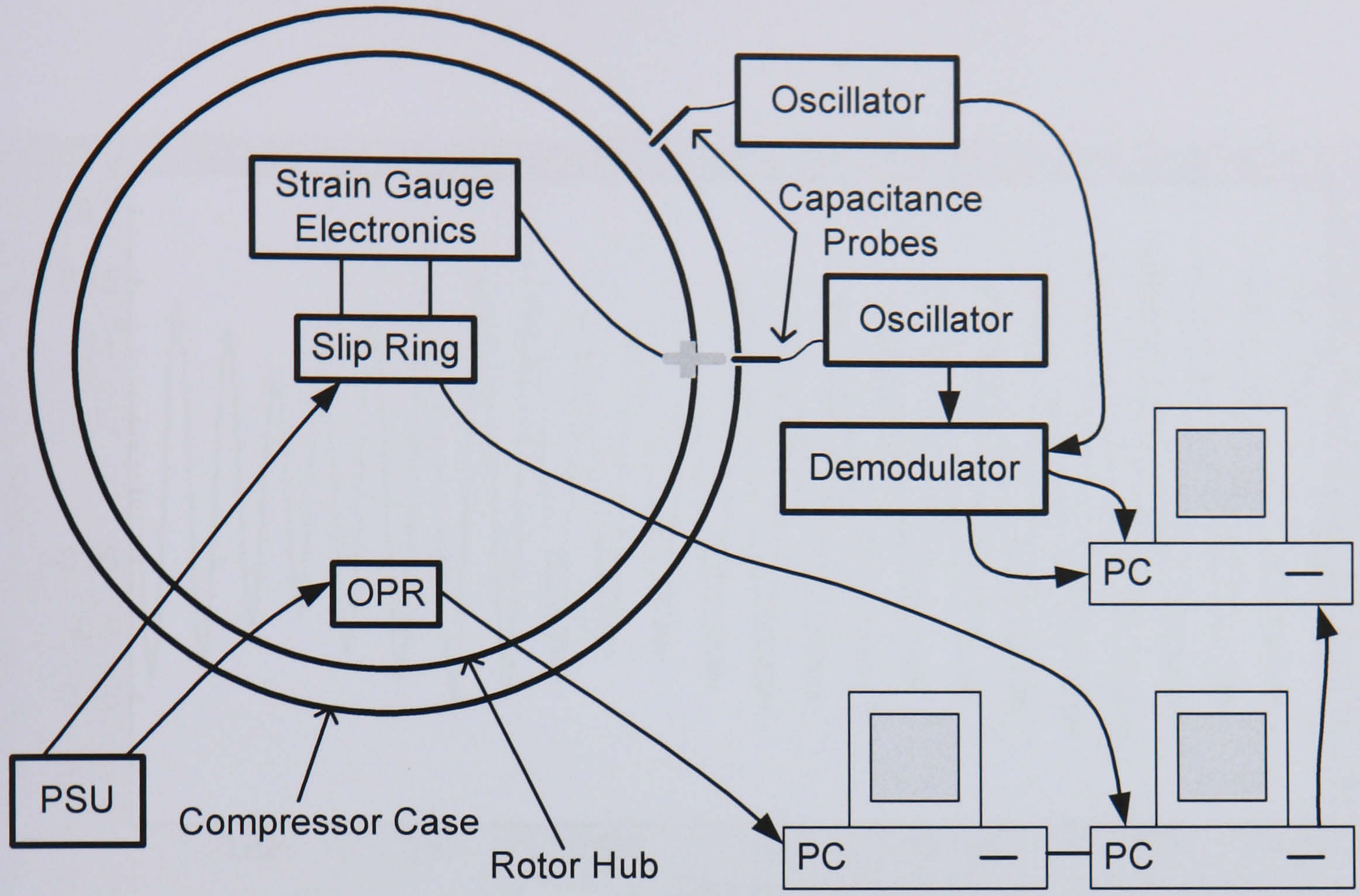

Figure E.6.3 - Quasi Blade On-Rotor Experiment Set-up

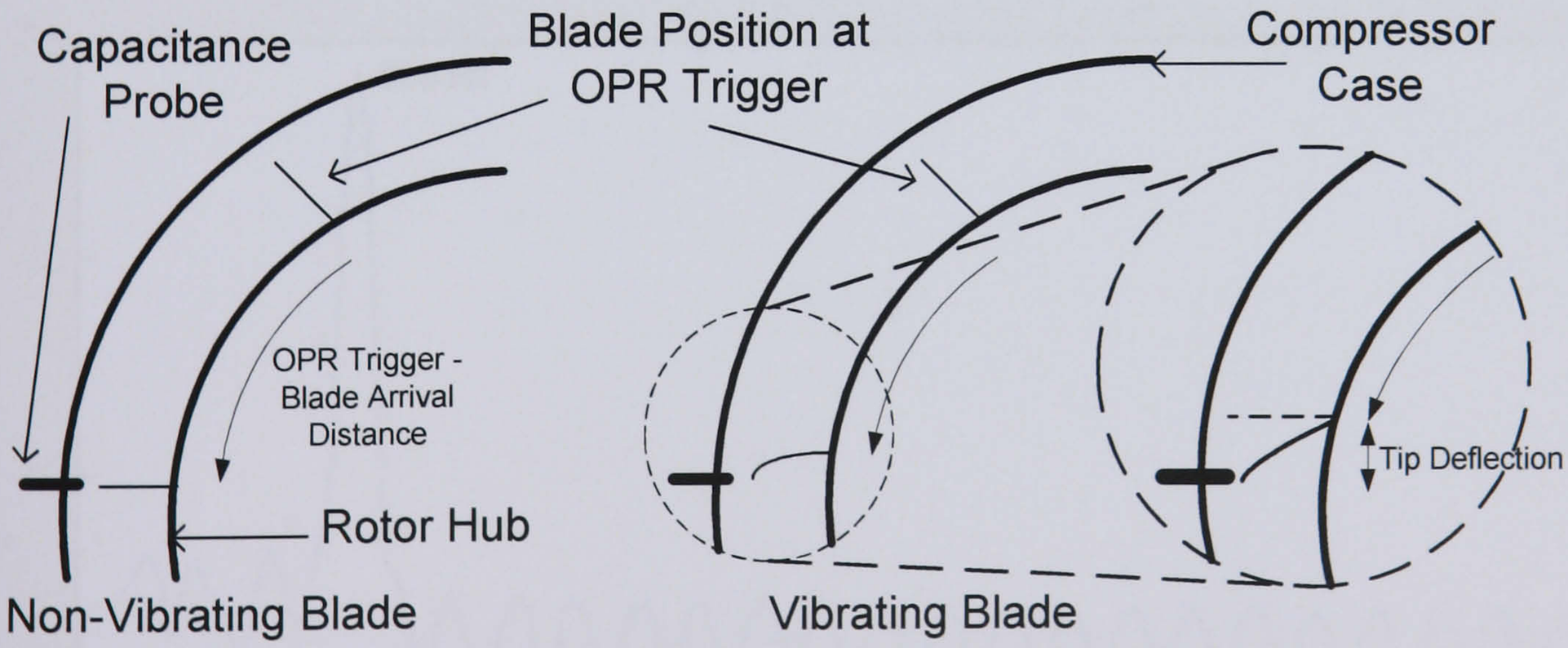

Figure E.6.4 - Blade's Travelled Distance

Appendix E.7 - Compressor Rotor Blade Vibration Results

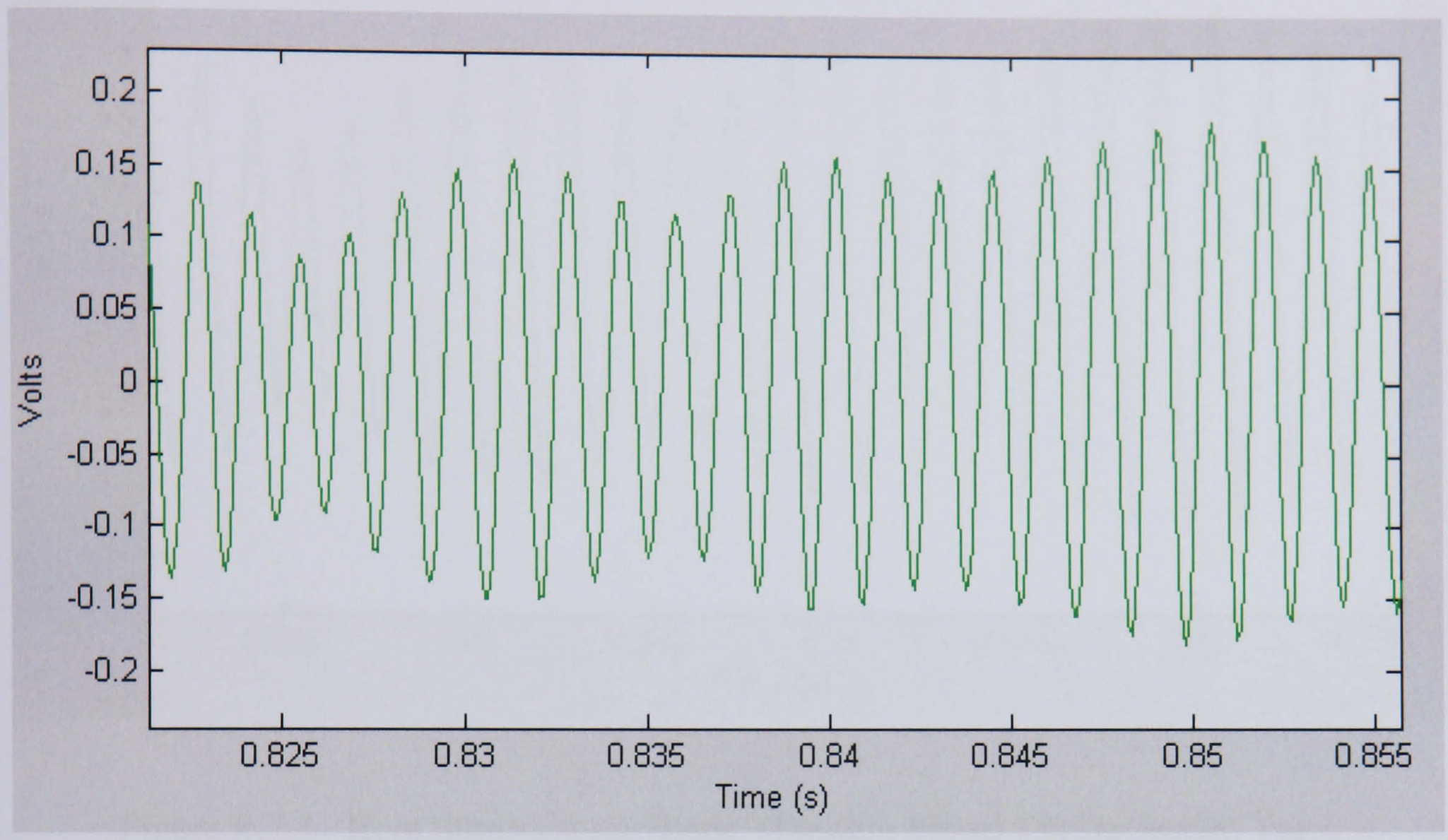

Figure E.7.1 - Root Strain Gauge Blade Vibration Signal Voltage Trace

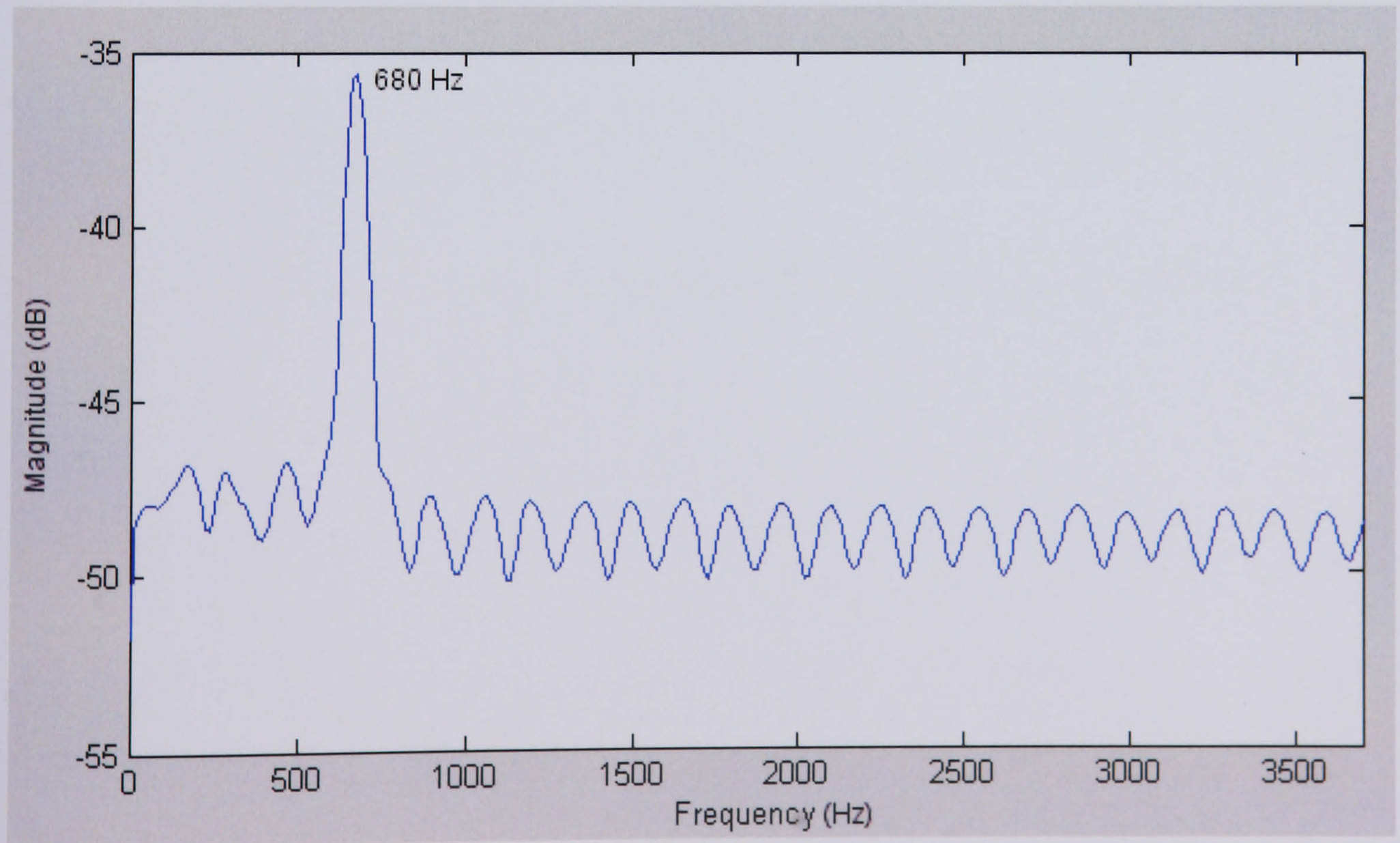

Figure E.7.2 - PSD of Strain Gauge Blade Vibration Signal

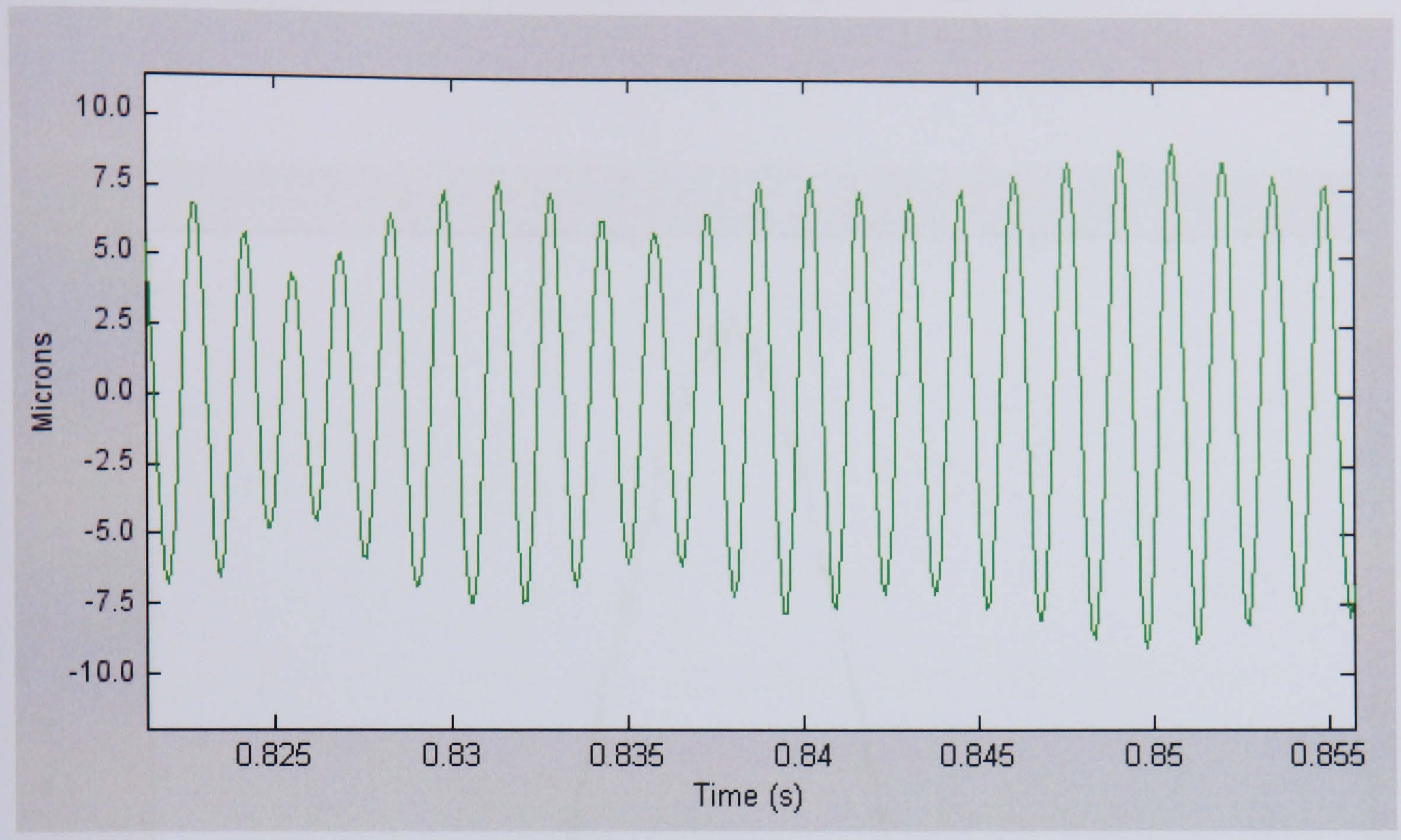

Figure E.7.3 - Root Strain Gauge Blade Vibration Signal Tip Deflection Trace

Appendix E.8 - Compressor Rotor Blade Tip Timing Results

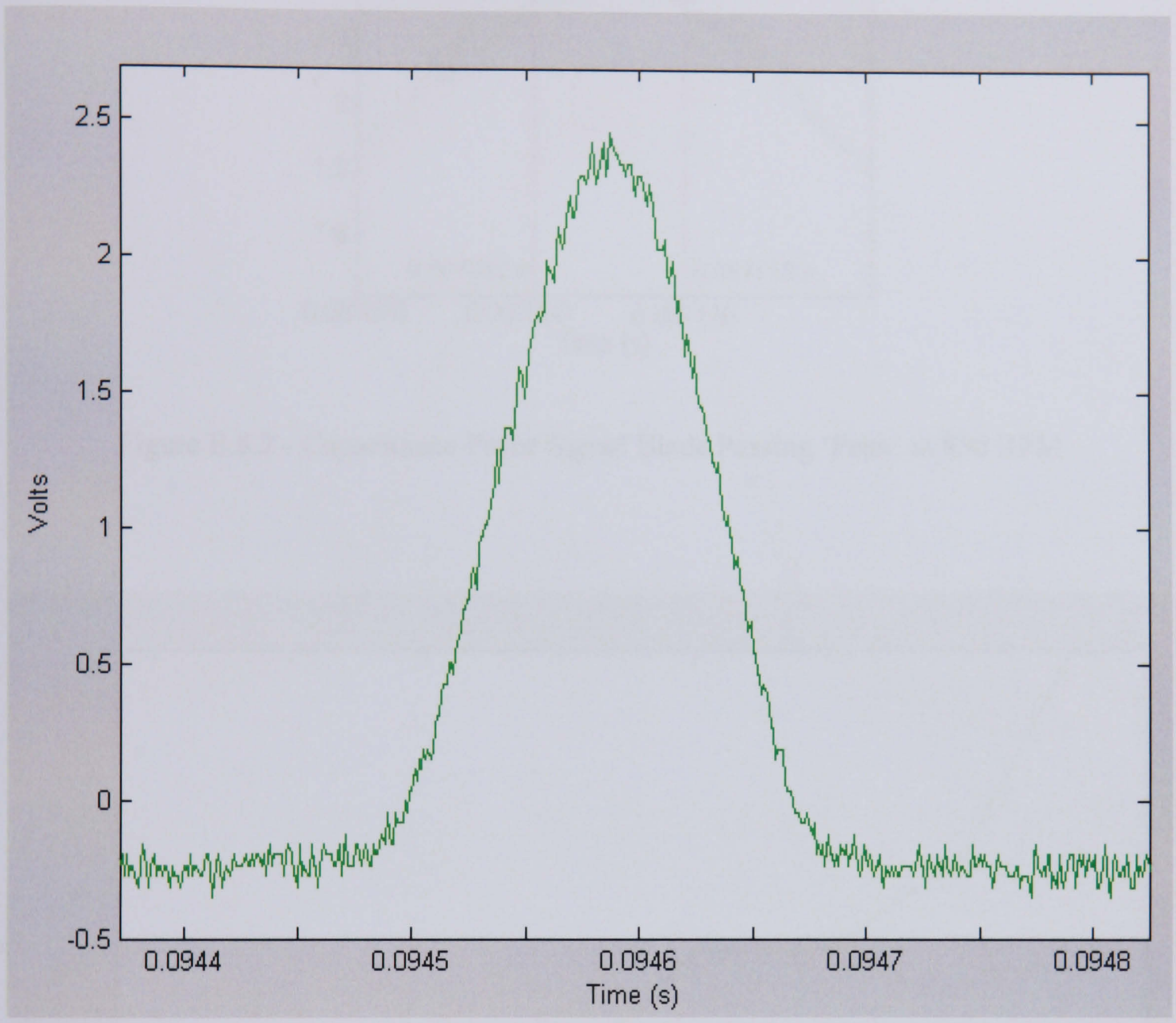

Figure E.8.1 - Capacitance Probe Signal Blade Passing Event at 850 RPM

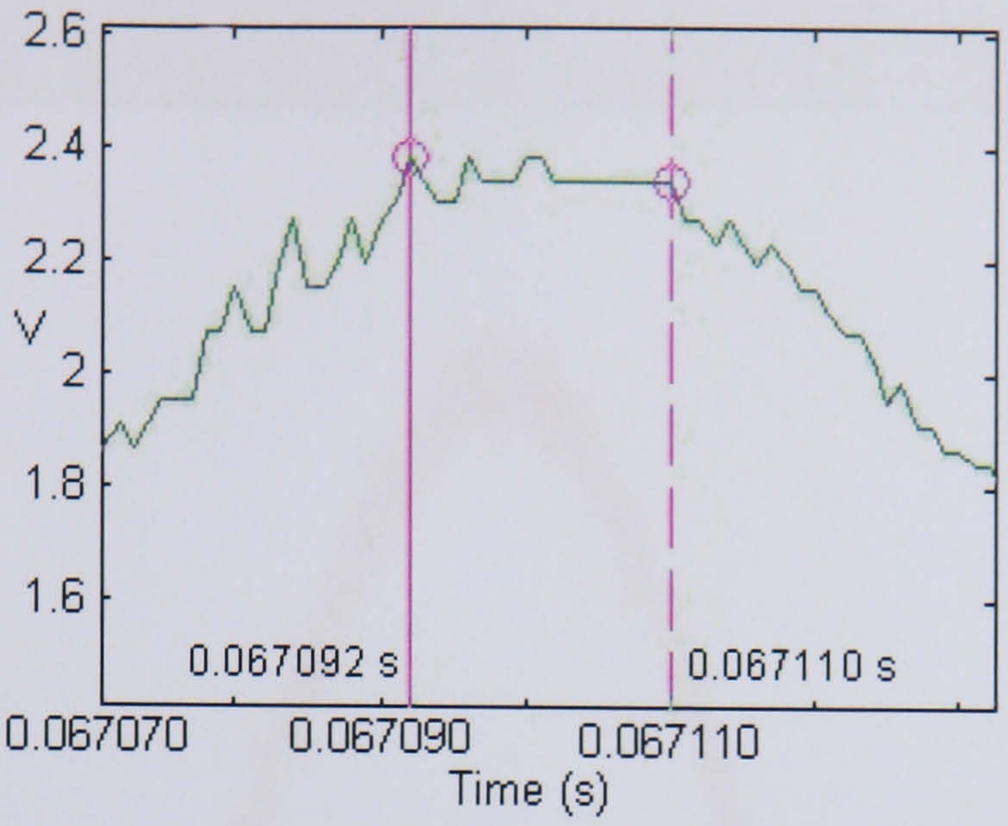

Figure E.8.2 - Capacitance Probe Signal Blade Passing 'Peak' at 850 RPM

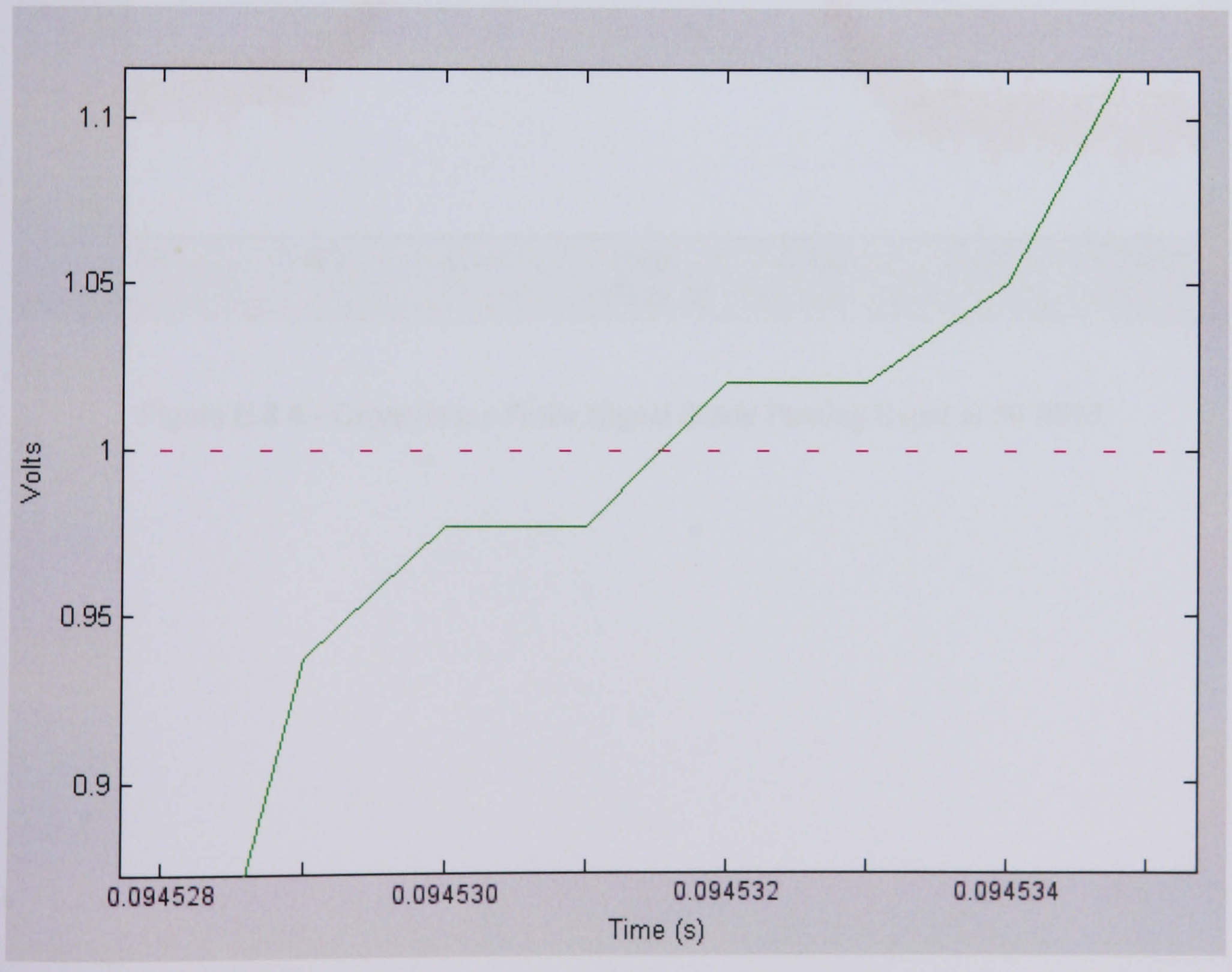

Figure E.8.3 - Capacitance Probe Signal Blade Passing Rising Edge at 850 RPM

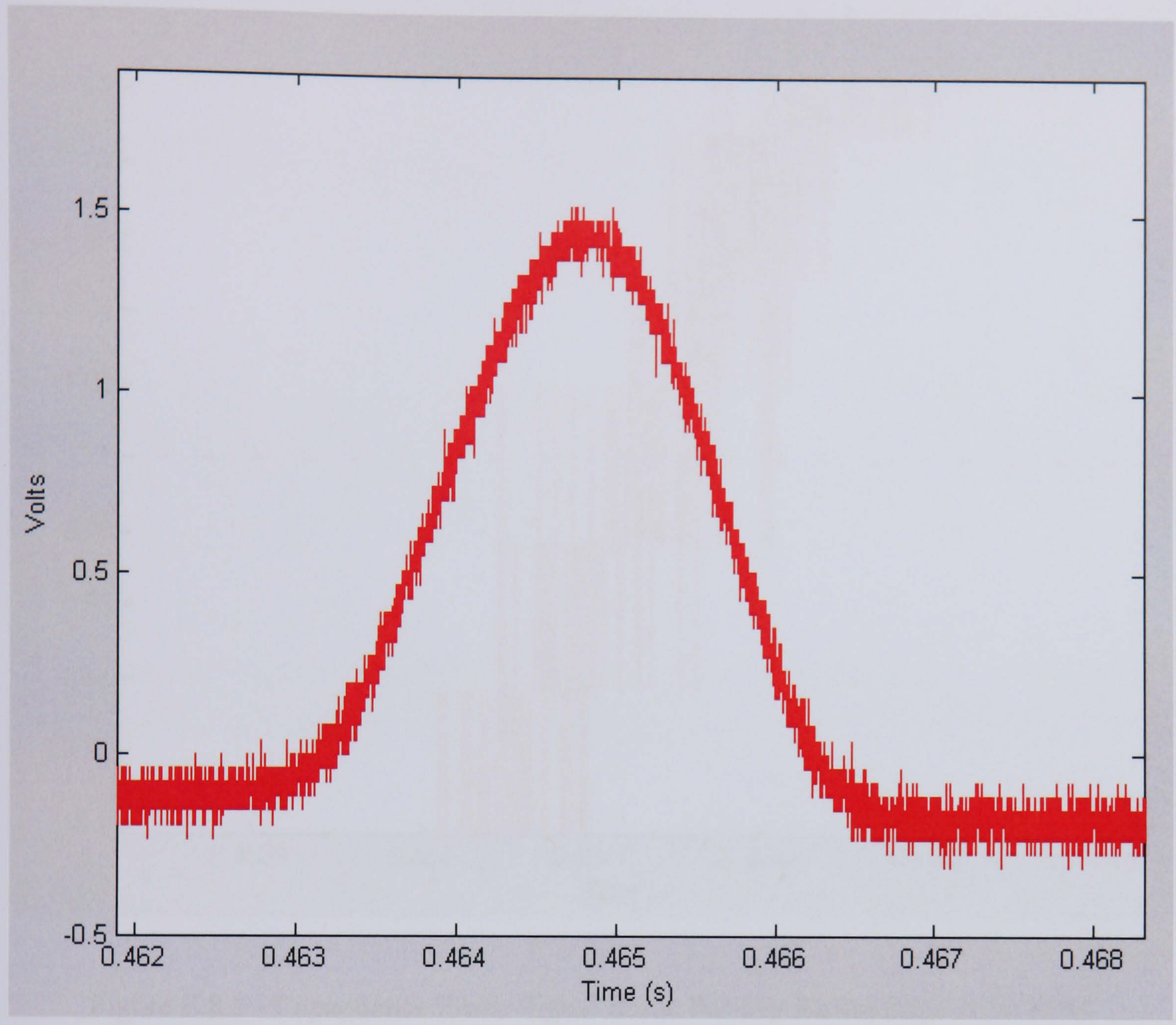

Figure E.8.4 - Capacitance Probe Signal Blade Passing Event at 50 RPM

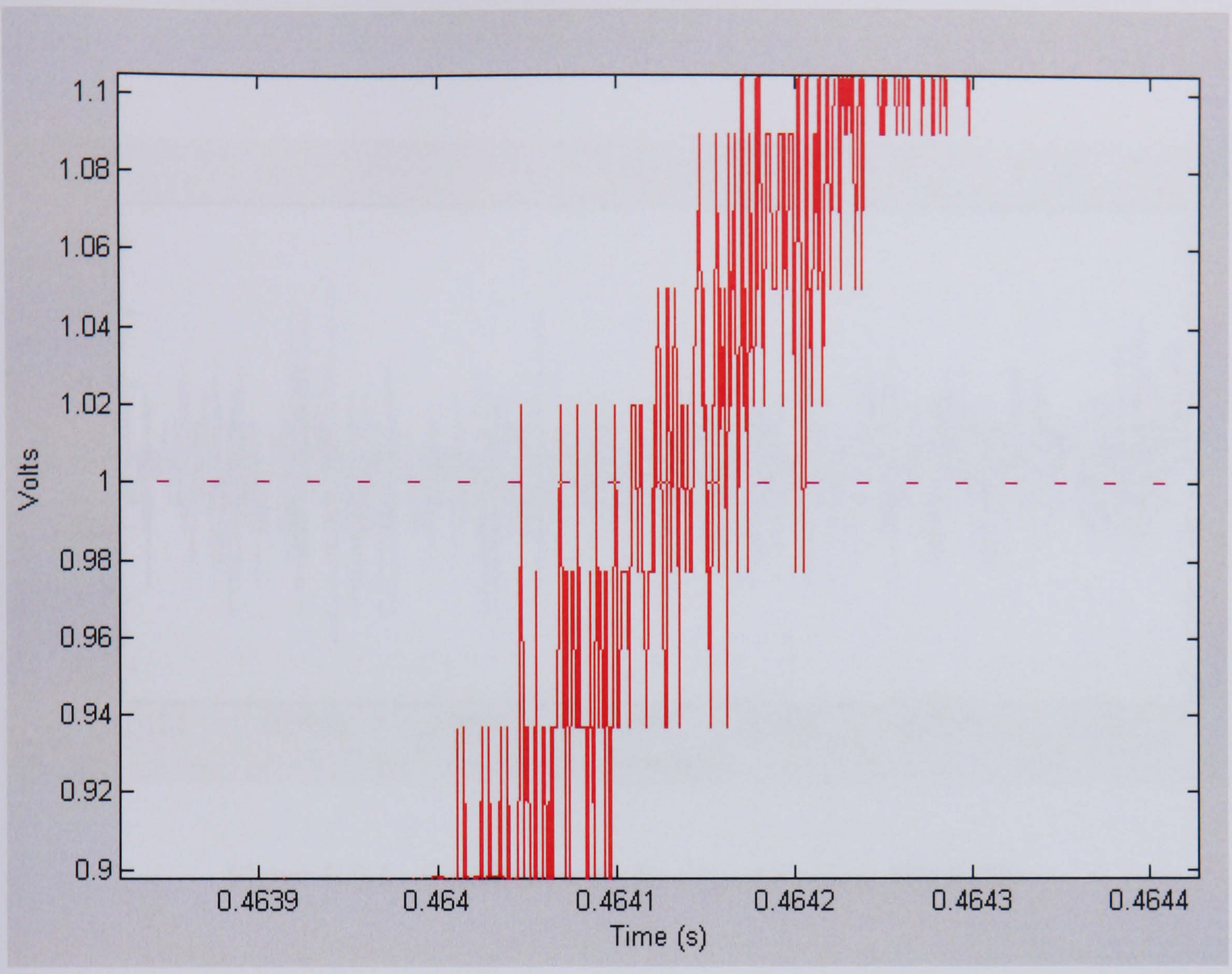

Figure E.8.5 - Capacitance Probe Signal Blade Passing Rising Edge at 50 RPM

Appendix E.9 - Compressor Rotor Blade Tip Timing Error Analysis

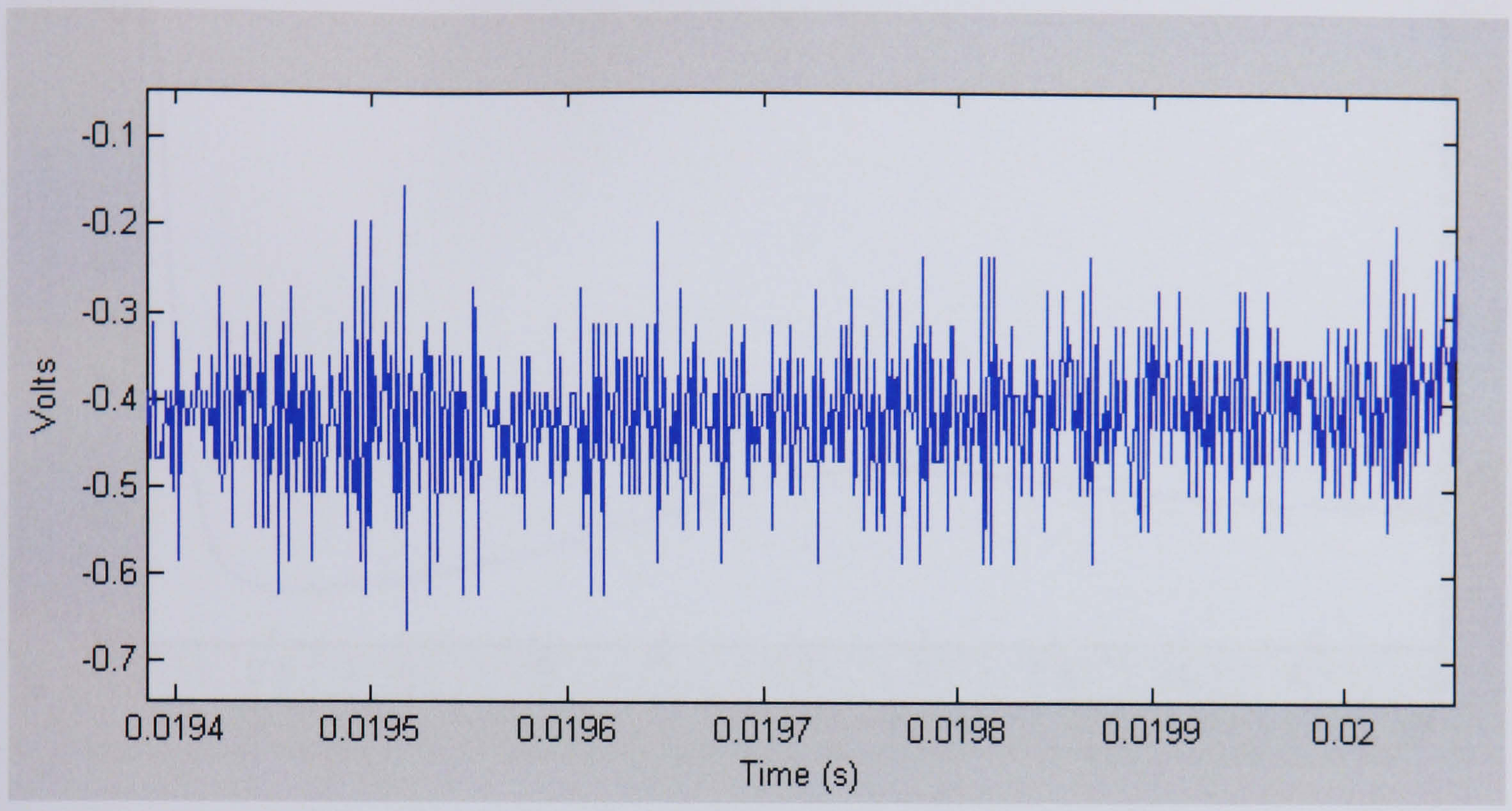

Figure E.9.1 - Capacitance Probe Signal Noise at 850 RPM

Figure E.9.2 - Capacitance Probe Signal Noise at Zero RPM

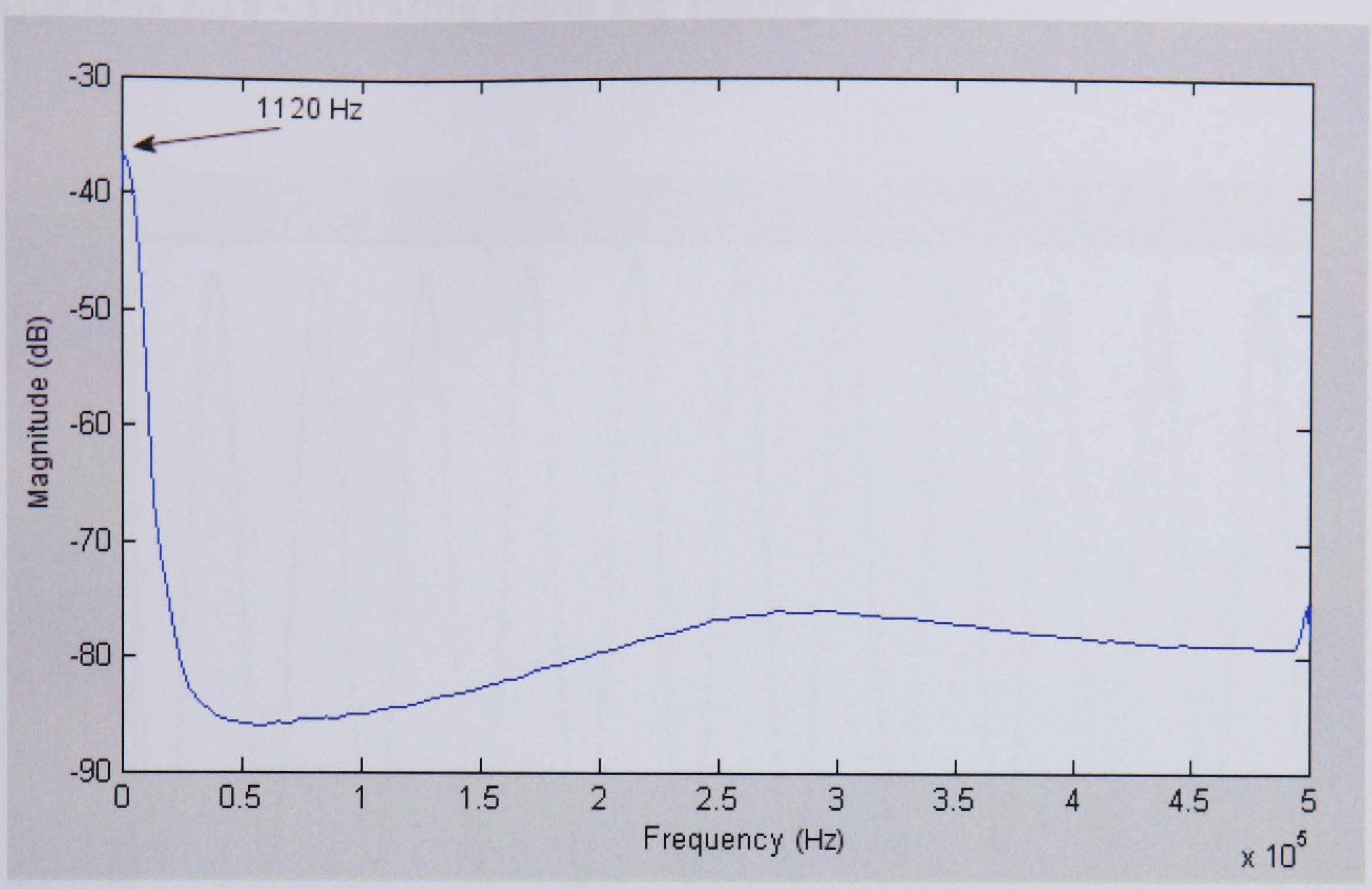

Figure E.9.3 - PSD of Capacitance Probe Blades Passing Signal

NB: Blade passing frequency = 850 x 79 / 60 = 1119.2 Hz

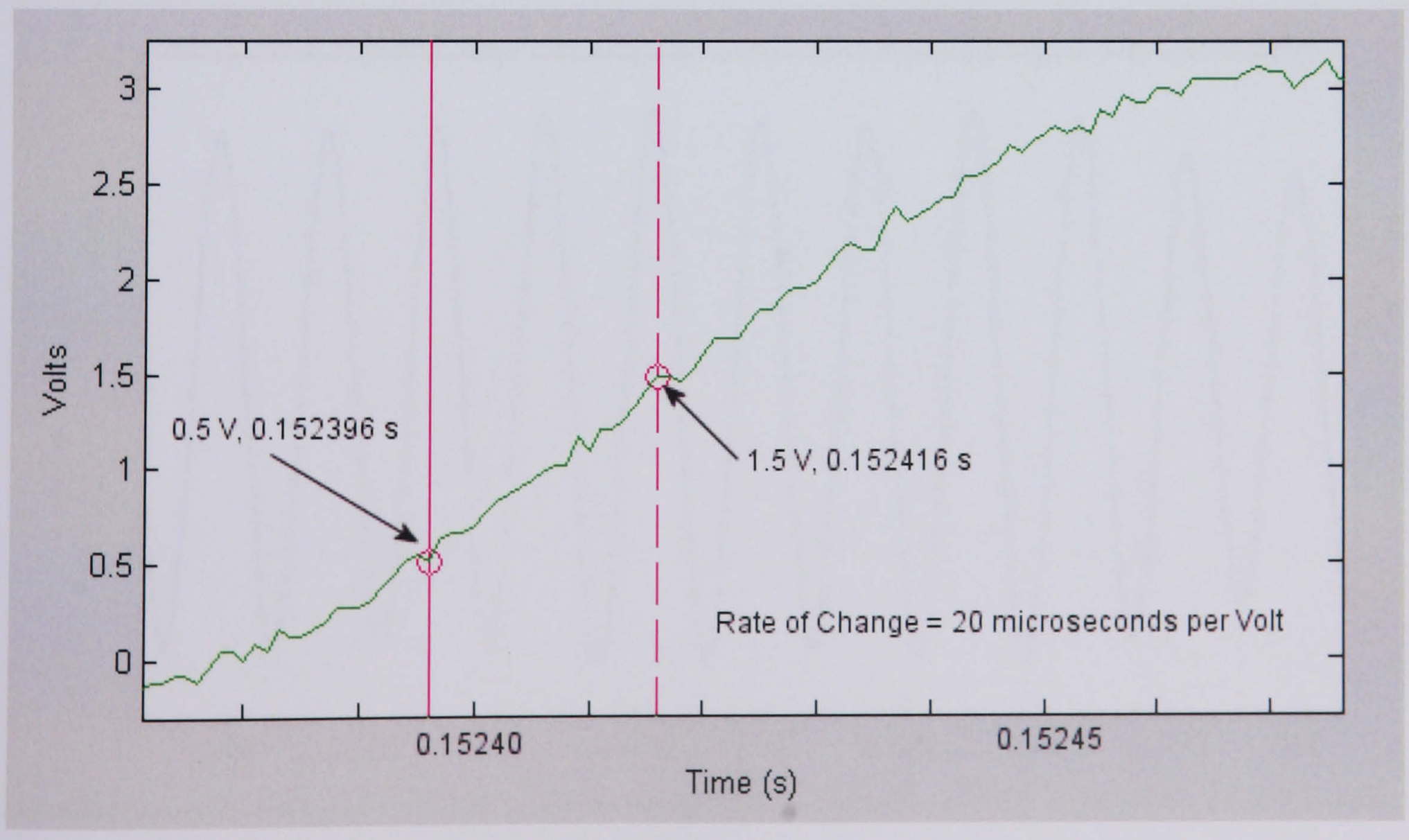

Figure E.9.4 - Capacitance Probe Signal Blade Passing Total Rising Edge at 850 RPM

Appendix E.10 - Vibrating Blade Tip Timing Results

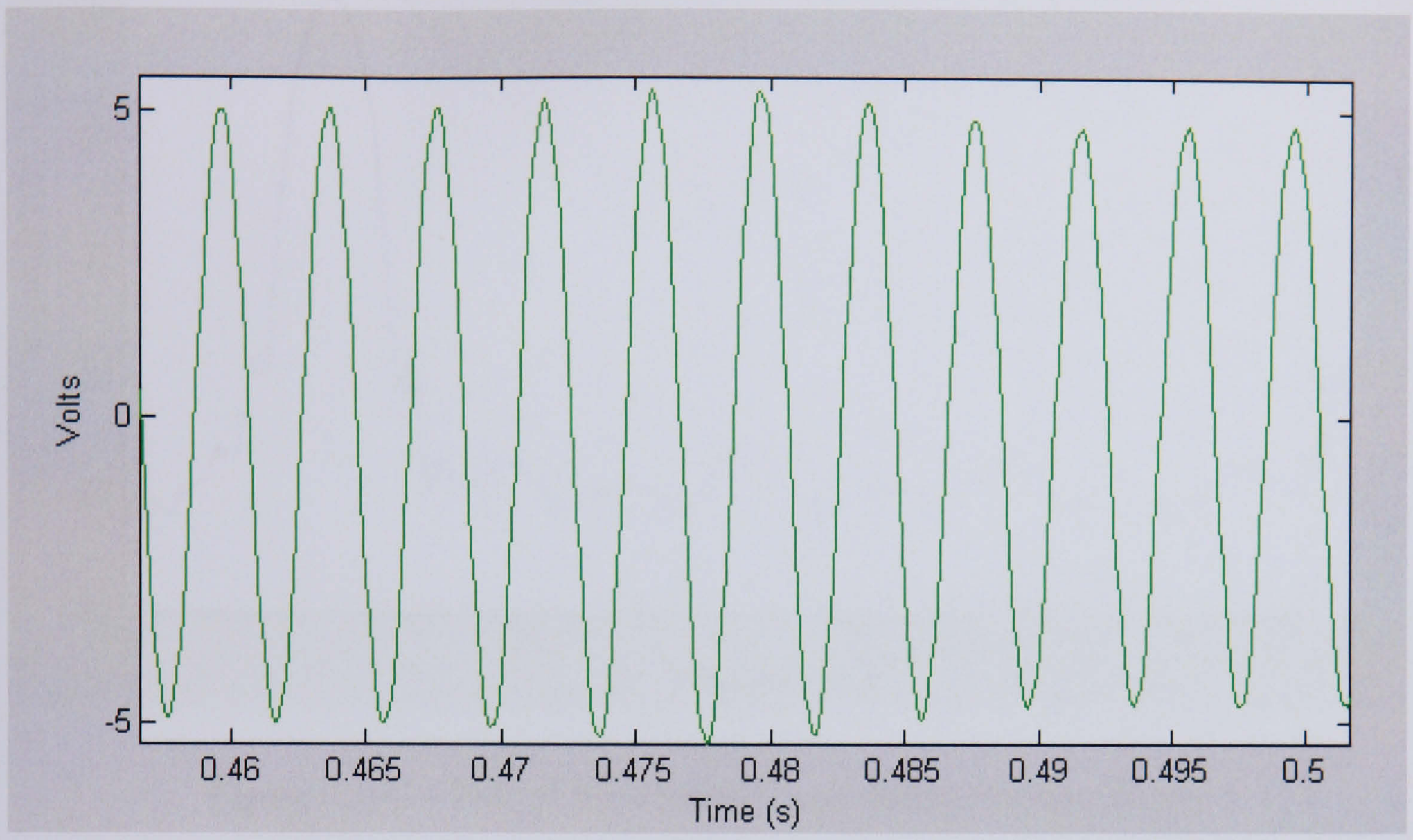

Figure E.10.1 - Root Strain Gauge Blade Vibration Signal Voltage Trace

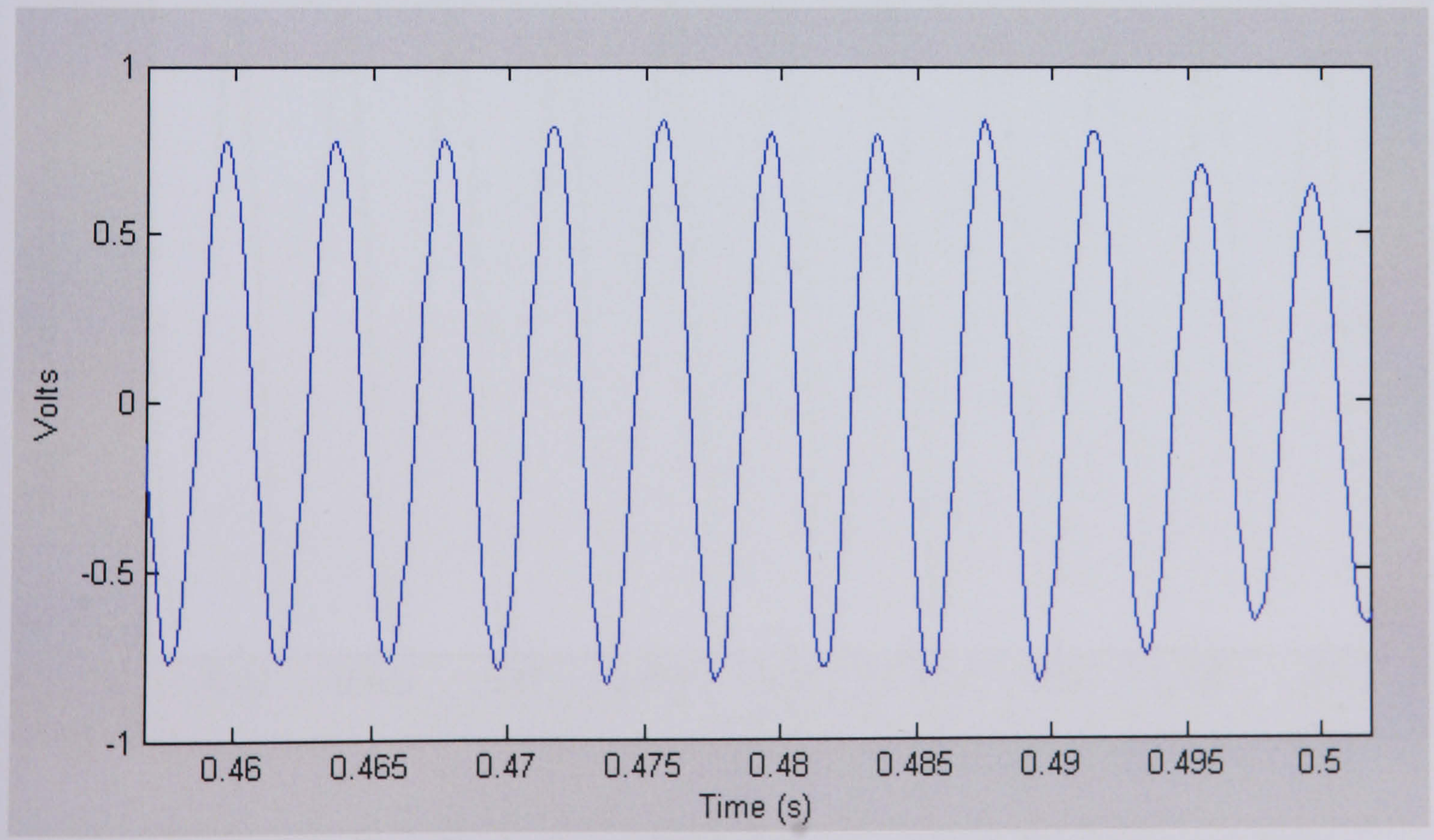

Figure E.10.2 - Leading Edge Strain Gauge Blade Vibration Signal Voltage Trace

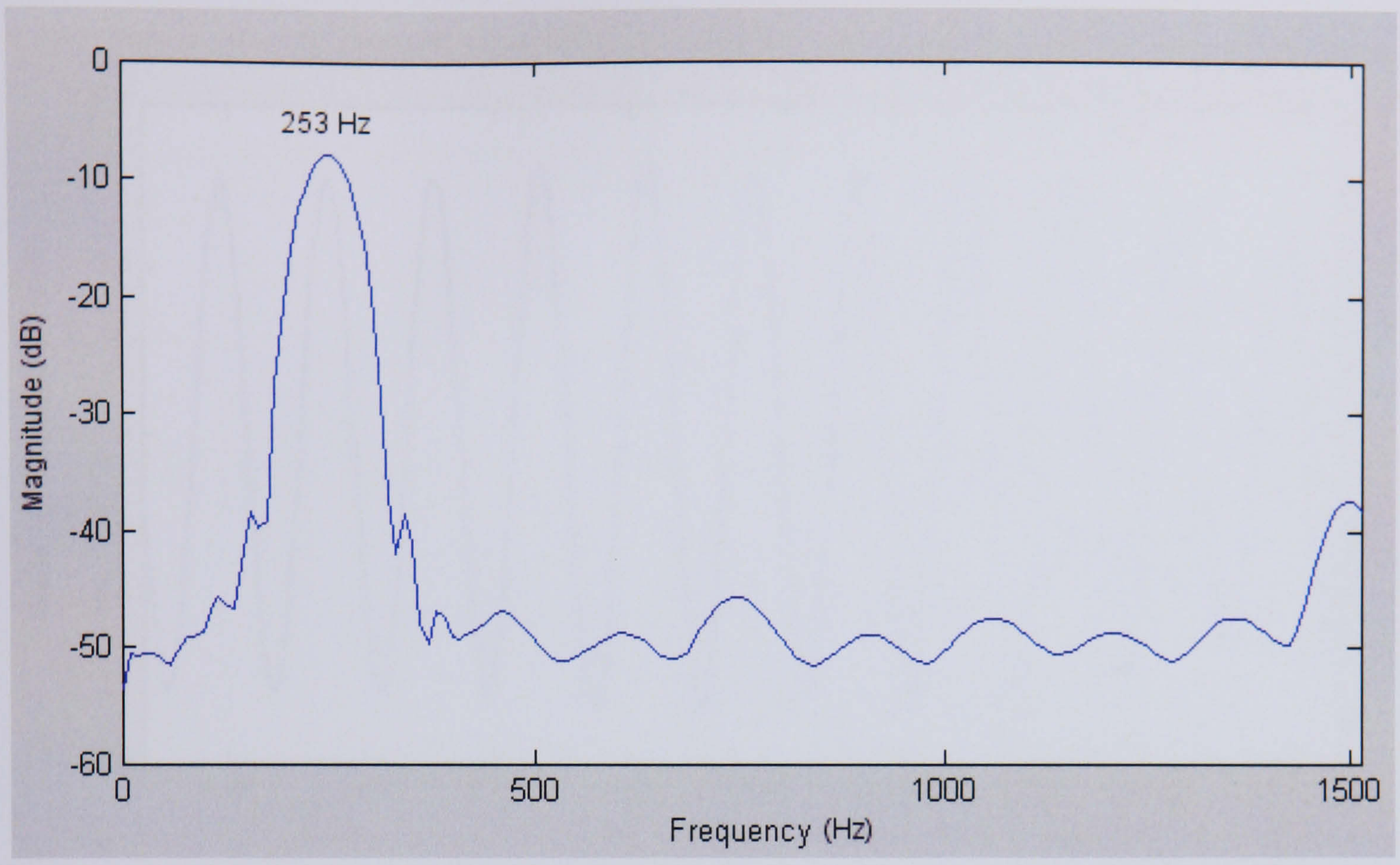

Figure E.10.3 - PSD of Root Strain Gauge Blade Vibration Signal

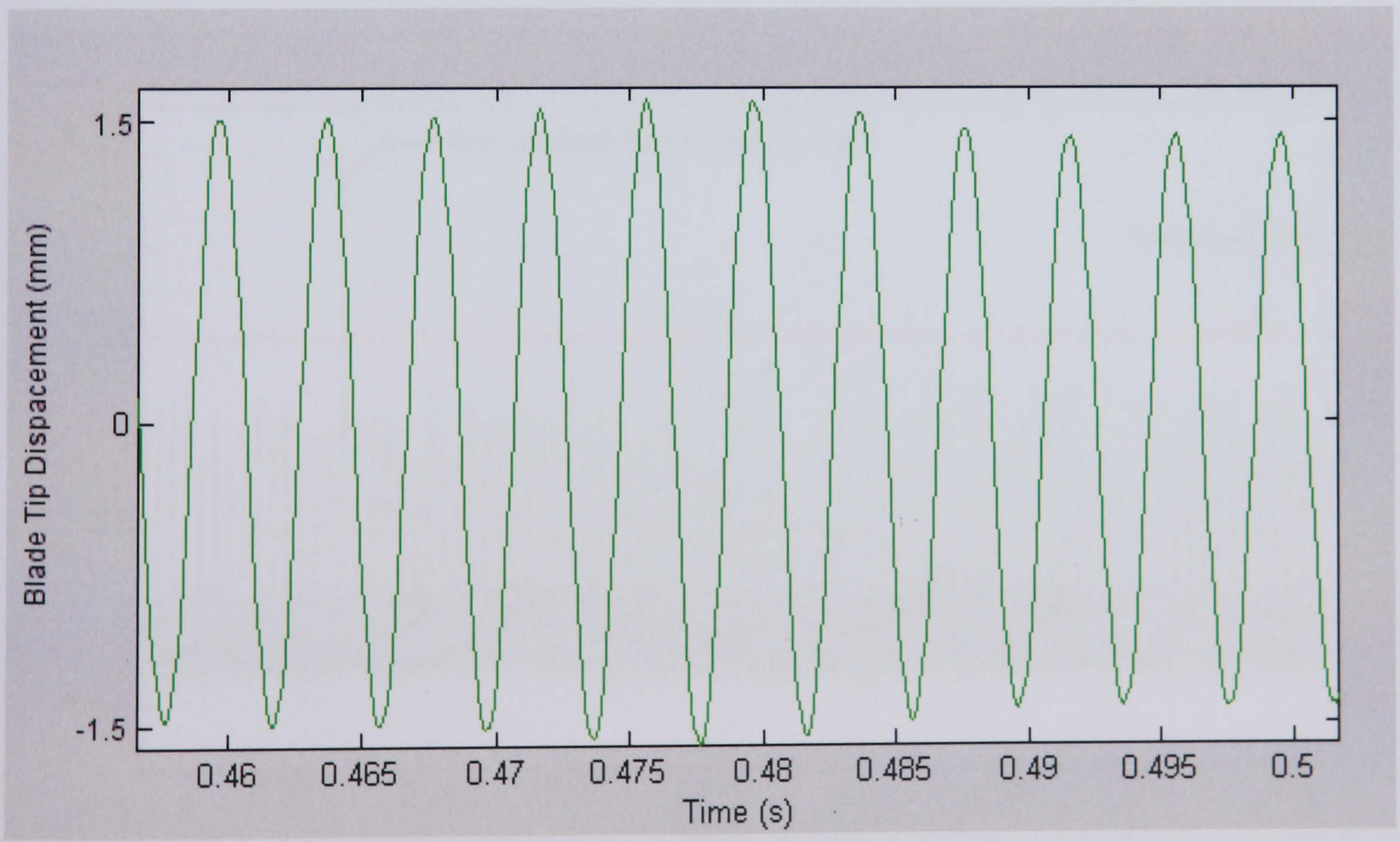

Figure E.10.4 - Root Strain Gauge Blade Vibration Signal Tip Deflection Trace

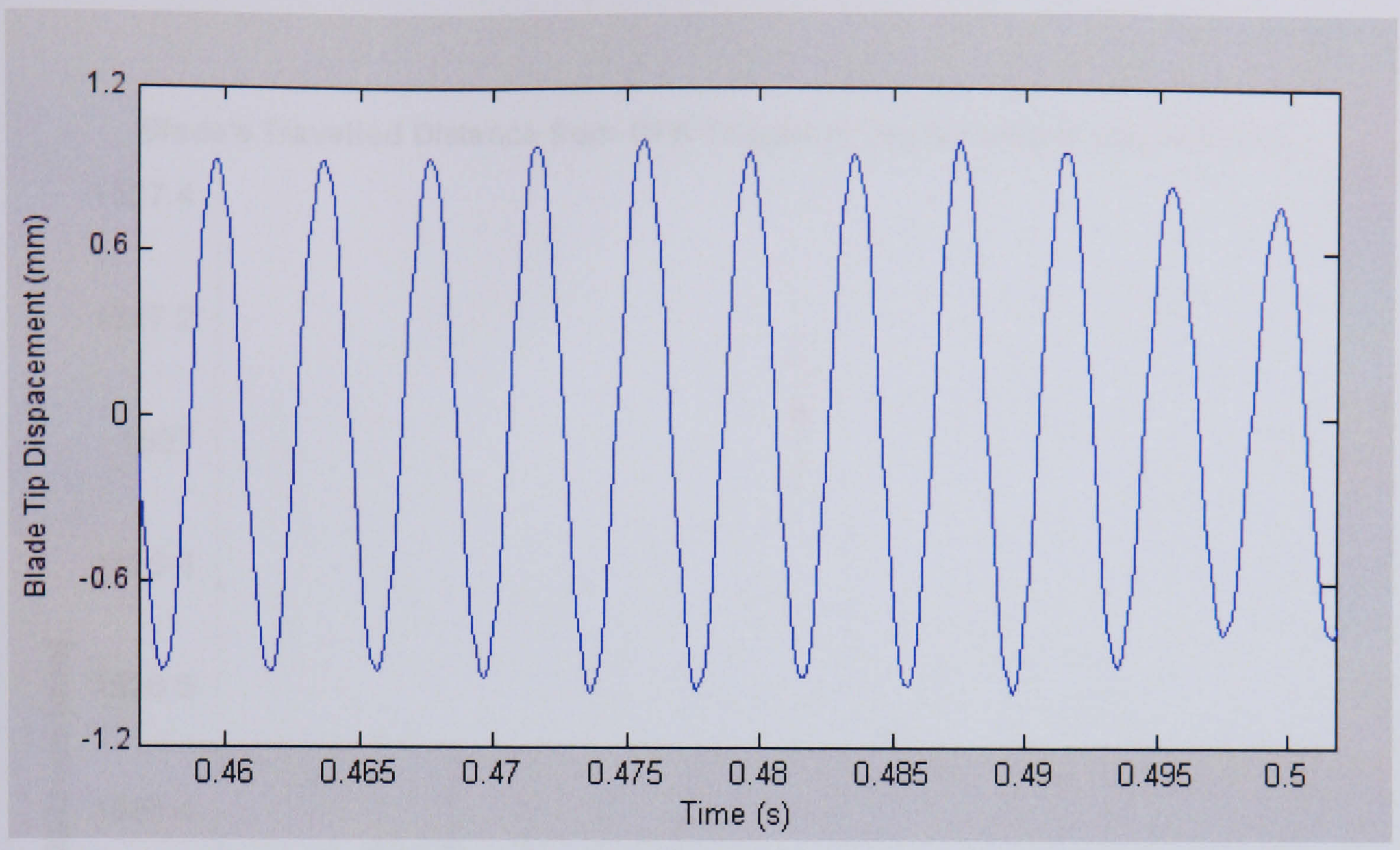

Figure E.10.5 - Leading Edge Strain Gauge Blade Vibration Signal Tip Deflection Trace

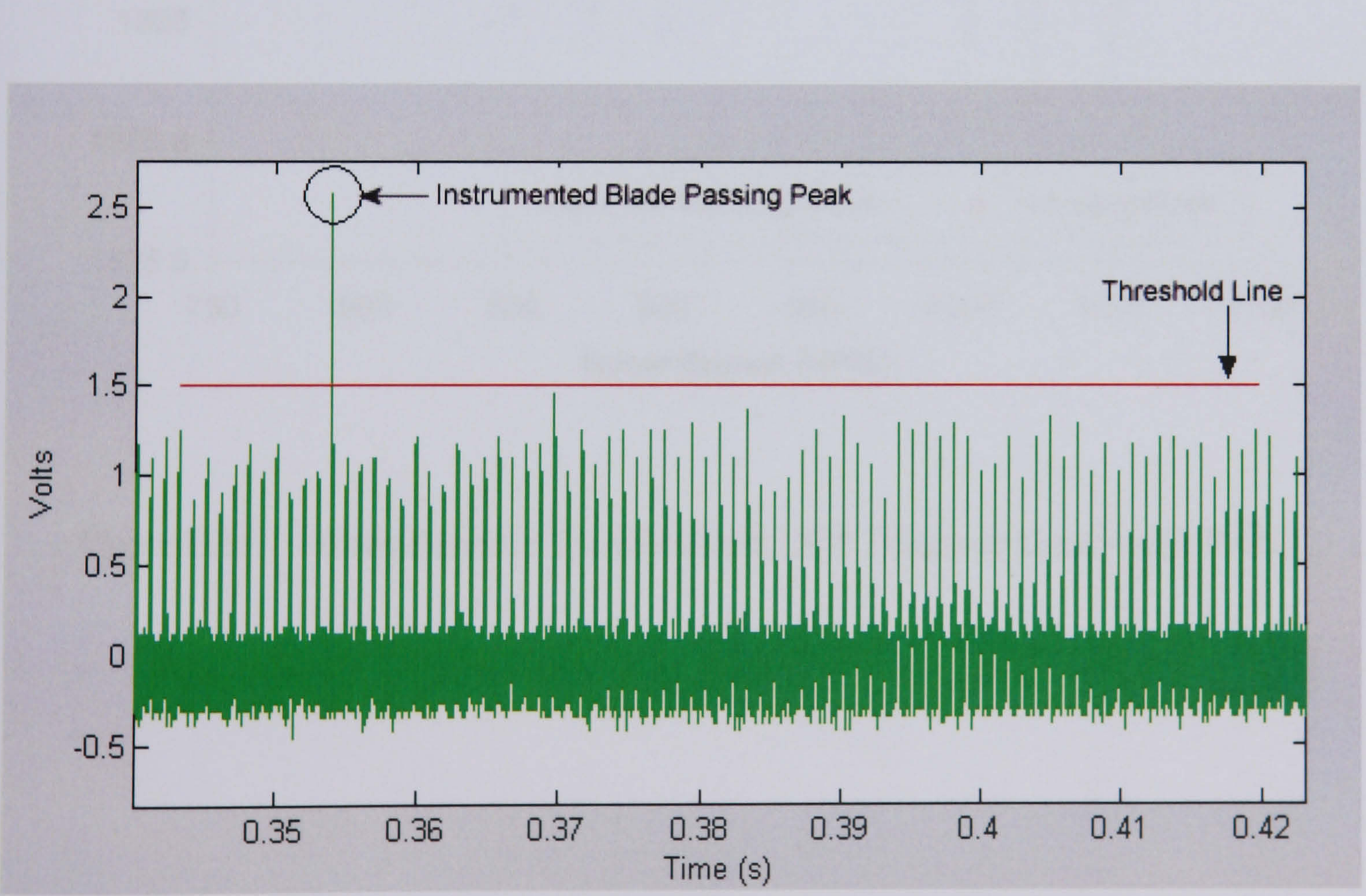

Figure E.10.6 - Capacitance Probe Blade Passing Signals from One Revolution

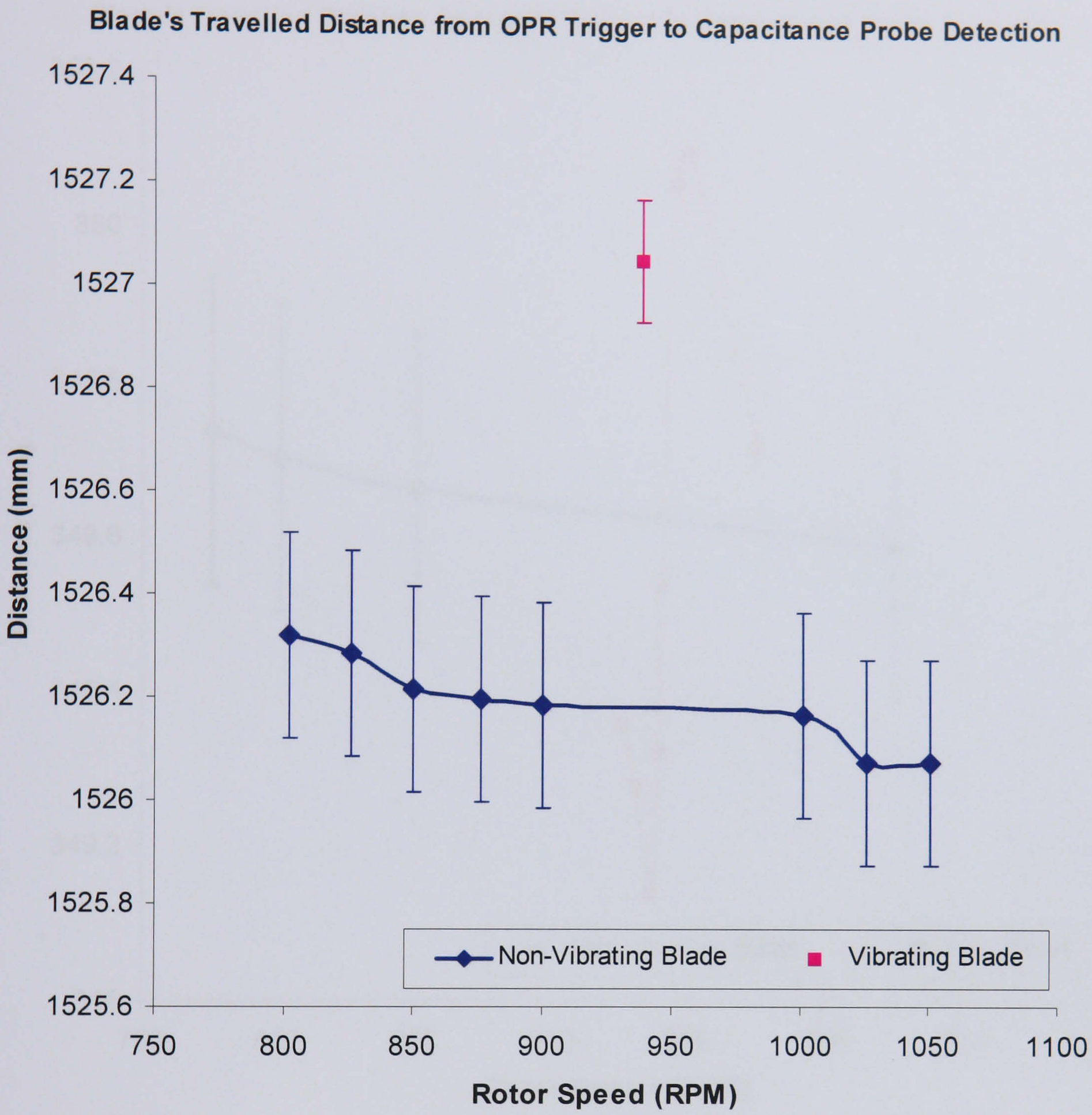

Figure E.10.7 - Blade Distance Travelled from OPR Trigger to Capacitance Probe

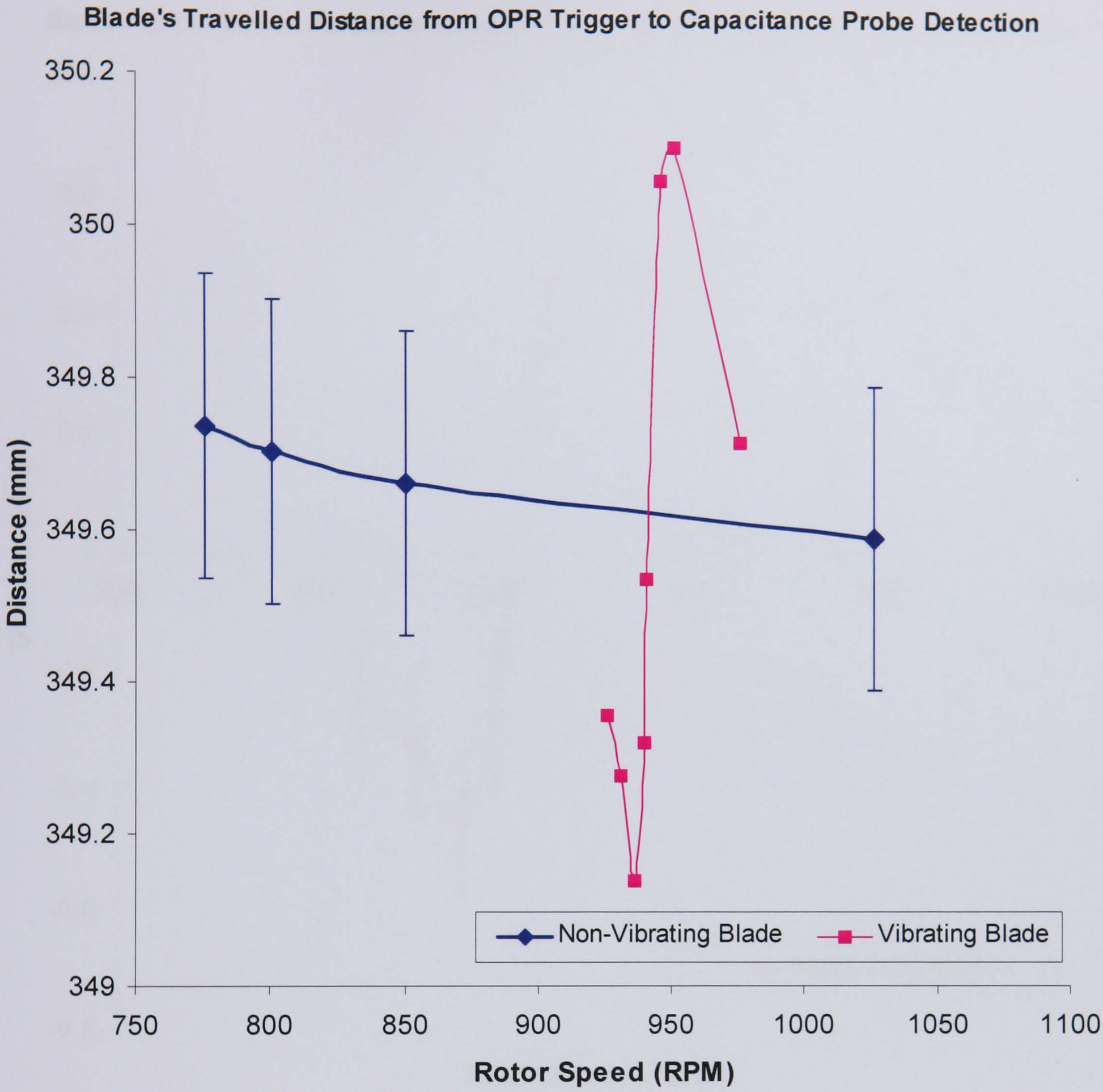

Figure E.10.8 - Blade Distance Travelled Over RPM Speed Across Resonance

NB: Error bars for the Vibrating Blade data shown here are illustrated in Figure E.10.9.

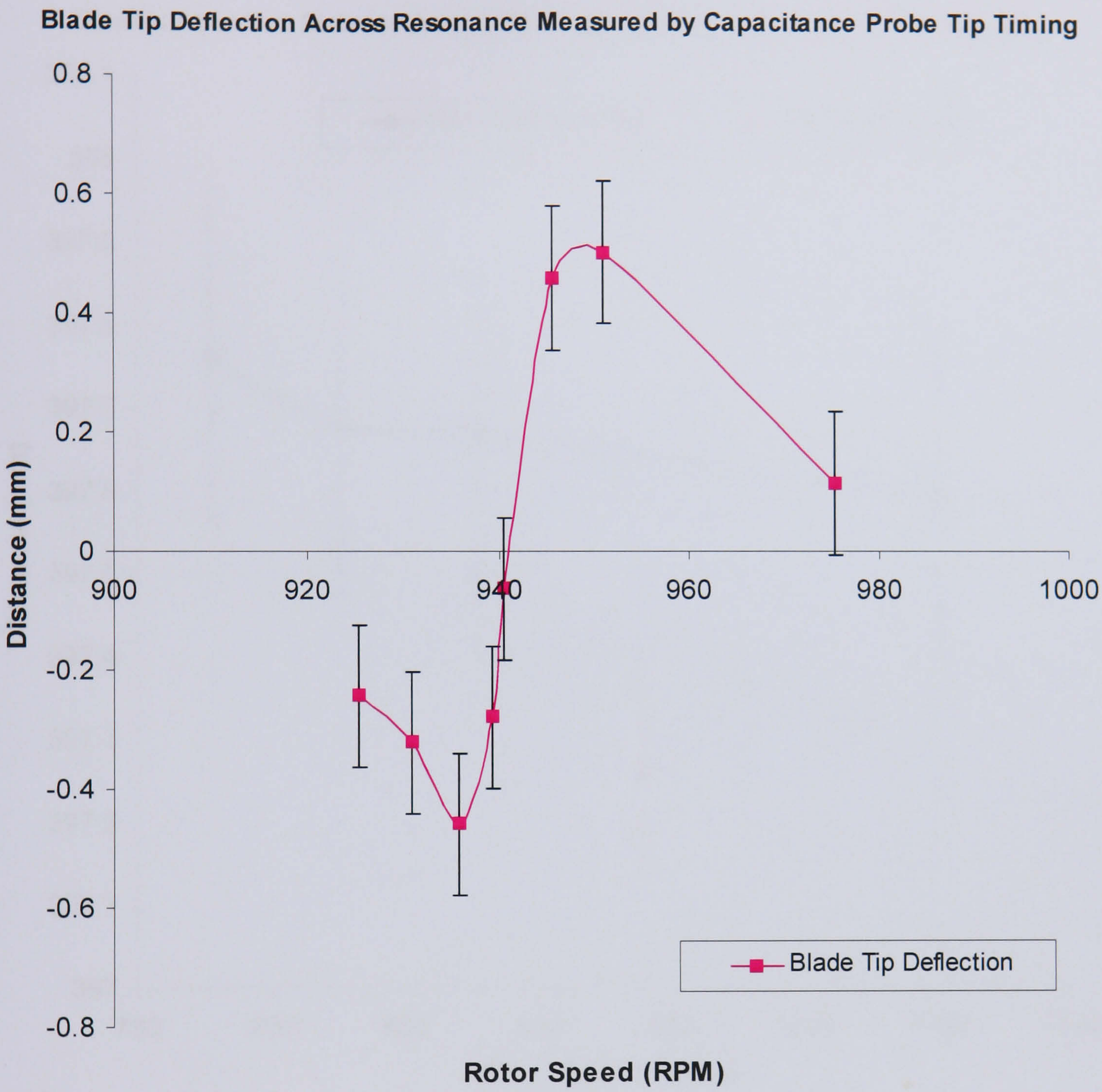

Figure E.10.9 - Blade Tip Deflection Measured Across Resonance by Tip Timing

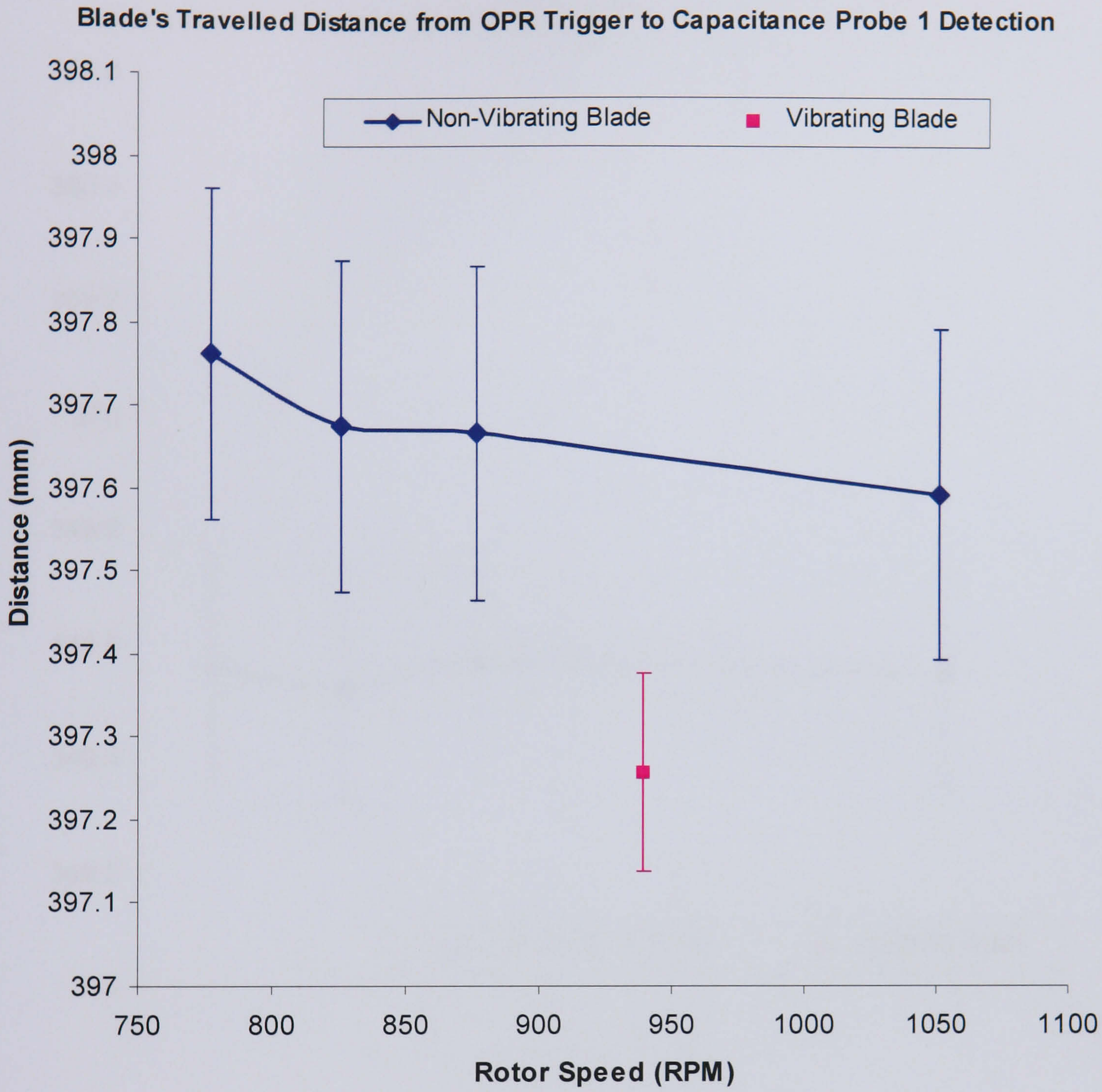

Figure E.10.10 - Blade Distance Travelled from OPR Trigger to Capacitance Probe 1

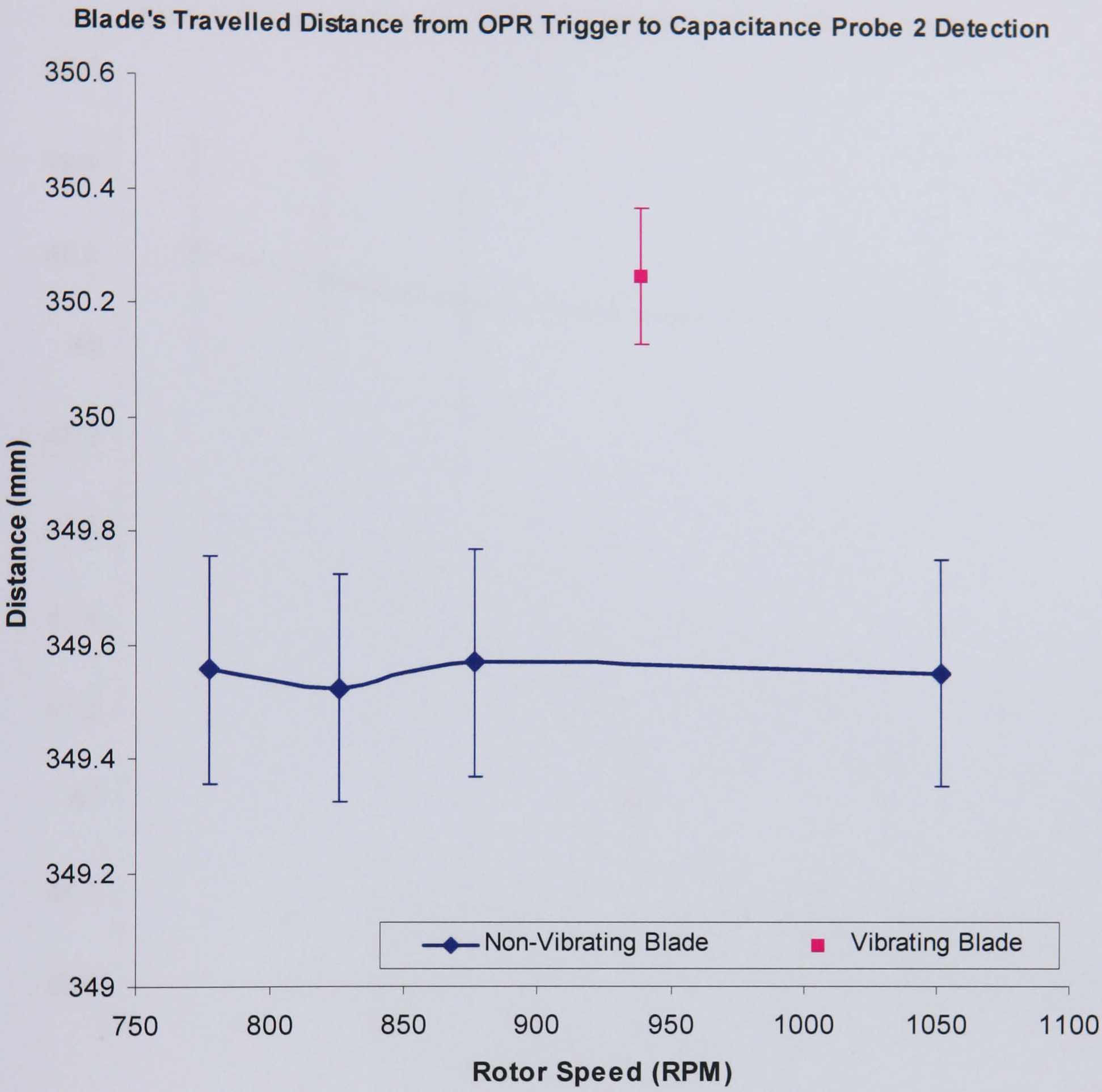

Figure E.10.11 - Blade Distance Travelled from OPR Trigger to Capacitance Probe 2

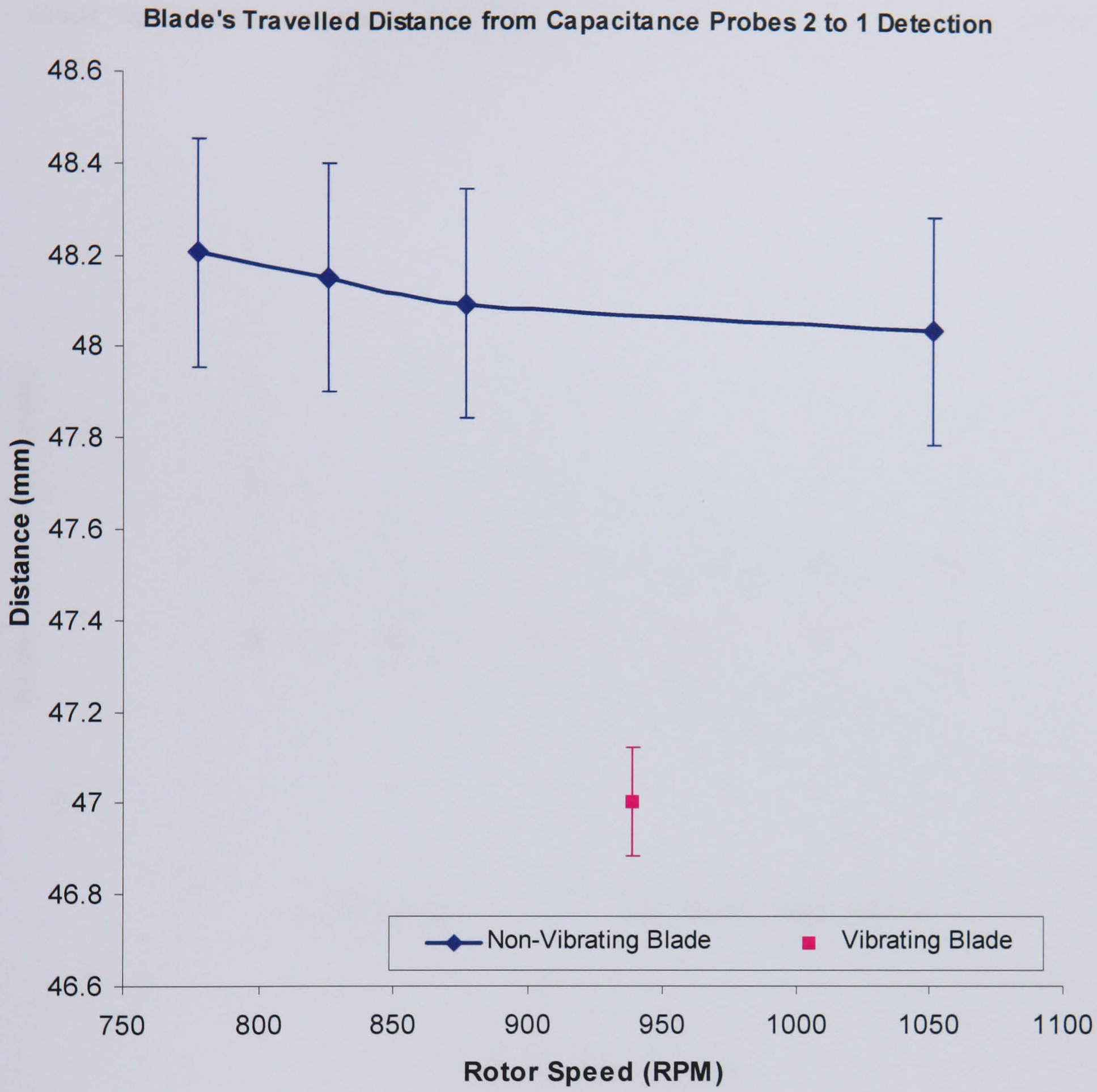

Figure E.10.12 - Blade Distance Travelled from Capacitance Probe 2 to Capacitance Probe 1

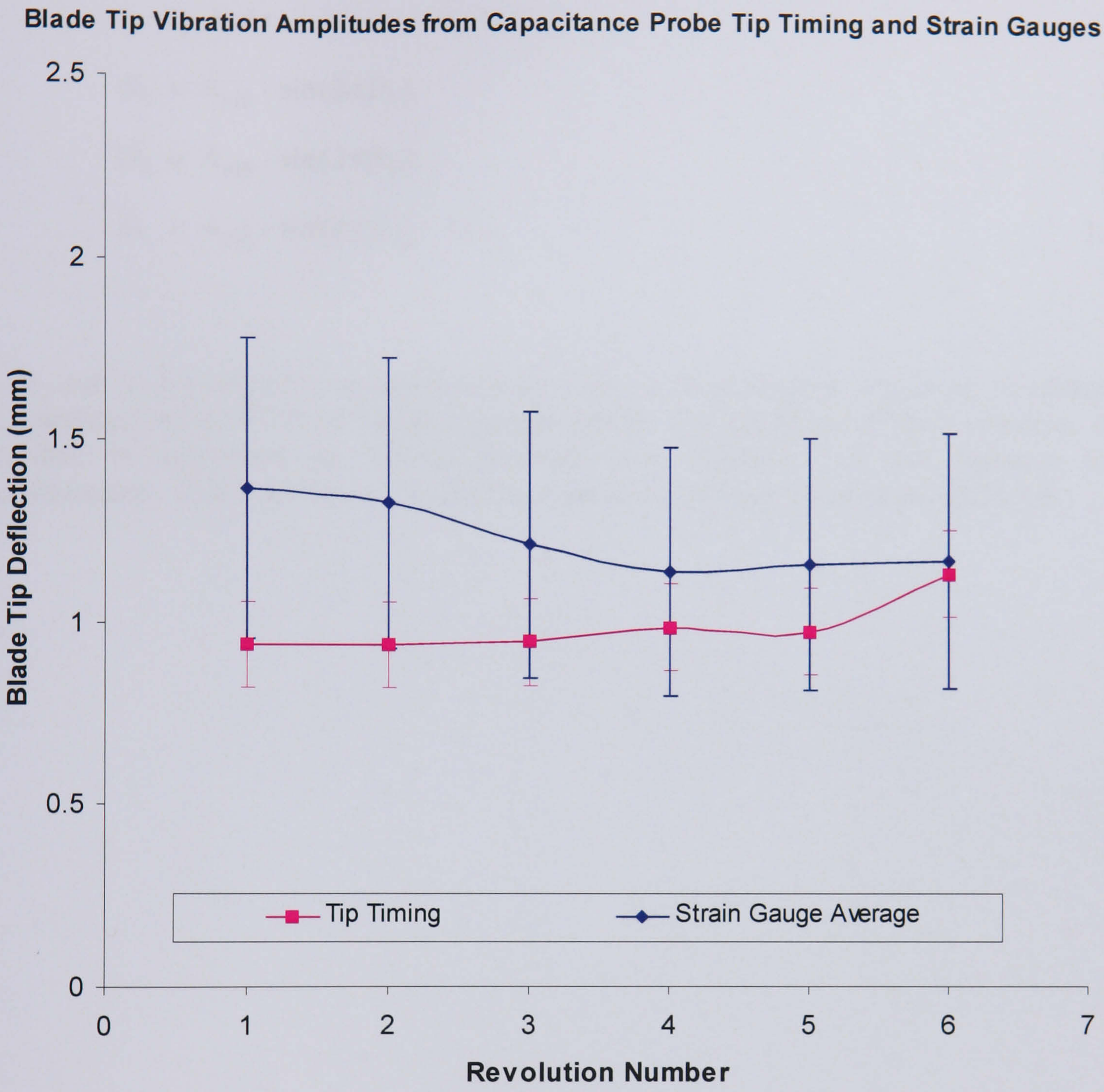

Figure E.10.13 - Blade Tip Vibration Amplitudes

Appendix E.11 - Blade Vibration Amplitude Calculation From Tip Timing

$$t_2 - t_1 = \Delta t \tag{E.7}$$

$$D_1 = A_{vib} \cdot \sin(2\pi f t_1) \tag{E.8}$$

$$D_2 = A_{vib} \cdot \sin(2\pi f t_2) \tag{E.9}$$

$$D_1 = A_{vib} \cdot \sin(2\pi f (t_2 - \Delta t)) \tag{E.10}$$

Δt, D_1 and D_2 are measured through dual capacitance probe tip timing. Frequency of vibration, f is calculated using FFT from the strain gauge signals. The amplitude of blade vibration, A_{vib} can then be calculated by solving Equation E.8, Equation E.9 and Equation E.10 simultaneously. This is performed by finding a solutions through iteration in MATLAB.